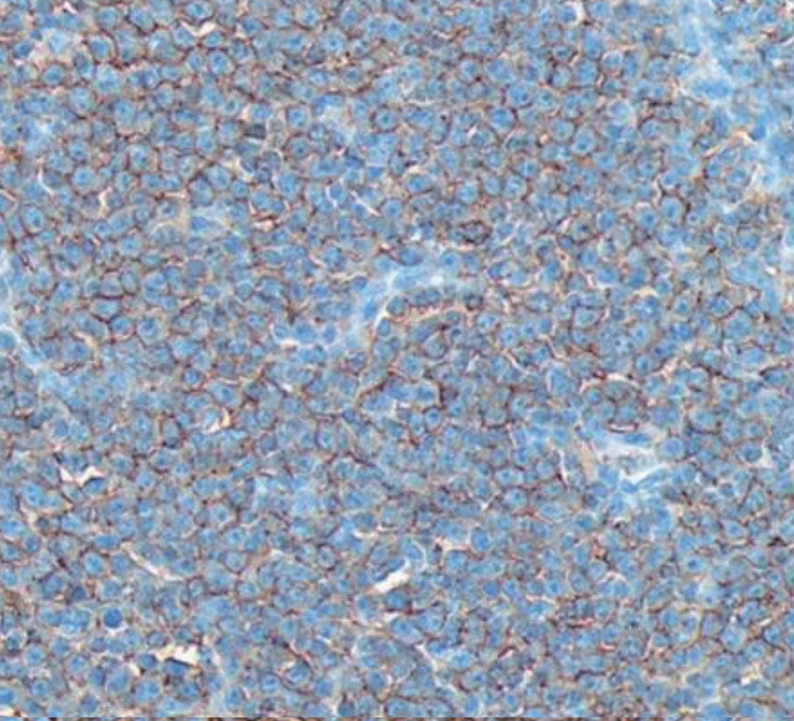


JPTM

Journal of Pathology
and Translational Medicine

March 2016
Vol. 50 / No. 2
jpatholm.org
pISSN: 2383-7837
eISSN: 2383-7845



***Sentinel Lymph Node
in Breast Cancer: Review
Article from a Pathologist's
Point of View***

Aims & Scope

The *Journal of Pathology and Translational Medicine* is an open venue for the rapid publication of major achievements in various fields of pathology, cytopathology, and biomedical and translational research. The Journal aims to share new insights into the molecular and cellular mechanisms of human diseases and to report major advances in both experimental and clinical medicine, with a particular emphasis on translational research. The investigations of human cells and tissues using high-dimensional biology techniques such as genomics and proteomics will be given a high priority. Articles on stem cell biology are also welcome. The categories of manuscript include original articles, review and perspective articles, case studies, brief case reports, and letters to the editor.

Subscription Information

To subscribe to this journal, please contact the Korean Society of Pathologists/the Korean Society for Cytopathology. Full text PDF files are also available at the official website (<http://jpatholm.org>). *Journal of Pathology and Translational Medicine* is indexed by PubMed, PubMed Central, Scopus, KoreaMed, KoMCI, WRPIM and CrossRef. Circulation number per issue is 700.

Editors-in-Chief

Hong, Soon Won, M.D. (*Yonsei University, Korea*)

Kim, Chong Jai, M.D. (*University of Ulsan, Korea*)

Associate Editors

Choi, Yoon Jung, M.D. (*National Health Insurance Service, Ilsan Hospital, Korea*)

Han, Jee Young, M.D. (*Inha University, Korea*)

Editorial Board

Ali, Syed Z. (*Johns Hopkins Hospital, U.S.A.*)

Avila-Casado, Maria del Carmen (*University of Toronto, Toronto General Hospital UHN, Canada*)

Bongiovanni, Massimo (*Centre Hospitalier Universitaire Vaudois, Switzerland*)

Cho, Kyung-Ja (*University of Ulsan, Korea*)

Choi, Yeong-Jin (*Catholic University, Korea*)

Chung, Jin-Haeng (*Seoul National University, Korea*)

Fadda, Guido (*Catholic University of the Sacred Heart, Italy*)

Gong, Gyung Yub (*University of Ulsan, Korea*)

Grignon, David J. (*Indiana University, U.S.A.*)

Ha, Seung Yeon (*Gachon University, Korea*)

Jang, Se Jin (*University of Ulsan, Korea*)

Jeong, Jin Sook (*Dong-A University, Korea*)

Kang, Gyeong Hoon (*Seoul National University, Korea*)

Katoh, Ryohei (*University of Yamanashi, Japan*)

Kerr, Keith M. (*Aberdeen University Medical School, U.K.*)

Kim, Aeree (*Korea University, Korea*)

Kim, Kyoung Mee (*Sungkyunkwan University, Korea*)

Kim, Kyu Rae (*University of Ulsan, Korea*)

Kim, Se Hoon (*Yonsei University, Korea*)

Kim, Seok-Hyung (*Sungkyunkwan University, Korea*)

Kim, Woo Ho (*Seoul National University, Korea*)

Kim, Youn Wha (*Kyung Hee University, Korea*)

Ko, Young Hyeoh (*Sungkyunkwan University, Korea*)

Koo, Ja Seung (*Yonsei University, Korea*)

Lee, C. Soon (*University of Western Sydney, Australia*)

Lee, Hye Seung (*Seoul National University, Korea*)

Lee, Kyung Han (*Sungkyunkwan University, Korea*)

Lee, Sug Hyung (*Catholic University, Korea*)

Lim, Beom Jin (*Yonsei University, Korea*)

Lkhagvadorj, Sayamaa (*Mongolian National University of Medical Sciences, Mongolia*)

Moon, Woo Sung (*Chonbuk University, Korea*)

Ngo, Quoc Dat (*Ho Chi Minh University of Medicine and Pharmacy, Vietnam*)

Park, Chan-Sik (*University of Ulsan, Korea*)

Park, Sanghui (*Ewha Womans University, Korea*)

Park, So Yeon (*Seoul National University, Korea*)

Park, Young Nyun (*Yonsei University, Korea*)

Pervez, Shahid (*Aga Khan University, Pakistan*)

Ro, Jae Y. (*Cornell University, The Methodist Hospital, U.S.A.*)

Romero, Roberto (*National Institute of Child Health and Human Development, U.S.A.*)

Schmitt, Fernando (*IPATIMUP [Institute of Molecular Pathology and Immunology of the University of Porto], Portugal*)

Shin, Eunah (*Cha University, Korea*)

Sung, Chang Ohk (*University of Ulsan, Korea*)

Tan, Puay Hoon (*National University of Singapore, Singapore*)

Than, Nandor Gabor (*Semmelweis University, Hungary*)

Tse, Gary M. (*Prince of Wales Hospital, Hongkong*)

Vielh, Philippe (*International Academy of Cytology Gustave Roussy Cancer Campus Grand Paris, France*)

Wildman, Derek (*University of Illinois, U.S.A.*)

Yatabe, Yasushi (*Aichi Cancer Center, Japan*)

Yoon, Bo Hyun (*Seoul National University, Korea*)

Yoon, Sun Och (*Yonsei University, Korea*)

Statistics Editors

Kim, Dong Wook (*National Health Insurance Service Ilsan Hospital, Korea*)

Yoo, Hanna (*Yonsei University, Korea*)

Manuscript Editor

Chang, Soo-Hee (*InfoLumi Co., Korea*)

Contact the Korean Society of Pathologists/the Korean Society for Cytopathology

Publishers: Min Cheol Lee, MD, So Young Jin, MD

Editors-in-Chief: Soon Won Hong, MD, Chong Jai Kim, MD

Published by the Korean Society of Pathologists/the Korean Society for Cytopathology

Editorial Office

Room 1209 Gwanghwamun Officia, 92 Saemunan-ro, Jongno-gu,

Seoul 03186, Korea/#406 Lilla Swami Bldg, 68 Dongsan-ro,

Seocho-gu, Seoul 06784, Korea

Tel: +82-2-795-3094/+82-2-593-6943

Fax: +82-2-790-6635/+82-2-593-6944

E-mail: office@jpatholm.org

Printed by ML communications Co., Ltd.

Jungang Bldg. 18-8 Wonhyo-ro 89-gil, Yongsan-gu, Seoul 04314, Korea

Tel: +82-2-717-5511 Fax: +82-2-717-5515 E-mail: ml@smileml.com

Manuscript Editing by InfoLumi Co.

210-202, 421 Pangyo-ro, Bundang-gu, Seongnam 13522, Korea

Tel: +82-70-8839-8800 E-mail: infolumi.chang@gmail.com

Front cover image: Semi-quantitative immunohistochemical scoring of CD20 expression. p98.

© Copyright 2016 by the Korean Society of Pathologists/the Korean Society for Cytopathology

© Journal of Pathology and Translational Medicine is an Open Access journal under the terms of the Creative Commons Attribution Non-Commercial License (<http://creativecommons.org/licenses/by-nc/3.0>).

© This paper meets the requirements of KS X ISO 9706, ISO 9706-1994 and ANSI/NISO Z.39.48-1992 (Permanence of Paper).

This journal was supported by the Korean Federation of Science and Technology Societies Grant funded by the Korean Government.

CONTENTS

REVIEW

- 83 Sentinel Lymph Node in Breast Cancer: Review Article from a Pathologist's Point of View
Sophia K. Apple

ORIGINAL ARTICLES

- 96 Prognostic Implication of Semi-quantitative Immunohistochemical Assessment of CD20 Expression in Diffuse Large B-Cell Lymphoma
Chang Hwan Choi, Young Hoon Park, Joo Han Lim, Suk Jin Choi, Lucia Kim, In Suh Park, Jee Young Han, Joon Mee Kim, Young Chae Chu
- 104 Upregulated Neuro-oncological Ventral Antigen 1 (NOVA1) Expression Is Specific to Mature and Immature T- and NK-Cell Lymphomas
Eun Kyung Kim, Sun Och Yoon, Soo Hee Kim, Woo Ick Yang, Yoon Ah Cho, Soo Jeong Kim
- 113 Meningeal Solitary Fibrous Tumors with Delayed Extracranial Metastasis
Nayoung Han, Hannah Kim, Soo Kee Min, Sun-Ha Paek, Chul-Kee Park, Seung-Hong Choi, U-Ri Chae, Sung-Hye Park
- 122 Prognostic Significance of Aquaporin 5 Expression in Non-small Cell Lung Cancer
Young Min Jo, Tae In Park, Hwa Young Lee, Ji Yun Jeong, Won Kee Lee
- 129 Interobserver Variability of Ki-67 Measurement in Breast Cancer
Yul Ri Chung, Min Hye Jang, So Yeon Park, Gyungyub Gong, Woo-Hee Jung, The Korean Breast Pathology Ki-67 Study Group
- 138 Comparison of Analytical and Clinical Performance of HPV 9G DNA Chip, PANArray HPV Genotyping Chip, and Hybrid-Capture II Assay in Cervicovaginal Swabs
Ho Young Jung, Hye Seung Han, Hyo Bin Kim, Seo Young Oh, Sun-Joo Lee, Wook Youn Kim
- 147 Morphologic Analysis of Cytomegalovirus Infected Cells in Bronchial Washing Cytology: Comparison of Liquid-Based Preparation and Conventional Smear
Jae Yeon Seok, Jungsuk An, Seung Yeon Ha, Dong Hae Chung, Sangho Lee, Hyunchul Kim

CASE REPORTS

- 155 **Clear Cell Adenocarcinoma Arising from Adenofibroma in a Patient with Endometriosis of the Ovary**
Inju Cho, Sung-Chul Lim
- 160 **An Adult Case of Bartter Syndrome Type III Presenting with Proteinuria**
Eun Jung Cha, Won Min Hwang, Sung-Ro Yun, Moon Hyang Park
- 165 **A Rare Case of Thymic Gangliocytic Paraganglioma**
Jung Wook Yang, Joungho Han, Hyun Woo Lee, Soo Youn Cho, Hong Kwan Kim
- 168 **Primary Neurilemmoma of the Thyroid Gland Clinically Mimicking Malignant Thyroid Nodule**
Young Sub Lee, Jee Soon Kim, Arthur Minwoo Chung, Woo Chan Park, Tae-Jung Kim

Instructions for Authors for *Journal of Pathology and Translational Medicine* are available at <http://jpatholm.org/authors/authors.php>

Sentinel Lymph Node in Breast Cancer: Review Article from a Pathologist's Point of View

Sophia K. Apple

Department of Pathology and Laboratory Medicine, University of California at Los Angeles (UCLA), Los Angeles, CA, USA

Received: November 11, 2015
Accepted: November 23, 2015

Corresponding Author

Sophia K. Apple, MD
Department of Pathology and Laboratory Medicine, University of California at Los Angeles (UCLA), Center of Health Science Bldg., Los Angeles, CA 90095-1732, USA
Tel: +1-310-825-9288
Fax: +1-310-825-2483
E-mail: sapple@mednet.ucla.edu

Breast cancer staging, in particular N-stage changed most significantly due to the advanced technique of sentinel lymph node biopsy two decades ago. Pathologists have more thoroughly examined and scrutinized sentinel lymph node and found increased number of small volume metastases. While pathologists use the strict criteria from the Tumor Lymph Node Metastasis (TNM) Classification, studies have shown poor reproducibility in the application of American Joint Committee on Cancer and International Union Against Cancer/TNM guidelines for sentinel lymph node classification in breast cancer. In this review article, a brief history of TNM with a focus on N-stage is described, followed by innate problems with the guidelines, and why pathologists may have difficulties in assessing lymph node metastases uniformly. Finally, clinical significance of isolated tumor cells, micrometastasis, and macrometastasis is described by reviewing historical retrospective data and significant prospective clinical trials.

Key Words: Sentinel lymph node; N-stage; Isolated tumor cells; Micrometastasis; Macrometastasis

The management and treatment of the axilla is moving towards conservatism since complete removal of axillary lymph nodes after sentinel lymph node (SLN) has not been affecting the overall survival and recurrence free survival. SLN biopsy has been as effective as axillary lymph node dissection (ALND) in staging, locoregional control and survival without morbidity such as lymphedema and swelling. Along with the advancement of SLN biopsy, pathologists have been scrutinizing assessment of SLN findings. Finding metastatic carcinoma in lymph nodes is a statistical exercise of probability. With more levels of blocks with hematoxylin and eosin (H&E) and immunohistochemical (IHC) stain sections we get, the probability of having positive lymph node increases. Pathologists have developed a robust way of detecting metastasis in SLN. In fact, with the application of IHC stain, negative SLN by a single level routine H&E slide can convert into positive SLN in 12%–29%,¹⁻⁶ most of them with small volume metastases such as isolated tumor cells (ITC) and micrometastasis, which are staged as pN0(i+) and pN1mi.

With the advent of detecting increasing number of small volume metastases in SLN, the following questions arose: Is ITC a true metastasis? What is the chance of having positive metastatic

lymph node when complete ALND is done with ITC in? Why is ITC considered pN0(i+) and not counted as a positive lymph node in Tumor Lymph Node Metastasis (TNM) staging? For that matter, is micrometastasis clinically significant metastasis? What is the chance of having positive metastatic lymph node when complete ALND is done? Why micrometastasis is considered pN1mi and counted as a positive lymph node in TNM staging? Is the volume or the number of tumor cells between ITC and micrometastasis so different that we should count as negative and positive in the N-stage respectively? Who should decide the cut-off number or size/volume of metastatic cells between pN0(i+) and pN1mi? Why was complete ALND recommend for pN1mi and macrometastasis in SLN but not for pN0(i+) traditionally? Are we (pathologists) uniformly and correctly assigning pN0(i+), pN1mi and macrometastasis in SLN? And even if we have accomplished such tasks successfully, is it clinically meaningful, and helpful to breast cancer patients in understanding prognosis? Lymph node staging is the most important prognostic factor for breast cancer. Is this still true? With numerous clinical trials published in literature suggesting that conservative management is currently more appropriate regardless of the size of metastasis in SLN, do we still need to split our

hairs dividing pN0(i+), pN1mi and pN1 in N-stage?

In this article, review of SLN in breast cancer is listed in the following order: Brief history of SLN staging, problems in determining metastatic SLN size in pathology, clinical significance of positive SLN, along with personal commentary and a plea to use evidence based practice to develop new and relevant standard criteria in SLN in the 8th edition of the American Joint Committee of Cancer (AJCC) staging systems.

BRIEF HISTORY OF SENTINEL LYMPH NODE STAGING

The TNM staging system was initially devised more than 50 years ago by Pierre Denoix in France.⁷ From then on, many revisions were made in advent of changes in breast cancer management and treatment.

In 1987, the International Union Against Cancer (UICC) and the AJCC staging systems were unified into a single TNM staging system to be able to communicate clinical information without ambiguity. “T is for the size or direct extent of the primary tumor, N is for the spread of regional lymph nodes and M is for the presence of distant metastasis.” Since the first publication in 1977, currently AJCC/UICC system revised and published the 7th edition.^{8,9}

It is arguable that N part of the staging changed most significantly since the SLN, biopsy first described by Giuliano *et al.*¹⁰ in 1994 in breast cancer as a potential altering the role of ALND by using intraoperative lymphatic mapping.

Along with SLN biopsy advancement by surgical oncologists, pathology assessment of SLN biopsy sample led to significant changes in N-stage by the AJCC Staging Manual. Starting from the 5th edition in 1997 when the first SLN was reported, the 6th edition in 2003 and the 7th edition in 2010 had some changes regarding SLN reporting. As SLN biopsy became more a standard treatment in the management of breast cancer, the AJCC Staging Manual needed revision to reflect the continual development and knowledge in this field. The 6th edition of the AJCC Cancer Staging Manual when compared to the previous one contains some of the most extensive and significant revisions pertaining to SLN related to the growing knowledge of new technology such as IHC staining and reverse transcriptase-polymerase chain reaction (RT-PCR). The principal changes are related to the size, number, location, and method of detection of regional metastases to the lymph nodes. A Breast Task Force was constituted to serve in an advisory role to the AJCC in the fall of 2001 and the 6th edition reflected the significant changes.

The Breast Task Force used the guideline to recommend changes and additions based on evidence-based findings in published clinical outcome data, reflecting a wide-spread clinical consensus and changes in nomenclature and coding system which support the uniform accrual of outcome information in national data-banks.^{11,12}

In the AJCC 5th edition, micrometastases were defined as metastatic lesions no larger than 2 mm in greatest dimension and classified as pN1. The terminology “occult metastases” was interchangeably used to describe a small metastatic carcinoma in the lymph node in the literature. The upper limit of 2 mm cutoff for separating micro- and macrometastases was determined by two studies 30 years ago.^{13,14}

The major change in the AJCC 6th edition was to define the lower limit for micrometastasis defined as a metastatic lesion larger than 0.2 mm in diameter and the upper limit was kept in 2 mm and ITC (single cells or cell deposits) no larger than 0.2 mm and classified as pN0. This lower limit of > 0.2 mm (10 times smaller than the upper limit) had been tested in only one retrospective study.¹⁵

With the advent of more sensitive technique, such as IHC stains, it was easier to detect ITC that were not readily visible from the H&E stain slides which was the gold standard for detection of metastatic carcinoma in the axillary lymph nodes. For example, when H&E stain shows no metastatic carcinoma but IHC stain with ITC, then the classifier became pN0(i+) for positive IHC, no cluster > 0.2 mm. The designation of pN1mi (i+) was used when H&E stain negative but IHC stain detected micrometastasis. So, “i” stands for IHC stain in the 6th edition AJCC.¹⁶

Separating the upper and lower limits of cutoff for ITC and micrometastatic lymph node is not an easy task since there is no “pure” study that has evaluated differences in overall survival compounding factors such as with or without tumor size, chemotherapy and radiation therapy.

The pN0(mol-) and pN0(mol+) classifiers were also added in the 6th edition of AJCC based on the molecular findings using RT-PCR.

The additional designation of (sn) for “sentinel node” was used in the classification of TNM staging system when only the SLN was excised without the full ALND. See Table 1.

With the advent of SLN biopsy, knowing sentinel nodes are more likely to contain metastases than non-SLNs, pathologists began to perform much more thorough and comprehensive examinations which included grossing by submitting the entire node by sectioning 2.0 mm thickness in a longest axis, serial

Table 1. AJCC 6th edition

pN0(sn)	No metastasis-sentinel lymph node
pN0(i+)	Isolated tumor cells (single cells or cell deposits) no larger than 0.2 mm
pN1mi	Metastatic lesion larger than 0.2–2.0 mm
pN1mi(i+)	H&E stain negative but IHC stain detected micrometastasis
pN0(mol-)	Negative molecular findings using RT-PCR
pN0(mol+)	Positive molecular findings using RT-PCR

AJCC, American Joint Committee of Cancer; H&E, hematoxylin and eosin; IHC, immunohistochemical; RT-PCR, reverse transcriptase-polymerase chain reaction.

sections for H&E stains instead of just one section, and adding IHC stains which deviated from the reference population assay in which lymph node examination was much simpler— one H&E section per node for pathologic examination before 1990s. Previously, grossly negative large lymph nodes were not necessarily entirely submitted for histologic examination.

Introduction of ITC was to prevent overtreatment of low-volume nodal involvement since some of the ITC is caused by passive tumor cell transport to the SLN after pre-operative fine needle aspiration (FNA) and/or core needle biopsy procedures and iatrogenic displacement due to breast massage causing benign epithelial elements in lymph node resulting false positive especially in papillary lesions.¹⁷

As we all know, finding metastatic carcinoma in lymph nodes is a statistical exercise of probability. With more H&E and IHC stain sections we get from the block, the probability of having positive node increases. We have the capability to detect even one cell in the SLN if this is clinically meaningful but first, we need to figure out whether this effort is paid off by clinical significance.

Also, there are differences in terminology in literature. Prior to AJCC 2003 and 2006, the term “isolated tumor cells” and “micrometastasis” were not clearly defined. Some studies referred to these as “occult metastasis.”

Later on the AJCC definition of SLN tumor deposits were measured using a micrometer and placed in one of three categories:⁹ macrometastasis, micrometastasis, or ITC. A macrometastasis was classified as “one or more tumor deposits greater than 2 mm.” A micrometastasis was classified as a tumor deposit “greater than 0.2 mm but not greater than 2.0 mm in largest dimension.” ITC were “defined as single cells or small cluster of cells not greater than 0.2 mm in largest dimension.” A cluster was defined as “a confluent focus of tumor cells touching other tumor cells.” The single largest cluster was measured by micrometer. Single dispersed cells throughout the lymph node were regarded as ITC if the largest cluster measured less than or equal

Table 2. AJCC 7th edition

pN0(i+)	Isolated tumor cells (single cells or cell deposits) no larger than 0.2 mm or fewer than 200 cells
pN1mi	Metastasis greater than 0.2 mm and/or more than 200 cells, but none greater than 2.0 mm
pN1a	Macrometastasis in 1 to 3 axillary lymph nodes, at least 1 metastasis greater than 2.0 mm
pN2a	Metastases in 4 to 9 axillary lymph nodes (at least 1 tumor deposit greater than 2.0 mm)
pN3a	Metastases in 10 or more axillary lymph nodes (at least 1 tumor deposit greater than 2.0 mm)

AJCC, American Joint Committee of Cancer.

to 0.2 mm.⁹ The presence of metastatic disease is measured by the size of the largest contiguous metastasis for multiple foci in SLN. The main differences between the AJCC 6th edition to the AJCC 7th edition in regards to SLN is to count the number of metastatic cells; if it is less than 200 cells versus over 200 cells for ITC and micrometastasis respectively. The label “i” stands for isolated tumor cells and not IHC stain for the 7th edition AJCC.

The main reason for a 200 cell cutoff was to have better reproducibility between pathologists. The arbitrary cutoff of the exact size and number was listed for improvement of agreement between pathologists without any clinical trial of the significance in prognosis and clinical validation. In fact, this was incorporated into the 7th edition for large cohesive, non-confluent tumor cells throughout the lymph node typically seen in metastatic lobular carcinoma. In addition, the 7th edition of AJCC states “these thresholds are meant to be guidelines, and not absolute cutoffs, to help pathologists determine if the tumor burden in a given lymph nodes is likely to be clinically important or not. The pathologist should use judgment and not an absolute cutoff of 0.2 mm or exact 200 cells, in determining the likelihood of whether the cluster of cells is an ITC or a true micrometastasis”. See Table 2.

According to the 7th edition AJCC, a positive node is defined as a metastasis measuring at least 0.2 mm, or > 200 tumor cells (pN1mi). Whenever there is a positive lymph node, the pathologist also needs to describe the following: the size of metastasis (or number of tumor cells), the anatomical node involved such as axilla, internal mammary, intramammary, infraclavicular or supraclavicular lymph node, the total number of positive nodes, and the method of detection such as clinical, FNA or tissue biopsy.

Positive intramammary lymph nodes are count in the total axillary lymph node count. Positive internal mammary SLN affects pN stage depending on status of other nodes (metastasis in clinically apparent ipsilateral internal mammary lymph nodes in the presence of 1 or more positive axillary lymph nodes; or in

more than 3 axillary lymph nodes and in internal mammary nodes with microscopic disease detected by SLN dissection but not clinically apparent). Positive infraclavicular node is staged as pN3a and supraclavicular node is staged as pN3c.

In addition, there is a troubling statement in the AJCC 2010 “Data elements with asterisks (small clusters of cells not greater than 0.2 mm or single tumor cells, or a cluster of fewer than 200 cells in a single histologic cross-section) are not required. However, these elements may be clinically important but are not yet validated or regularly used in patient management.”

Further disclaimer statements in the 7th edition of AJCC are as follows: “Approximately 1,000 tumor cells are contained in a 3-dimensional 0.2-mm cluster. Thus, if more than 200 individual tumor cells are identified as single dispersed tumor cells or as a nearly confluent elliptical or spherical focus in a single histologic section of a lymph node, there is a high probability that more than 1,000 cells are present in the node. In these situations, the node should be classified as containing a micrometastasis (pN1mi). Cells in different lymph node cross sections or longitudinal sections or levels of the block are not added together; the 200 cells must be in a single node profile even if the node has been thinly sectioned into multiple slices. It is recognized that there is substantial overlap between the upper limit of the ITC and the lower limit of the micrometastasis categories because of inherent limitations in pathologic nodal evaluation and detection of minimal tumor burden in lymph nodes. Thus, the threshold of 200 cells in a single cross-section is a guideline to help pathologists distinguish between these 2 categories.”⁹ And final statement is as follows: “The pathologist should use judgment regarding whether it is likely that the cluster of cells represents a true micrometastasis or is simply a small group of isolated tumor cells.”

In 2010, both the UICC and TNM joined in the provision in guidelines for SLN classification, however, studies have shown poor reproducibility in the application of in both invasive ductal and invasive lobular carcinomas.

Furthermore, previous studies have shown that application of IHC stain on H&E negative lymph node can detect small volume metastatic carcinoma in 12%–29% of cases. However, all the previous data of prognosis based on lymph node status has been from one H&E section evaluation. Therefore due to more thorough examination of SLN, more cases of ITC have been reported.¹⁻⁶

For this reason, the College of American Pathologists (CAP) published a consensus statement in July 2000 recommending a single H&E slide section from each lymph node block without

gross evidence of metastasis without routine cytokeratin IHC stain or routine serial sectioning based on the preliminary study from John Wayne Cancer Center which found no differences in five-year disease-free survival rate between node negative by H&E negative, IHC negative versus H&E negative, IHC positive groups.¹⁸⁻²⁰

Although CAP guidelines and recommendations for SLN biopsy for pathologists did not include serial sectioning with multiple H&E slides and IHC stains, many pathologists reported and continued to perform comprehensive evaluation on SLN including our institution to this date. With the advent of the comprehensive SLN evaluation, probability of finding small metastasis increased and the natural question is whether to perform completion ALND on these cases. It is reported that among patients with a positive SLN by H&E stain were found to have additional nodal metastasis in ALND in 48.3% of cases.²¹ In addition, metastatic carcinoma is found in non-sentinel nodes during ALND in 9%–15% and 15%–35% of patients with ITC and micrometastasis in the SLN respectively.²²⁻²⁵

Traditionally, complete ALND was done for SLN with pN1mi and macrometastasis but not for pN0(i+). Also adjuvant chemotherapy may have been added to pN1mi and macrometastasis. This was true in many practices including our institution. And therefore, it would be important to distinguish an accurate size of metastatic tumor deposits in the SLN.

PROBLEMS IN DETERMINING METASTATIC SENTINEL LYMPH NODE SIZE IN PATHOLOGY

Grossing axillary SLN

How best to gross SLN is not stated in the AJCC Staging Manuals. Most pathologists submit clinically negative SLN entirely for microscopic examination by slicing lymph node in a longest axis into 0.2 cm thickness based on CAP guideline. CAP states that a single H&E section from each block is sufficient and multiple level sections and IHC stain for keratin are not necessary. However, there are many institutions performing multiple levels and IHC stains for each block for SLN. The “correct” method is still a matter of debate. In our institution, we get 3 multiple levels for H&E stain and 2 intervening keratin IHC stains for entirely submitted each SLN blocks. The reason for this is that IHC stain highlights small metastatic cells easier than H&E stain, especially for the metastatic lobular carcinoma cases.

Microscopic examination of SLN

While the 7th edition AJCC criteria and definition are fairly

straightforward, its' application may be difficult in reality for pathologists to uniformly classify N-stage correctly. Initially, in 2006, Dr. Connolly²⁶ described some of the most practical challenges in the classification in the assessment of SLN biopsy separating ITC, micrometastases, and macrometastases.

Cserni *et al.*²⁷ reported that there is 24% discordance in their review of 512 cases of low-volume nodal metastasis and a plea for better formulated supplemented TNM definition.

Literature reported the kappa values for pathologist's agreement is at best moderate to substantial reproducibility.²⁸⁻³² The kappa value for interobserver agreement was reported moderate (0.55 and 0.56) for pN0(i+) and substantial (0.62) for pN1mi. This is an improvement from the previous interobserver agreement amongst expert breast pathologists (kappa: 0.49) and community hospital-based pathologists (kappa: 0.47) based on European Working Group for Breast Screening Pathology (EWGBSP). Despite the intent for the better interpretation of metastatic tumor cells in lymph node in the 7th edition AJCC, many issues have not been resolved. In 2012, Netherlands group published the discrepancy rate between central to local pathologists in which changed pN status in 24% with kappa value of 0.69.³³

This is stating that one of four cases in breast cancer, pathologists do not agree with N-stage even though the descriptor for N-stage is easily understandable in the AJCC Staging Manual. There are still some circumstances pathologists have difficulties knowing how to accurately assign N- stage based on the 7th edition AJCC. Here are some of the examples:

1. Multiple discontinuous foci of metastatic carcinoma as seen in Figs. 1 and 2. The entire area of metastatic carcinoma is >2 mm but the largest contiguous metastatic carcinoma measures <0.2 mm. Is this macrometastasis or micrometastasis? The AJCC staging criteria states that we should not add these non-contiguous metastatic foci but shouldn't there be an upper limit to number of foci of micrometastases to upgrade to macrometastasis based on the sheer volume of tumor deposits? Does this actually make a common sense to classify as pN1mi? All the other organs in pathology staging would classify this kind of scenario as "metastatic carcinoma." Using the best pathologist's "judgment," macrometastasis may be best for this case although by strict criteria, it is pN1mi.

2. Multiple discontinuous foci of metastatic carcinoma as seen in Fig. 3. The entire area will be classified as micrometastasis but one of the longest contiguous areas will be classified as ITC. Counting the number of metastatic carcinoma may be <200 cells. Is this micrometastasis (pN1mi) or ITC [pN0(i+)]? How should we best judge?

3. Metastatic carcinoma seen in axillary adipose or fibrous tissue without any residual and apparent lymph node structure. Should this be counted as positive lymph node or a carcinoma arising in axillary breast tissue? Based on the 6th edition, cancerous nodules in the axillary fat without evidence of residual lymph node tissue should be classified as positive axillary lymph nodes. But what if these cancerous nodules in the axilla are can-

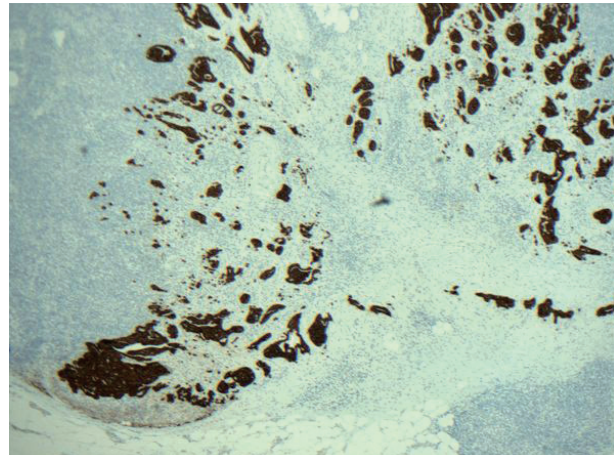


Fig. 1. Keratin immunohistochemical stain. Multiple discontinuous foci of keratin positive metastatic tumor deposits are noted. The largest cluster seen on the lower left corner is <2 mm. Is this macrometastasis or micrometastasis? The American Joint Committee of Cancer (AJCC) staging criteria states that we should not add these non-contiguous metastatic foci but shouldn't there be an upper limit to number of foci of micrometastases to upgrade to macrometastasis based on the sheer volume of tumor deposits? Does this actually make common sense to classify as pN1mi as the criteria written in the 7th edition AJCC? All the other organs in pathological N staging would classify this kind of scenario as "metastatic carcinoma."

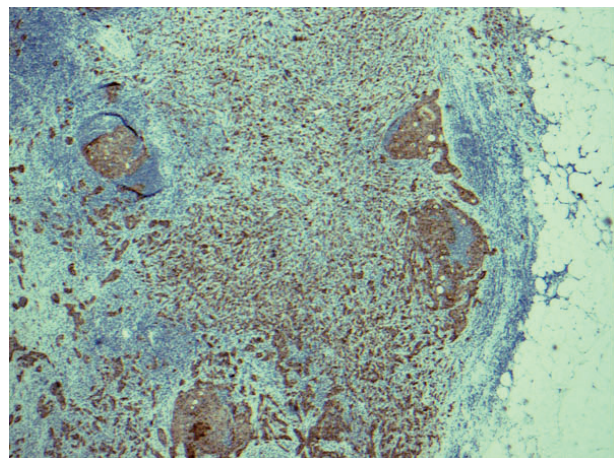


Fig. 2. Keratin immunohistochemical stain. Most pathologists would classify this image as macrometastatic lymph node but technically each cluster or group of cells are not touching each other in a confluent or contiguous manner, and therefore, each cluster should be considered independent and measured independently.

cer cells from the axillary breast tissue? Should it be classified as extensive extracapsular extension? Many pathologists do not classify cancerous nodules in axilla without apparent lymph node structure as lymph node metastasis (unpublished personal observation). The dimension of the tumor from this scenario may end up in T-stage rather than in N-stage. See Fig. 4.

4. When there is pericapsular lymph-vascular invasion (LVI) in which tumor cells are not in the parenchyma or subcapsular part of lymph node, is that considered metastatic or LVI? Deeper sections still did not show intracapsular or intraparenchymal involvement. Anecdotally, this kind of the case was sent out to other breast pathology experts and came back with different opinions; some considered metastatic carcinoma pN0(i+) or pN1mi depending on the size of the largest contiguous dimension of metastatic focus and some just LVI. See Figs. 5 and 6. Based on CAP guidelines, capsular LVI is considered metastatic carcinoma and the largest dimension is measured as the size of metastasis. However the 7th edition AJCC does not specify this scenario.

5. When most of the metastatic carcinoma is seen outside the lymph node capsule (in this case by metastatic lobular carcinoma) with only one ITC within the lymph node parenchyma, is it considered extracapsular invasion with ITC or is it micrometastasis based on the total number of cells of > 200 or > 0.2 mm? See Figs. 7 and 8. Should the extracapsular extension be included as a maximum linear dimension of metastasis?

6. Matted lymph nodes with metastatic carcinoma; how should we count? One matted lymph node or identifiable appar-

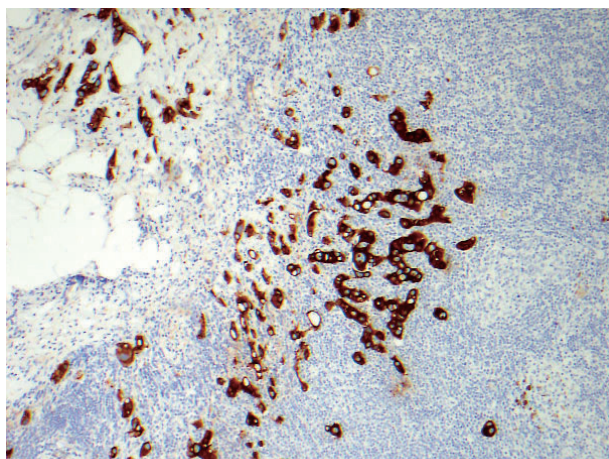


Fig. 3. Keratin immunohistochemical stain. Multiple discontinuous foci of metastatic carcinoma each cluster measuring no larger than 0.2 mm and fewer than 200 cells. Is this micrometastasis (pN1mi) or isolated tumor cells [pN0(i+)]? There is even extracapsular invasion seen on the upper left corner.

ent lymph nodes involved with metastatic tumor? This may alter pN1a or above in some cases.

7. Invasive lobular carcinoma often has loss of E-cadherin

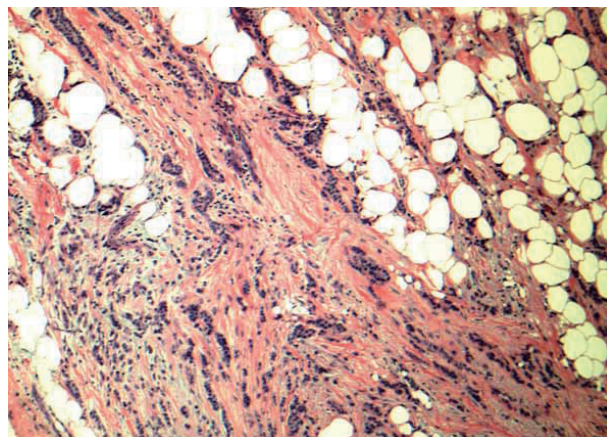


Fig. 4. Low grade invasive tumor is seen from axillary fat without adjacent residual and apparent lymph node structure. Should this be counted as positive lymph node or a carcinoma arising in axillary breast tissue? Based on the 6th edition, cancerous nodules in the axillary fat without evidence of residual lymph node tissue should be classified as positive axillary lymph nodes. There is no normal breast tissue or ductal carcinoma *in situ* around this tumor. Is this axillary breast tissue with carcinoma, totally effaced lymph node with metastatic carcinoma or extensive extracapsular invasion? Many pathologists do not classify cancerous nodules in axilla as lymph node metastases.

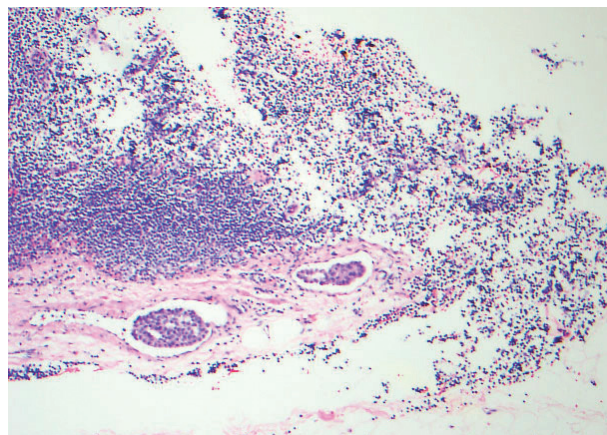


Fig. 5. Pericapsular lymph-vascular invasion (LVI) in which tumor cells is not seen in the parenchyma or subcapsular part of lymph node. Should this be classified as metastatic [either pN0(i+) or pN1mi depending on the maximum linear dimension] or LVI? Tumor deposits seen in afferent vessel and not intracapsular or intraparenchymal involvement is technically LVI, a transient step before metastasis into lymph node. Based on College of American Pathologists (CAP) guidelines, capsular LVI is considered metastatic carcinoma and the largest dimension is measured as the size of metastasis. However the 7th edition American Joint Committee of Cancer (AJCC) does not specify this scenario.

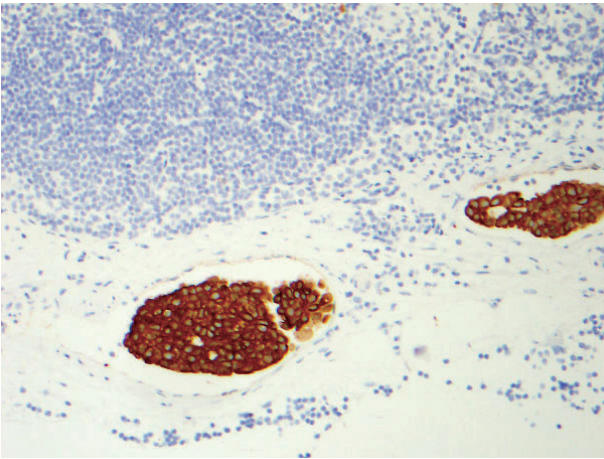


Fig. 6. Keratin stain from the same case as Fig. 5.

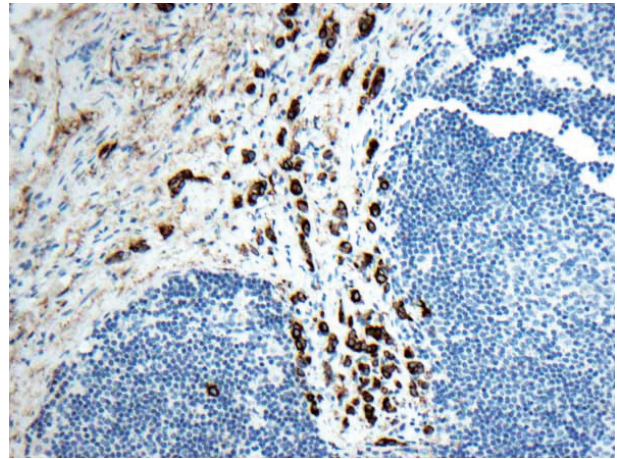


Fig. 8. Keratin stain from the same case as Fig. 7.

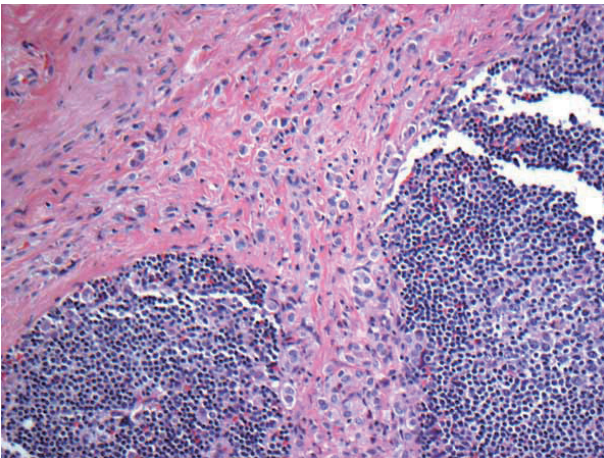


Fig. 7. Metastatic lobular carcinoma is seen mostly outside the lymph node capsule with only one isolated tumor cell within the lymph node parenchyma. Should the extracapsular extension be included as maximum linear dimension of metastasis or is it considered extracapsular invasion with isolated tumor cells?

which results in individual cell pattern in both breast and lymph node. This scenario was written by Turner *et al.*³⁰ who reported inconsistency in nodal metastases by breast pathologists with the initial kappa before the training program was 0.575 and post-test was 0.947. We reported that strict adherence of the 6th edition AJCC criteria will result in down staging N in many lobular carcinoma cases.³⁴

The 7th edition AJCC was bit more helpful in this situation because one needs to count the number of metastatic cells in SLN; if it is less than 200 cells versus over 200 cells for isolated tumor cells and micrometastasis respectively. However, the number 200 cells is arbitrarily chosen without any background published research data with clinical follow-up. Although some metastatic lobular carcinoma cases have obvious macrometasta-

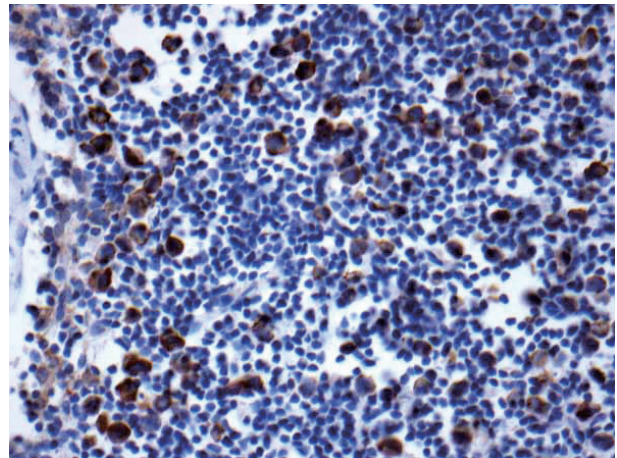


Fig. 9. Keratin stain. Dispersed pattern of multiple and numerous foci metastatic lobular carcinoma to lymph node is commonly seen. If these cells are more than 200 cells or less than 200 cells, then, it is classified as micrometastasis (pN1mi) and ITC [pN0(i+)] respectively. All cases such as this will be classified as pN1mi based on >200 cells but why can't it be macrometastasis? Is there an upper limit such as 500 cells or 1,000 cells to qualify as macrometastasis?

sis, diffuse single or few cell clusters of infiltrating pattern is typical for invasive lobular carcinoma metastatic to lymph node (Fig. 9). All cases such as this will be classified as pN1mi based on > 200 cells but why can't it be macrometastasis? Is there an upper limit such as 500 cells or 1,000 cells to qualify as macrometastasis?

8. For N-stage, if there is stromal desmoplasia or stromal proliferation around small volume metastasis, the 6th edition AJCC states that the size of the tumor deposit should include the stromal reaction. The 7th edition AJCC recognized that this distinction is highly subjective. In general, after neoadjuvant chemotherapy, the classification of lymph nodes should be the same as the patients who did not have neoadjuvant chemo-

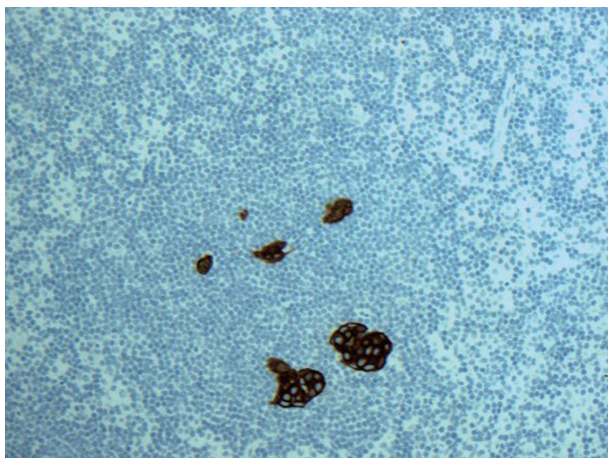


Fig. 10. Keratin stain. Isolated tumor cells are seen (<200) within the parenchyma of the lymph node. Most American pathologists will classify this as pN0(i+) but many of European pathologists may classify this as micrometastasis based on previous International Union Against Cancer (UICC) related publications.

therapy. Lymph nodes after neoadjuvant chemotherapy more frequently show stromal fibrosis without “typical desmoplasia,” foamy histiocytes with multinucleated giant cell reaction, elastosis and small clusters of non-confluent residual and viable metastatic tumor cells. How should we classified- is this ypN0 (i+) or ypN1? After all, even small residual metastatic deposits after neoadjuvant chemotherapy is probably not true ITC but a remnant of macrometastasis prior to therapy and hence, it should be classified as pN1. Currently, the AJCC Staging Manual is not clear about this scenario and hence, pathologists are stating in their report how they measured the size of metastatic deposit with a long explanation.

9. Location of metastatic tumor cells whether it is subcapsular or intraparenchymal is not specified in the 7th edition AJCC, however, many European pathologists based on previous UICC related publications, tumor cells located within the parenchyma measuring even less than 0.2 mm is considered micrometastasis and not considered as ITC. Regardless of the location, most of American pathologists would consider ITC purely depending on the size of metastasis. See Fig. 10.

The above stated scenarios are difficult to resolve and ultimately depends on the pathologists to make appropriate judgments resulting high subjectivity and inconsistency in N-stage. Finally, we need to ask ourselves, is this distinction between pN0 (i+) and pN1mi useful for patient’s prognosis, treatment plans and overall survival? For that matter, is macrometastasis different in prognosis and overall survival when compared to pN0(i+) and pN1mi? Our goal is to determine the significance of these

findings, albeit that there is difficulty in interobserver reproducibility among the pathologists. Also we should keep in mind that both retrospective and prospective studies in literature composed of variability in interpretation of N-stages; pN0(i+), pN1mi and pN1a even with the best intention of adhering to AJCC criterion. Also the mode of detection of metastatic SLN has been different in literature.

CLINICAL SIGNIFICANCE OF SENTINEL LYMPH NODE

In 2005, an American Society of Clinical Oncology (ASCO) guideline recommendation for SLN biopsy in early-breast cancer was published. The recommendation and guideline were based on the literature review from one prospective randomized controlled trial, four limited meta-analysis, 69 published single-institution and multicenter trials. SLN biopsy alone without complete ALND is considered standard of care for SLN negative patients. Completion ALND was standard treatment for patients who had macro- and micrometastasis in SLN for T1 and T2 tumors. “For large or locally advanced inflammatory breast cancer (T3 and T4), ductal carcinoma *in situ*, when breast-conserving surgery is to be done, pregnancy, in the setting of prior non-oncologic breast surgery or axillary surgery, and in the presence of clinically suspicious axillary lymph node, SLN biopsy was not recommended.”³⁵

Survival data on pN0(i+), pN1mi and pN1 showed mixed results. Survival benefit of performing ALND after ITC and/or micrometastasis in SLN was not clear cut. Some reported an adverse effect on survival and others have shown no effect. Again, the mixed results may have been due to the variable definitions of micrometastases and ITC in literature and different mode of detection.

Retrospective clinical data

The Surveillance Epidemiology and End Results (SEER) database reported that micrometastasis represents a significant prognostic marker. Their data consists of 209,720 patient numbers between 1992 and 2003 and the 10 year survival among pN1, pN1mi and pN0(i+) is 73%, 77%, and 78%, respectively. Also, N1mi diagnoses increased from 2.3% to 7%.³⁶

de Boer *et al.*³⁷ published MIRROR (Micrometastasis and Isolated Tumor Cells: Relevant and Robust Or Rubbish?) study in Netherlands which included three cohorts with the median follow-up of 5.1 years: 865 patient with negative regional lymph nodes who did not receive adjuvant chemotherapy, 865 patients

with either ITC or micrometastasis in lymph nodes who did not receive adjuvant chemotherapy and 994 with either ITC or micrometastasis in lymph nodes who did receive adjuvant chemotherapy. The authors found ITC or micrometastases in regional lymph nodes were associated with a reduced disease-free survival who did not receive adjuvant chemotherapy and those who received adjuvant chemotherapy had improved disease-free survival rate.³⁷

Pugliese *et al.*³⁸ studied a total of 954 SLN biopsies consist of 491 N0(i-), 86 N0(i+), 73 N1mi, 146 N1a, 29 N2a, and 11 N3a patients with a median follow-up of 45.4 months and found no differences in overall survival (OS) and relapse-free survival (RFS) between pN0(i-) and pN0(i+) or pN1mi but worse prognosis was noted when the size of the metastases reached the pN1a.

Hansen *et al.*³⁹ reported no difference in disease-free survival and OS with a median follow up of 8 years between pN0, pN0(i+) and pN1mi in their study cohort of 790 with patients. Their cohort consisted >90% who had received adjuvant chemotherapy. Only patients with macrometastasis had a statistical significant decrease in disease-free survival and OS.

Bilimoria *et al.*⁴⁰ reported a retrospective study from the National Cancer Data Base on 97,314 SLN positive patients from 1998–2006 subdivided into those who had ALND and those who did not have ALND had a similar axillary local recurrence and 5 year relative survival; 23% macrometastases (pN1) and 55% with SLN micrometastases (pN1mi).

The SEER Database by Yi *et al.*⁴¹ reported a total of 26,986 composed of 11% pN1 and 33% pN1mi from 1998–2004 had no difference in OS at a median follow-up of 50 months.

In addition, there are nine smaller studies comprising a total of 1,035 patients with positive SLN without ALND and reported low axillary local recurrence rate, in the range of 0% to 2% at 28–82 months follow-up.⁴²

Our institution also supported that SLN biopsy alone as adequate intervention in 302 patients with an average clinical follow-up of 24 months.⁴³ Even for the mastectomy cases with pN1 disease in SLN did not affect OS and RFS between the radiation therapy without ALND and complete ALND surgery.⁴⁴

Prospective clinical data

There are three significant prospective randomized studies relevant to SLN metastasis: the National Surgical Adjuvant Breast and Bowel Project (NSABP) trial-32, the American College of Surgeons Oncology Group (ACOSOG) trial Z0011, and the International Breast Cancer Study Group (IBCSG 23-01).⁴⁵⁻⁴⁷

The NSABP B-32 was a randomized controlled phase 3 trial composed of 5,611 patient sample divided into group 1 (SLN and ALND) and group 2 (SLN alone if no metastasis SLN with ALND if metastatic carcinoma was present in SLN). The adjuvant chemotherapy and radiation therapy was relatively equally divided in between these groups: 85% in group 1 and 84.1% in group 2. The clinical follow-up was 95.6 months and the endpoint was overall survival. The authors found no differences in OS, disease-free survival and regional control between two groups. NSABP B-32 also looked into clinical significance in “occult metastasis” comparing pN0, pN0(i+) and pN1mi groups and found no difference in overall survival among these groups during 5-year follow-up period. The authors concluded that additional evaluation including IHC stains and multiple levels of SLN are not indicated because a clinical benefit was not significant.^{48,49}

The ACOSOG Z0011 trial 2 is a landmark article that changed paradigm shifts in 2011. ACOSOG Z0011 is a randomized trial, non-inferiority study which suggested that completion ALND is not necessary in T1 and T2 breast cancer patients who received whole-breast radiation since disease-free survival and recurrence rates did not appear to differ between the patients who had completion ALND versus those who had SLN biopsy alone and had up to two positive SLNs. All patients in this study received adjuvant radiation therapy. The study consisted of 813 positive SLN patients randomized to 388 patients who had ALND and 425 patients without ALND. Criticisms of ACOSOG Z0011 study have been that the case selection was biased toward older women, predominantly estrogen receptor (ER) positive tumors (younger women with ER negative tumors were under-represented), lost to follow-up was significant (21% in the complete ALND and 17% in the SLN alone groups) and short clinical follow-up of 6.3 years.

The IBCSG 23-01 was a multicenter randomized phase 3 trial in breast cancer size of less or equal to 5 cm, separating pN0(i+) and pN1mi without extracapsular invasion of SLN based on H&E slide to 464 patients who had ALND and 467 patients who did not have ALND with a median follow-up of 5 years. The result was similar to the ACOSOG Z0011 trial stating that ALND was not necessary since there is no adverse effect on survival.⁵⁰

Additionally, the European Organization for Research and Treatment of Cancer (EORTC) 10981-22023, the After Mapping of the Axilla: Radiotherapy or Surgery (AMAROS) which is a randomized, multicentric, phase 3 non-inferiority trial also supported ACOSOG Z0011 findings that there are no differences when complete ALND verses axillary radiation therapy from

positive SLN patients in early breast cancer when the usage of chemotherapy, or hormone therapy was factored in. Traditionally ALND has been a guide to adjuvant chemotherapy and based on this study, the information provided by complete ALND is no longer useful.^{51,52}

Another prospective clinical trial study, the POSNOC (Positive Sentinel Node: Adjuvant Therapy Alone versus Adjuvant Therapy Plus Clearance or Axillary Radiotherapy) trial is still open and recruiting patients till 3/31/18 in the United Kingdom which is a pragmatic, randomized, multicentric and non-inferiority trial for early breast cancer with one or two SLN macrometastases.

CONCLUSION AND COMMENTARY

The growing body of literature from both retrospective and prospective studies advocates conservatism. Completion ALND is not providing benefit of OS and disease-free survival in microscopic metastatic SLN [pN0(i+) and pN1mi]. Even macrometastasis in one or two SLN(s) in ACOSOG Z0011 did not affect OS. There is mounting evidence to support that SLN biopsy alone can be a standard practice demonstrating its efficacy, accuracy in staging and equivalent survival outcome when compared to complete ALND and SLNB alone in T1–T2 breast cancer.^{45,53–57}

Recently, Danish Breast Cancer Cooperative Group (DBCG) looked into 2,074 patients who had either ITC or micrometastasis in SLN and found no significant difference in OS and axillary recurrence rate between patients who had completion ALND or no ALND. The study adds growing literature that it is safe to omit ALND in minimal metastatic disease in the SLN.⁵⁸

From a pathologists' point of view, we need to ask the following questions: Are we reporting small volume metastasis in vain? Is separating pN0(i+) or pN1mi really necessary? While most of the cases N-staging are straightforward, we do still face ambiguous cases. When we perform tedious work by counting metastatic tumor cells, we want to make sure this work has value in clinical contribution. The evidence shows that separating small volume N-stage or even macrometastasis is not affecting clinical management to perform completion ALND or OS in early stage breast cancers. Also all other organ systems in the same AJCC Staging Manual for colon cancer, gynecologic cancer, even melanoma which the technique of SLN was first described do not practice as in breast N-staging; there is no pN0(i+) or pN1mi. Metastatic carcinoma when seen by either H&E or IHC stain slide is called metastatic carcinoma. IHC stain is

used discretionally by pathologists to confirm the presence of metastasis as needed if there is suspicious area by H&E slide. Why should breast cancer N-stage be any different from other organs?

As we understand that ALND dissection is no longer needed or necessary in many early breast cancers, the necessity of performing multiple levels, IHC stain, frozen section and molecular studies on SLN needs to be revisited.

Recently the AJCC Executive Committee announced a mid-2016 publication date for the 8th edition AJCC Cancer Staging System during its September 2013 Annual Meeting held in Chicago. The 8th edition will be effective for all cancer cases recorded on or after January 1, 2017. Key activities prior to the 2016 publication data are 1. Analysis of data collected since the 7th edition's release in 2010, 2. Validation of prognostic and predictive factors for incorporation in the staging system and 3. Collaboration with the cancer care and surveillance community to set the standard to anticipate, communicate, and help incorporate staging system changes. Breast Expert Panel leaders are Gabriel N. Hortobagyi, MD, Breast Medical Oncologist and Armando Giuliano, MD, Breast Surgical Oncologist.

As a pathologist, I hope to see the 8th edition AJCC Cancer Staging System for N-stage to be clinically relevant with simple and practical application without further arbitrary cutoffs to reduce subjective interpretation and to enhance agreement between both academic and community based pathologists all over the world.

Conflicts of Interest

No potential conflict of interest relevant to this article was reported.

REFERENCES

1. Trojani M, de Mascarel I, Bonichon F, Coindre JM, Delsol G. Micrometastases to axillary lymph nodes from carcinoma of breast: detection by immunohistochemistry and prognostic significance. *Br J Cancer* 1987; 55: 303-6.
2. Hainsworth PJ, Tjandra JJ, Stillwell RG, *et al.* Detection and significance of occult metastases in node-negative breast cancer. *Br J Surg* 1993; 80: 459-63.
3. Clare SE, Sener SF, Wilkens W, Goldschmidt R, Merkel D, Winchester DJ. Prognostic significance of occult lymph node metastases in node-negative breast cancer. *Ann Surg Oncol* 1997; 4: 447-51.
4. Sedmak DD, Meineke TA, Knechtges DS, Anderson J. Prognostic significance of cytokeratin-positive breast cancer metastases. *Mod*

- Pathol 1989; 2: 516-20.
5. Chen ZL, Wen DR, Coulson WF, Giuliano AE, Cochran AJ. Occult metastases in the axillary lymph nodes of patients with breast cancer node negative by clinical and histologic examination and conventional histology. *Dis Markers* 1991; 9: 239-48.
 6. de Mascarel I, Bonichon F, Coindre JM, Trojani M. Prognostic significance of breast cancer axillary lymph node micrometastases assessed by two special techniques: reevaluation with longer follow-up. *Br J Cancer* 1992; 66: 523-7.
 7. Denoix PF. Tumor, node and metastasis (TNM). *Bull Inst Nat Hyg (Paris)* 1944; 1: 1-69.
 8. Sobin LH, Gospodarowicz MK, Wittekind C. TNM classification of malignant tumours. 7th ed. New York: John Wiley and Sons Inc., 2009.
 9. Edge SB, Byrd DR, Compton CC, Fritz AG, Greene FL, Trotti A. AJCC cancer staging manual. 7th ed. New York: Springer, 2009.
 10. Giuliano AE, Kirgan DM, Guenther JM, Morton DL. Lymphatic mapping and sentinel lymphadenectomy for breast cancer. *Ann Surg* 1994; 220: 391-8.
 11. Fleming ID, Cooper JS, Hensen DE, *et al.* AJCC cancer staging manual. 5th ed. Philadelphia: Lippincott-Raven, 1997.
 12. Singletary SE, Allred C, Ashley P, *et al.* Staging system for breast cancer: revisions for the 6th edition of the AJCC Cancer Staging Manual. *Surg Clin North Am* 2003; 83: 803-19.
 13. Huvos AG, Hutter RV, Berg JW. Significance of axillary macrometastases and micrometastases in mammary cancer. *Ann Surg* 1971; 173: 44-6.
 14. Fisher ER, Palekar A, Rockette H, Redmond C, Fisher B. Pathologic findings from the National Surgical Adjuvant Breast Project (Protocol No. 4). V. Significance of axillary nodal micro- and macrometastases. *Cancer* 1978; 42: 2032-8.
 15. Nasser IA, Lee AK, Bosari S, Saganich R, Heatley G, Silverman ML. Occult axillary lymph node metastases in "node-negative" breast carcinoma. *Hum Pathol* 1993; 24: 950-7.
 16. Greene FL, Page DL, Fleming ID, *et al.* AJCC cancer staging manual. 6th ed. New York: Springer-Verlag, 2002.
 17. Bleiweiss IJ, Nagi CS, Jaffer S. Axillary sentinel lymph nodes can be falsely positive due to iatrogenic displacement and transport of benign epithelial cells in patients with breast carcinoma. *J Clin Oncol* 2006; 24: 2013-8.
 18. Fitzgibbons PL, Page DL, Weaver D, *et al.* Prognostic factors in breast cancer. College of American Pathologists Consensus Statement 1999. *Arch Pathol Lab Med* 2000; 124: 966-78.
 19. Hansen NM, Grube BJ, Giuliano AE. The time has come to change the algorithm for the surgical management of early breast cancer. *Arch Surg* 2002; 137: 1131-5.
 20. Singletary SE, Connolly JL. Breast cancer staging: working with the sixth edition of the AJCC Cancer Staging Manual. *CA Cancer J Clin* 2006; 56: 37-47.
 21. Kim T, Giuliano AE, Lyman GH. Lymphatic mapping and sentinel lymph node biopsy in early-stage breast carcinoma: a metaanalysis. *Cancer* 2006; 106: 4-16.
 22. McCready DR, Yong WS, Ng AK, Miller N, Done S, Youngson B. Influence of the new AJCC breast cancer staging system on sentinel lymph node positivity and false-negative rates. *J Natl Cancer Inst* 2004; 96: 873-5.
 23. Cserni G, Gregori D, Merletti F, *et al.* Meta-analysis of non-sentinel node metastases associated with micrometastatic sentinel nodes in breast cancer. *Br J Surg* 2004; 91: 1245-52.
 24. Viale G, Maiorano E, Mazzarol G, *et al.* Histologic detection and clinical implications of micrometastases in axillary sentinel lymph nodes for patients with breast carcinoma. *Cancer* 2001; 92: 1378-84.
 25. van Deurzen CH, de Boer M, Monnikhof EM, *et al.* Non-sentinel lymph node metastases associated with isolated breast cancer cells in the sentinel node. *J Natl Cancer Inst* 2008; 100: 1574-80.
 26. Connolly JL. Changes and problematic areas in interpretation of the AJCC Cancer Staging Manual, 6th Edition, for breast cancer. *Arch Pathol Lab Med* 2006; 130: 287-91.
 27. Cserni G, Bianchi S, Vezzosi V, *et al.* Variations in sentinel node isolated tumour cells/micrometastasis and non-sentinel node involvement rates according to different interpretations of the TNM definitions. *Eur J Cancer* 2008; 44: 2185-91.
 28. Cserni G, Bianchi S, Boecker W, *et al.* Improving the reproducibility of diagnosing micrometastases and isolated tumor cells. *Cancer* 2005; 103: 358-67.
 29. Cserni G, Sapino A, Decker T. Discriminating between micrometastases and isolated tumor cells in a regional and institutional setting. *Breast* 2006; 15: 347-54.
 30. Turner RR, Weaver DL, Cserni G, *et al.* Nodal stage classification for breast carcinoma: improving interobserver reproducibility through standardized histologic criteria and image-based training. *J Clin Oncol* 2008; 26: 258-63.
 31. de Mascarel I, MacGrogan G, Debled M, Brouste V, Mauriac L. Distinction between isolated tumor cells and micrometastases in breast cancer: is it reliable and useful? *Cancer* 2008; 112: 1672-8.
 32. Cserni G, Amendoeira I, Bianchi S, *et al.* Distinction of isolated tumour cells and micrometastasis in lymph nodes of breast cancer patients according to the new Tumour Node Metastasis (TNM) definitions. *Eur J Cancer* 2011; 47: 887-94.
 33. Vestjens JH, Pepels MJ, de Boer M, *et al.* Relevant impact of central pathology review on nodal classification in individual breast cancer patients. *Ann Oncol* 2012; 23: 2561-6.

34. Apple SK, Moatamed NA, Finck RH, Sullivan PS. Accurate classification of sentinel lymph node metastases in patients with lobular breast carcinoma. *Breast* 2010; 19: 360-4.
35. Lyman GH, Giuliano AE, Somerfield MR, *et al.* American Society of Clinical Oncology guideline recommendations for sentinel lymph node biopsy in early-stage breast cancer. *J Clin Oncol* 2005; 23: 7703-20.
36. Chen SL, Hoehne FM, Giuliano AE. The prognostic significance of micrometastases in breast cancer: a SEER population-based analysis. *Ann Surg Oncol* 2007; 14: 3378-84.
37. de Boer M, van Deurzen CH, van Dijck JA, *et al.* Micrometastases or isolated tumor cells and the outcome of breast cancer. *N Engl J Med* 2009; 361: 653-63.
38. Pugliese MS, Beatty JD, Tickman RJ, *et al.* Impact and outcomes of routine microstaging of sentinel lymph nodes in breast cancer: significance of the pN0(i+) and pN1mi categories. *Ann Surg Oncol* 2009; 16: 113-20.
39. Hansen NM, Grube B, Ye X, *et al.* Impact of micrometastases in the sentinel node of patients with invasive breast cancer. *J Clin Oncol* 2009; 27: 4679-84.
40. Bilimoria KY, Bentrem DJ, Hansen NM, *et al.* Comparison of sentinel lymph node biopsy alone and completion axillary lymph node dissection for node-positive breast cancer. *J Clin Oncol* 2009; 27: 2946-53.
41. Yi M, Giordano SH, Meric-Bernstam F, *et al.* Trends in and outcomes from sentinel lymph node biopsy (SLNB) alone vs. SLNB with axillary lymph node dissection for node-positive breast cancer patients: experience from the SEER database. *Ann Surg Oncol* 2010; 17 Suppl 3: 343-51.
42. Cyr A, Gao F, Gillanders WE, Aft RL, Eberlein TJ, Margenthaler JA. Disease recurrence in sentinel node-positive breast cancer patients forgoing axillary lymph node dissection. *Ann Surg Oncol* 2012; 19: 3185-91.
43. Vergara-Lluri ME, Prati R, Petersen J, Omidvar Y, Apple SK. Recurrence rates in breast cancer patients who had sentinel lymph node biopsy alone versus completion axillary lymph node dissection: a 7-year clinical follow-up study. *Breast J* 2014; 20: 666-8.
44. Fu Y, Chung D, Cao MA, Apple S, Chang H. Is axillary lymph node dissection necessary after sentinel lymph node biopsy in patients with mastectomy and pathological N1 breast cancer? *Ann Surg Oncol* 2014; 21: 4109-23.
45. Krag DN, Anderson SJ, Julian TB, *et al.* Sentinel-lymph-node resection compared with conventional axillary-lymph-node dissection in clinically node-negative patients with breast cancer: overall survival findings from the NSABP B-32 randomised phase 3 trial. *Lancet Oncol* 2010; 11: 927-33.
46. Giuliano AE, Hunt KK, Ballman KV, *et al.* Axillary dissection vs no axillary dissection in women with invasive breast cancer and sentinel node metastasis: a randomized clinical trial. *JAMA* 2011; 305: 569-75.
47. Galimberti V, Cole BF, Zurrada S, *et al.* Axillary dissection versus no axillary dissection in patients with sentinel-node micrometastases (IBCSG 23-01): a phase 3 randomised controlled trial. *Lancet Oncol* 2013; 14: 297-305.
48. Weaver DL, Ashikaga T, Krag DN, *et al.* Effect of occult metastases on survival in node-negative breast cancer. *N Engl J Med* 2011; 364: 412-21.
49. Weaver DL, Le UP, Dupuis SL, *et al.* Metastasis detection in sentinel lymph nodes: comparison of a limited widely spaced (NSABP protocol B-32) and a comprehensive narrowly spaced paraffin block sectioning strategy. *Am J Surg Pathol* 2009; 33: 1583-9.
50. Hieken TJ, Boughey JC. Axillary dissection versus no axillary dissection in patients with sentinel-node micrometastases: commentary on the IBCSG 23-01 Trial. *Gland Surg* 2013; 2: 128-32.
51. Straver ME, Meijnen P, van Tienhoven G, *et al.* Role of axillary clearance after a tumor-positive sentinel node in the administration of adjuvant therapy in early breast cancer. *J Clin Oncol* 2010; 28: 731-7.
52. AMAROS. The EORTC 10981-22023 AMAROS trial [Internet]. AMAROS, 2010 [cited 2015 Oct 1]. Available from: <http://research.nki.nl/amaros/>.
53. Mansel RE, Fallowfield L, Kissin M, *et al.* Randomized multicenter trial of sentinel node biopsy versus standard axillary treatment in operable breast cancer: the ALMANAC Trial. *J Natl Cancer Inst* 2006; 98: 599-609.
54. Gill G; SNAC Trial Group of the Royal Australasian College of Surgeons (RACS) and NHMRC Clinical Trials Centre. Sentinel-lymph-node-based management or routine axillary clearance? One-year outcomes of sentinel node biopsy versus axillary clearance (SNAC): a randomized controlled surgical trial. *Ann Surg Oncol* 2009; 16: 266-75.
55. Lucci A, McCall LM, Beitsch PD, *et al.* Surgical complications associated with sentinel lymph node dissection (SLND) plus axillary lymph node dissection compared with SLND alone in the American College of Surgeons Oncology Group Trial Z0011. *J Clin Oncol* 2007; 25: 3657-63.
56. Cote RJ, Peterson HF, Chaiwun B, *et al.* Role of immunohistochemical detection of lymph-node metastases in management of breast cancer. International Breast Cancer Study Group. *Lancet* 1999; 354: 896-900.
57. Guenther JM, Hansen NM, DiFronzo LA, *et al.* Axillary dissection is not required for all patients with breast cancer and positive sen-

- tincl nodes. Arch Surg 2003; 138: 52-6.
58. Tvedskov TF, Jensen MB, Ejlersen B, Christiansen P, Balslev E, Kroman N. Prognostic significance of axillary dissection in breast cancer patients with micrometastases or isolated tumor cells in sentinel nodes: a nationwide study. Breast Cancer Res Treat 2015; 153: 599-606.

Prognostic Implication of Semi-quantitative Immunohistochemical Assessment of CD20 Expression in Diffuse Large B-Cell Lymphoma

Chang Hwan Choi^{a*}
Young Hoon Park^{1*} · Joo Han Lim¹
Suk Jin Choi · Lucia Kim
In Suh Park · Jee Young Han
Joon Mee Kim · Young Chae Chu

Departments of Pathology and
¹Hematology-Oncology, Inha University Hospital,
Inha University School of Medicine, Incheon,
Korea

Received: November 19, 2015
Revised: January 4, 2016
Accepted: January 12, 2016

Corresponding Author

Suk Jin Choi, MD
Department of Pathology, Inha University Hospital,
Inha University School of Medicine, 27 Inhang-ro,
Jung-gu, Incheon 22332, Korea
Tel: +82-32-890-3972
Fax: +82-32-890-3464
E-mail: sukjinchoi007@gmail.com

*Chang Hwan Choi and Young Hoon Park
contributed equally to this work.

^aPresent address: Scientific Investigation Laboratory,
Criminal Investigation Command, Ministry of
National Defense, Seoul, Korea.

Background: Immunohistochemical demonstration of CD20 in diffuse large B-cell lymphoma (DLBCL) is prerequisite not only for the diagnosis but also for assigning patients to rituximab-containing chemotherapy. However, little is known about the impact of abundance of CD20 expression assessed by immunohistochemistry on the clinical outcome of DLBCL. We performed a semi-quantitative immunohistochemical analysis of CD20 expression in DLBCL to examine the prognostic implication of the level of CD20 expression. **Methods:** Pre-treatment diagnostic tissue samples from 48 DLBCL patients who were treated with rituximab, cyclophosphamide, doxorubicin, vincristine, and prednisone (R-CHOP) regimen were represented in a tissue microarray and immunostained for CD20. The relative abundance of CD20 expression was semi-quantitatively scored using a web-based ImmunoMembrane plug-in. Receiver operating characteristic curve analysis was used to determine a prognostically relevant cut-off score in order to dichotomize the patients into CD20-high versus CD20-low groups. **Results:** The levels of CD20 expression were heterogeneous among the patients, with a wide and linear distribution of scores. Patients in CD20-low group showed significantly poor clinical outcome. **Conclusions:** The levels of CD20 expression in DLBCL are heterogeneous among the patients with DLBCL. A subgroup of the patients with CD20 expression levels below the cut-off score showed poor clinical outcome.

Key Words: Antigen, CD20; Lymphoma, large B-cell; Immunohistochemistry; Tissue array analysis

Diffuse large B-cell lymphoma (DLBCL) is the most aggressive non-Hodgkin lymphoma that is potentially curable with conventional cyclophosphamide, doxorubicin, vincristine, and prednisone (CHOP) chemotherapy.¹ Even though the addition of rituximab to standard CHOP chemotherapy dramatically improved the survival of the patients, some patients fail to respond to rituximab, cyclophosphamide, doxorubicin, vincristine, and prednisone (R-CHOP) regimen. Furthermore, relapse of disease after standard chemoimmunotherapy has been documented to be roughly up to 50%.² In rituximab-era, immunohistochemical demonstration of CD20 in the cell membrane of the lymphoma-cells is prerequisite not only for histopathologic diagnosis of DLBCL but also for assignment of the patients to front-line rituximab-containing immunochemotherapy. However, the

prognostic significance of relative abundance of immunohistochemically assessed CD20 expression on the formalin-fixed paraffin-embedded tissue (FFPET) sections of the diagnostic tissue samples has not yet been investigated.

Rituximab is a CD20-directed chimeric monoclonal antibody that depletes the tumor cells with CD20 expression in their cytoplasmic membrane through mechanisms including inhibition of cell proliferation, induction of apoptosis, and antibody/complement-dependent cytotoxicity.³ Accordingly, the relative abundance of CD20 in tumor cells could be implicated in the clinical outcome of the patients treated with R-CHOP regimen. However, there is no immunohistochemical marker that can discriminate patients who are beyond the benefits of the addition of rituximab to conventional standard chemotherapy. We

hypothesized the relative abundance of CD20, the target molecules of rituximab on the cell membrane of the tumor cells, could be implicated in the prognosis of DLBCL patients treated with standard R-CHOP therapy. In this study, we performed a semi-quantitative immunohistochemical analysis of CD20 expression in a tissue microarray (TMA) cohort of DLBCL tumor tissues and correlated the CD20 level with clinical outcome.

MATERIALS AND METHODS

TMA cohort

We searched the surgical pathology archives for cases diagnosed with de novo DLBCL in Inha University Hospital between January 2006 and December 2013. Among them, we included the patients who received six to eight cycles of standard R-CHOP chemotherapy. Having excluded the primary central nervous

system lymphomas and cases diagnosed based on small biopsy specimens such as endoscopic biopsy or needle biopsy, a total of 48 patients with complete outcome data were eligible for the preparation of TMA cohort, including 27 male and 21 female with a median age of 58.5 years (range, 20 to 81 years). Two 1-mm duplicate cores from the diagnostic FFPET samples were represented on a TMA by using a self-made TMA and a home-made recipient block as described previously.⁴

Immunohistochemical staining of TMA sections

Using an automated immunohistochemical stainer (BenchMarkXT, Ventana, Tucson, AZ, USA), sections of the TMA cut in 4- μ m thickness were routinely processed for immunohistochemical stains for CD20 (1:500, H1, heat-induced antigen retrieval, BD Pharmingen, San Jose, CA, USA), BCL2 (1:100, 124, heat-induced antigen retrieval, Dako, Carpinteria, CA, USA),

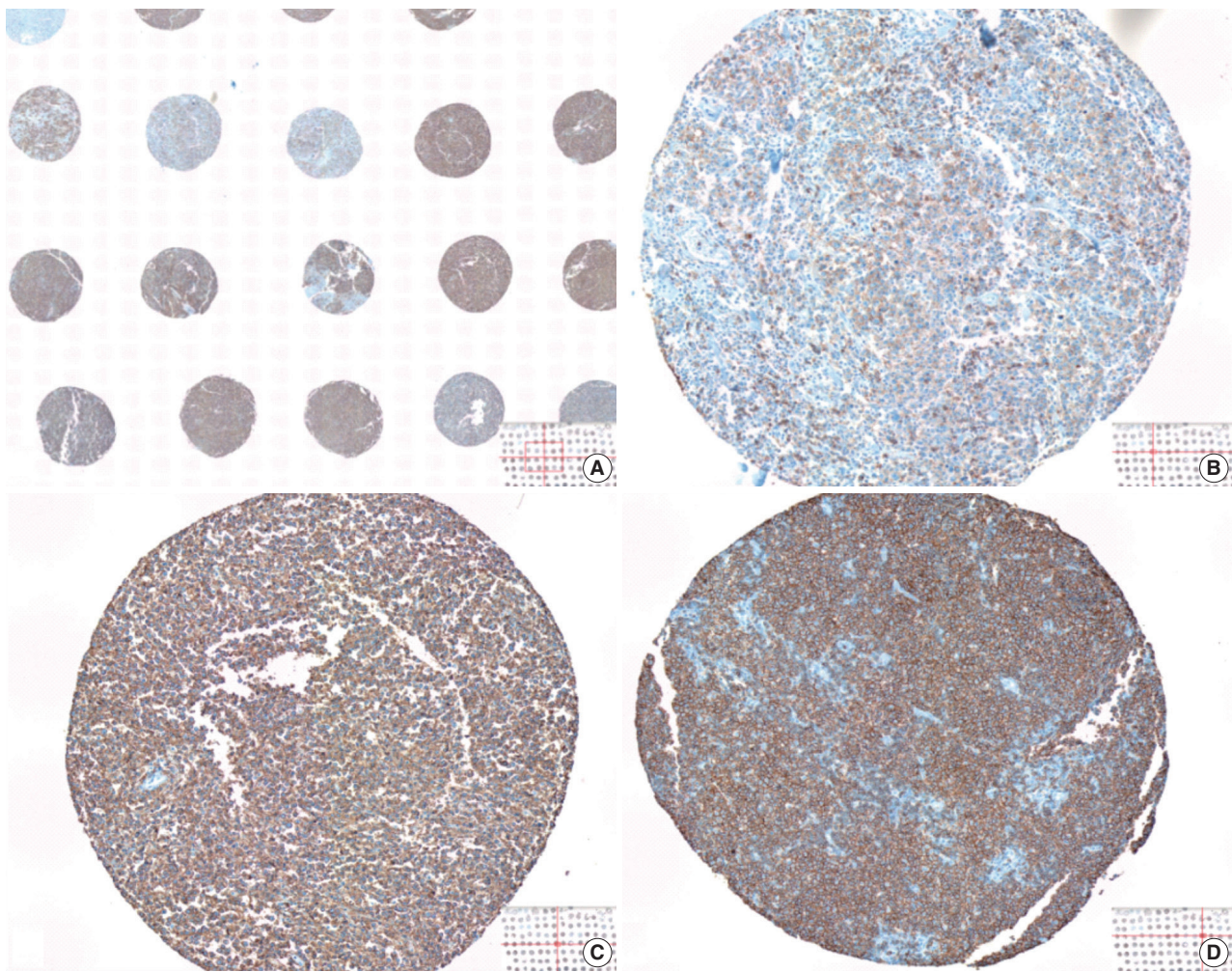


Fig. 1. Visual heterogeneity in the intensity of CD20 staining in large B-cell lymphoma tumor tissues represented in a tissue microarray. The levels of CD20 expression is visually heterogeneous among tumor tissues (A), ranging from weak (B), intermediate (C), to strong (D) intensity of the 3,3'-diaminobenzidine (DAB) signal.

BCL6 (1:30, PG-B6p, heat-induced antigen retrieval, Dako), CD10 (pre-diluted, SP67, heat-induced antigen retrieval, Ventana), and MUM1 (1:100, MUM1p, heat-induced antigen retrieval, Dako). Cases were designated as positive when $\geq 30\%$ of the tumor cells were immunoreactive for all antibodies except for CD20.⁵ Cases were classified into germinal center B-cell versus non-germinal center B-cell type according to Hans classification.⁶

Quantification of CD20 levels

The whole image of CD20-stained TMA section was digitalized using a digital slide scanner (VM600, Motic, Ximen, China) using a $\times 20$ objective (Fig. 1). Then, representative JPEG images were acquired from each tissue sample (Fig. 1). CD20 immunoreactivity within each JPEG image was semi-quantitatively assessed using ImageJ software (<http://rsbweb.nih.gov/ij/>) coupled with ImmunoMembrane plug-in (<http://imtmicroscope.uta.fi/immunomembrane>).⁷ Completeness (0–10 points) and intensity (0–10 points) of membrane staining was added for a score (0–20 points) (Fig. 2). Then, we used the average of the duplicates in analysis as the arbitrary level of CD20 for each case.

Statistical analysis

The primary outcomes of interest in this study were overall survival (OS) and event-free survival (EFS). OS was defined as the time interval between the date of diagnosis and the date of death by any cause. EFS was estimated from the date of diagnosis to the

date of disease progression, relapse, last contact, or death. Complete response (CR) was determined according to the conventional response criteria. Receiver operating characteristic (ROC) curve analysis was used to select a prognostically relevant cut-off score of CD20 expression that can dichotomize the patients in terms of clinical outcome.^{8,9} Kaplan-Meier analysis was used to estimate cumulative survivals and the differences between survival curves were analyzed using log-rank test. Chi-square test or Fisher exact test were used to compare the differences in frequency of categorical variables between two groups. Mann-Whitney U test and Kruskal-Wallis test were used to assess mean differences between the groups. Multivariate regression analysis using the Cox proportional hazards model was performed to determine the hazard ratios (HRs) of the clinicopathologic factors and CD20 levels. All p-values presented were two-sided, and $p < .05$ was considered statistically significant. All statistical analyses were performed using SPSS ver. 19.0 (IBM Co., Armonk, NY, USA).

RESULTS

Heterogeneity in CD20 levels among patients with DLBCL

The TMA section immunostained for CD20 exhibited heterogeneous CD20 levels among patients, with a high degree of reproducibility in scores between duplicate tissue cores to duplicate runs (Fig. 3). As indicated by a wide and linear range of the

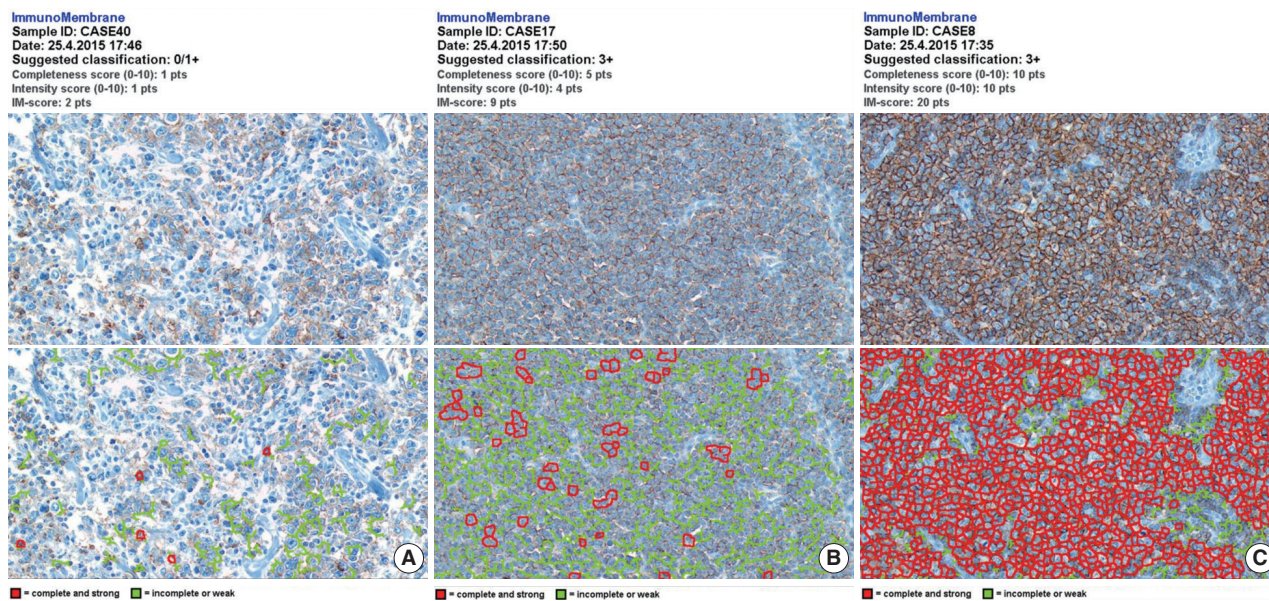


Fig. 2. Semi-quantitative immunohistochemical scoring of CD20 expression. The images of weak and incomplete (A, upper), weak and complete (B, upper), and strong and complete (C, upper) staining for CD20 are digitally analyzed using the free web-based ImmunoMembrane (IM) plug-in that produces a combined score of 2 (A, lower), 9 (B, lower), and 20 (C, lower) in its pseudo-color image, respectively.

semi-quantitative scores with a negatively skewed distribution of data on the frequency histogram (Fig. 4), the level of CD20 expression was significantly lower in patients who died of disease compared to those survived ($p = .012$) (Fig. 5).

Association between CD20 level and clinical outcome

The median follow-up period was 58.5 months (range, 11 to 125 months). Overall, there were 27 male (56.3%) and 21 female (43.7%) patients, and the median age was 58.5 years (range, 20

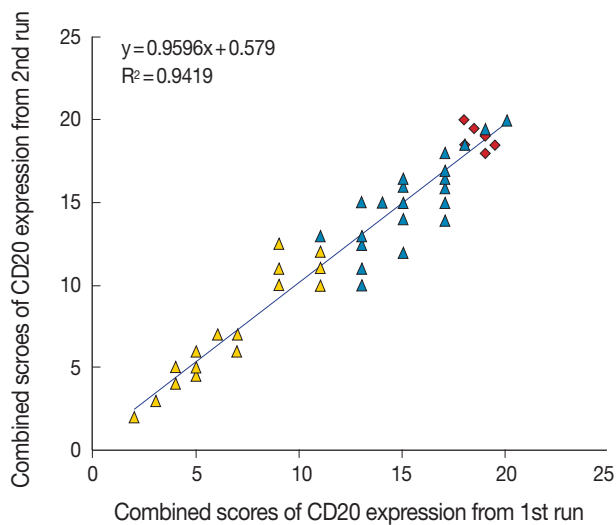


Fig. 3. Reproducibility of the immunohistochemical scoring. The combined scores of CD20 expression obtained from the first run of semi-quantitative immunohistochemical scoring are reproducible in the second run. Yellow triangle, CD20-low group; blue triangle, CD20-high group; red rhombus, germinal center of the tonsil as control tissue.

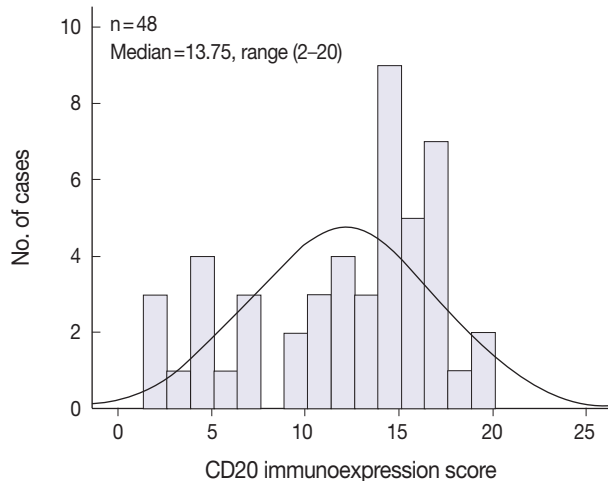


Fig. 4. Negatively skewed distribution of the combined scores of CD20 expression. The frequency histogram of the scores illustrates a wide and linear range of the semi-quantitative scores with negatively skewed distribution.

to 81 years). After six to eight cycles of R-CHOP chemotherapy, CR was achieved in 41 patients (85.4%) and 11 (11/41, 26.8%) of them experienced relapse.

The outcome-based ROC curve analysis produced a predictive cut-off score of 11.75 in CD20 levels (with an area under the

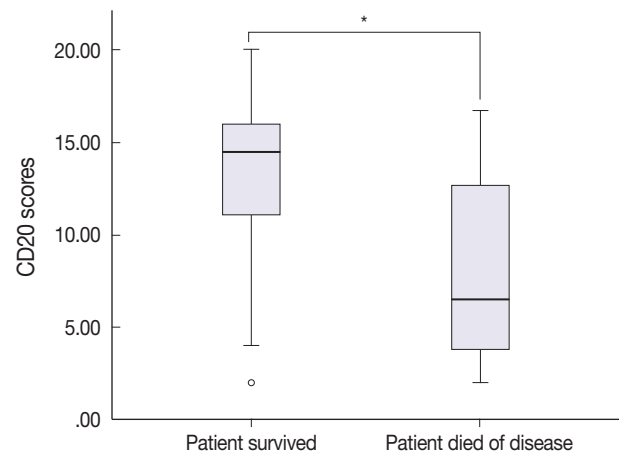


Fig. 5. High inter- and intra-group variation in the levels of CD20 expression between patients who survived and those died. The mean of combined scores of CD20 expression was significantly lower in patients who died of disease compared to those who survived (Mann-Whitney test, $*p = .012$).

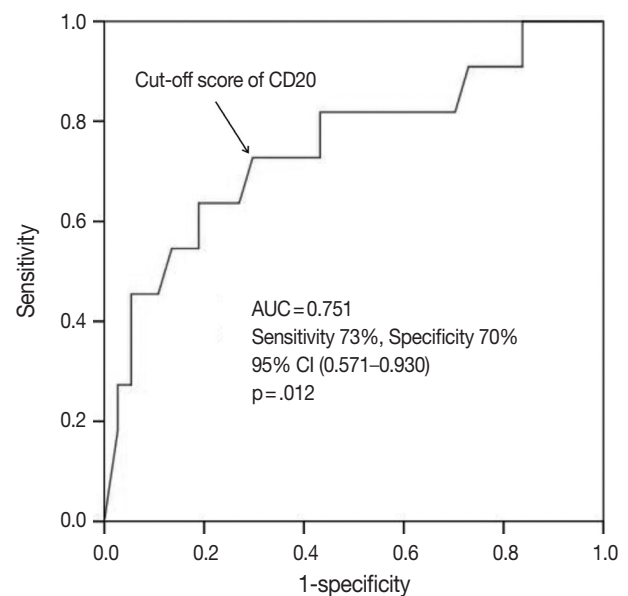


Fig. 6. Determination of a cut-off score of CD20 expression level for poor survival outcome. Receiver operating characteristic (ROC) curve analysis was used to determine a statically optimal cut-off score of CD20 expression level for prediction of disease-associated deaths. The cut-off score of 11.75 derived from the ROC curve analysis maximized the sum of sensitivity and specificity (sensitivity, 72.7%; specificity, 70.3%; $p = .012$). AUC, area under the ROC curve; CI, confidence interval.

ROC curve of 0.751; 95% confidence interval [CI], 0.571 to 0.930; sensitivity, 72.7%; specificity, 70.3%; $p = .012$) that could predict poor prognosis in terms of OS (Fig. 6). Based on the predictive cut-off score, the overall patients in our cohort were dichotomized into the CD20-low ($n = 20$, 41.7%) and CD20-high ($n = 28$, 58.3%).

Table 1 shows the distribution of the clinical background characteristics of the patients in the two groups divided according to the CD20 expression level. There were no significant differences in clinicopathologic parameters between the two groups. CR was achieved in 15 patients (75%) in the CD20-low group and 26 patients (92.9%) in the CD20-high group, with no sig-

nificant difference in CR rate between these two groups ($p = .197$). Eventually, disease relapse was experienced by four out of 15 patients (26.7%) in the CD20-low group and by seven out of 26 patients (26.9%) in CD20-high group, with no significant difference in relapse rate between these two groups. Clinical events including disease progression were more frequently observed in CD20-low group (14/20, 70%) compared to CD20-high group (13/28, 46.4%), with a significant difference in EFS (median, 37 months [range, 4 to 100 month] vs 96 months [range, 6 to 100 months]) for the CD20-high group ($p = .032$) (Fig. 7A). The 5-year EFS were 39.4% in CD20-low group and 66.5% in CD20-high group, respectively. Overall, nine patients died,

Table 1. Clinical and pathologic parameters in patients according to CD20 level

Characteristic	CD20 level above the cut-off score	CD20 level below the cut-off score	p-value
No. of patients	28	20	
Age, median (range, yr)	54 (20–75)	61 (34–81)	.446
> 60 yr	11 (45.8)	11 (57.9)	.175
Sex			.169
Male	13 (46.4)	14 (70)	
Female	15 (53.6)	6 (30)	
ECOG PS			.212
<2	18 (64.3)	10 (50)	
≥2	10 (35.7)	10 (50)	
Stage			.583
I/II	16 (57.1)	13 (65)	
III/IV	12 (42.9)	7 (35)	
Serum LDH level			.299
Normal	4 (14.3)	1 (5)	
Elevated	24 (85.7)	19 (95)	
No. of extranodal sites			1
<2	24 (85.7)	17 (85)	
≥2	4 (14.3)	3 (15)	
IPI risk stratification			.269
Low/Low-intermediate	21 (75)	12 (60)	
High-intermediate/High	7 (25)	8 (40)	
Presence of B symptom			.176
Yes	5 (17.9)	7 (35)	
No	23 (82.1)	13 (65)	
BM involvement			.369
Negative	25 (89.3)	16 (80)	
Positive	3 (10.7)	4 (20)	
Subtype by IHC			.175
GCB-like	9 (32.1)	3 (15)	
Non-GCB-like	19 (67.9)	17 (85)	
BCL2 IHC			.212
Negative	9 (32.1)	10 (50)	
Positive	19 (67.9)	10 (50)	
Response			.197
CR	26 (92.9)	15 (75)	
No CR	2 (7.1)	5 (25)	

Values are presented as number (%).

ECOG PS, Eastern Cooperative Oncology Group Performance status; LDH, lactate dehydrogenase; IPI, International Prognostic Index; BM, bone marrow; IHC, immunohistochemistry; GCB, germinal center B cell; CR, complete response.

including six deaths in the CD20-low group and three deaths in the CD20-high group. Median OS was 50 months (range, 11 to 100 months) for the CD20-low group and 71 months (range, 15 to 125 months) for the CD20-high group, with a significantly shorter 5-year EFS (39.4% vs 66.5%) and OS (59.9% vs 90.6%) in CD20-low group (Fig. 7B).

Prognostic factor analyses

In the univariate analysis of prognostic factors, following parameters were significantly associated with worse prognosis in terms of both EFS and OS: CD20 level lower than the cut-off score ($p = .039$ and $p = .035$) and two or more sites of extranodal involvement ($p = .034$ and $p = .044$). In addition, poor perfor-

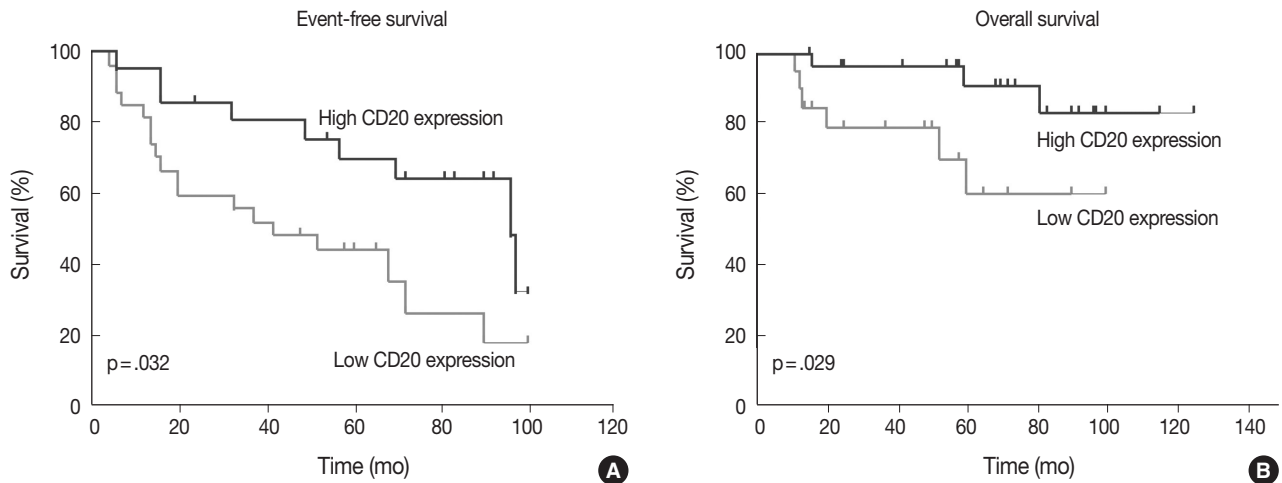


Fig. 7. Event-free survival (A) and overall survival (B) of the patients with diffuse large B-cell lymphoma according to the relative abundance of CD20 expression.

Table 2. Univariate and multivariate analysis of clinicopathologic parameters for event-free survival and overall survival

Variable	Event-free survival				Overall survival			
	Univariate		Multivariate		Univariate		Multivariate	
	HR (95% CI)	p-value	HR (95% CI)	p-value	HR (95% CI)	p-value	HR (95% CI)	p-value
Age								
<60 yr vs >60 yr	0.884 (0.413–1.890)	.750	-	-	0.599 (0.150–2.397)	.464	-	-
Serum LDH level								
Elevated vs normal	1.698 (0.268–3.699)	.562	-	-	1.487 (0.258–5.614)	.658	-	-
ECOG PS								
≥2 vs <2	2.228 (1.030–4.819)	.042	1.421 (0.598–3.581)	.125	2.802 (0.730–10.752)	.071	-	-
Stage								
III/IV vs I/II	1.372 (0.633–2.976)	.423	-	-	1.453 (0.389–5.422)	.576	-	-
Extranodal site								
≥2 vs <2	2.953 (1.087–8.024)	.034	2.768 (1.028–7.571)	.047	3.58 (1.485–20.974)	.044	2.35 (0.798–12.257)	.098
IPI score								
≥3 vs <3	1.943 (0.883–4.276)	.099	-	-	1.560 (0.385–6.318)	.530	-	-
B symptoms								
Positive vs negative	3.090 (1.404–6.810)	.023	2.255 (0.825–4.287)	.095	2.268 (0.892–17.258)	.085	-	-
BCL2								
Positive vs negative	0.612 (0.284–1.321)	.204	-	-	1.036 (0.257–4.169)	.960	-	-
BCL6								
Negative vs positive	1.128 (0.515–2.472)	.763	-	-	0.969 (0.259–3.624)	.962	-	-
Subtype by IHC								
Non-GCB vs GCB	1.324 (0.569–3.080)	.509	-	-	1.298 (0.326–5.218)	.712	-	-
CD20 level								
Below vs above the cut-off	2.261 (1.047–4.875)	.039	2.187 (1.015–4.745)	.048	4.89 (1.043–17.857)	.035	4.291 (1.012–17.724)	.043

mance status with Eastern Cooperative Oncology Group (ECOG) score ≥ 2 ($p = .042$) and presence of B symptoms ($p = .023$) were significantly associated with a poor prognosis in terms of EFS, but not in terms of OS. The stage at diagnosis and International Prognostic Index score were not significantly associated with EFS ($p = .423$ and $p = .099$) and OS ($p = .576$ and $p = .530$). When all the parameters significant in univariate analysis were included in multivariate analysis, lower CD20 level remained an independent prognostic factor for EFS (HR, 2.187; 95% CI, 1.015 to 4.745; $p = .048$) and for OS (HR, 4.291; 95% CI, 1.012 to 17.724; $p = .043$) (Table 2). Two or more sites of extranodal involvement was an independent prognostic factor (HR, 2.768; 95% CI, 1.028 to 7.571; $p = .047$) for EFS but it was not of prognostic relevance with regard to OS ($p = .098$). ECOG performance status (ECOG PS) ≥ 2 ($p = .125$) and presence of B symptoms ($p = .095$) were not found to be in correlation with OS in multivariate analysis.

DISCUSSION

The prognostic significance of the traditional clinicopathologic parameters of DLBCL seems to be overshadowed by the introduction of R-CHOP as a standard regimen for DLBCL.⁸⁻¹⁰ Bcl-2 expression assessed by immunohistochemical staining seems to be no longer associated with a poor outcome in DLBCL patients treated with R-CHOP.¹¹ In addition, the prognostic value of immunophenotypic subtype determined by immunohistochemistry for CD10, Bcl-6, and MUM1 is questioned in rituximab era.^{12,13} Furthermore, the predictive significance of International Prognostic Index that has been the most important prognostic factor for DLBCL in pre-rituximab era also seems to be overridden by the addition of rituximab to CHOP regimen.¹⁴

When assessed semi-quantitatively using flow cytometry (FCM) analysis, the levels of CD20 expression in the fresh tissue sample were quite heterogeneous both among and within different types of non-Hodgkin B-cell lymphomas.^{15,16} In addition, the level of CD20 expression at the onset of disease seems to be an independent predictor for poor outcomes in patients treated with R-CHOP.^{15,17,18} FCM analysis of fresh tissue sample, however, is not a routine practice in many institutions with limited resources. Furthermore, fresh tissue samples for FCM analysis are not always available. Accordingly, immunohistochemical assessment of CD20 expression in diagnostic tissue samples in forms of paraffin blocks should be a more feasible method both in terms of low cost and convenience in sample recruitment.

There has been no previous literature specific to the distribution of immunohistochemical levels of CD20 expression in the

diagnostic FFPET samples of DLBCL and their association with the prognosis of the patients. In this study, we used a free web-based image analysis tool that enabled us to acquire objective semi-quantitative scores of CD20 expression levels based on intensity and completeness of CD20-immunostaining of the FFPET sections. As indicated by the previous investigations using FCM analysis of fresh tissue samples, the levels of CD20 expression assessed by semi-quantitative immunohistochemistry were quite heterogeneous among the patients, with scores spread over a wide and linear range. By correlating the expression level of CD20 with the clinical outcomes, we were able to identify a subgroup of DLBCL patients with CD20 expression levels below the cut-off score, who showed poor EFS and OS independent of other known clinical and pathologic parameters. Further studies are warranted to validate the prognostic role of the relative abundance of CD20 expression in a larger cohort.

Interestingly, Shimizu *et al.*¹⁹ recently reported that histone deacetylase (HDAC) inhibitors augment cytotoxic effect of rituximab by increasing the level of CD20 in the cell lines of DLBCL. Accordingly, the patients with lower levels of CD20 expression who could be less amenable to rituximab therapy could probably benefit from pretreatment of HDAC inhibitors such as valproic acid prior to the standard R-CHOP treatment.²⁰ Alternatively, they could more likely benefit from the treatment with novel anti-CD20 monoclonal antibodies which show more anti-cancer activity in CD20 low-expression B-cell lymphomas. For example, ofatumumab (a fully human anti-CD20 monoclonal antibody) and obinutuzumab (a humanized type II antibody targeted against CD20) have been shown to be active and safe in clinical trials that had included patients with chronic lymphocytic leukemia which is known to have relatively lower levels of CD20 expression.^{21,22}

In conclusion, a level of CD20 expression is heterogeneous in DLBCL and lower level of CD20 expression is a poor prognostic marker for survival in patients with DLBCL who are treated with R-CHOP chemotherapy. Semi-quantitative immunohistochemical estimation of CD20 expression can be used to identify a subgroup of DLBCL patients with poor outcome who might possibly benefit from the pretreatment with agents that can increase the level of CD20 expression in the cell membranes of the tumor cells.

Conflicts of Interest

No potential conflict of interest relevant to this article was reported.

Acknowledgments

This work was supported by Inha University Research Grant. The authors wish to thank Yu Hwan Lim, Kyung Hwan Jang, Yong Hoon Lee, Young Min Lee, and Seok Joon Hong in the histology lab for their technical support and advice in the construction of the TMA blocks and Kyung Shin Kim and Eun Sook Kim in the immunopathology section for their excellent immunohistochemistry.

REFERENCES

- Stein H, Warnke RA, Chan WC, *et al.* Diffuse large B-cell lymphoma, not otherwise specified. In: Swerdlow SH, Campo E, Harris NL, *et al.*, eds. WHO classification of tumours of haematopoietic and lymphoid tissues. 4th ed. Lyon: IARC Press, 2008; 233-7.
- Coiffier B. State-of-the-art therapeutics: diffuse large B-cell lymphoma. *J Clin Oncol* 2005; 23: 6387-93.
- Boross P, Leusen JH. Mechanisms of action of CD20 antibodies. *Am J Cancer Res* 2012; 2: 676-90.
- Kim KH, Choi SJ, Choi YI, *et al.* In-house manual construction of high-density and high-quality tissue microarrays by using homemade recipient agarose-paraffin blocks. *Korean J Pathol* 2013; 47: 238-44.
- Berglund M, Thunberg U, Amini RM, *et al.* Evaluation of immunophenotype in diffuse large B-cell lymphoma and its impact on prognosis. *Mod Pathol* 2005; 18: 1113-20.
- Hans CP, Weisenburger DD, Greiner TC, *et al.* Confirmation of the molecular classification of diffuse large B-cell lymphoma by immunohistochemistry using a tissue microarray. *Blood* 2004; 103: 275-82.
- Tuominen VJ, Tolonen TT, Isola J. ImmunoMembrane: a publicly available web application for digital image analysis of HER2 immunohistochemistry. *Histopathology* 2012; 60: 758-67.
- Salles G, de Jong D, Xie W, *et al.* Prognostic significance of immunohistochemical biomarkers in diffuse large B-cell lymphoma: a study from the Lunenburg Lymphoma Biomarker Consortium. *Blood* 2011; 117: 7070-8.
- Culpin RE, Sieniawski M, Angus B, *et al.* Prognostic significance of immunohistochemistry-based markers and algorithms in immunotherapy-treated diffuse large B cell lymphoma patients. *Histopathology* 2013; 63: 788-801.
- Coiffier B. Rituximab therapy in malignant lymphoma. *Oncogene* 2007; 26: 3603-13.
- Mounier N, Briere J, Gisselbrecht C, *et al.* Rituximab plus CHOP (R-CHOP) overcomes bcl-2-associated resistance to chemotherapy in elderly patients with diffuse large B-cell lymphoma (DLBCL). *Blood* 2003; 101: 4279-84.
- Nyman H, Adde M, Karjalainen-Lindsberg ML, *et al.* Prognostic impact of immunohistochemically defined germinal center phenotype in diffuse large B-cell lymphoma patients treated with immunochemotherapy. *Blood* 2007; 109: 4930-5.
- Winter JN, Weller EA, Horning SJ, *et al.* Prognostic significance of Bcl-6 protein expression in DLBCL treated with CHOP or R-CHOP: a prospective correlative study. *Blood* 2006; 107: 4207-13.
- Sehn LH, Berry B, Chhanabhai M, *et al.* The revised International Prognostic Index (R-IPI) is a better predictor of outcome than the standard IPI for patients with diffuse large B-cell lymphoma treated with R-CHOP. *Blood* 2007; 109: 1857-61.
- Johnson NA, Boyle M, Bashashati A, *et al.* Diffuse large B-cell lymphoma: reduced CD20 expression is associated with an inferior survival. *Blood* 2009; 113: 3773-80.
- Olejniczak SH, Stewart CC, Donohue K, Czuczman MS. A quantitative exploration of surface antigen expression in common B-cell malignancies using flow cytometry. *Immunol Invest* 2006; 35: 93-114.
- Horvat M, Kloboves Prevodnik V, Lavrencak J, Jezersek Novakovic B. Predictive significance of the cut-off value of CD20 expression in patients with B-cell lymphoma. *Oncol Rep* 2010; 24: 1101-7.
- Suzuki Y, Yoshida T, Wang G, *et al.* Association of CD20 levels with clinicopathological parameters and its prognostic significance for patients with DLBCL. *Ann Hematol* 2012; 91: 997-1005.
- Shimizu R, Kikuchi J, Wada T, Ozawa K, Kano Y, Furukawa Y. HDAC inhibitors augment cytotoxic activity of rituximab by upregulating CD20 expression on lymphoma cells. *Leukemia* 2010; 24: 1760-8.
- Damm JK, Gordon S, Ehinger M, *et al.* Pharmacologically relevant doses of valproate upregulate CD20 expression in three diffuse large B-cell lymphoma patients *in vivo*. *Exp Hematol Oncol* 2015; 4: 4.
- Coiffier B, Lepage S, Pedersen LM, *et al.* Safety and efficacy of ofatumumab, a fully human monoclonal anti-CD20 antibody, in patients with relapsed or refractory B-cell chronic lymphocytic leukemia: a phase 1-2 study. *Blood* 2008; 111: 1094-100.
- Goede V, Fischer K, Busch R, *et al.* Obinutuzumab plus chlorambucil in patients with CLL and coexisting conditions. *N Engl J Med* 2014; 370: 1101-10.

Upregulated Neuro-oncological Ventral Antigen 1 (NOVA1) Expression Is Specific to Mature and Immature T- and NK-Cell Lymphomas

Eun Kyung Kim¹ · Sun Och Yoon¹
Soo Hee Kim^{1,2} · Woo Ick Yang¹
Yoon Ah Cho¹ · Soo Jeong Kim³

¹Department of Pathology, Yonsei University College of Medicine, Seoul; ²Anatomic Pathology Reference Lab, Seegene Medical Foundation, Seoul; ³Department of Internal Medicine, Division of Hematology, Yonsei University College of Medicine, Seoul, Korea

Received: January 12, 2016

Revised: February 5, 2016

Accepted: February 8, 2016

Corresponding Author

Sun Och Yoon, MD, PhD
Department of Pathology, Yonsei University College of Medicine, 50-1 Yonsei-ro, Seodaemun-gu, Seoul 03722, Korea
Tel: +82-2-2228-1763
Fax: +82-2-362-0860
E-mail: sooyoon@yuhs.ac

Background: Recent studies have revealed that the splicing factor neuro-oncological ventral antigen 1 (NOVA1) is enriched in fibroblasts and accumulated T cells of tertiary lymphoid structures. In the present study, we investigated NOVA1 expression in various subtypes of mature and immature T- and natural killer (NK)-cell lymphomas as well as in various B-cell lymphoma subtypes.

Methods: NOVA1 immunoexpression was evaluated in hyperplastic palatine tonsils (n = 20), T- and NK-cell lymphomas (n = 177), diffuse large B-cell lymphomas (n = 151), and other types of B cell lymphomas (n = 31). Nuclear staining intensity and percentage of positive tumor cells were graded. NOVA1 mRNA expression was analyzed in various lymphoma cell lines. **Results:** Tumor cells of T- and NK-cell lymphomas showed higher expression levels of NOVA1 than did normal paracortical T cells, and 56.5% of T- and NK-cell lymphoma cases showed diffuse and strong expression. The NOVA1 expression level varied according to the subtype; it was higher in angio-immunoblastic T-cell lymphoma, anaplastic lymphoma kinase (ALK)-negative anaplastic large cell lymphoma (ALCL), and T lymphoblastic leukemia/lymphoma (T-LBL), but it was lower in ALK-positive ALCL. In almost all B-cell lymphomas, NOVA1 expression was very low or negative. NOVA1 mRNA was also expressed in Jurkat, a T-LBL cell line. **Conclusions:** The present findings suggest that NOVA1 upregulation may be involved in certain subtypes of T- and NK-cell lymphomas, but not in B-cell lymphomas. Upregulated NOVA1 expression seems to be a specific biological feature of activated T cells such as T- and NK-cell lymphomas.

Key Words: NOVA1; Lymphoma, T-cell; NK cell lymphoma; Splicing factor

Neuro-oncological ventral antigen 1 (NOVA1) is known to play a role in the neuronal splicing program.¹⁻⁴ A recent study revealed that the splicing programs of epithelial cells, fibroblasts, and endothelial cells are specifically regulated by the epithelial splicing regulatory protein 1 (ESRP1) and ESRP2, muscle blind-like splicing regulator 1 (MBNL1), NOVA1, and polypyrimidine tract binding protein 1 (PTBP1). Furthermore, RNA binding protein, fox-1 homolog 2 (RFX2) splicing factors, and NOVA1 are found enriched in fibroblasts.⁵ In our recent study,⁶ we also confirmed that NOVA1 is highly expressed in fibroblasts/stromal spindle cells in normal tissues.

In addition, we observed that NOVA1 is frequently upregulated in accumulated T lymphocytes in tertiary lymphoid structures formed by chronic inflammation, whereas only small numbers of T lymphocytes express NOVA1 in the secondary lymphoid organs, such as hyperplastic palatine tonsils.⁶⁻⁸ These findings suggest that NOVA1 upregulation may be involved in T cell activation and proliferation.⁶ Given that fibroblasts/stromal spin-

dle cells actively regulate immune cells within the tissue microenvironment through direct interaction with immune B cells or T cells,^{9,10} NOVA1-related regulation in stromal fibroblasts/spindle cells may also occur in immune cells.

We hypothesized that NOVA1 upregulation could be involved in the pathogenesis of malignant lymphoma, which is a neoplasm of activated or transformed immune cells. In our previous study, peripheral T-cell lymphoma cases frequently showed strong NOVA1 expression while mature B-cell lymphoma cases did not,⁶ although the investigation was done on a small scale. In the present study, we extended our study to confirm the role of NOVA1 in the pathogenesis of malignant lymphoma. We thoroughly investigated NOVA1 expression in a large number of various subtypes of mature and immature T- and natural killer (T/NK)-cell lymphomas, and the expression of NOVA1 was also compared in various subtypes of B-cell lymphomas.

MATERIALS AND METHODS

Patients and clinical data

Archival tissues of formalin-fixed, paraffin-embedded (FFPE) tumor blocks were retrieved from consecutively archived specimens. A set of 177 T/NK-cell lymphomas diagnosed in Severance Hospital from 1999 to 2013 were included. The subtypes of T/NK-cell lymphomas were as follows: extranodal NK/T-cell lymphoma, nasal type (NKTL; $n = 60$), peripheral T-cell lymphoma, not otherwise specified (PTCL-NOS; $n = 44$), angioimmunoblastic T-cell lymphoma (AITL; $n = 16$), anaplastic large cell lymphoma (ALCL; anaplastic lymphoma kinase [ALK]-positive, $n = 16$; ALK-negative, $n = 17$), T lymphoblastic leukemia/lymphoma (T-LBL; $n = 20$) and other types ($n = 4$; hepatosplenic T-cell lymphoma, $n = 2$; subcutaneous panniculitis-like T-cell lymphoma, $n = 1$; cutaneous gamma-delta T-cell lymphoma, $n = 1$). Clinical information was obtained from patient medical records and 139 had clinical data available. The clinicopathological characteristics are summarized in Appendix 1.

A set of 151 diffuse large B cell lymphoma (DLBCL) and other types of 31 B-cell lymphomas, which were diagnosed in Severance Hospital from 2005 to 2011, were included. Other types of B-cell lymphomas were as follows: follicular lymphoma ($n = 14$), mantle cell lymphoma ($n = 5$), marginal zone B-cell lymphoma ($n = 7$), and Burkitt lymphoma ($n = 5$). Hyperplastic palatine tonsil tissues of cancer-free individuals ($n = 20$) were randomly retrieved. All tumor samples were reviewed by hematopathologists based on the current World Health Organization (WHO) criteria.¹¹ The institutional review board approved this study.

Tissue microarray preparation and immunohistochemistry

Sections of FFPE tissues were prepared and stained with hematoxylin and eosin. Under the microscope, the representative area was confirmed and selected for a 3-mm-core sized tissue microarray (TMA). One or two different representative areas per case were selected and 29 cores were embedded in a TMA block.

Immunohistochemistry of NOVA1 (1:500, Abcam, Cambridge, UK) was performed on 4- μ m tissue sections using the Ventana BenchMark XT Autostainer (Ventana Medical Systems, Tucson, AZ, USA). Immunohistochemistry with other primary antibodies was performed for diagnostic purposes and the tested antibodies are listed in Appendix 2.

Analysis of immunohistochemistry

NOVA1 expression was semiquantitatively determined according to the H-score method with a total score range of 0–300.¹²

The dominant intensity score of nuclear staining (0, absent; 1, weak or barely detectable; 2, distinct brown; and 3, strong dark brown) was multiplied by the percentage of positive tumor cell nuclei. The NOVA1 protein expression score ranged from 0 to 300, as high ($200 < \text{H-score} \leq 300$), intermediate ($100 < \text{H-score} \leq 200$), or low ($0 \leq \text{H-score} \leq 100$) expression.

Cell lines and reagents

Jurkat, a T-LBL cell line, was maintained in RPMI1640 medium (22400-089, Gibco, Life Technologies, Carlsbad, CA, USA) supplemented with 10% heat-inactivated fetal bovine serum (FBS; 6000-044, Gibco, Life Technologies). HH, a cell line derived from CD30-positive cutaneous T-cell lymphoma, and MAC1, a cell line derived from CD30-positive ALK-negative ALCL, were maintained in RPMI1640 medium supplemented with 20% heat-inactivated FBS. SNK6, derived from Epstein-Barr virus (EBV)-positive NKTL, was cultured in RPMI1640 medium supplemented with 10% heat-inactivated human plasma and 700 U/mL of recombinant interleukin 2. YT, an EBV-positive human NK-like leukemic cell line, was cultured in Iscove's modified Dulbecco's medium (12440-046, Gibco) supplemented with 20% heat-inactivated FBS. All the cell lines derived from T- or NK-cell lymphomas were kindly provided by Prof. Jeon YK (Seoul National University College of Medicine, Seoul, Korea). Toledo, a DLBCL cell line, was purchased from the American Type Culture Collection (ATCC, Manassas, VA, USA) and maintained in RPMI1640 supplemented with 10% heat-inactivated FBS.

RNA isolation and quantitative polymerase chain reaction

RNA isolation was performed using an RNeasy plus mini kit (74134, Qiagen, Hilden, Germany), and cDNA was constructed using a cDNA synthesis kit (11754-050, Invitrogen, Carlsbad, CA, USA). The TaqMan probes used were as follows: *GAPDH* (Hs99999905-m1, AB, Life Technologies) and *NOVA1* (Hs00359592-m1, AB, Life Technologies). Quantitative polymerase chain reaction was performed using ABI StepOnePlus under the following conditions: 50°C for 2 minutes, 95°C for 5 minutes, 40 cycles of 95°C for 15 seconds, and 60°C for minutes. Relative mRNA expression levels of *NOVA1* were determined by the comparative method ($2^{-\Delta\Delta C_t}$) against the reference *GAPDH*.

Statistical analysis

The Kruskal-Wallis (K-W), Mann-Whitney U (M-W), t and χ^2 tests were used to analyze differences between the variables ex-

amined. Survival rates were analyzed with the Kaplan-Meier method, and differences were compared using the log-rank test. Two-sided *p*-values less than .05 were considered statistically significant. Statistical analyses were done using the IBM SPSS ver. 22 (IBM Corp., Armonk, NY, USA).

RESULTS

Expression of NOVA1 in the palatine tonsils

The NOVA1 expression patterns in the cell nuclei were similar to those reported in a previous study.⁶ Stromal spindle cells/fibroblasts showed strong and constant expression of NOVA1. Endothelial cells variably expressed NOVA1 with negative to moderate intensity. Almost all B cells of the germinal centers or outside the germinal centers were negative for NOVA1. As for T cells, occasional expression of NOVA1 (intensity grade 2–3 with 5% or less percentage of T cells) was noted in the paracortical area (Table 1).

Expression of NOVA1 in T/NK-cell lymphomas

T/NK-cell lymphomas showed low to high NOVA1 expression and 99 (56.5%) showed high NOVA1 expression (Table 1, Fig. 1). The expression level (score) of NOVA1 was higher in tumor cells of T/NK-cell lymphomas when compared to normal T cells of tonsil tissues (mean score, 209 vs. 7; *p* < .001; non-parametric M-W) (Fig. 2A). Within T/NK-cell lymphomas,

precursor T-LBL showed a relatively higher level of NOVA1 expression than did NKTL or mature (peripheral) T-cell lymphomas, although a statistically significant difference was not noted (*p* = .226; K-W) (Fig. 2B). According to the specific subtypes of T/NK-cell lymphomas, the expression level of NOVA1 in tumor cells varied (*p* = .011; K-W). AITL, ALK-negative ALCL, and T-LBL showed relatively higher NOVA1 expression levels when compared to other subtypes (Table 1, Fig. 2C). Specifically, ALK-positive ALCL revealed a lower level of NOVA1 expression when compared to ALK-negative ALCL (mean score, 156 vs. 259; *p* = .027; M-W) and ALK-positive ALCL showed the lowest expression level among subtypes of T/NK-cell lymphomas (Table 1, Fig. 2C). The rate of high, intermediate, or low expression of NOVA1 was also different according to subtype (*p* < .001); high expression was relatively more frequent in AITL, ALK-negative ALCL, and T-LBL cells, while low expression was relatively more frequent in NKTL and ALK-positive ALCL (Table 1, Fig. 2D).

Expression of NOVA1 in DLBCLs

In DLBCL, high NOVA1 expression was not noted in any cases. The tested 151 DLBCL cases revealed an expression pattern with a score less than 10. Furthermore, in the various types of other B-cell lymphomas, high NOVA1 expression was not noted (Table 1, Fig. 3).

Table 1. NOVA1 expression in several types of normal and tumor immune cells

Tissue category	Case No.	General pattern	NOVA1 expression			H-score (mean)
			Frequency of expression category (%)			
			High	Intermediate	Low	
Palatine tonsils	20	Small numbers of T cells	0	0	100	7
T- and NK-cell lymphomas	177	Strong and diffuse	56.5	18.6	24.9	209
NKTL	60	Lower	54.2	13.6	32.2	195
PTCL-NOS	44	Diverse	38.6	40.9	20.5	194
AITL	16	Higher	81.2	6.2	12.5	255
ALK-negative ALCL	17	Higher	82.4	5.9	11.8	259
ALK-positive ALCL	16	Lower	40	13.3	46.7	156
T-LBL	20	Higher	75	5	20	237
Other types ^a	4	NA	25	50	25	175
B-Cell lymphomas	182	Almost negative	0	0	100	7
DLBCL	151	Almost negative	0	0	100	8
Other types ^b	31	Almost negative	0	0	100	5

NOVA1, neuro-oncological ventral antigen 1; NK, natural killer; NKTL, extranodal natural killer/T-cell lymphoma, nasal type; PTCL-NOS, peripheral T-cell lymphoma, not otherwise specified; AITL, angioimmunoblastic T-cell lymphoma; ALK, anaplastic lymphoma kinase; ALCL, anaplastic large cell lymphoma; T-LBL, T lymphoblastic leukemia/lymphoma; DLBCL, diffuse large B-cell lymphoma.

^aThe T- or NK-cell lymphomas of the “other type” category included hepatosplenic T-cell lymphoma (*n* = 2), subcutaneous panniculitis-like T-cell lymphoma (*n* = 1), and cutaneous gamma-delta T-cell lymphoma (*n* = 1). The case number for this category was too small (only 4 cases), and therefore NOVA1 expression may not be representative for this category; ^bThe set of “other type” B-cell lymphomas was composed of follicular lymphoma (*n* = 14), mantle cell lymphoma (*n* = 5), marginal zone B-cell lymphoma (*n* = 7), and Burkitt lymphoma (*n* = 5).

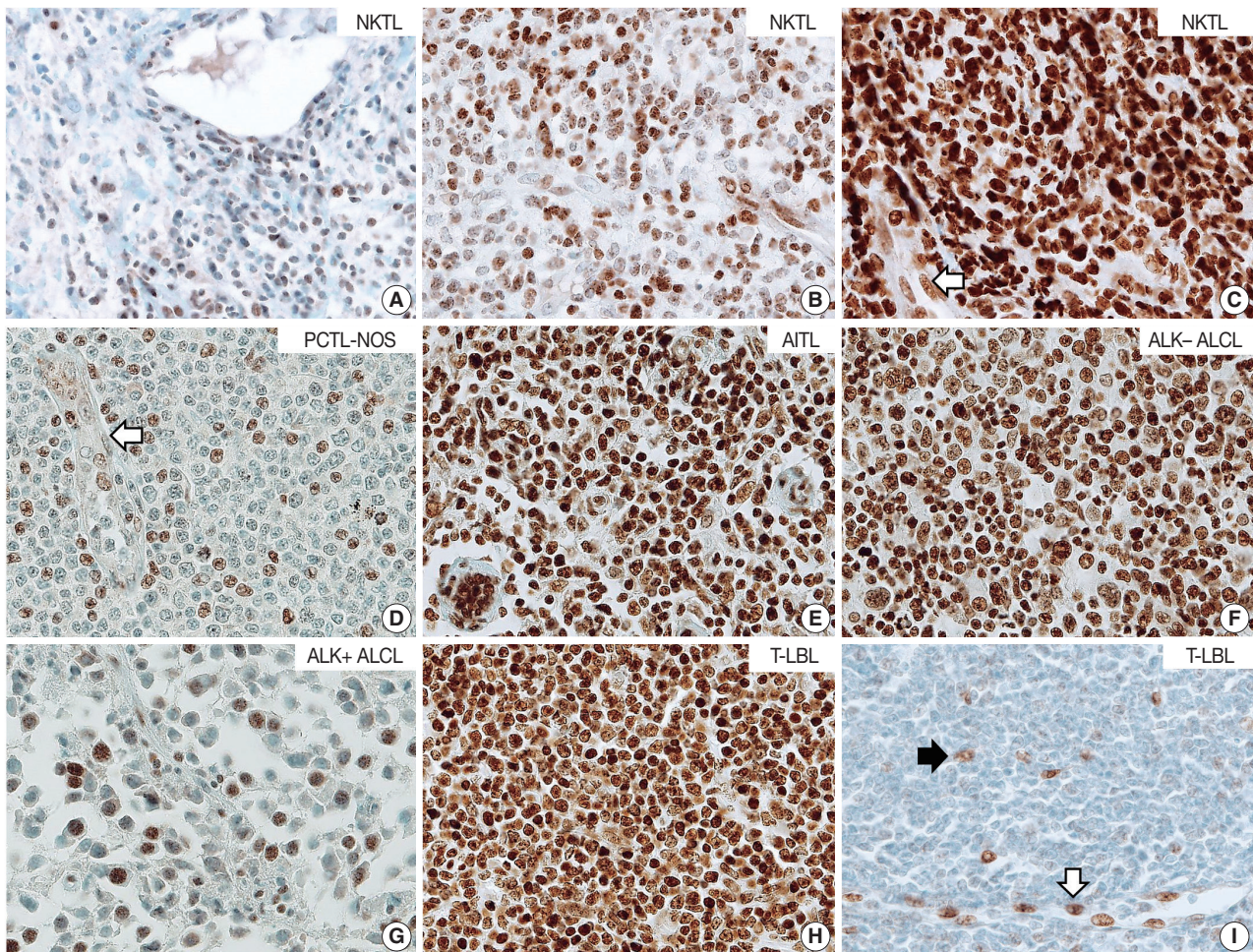


Fig. 1. Representative cases of T- and natural killer (NK)-cell lymphoma. Representative cases of extranodal NK/T-cell lymphoma, nasal type (NKTL) are presented, which show low (A), intermediate (B), and high (C) levels of neuro-oncological ventral antigen 1 (NOVA1) expression. Among mature (peripheral) T-cell lymphoma cases, low to high expression of NOVA1 is variably observed (D–G). (D) A case of peripheral T cell lymphoma, not otherwise specified (PTCL-NOS), reveals low NOVA1 expression. A case of angioimmunoblastic T-cell lymphoma (AITL) (E) and a case of anaplastic lymphoma kinase (ALK)-negative anaplastic large cell lymphoma (ALCL) (F) exhibits high NOVA1 expression. A case of ALK-positive ALCL (G) demonstrates low NOVA1 expression. A case of precursor T lymphoblastic lymphoma/leukemia (T-LBL) (H) shows high NOVA1 expression while a case of T-LBL shows low NOVA1 expression. Endothelial cells exhibit high or low NOVA1 expression in accordance with the NOVA1 status of tumor T cells (white arrow in panels in C and D). In cases where most tumor cells showed negative NOVA1 expression, stromal fibroblasts (black arrow in panel I) and endothelial cells (white arrow in panel I) demonstrate positive NOVA1 expression.

NOVA1 gene expression in human lymphoma cell lines

NOVA1 mRNA was expressed only in the Jurkat cell line, which corresponds to T-LBL. NOVA1 mRNA was not detected in other tested cell lines of HH (correspondent to peripheral, mature T cell lymphoma), MAC1 (peripheral, mature T-cell lymphoma), SNK6 (NKTL), YT (NK cell leukemia), or Toledo (DLBCL) (Fig. 4).

NOVA1 expression and its clinicopathologic correlation in T/NK-cell lymphomas

The NOVA1 expression level in tumor cells was not different

according to the organ/sites where lymphomas were growing (Appendix 3). The known clinicopathological prognostic factors such as age, lactate dehydrogenase level, Ann-Arbor stage, or International Prognostic Index (IPI) risk scores showed no correlation with NOVA1 expression. In cases of mature (peripheral) T-cell lymphomas, high expression of NOVA1 tended to be related to shorter overall survival rate in comparison to low or intermediate NOVA1 expression, although statistical significance was not observed (Fig. 5A, B). In other subtypes, such as NKTL and T-LBL, no correlation was noted between NOVA1 expression and overall survival rate.

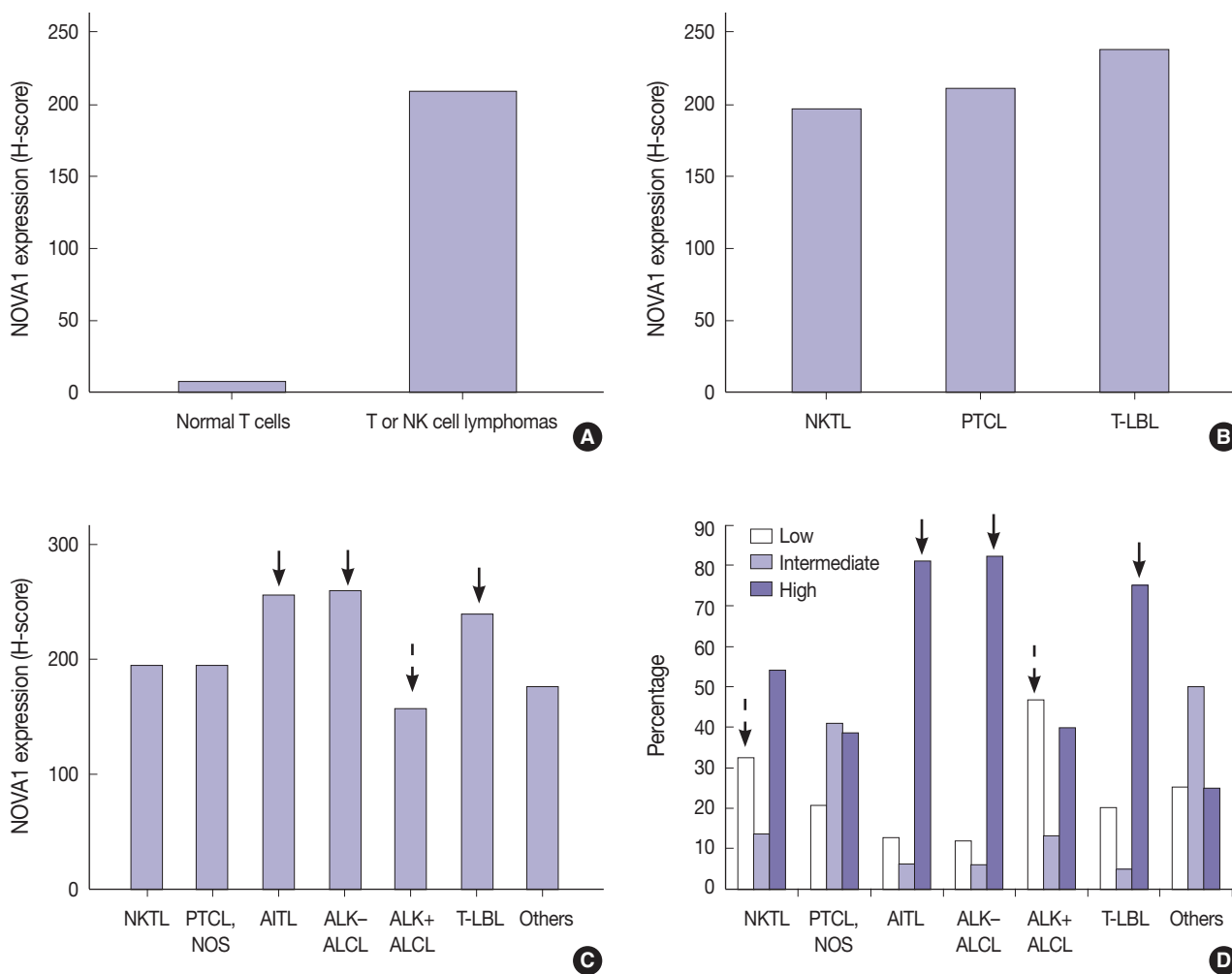


Fig. 2. Expression level of neuro-oncological ventral antigen 1 (NOVA1) in T- and natural killer (NK) cell lymphomas and normal T cells. (A) Expression level (score) of NOVA1 is higher in tumor cells of T/NK-cell lymphomas when compared to normal T cells of tonsil tissues (mean score, 7 vs 209; $p < .001$). (B) Within T/NK-cell lymphomas, T lymphoblastic leukemia/lymphoma (T-LBL) shows relatively higher levels of NOVA1 expression than do extranodal NK/T-cell lymphoma, nasal type (NKTL) or mature (peripheral) T-cell lymphomas, although a statistically significant difference is not noted ($p = .226$). (C) According to the specific subtypes of T/NK-cell lymphomas, the expression levels of tumor cells are different ($p = .012$). Angioimmunoblastic T-cell lymphoma (AITL), anaplastic lymphoma kinase (ALK)-negative anaplastic large cell lymphoma (ALCL), and T-LBL shows a relatively higher level of NOVA1 expression (arrow) when compared to other subtypes. ALK-positive ALCL reveals lower NOVA1 expression (dotted arrow) when compared to ALK-negative ALCL (mean score, 159 vs 256; $p = .027$) and ALK-positive ALCL shows the lowest expression among subtypes of T/NK cell lymphomas. (D) The rates of high, intermediate, and low expression of NOVA1 are different according to subtype ($p < .001$); high expression is relatively more frequent in AITL, ALK-negative ALCL, and T-LBL (solid arrow), while low expression is relatively more frequent in ALK-positive ALCL and NKTL (dotted arrow). The case number in the “others” category is too small (only 4 cases), and therefore, the NOVA1 expression may not be representative of this category. PTCL, peripheral T-cell lymphoma; PTCL-NOS, peripheral T-cell lymphoma, not otherwise specified.

DISCUSSION

In this study, we found that NOVA1 was frequently and highly expressed in various subtypes of T/NK-cell lymphomas, with about 60% of T/NK-cell lymphoma cases showing high NOVA1 expression, whereas only a small number of T cells expressed NOVA1 in the hyperplastic palatine tonsils. As for B-cell lymphomas,

NOVA1 was negative in various types of B-cell lymphomas other than DLBCL, or normal B cells. In DLBCL, NOVA1 was expressed in a few cases; however, high expression was not noted in any cases.

Our previous study⁶ revealed high expression of NOVA1 in activated T cells and the present study also confirmed that finding. Moreover, NOVA1 was upregulated in lymphomas derived

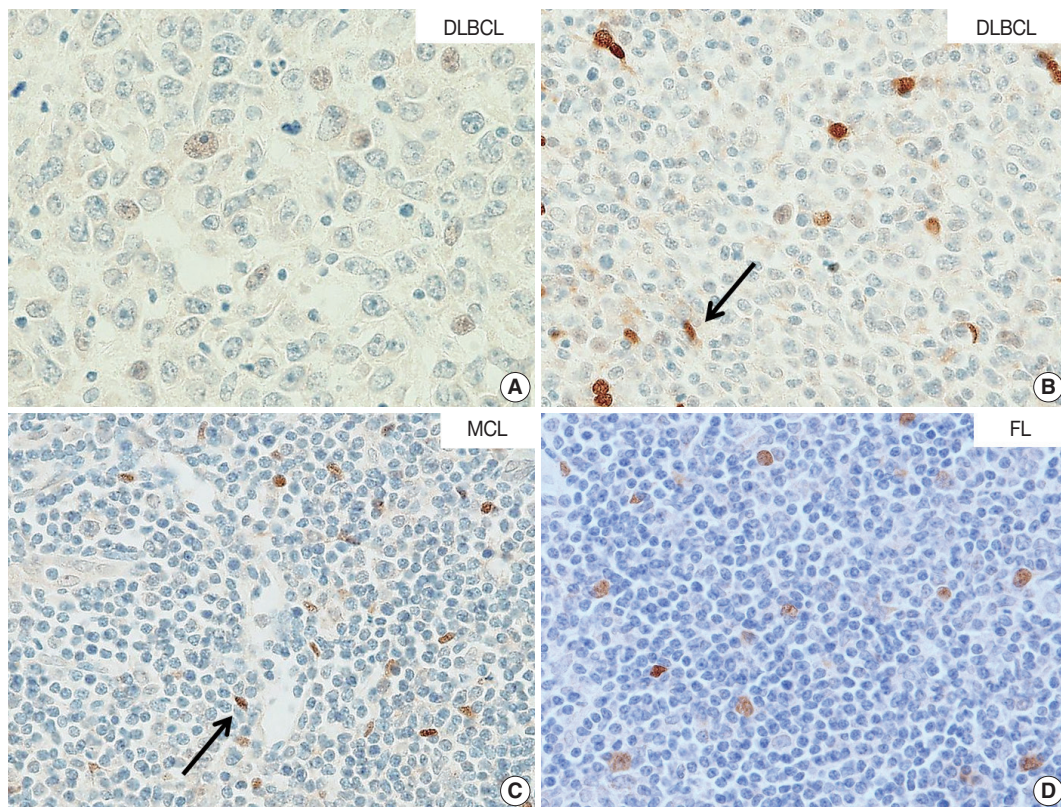


Fig. 3. Neuro-oncological ventral antigen 1 (NOVA1) expression in B-cell lymphomas. (A, B) In the representative cases of diffuse large B-cell lymphoma (DLBCL), almost all tumor cells are negative for NOVA1. In some DLBCL cases, NOVA1-expressing fibroblasts/stromal support cells are occasionally found throughout the microenvironment (arrow in panel B). (C, D) In cases of mantle cell lymphoma (MCL) or follicular lymphoma (FL), tumor cells are negative for NOVA1, and fibroblasts/stromal support cells are positive for NOVA1 (arrow).

from immature T cells such as precursor T-LBL and NKTL. However, in contrast to T/NK cells, NOVA1 might not be involved in B cell lesions, either malignant lymphomas or non-neoplastic B cells, as shown in our studies.

Among subtypes of T/NK-cell lymphomas, the expression level in tumor cells was different. Regarding the different biological characteristics and pathogenesis of each subtype of T/NK-cell lymphoma, NOVA1 expression may be affected by various intrinsic biological factors related to each subtype. The AITL, ALK-negative ALCL, and T-LBL subtypes, which showed distinctively high NOVA1 expression, are biologically characteristic entities.¹¹ Interestingly, the NOVA1 expression pattern was different even within ALCL specimens, according to ALK expression status. ALK-negative ALCL showed distinctively high NOVA1 expression while ALK-positive ALCL exhibited low NOVA1 expression. Both types of ALCL share common morphologic features of CD30 positivity, large anaplastic “hallmark” cells, frequent loss of pan-T-cell antigens, and expression of cytotoxic molecules, and are classified as the same disease. However, ALK-positive ALCL and ALK-negative ALCL are thought to be

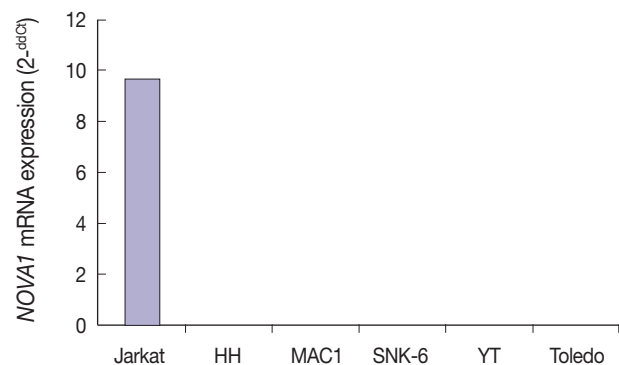


Fig. 4. Neuro-oncological ventral antigen 1 (NOVA1) mRNA expression in various cell lines. NOVA1 mRNA are expressed only in Jurkat cell lines, which correspond to T lymphoblastic leukemia/lymphoma. NOVA1 mRNA are not detected in other tested cell lines of HH, MAC1, SNK6, YT, or Toledo.

different entities; the clinical features, prognosis, and gene expression signatures have been noted to be different.¹¹ Therefore, the differences in NOVA1 expression may be related to the intrinsic biologic characteristics of these two types. There are no known studies that can explain the distinctively low NOVA1

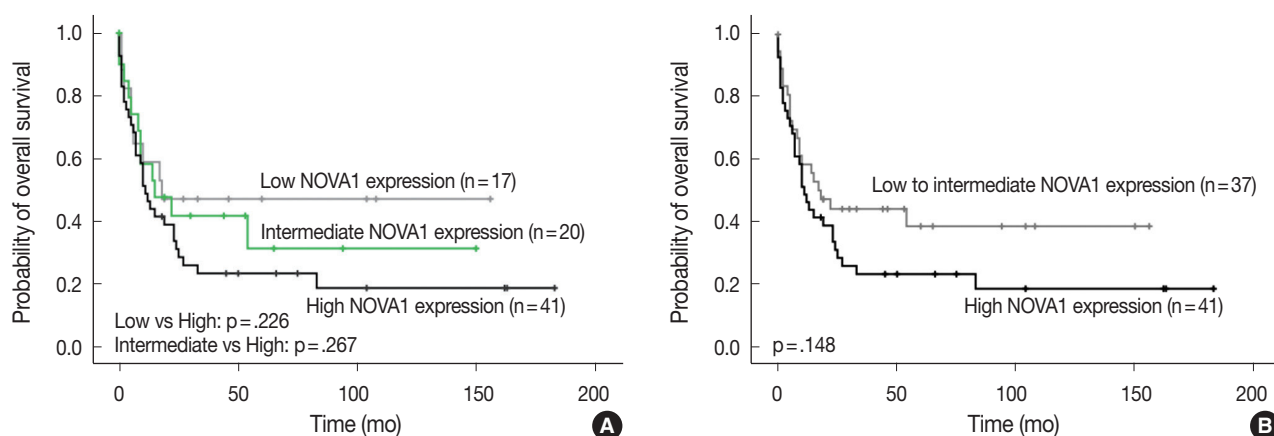


Fig. 5. Patient overall survival according to neuro-oncological ventral antigen 1 (NOVA1) expression in peripheral T-cell lymphoma, not otherwise specified; three-tiered (A) and two-tiered (B) analysis by Kaplan-Meier with log-rank test. High expression of NOVA1 tends to be related to shorter overall survival than low or intermediate expression, although statistical significance is not observed.

expression in ALK-positive ALCL. We thought that nucleophosmin (NPM), the fusion partner of ALK-NPM translocation/ $t(2;5)$ in ALK-positive ALCLs, may be associated. NPM is a putative ribosome assembly factor involved in processing pre-RNA molecules.¹³ Mutated NPM molecules are abnormally localized in the cytoplasm because of impaired nuclear localization, and this abnormal localization of NPM is thought to be associated with abnormal ribosome biogenesis.¹³ The aberrant function of mutated NPM may be related to inhibiting NOVA1 function in the splicing process of pre-RNA molecules via abnormal ribosome biogenesis. PTCL-NOS showed a relatively diverse pattern of NOVA1 expression. The proportion of cases showing an intermediate level of NOVA1 expression was relatively higher than that in other subtypes. This difference may be because PTCL-NOS is a disease group of heterogeneous entities of mature (peripheral) T-cell lymphomas.

NOVA1 expression did not vary according to the organ site where the lymphoma developed. These findings indicate that NOVA1 expression may be primarily dependent on the intrinsic characteristics of the tumor cell itself rather than extrinsic factors such as the organ-specific microenvironment, which is pre-formed before tumor growth. In association with patient prognosis, NOVA1 expression showed no statistical significance. However, in mature (peripheral) T-cell lymphomas, high NOVA1 expression tended to be related to an inferior overall survival rate. In our previous study, high NOVA1 expression levels in reactive, non-neoplastic (mature) T cells, which accumulate within the tertiary lymphoid structures of gastric carcinoma microenvironment, were associated with favorable patient prognosis. Suppression of NOVA1 in such reactive T cells was related with poor patient prognosis, and this effect is thought to be related to the

suppression of regulatory T cell functions.⁶ From these findings, the role of NOVA1 in tumor T cells of malignant lymphomas and non-tumor T cells of tissues seems to be different. In normal physiologic conditions, NOVA1 upregulation seems to be involved in normal immune regulation. In neoplastic T cells, however, NOVA1 upregulation seems to be involved in tumor progression.

Alternative splicing of pre-mRNA is the main mechanism of transcriptome and proteome diversity,^{4,14} and the splicing program relies on the action of splicing factors¹ like NOVA1. The action of splicing factors is cell type-specific and independent of organ origin.^{2,3,5} Previous studies have suggested or shown that normal and tumorous hematopoietic cells are regulated by specific alternative splicing programs and alternative transcript variants such as *c-myc*, a transcription factor of hematopoietic cells; CD45, a transmembrane protein tyrosine phosphatase of T cells, B cells, and other hematopoietic cells; and CD20, a surface marker of mature B cells.¹⁵⁻¹⁷ Likewise, NOVA1 may work as an alternative splicing factor in the lymphoreticular system and in lymphomagenesis of T/NK-cell lineage.

Among the tested cell lines, only Jurkat cells, which corresponded to immature T cells, expressed the *NOVA1* gene. These findings could partially support the findings observed in clinical patient samples. The functional role of NOVA1 in lymphoid cells and target genes regulated by NOVA1 in lymphomagenesis should be identified through further studies.

In summary, NOVA1 was frequently upregulated in various subtypes of T/NK-cell lymphomas. NOVA1 expression may be a new biomarker for T/NK-cell lymphomas and should be studied as a possible therapeutic target for this type of lymphoma.

Conflicts of Interest

No potential conflict of interest relevant to this article was reported.

Acknowledgments

The study was supported by the Basic Science Research Program through the National Research Foundation of Korea (NRF) funded by the Ministry of Education, Science and Technology (2012R1A1A2007344).

REFERENCES

1. Barash Y, Calarco JA, Gao W, *et al.* Deciphering the splicing code. *Nature* 2010; 465: 53-9.
2. de la Grange P, Gratadou L, Delord M, Dutertre M, Auboeuf D. Splicing factor and exon profiling across human tissues. *Nucleic Acids Res* 2010; 38: 2825-38.
3. Merkin J, Russell C, Chen P, Burge CB. Evolutionary dynamics of gene and isoform regulation in mammalian tissues. *Science* 2012; 338: 1593-9.
4. Kalsotra A, Cooper TA. Functional consequences of developmentally regulated alternative splicing. *Nat Rev Genet* 2011; 12: 715-29.
5. Mallinjoind P, Villemin JP, Mortada H, *et al.* Endothelial, epithelial, and fibroblast cells exhibit specific splicing programs independent of their tissue of origin. *Genome Res* 2014; 24: 511-21.
6. Yoon SO, Kim EK, Lee M, *et al.* NOVA1 inhibition by miR-146b-5p in the remnant tissue microenvironment defines occult residual disease after gastric cancer removal. *Oncotarget* 2016; 7: 2475-95.
7. Drayton DL, Liao S, Mounzer RH, Ruddle NH. Lymphoid organ development: from ontogeny to neogenesis. *Nat Immunol* 2006; 7: 344-53.
8. Ruddle NH, Akirav EM. Secondary lymphoid organs: responding to genetic and environmental cues in ontogeny and the immune response. *J Immunol* 2009; 183: 2205-12.
9. Buckley CD, Barone F, Nayar S, Bénézech C, Caamaño J. Stromal cells in chronic inflammation and tertiary lymphoid organ formation. *Annu Rev Immunol* 2015; 33: 715-45.
10. Kalluri R, Zeisberg M. Fibroblasts in cancer. *Nat Rev Cancer* 2006; 6: 392-401.
11. Swerdlow SH, Campo E, Harris NL, *et al.* WHO classification of tumours of haematopoietic and lymphoid tissues. 4th ed. Lyon: IARC Press, 2008.
12. Park E, Park SY, Kim H, *et al.* Membranous insulin-like growth factor-1 receptor (IGF1R) expression is predictive of poor prognosis in patients with epidermal growth factor receptor (EGFR)-mutant lung adenocarcinoma. *J Pathol Transl Med* 2015; 49: 382-8.
13. Falini B, Nicoletti I, Bolli N, *et al.* Translocations and mutations involving the nucleophosmin (*NPM1*) gene in lymphomas and leukemias. *Haematologica* 2007; 92: 519-32.
14. Kelemen O, Convertini P, Zhang Z, *et al.* Function of alternative splicing. *Gene* 2013; 514: 1-30.
15. Oberdoerffer S, Moita LF, Neems D, Freitas RP, Hacohen N, Rao A. Regulation of CD45 alternative splicing by heterogeneous ribonucleoprotein, hnRNPLL. *Science* 2008; 321: 686-91.
16. O'Rourke JP, Ness SA. Alternative RNA splicing produces multiple forms of c-Myb with unique transcriptional activities. *Mol Cell Biol* 2008; 28: 2091-101.
17. Henry C, Deschamps M, Rohrlisch PS, *et al.* Identification of an alternative CD20 transcript variant in B-cell malignancies coding for a novel protein associated to rituximab resistance. *Blood* 2010; 115: 2420-9.

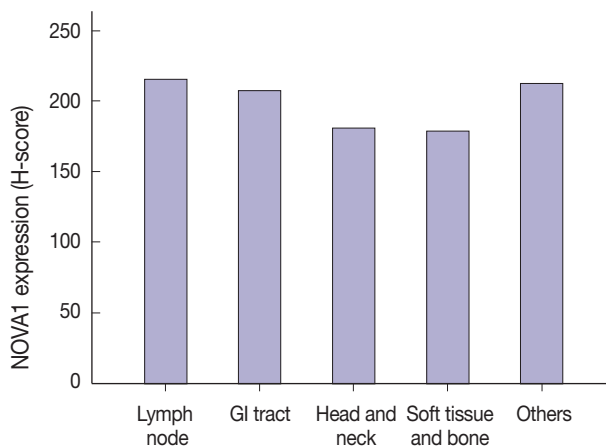
Appendix 1. Clinicopathological characteristics of T/NK-cell lymphoma cases

Characteristic	No. (%) (n = 139)
Sex (male vs female)	94 (67.1):45 (32.9)
Age (<60 yr vs ≥60 yr)	91 (65.0):49 (35.0)
Subtype	
NKTL	45 (32.4)
PTCL	38 (27.3)
AITL	14 (10.1)
ALCL, ALK-negative	12 (8.6)
ALCL, ALK-positive	12 (8.6)
T-LBL	15 (10.8)
Others	3 (2.2)
Primary site of tumor	
H&N vs LN vs GI vs soft tissue and bone vs others (solid organs)	37 (26.4):72 (51.4):9 (6.4):14 (10.0):8 (5.7)
Ann Arbor stage (I & II vs III&IV vs not evaluable)	29 (27.9):77 (55.0):34 (24.3)
LDH level (normal vs elevated vs not evaluable)	39 (27.9):60 (42.9):41 (29.3)
BM involvement (absent vs present vs not evaluable)	77 (55.0):33 (23.6):30 (21.4)
IPI score (0–2 vs 3–5 vs not evaluable)	65 (46.4):43 (30.7):32 (22.9)
Initial treatment modality	
CTx alone vs CTx with RTx vs RTx alone vs no Tx vs not evaluable	63 (45.0):27 (19.3):1 (0.7):1 (0.7):48 (34.3)

NK, natural killer; NKTL, extranodal natural killer/T-cell lymphoma, nasal type; PTCL, peripheral T-cell lymphoma; AITL, angioimmunoblastic T-cell lymphoma; ALCL, anaplastic large cell lymphoma; ALK, anaplastic lymphoma kinase; T-LBL, T lymphoblastic leukemia/lymphoma; H&N, head and neck; LN, lymph node; GI, gastrointestinal tract; LDH, lactate dehydrogenase; BM, bone marrow; IPI, International Prognostic Index; CTx, chemotherapy; RTx, radiotherapy; Tx, treatment.

Appendix 2. List of primary antibodies and their dilutions

Antibody	Dilution	Type	Company
CD20	1:1600	Mouse	DAKO, Glostrup, Denmark
CD3	1:200	Rabbit	LabVision, Fremont, CA, USA
CD4	1:200	Rabbit	Cell Marque, Rocklin, CA, USA
CD8	1:100	Mouse	Cell Marque, Rocklin, CA, USA
CD56	1:200	Rabbit	Cell Marque, Rocklin, CA, USA



Appendix 3. Neuro-oncological ventral antigen 1 (NOVA1). NOVA1 protein expression in various organ/sites of lymphomas. NOVA1 expression level in tumor cells does not vary according to the organ/sites where lymphomas were growing. GI, gastrointestinal.

Meningeal Solitary Fibrous Tumors with Delayed Extracranial Metastasis

Nayoung Han^{1*} · Hannah Kim^{1*}
Soo Kee Min² · Sun-Ha Paek³
Chul-Kee Park³ · Seung-Hong Choi⁴
U-Ri Chae⁵ · Sung-Hye Park^{1,6}

¹Department of Pathology, Seoul National University College of Medicine, Seoul;

²Department of Pathology, Hallym University Sacred Heart Hospital, Hallym University

College of Medicine, Anyang; Departments of ³Neurosurgery and ⁴Radiology, Seoul National University College of Medicine, Seoul;

⁵Department of Industrial Engineering, Ajou University, Suwon; ⁶Neuroscience Institute, Seoul National University College of Medicine, Seoul, Korea

Received: August 3, 2015

Revised: October 11, 2015

Accepted: October 30, 2015

Corresponding Author

Sung-Hye Park, MD

Department of Pathology, Seoul National University College of Medicine, 103 Daehak-ro, Jongno-gu, Seoul 03080, Korea

Tel: +82-2-740-8278

Fax: +82-2-765-5600

E-mail: shparknp@snu.ac.kr

*Nayoung Han and Hannah Kim contributed equally to this work.

Background: The term solitary fibrous tumor (SFT) is preferred over meningeal hemangiopericytoma (HPC), because *NAB2-STAT6* gene fusion has been observed in both intracranial and extracranial HPCs. HPCs are now considered cellular variants of SFTs. **Methods:** This study analyzes 19 patients with STAT6-confirmed SFTs, who were followed for over 11 years in a single institution. Ten patients (10/19, 56.2%) had extracranial metastases (metastatic group), while the remainder (9/19) did not (non-metastatic group). These two groups were compared clinicopathologically. **Results:** In the metastatic group, the primary metastatic sites were the lungs (n=6), bone (n=4), and liver (n=3). There was a mean lag time of 14.2 years between the diagnosis of the initial meningeal tumor to that of systemic metastasis. The median age at initial tumor onset was 37.1 years in the metastatic group and 52.5 in the non-metastatic group. The 10-year survival rates of the metastatic- and non-metastatic groups were 100% and 33%, respectively. The significant prognostic factors for poor outcomes on univariate analysis included advanced age (≥ 45 years) and large initial tumor size (≥ 5 cm). In contrast, the patients with higher tumor grade, high mitotic rate ($\geq 5/10$ high-power fields), high Ki-67 index ($\geq 5\%$), and the presence of necrosis or CD34 positivity showed tendency of poor prognosis but these parameters were not statistically significant poor prognostic markers. **Conclusions:** Among patients with SFTs, younger patients (< 45 years) experienced longer survival times and paradoxically had more frequent extracranial metastases after long latent periods than did older patients. Therefore, young patients with SFTs require careful surveillance and follow-up for early detection of systemic metastases.

Key Words: Central nervous system; Hemangiopericytoma; Neoplasm metastases; *NAB2-STAT6* gene fusion; Solitary fibrous tumors

Solitary fibrous tumors (SFTs), first described in 1931 by Kiemperer and Coleman,¹ are rare spindle-cell mesenchymal tumors that often arise in the pleural cavity. However, SFTs can arise in the extrapleural sites such as thoracic wall, mediastinum, pericardium, retroperitoneum, and abdominal cavity. They can also occur in the subcutaneous and deep soft tissues of the extremities and extracompartmentally in the head and neck.^{1,2} More than 100 cases of intracranial SFTs have been reported to date. However, the exact incidence of intracranial SFTs is unknown. The current consensus is that extracranial hemangiopericytomas (HPCs) and SFTs are synonymous. Such tumors should be called SFTs (rather than HPCs), because HPCs do not originate from or differentiate into pericytes.² The prototypical pericytic neoplasms are myopericytomas and sinonasal HPCs.² However, in

the central nervous system (CNS), HPCs and SFTs exhibit distinct biological behavior, and are therefore considered separate entities. For instance, intracranial HPCs tend to be aggressive, while intracranial SFTs are typically relatively benign.³

Recently, *NAB2-STAT6* gene fusions have been identified using whole-exome sequencing in intracranial and extracranial soft tissue HPCs and SFTs.⁴ Therefore, the use of a single, unifying term to describe intracranial SFTs is preferred than HPCs with the HPC morphology implies a “cellular and aggressive variant,” and SFT morphology a “fibrous and benign variant” of the same disease.⁵

Meningeal HPCs commonly occur around the same age as do meningiomas (range, 26 to 73 years; mean, 48 years). However, compared to meningiomas, HPCs are more common in men

than in women.⁶ According to PISTOLESI *et al.*'s report,⁷ the mean time to the first local recurrence and to the appearance of extracranial metastases of meningeal HPCs were 3.9 years and 8.3 years, respectively. The 10-year survival rate was 83.9%.⁶

This study was designed to clarify the clinicopathological characteristics of metastatic and non-metastatic meningeal SFTs. We analyzed meningeal SFTs (cellular variant) displaying extracranial dissemination, and compared them with non-metastatic meningeal SFTs. Patients with metastatic meningeal SFTs (metastatic group) were significantly younger than were those with non-metastatic tumors (non-metastatic group). Interestingly, the metastatic group exhibited better long-term survival than did the non-metastatic group.

MATERIALS AND METHODS

All cases of meningeal SFTs/HPCs between January 1995 and

January 2013 were retrieved from the pathology archives at the Seoul National University Hospital (SNUH). We selected cases that matched the search term “solitary fibrous tumor” or “hemangiopericytoma,” and 48 cases of meningeal HPCs/SFTs were selected from this 18-year period. There was no sex predominance. The mean patient age was 48.1 years (range, 21 to 77 years). We selected 19 cases of pathologically and STAT6 immunohistochemically confirmed meningeal SFTs that were followed up for more than 11 years. Ten cases presented with systematic extracranial metastases (metastatic group), while nine had no extracranial metastases (non-metastatic group). The medical and pathological records of the 19 cases are summarized in Table 1.

Two pathologists (N.H and S.-H.P) performed all of the pathological reviews. A Ventana autostainer was used for immunohistochemical staining, according to the manufacturer guidelines. Primary antibodies against STAT6 (1:1,000, clone Sc-621, Santa Cruz Biotechnology, Santa Cruz, CA, USA), CD34 (1:200,

Table 1. Summary of the patients with and without meningeal SFT/HPC and extracranial metastasis, treated in Seoul National University Hospital (SNUH)

No.	Age at first diagnosis (yr)	Sex	Dx	Site	Site of metastasis	Symptoms	Initial Tx	Adjuvant Tx	Local recurrence	Time for metastasis (yr)	Mortality and cause of death
1	26	F	HPC	Cerebellum	Bone, lung	Headache	GTR	RT	No	11.3	DBD
2	56	F	HPC	Rt. frontal	Lung	L/E weakness	GTR	CT (VIP #1)	Yes	11.0	DBD
3	24	F	HPC	Lt. occipital	Liver	Headache	GTR	GKS, CT (ifosfamide #1)	Yes	17.6	Alive
4	36	M	HPC	Lt. sagittal	Bone	Headache	STR	RT	Yes	11.7	Alive
5	52	F	HPC	Rt. temporal	Bone, EAC	Headache	GTR	GKS, RT	Yes	5.7	DBD
6	30	M	HPC	Rt. CPA	Lung, liver, orbit, spinal cords	Dizziness	GTR	Cyberknife	Yes	5.6	DBD
7	32	M	HPC	Lt. T-P-O	Lung	Headache	GTR	GKS	Yes	22.8	Alive
8	44	M	HPC	Cerebellum	Bone, lung	Headache, L/E weakness	GTR	GKS, RT	Yes	24.2	DBD
9	29	F	HPC	Lt. frontal	Lung	Incidental	GTR	None	No	22.1	Alive
10	43	F	SFT	Rt. F-T	Liver, breast, lung	Double vision	GTR	Preop-RT	No	10.3	Alive
11	73	F	HPC	Rt. fronto-parietal	NA	L/E weakness	GTR	Re-GTR	Yes	NA	Alive
12	47	F	HPC	Lt. frontal	NA	Thyroid cancer work up	GTR	None	Unknown	NA	Death
13	34	M	HPC	Cerebellum	NA	Headache	GTR	RT	No	NA	Alive
14	61	F	HPC	Lt. occipital	NA	Headache	GTR	GKS, RT	Yes	NA	DBD
15	62	F	HPC	Medial parietal	NA	L/E weakness	GTR	GKS, RT	Yes	NA	DBD
16	58	F	HPC	Parasagittal	NA	Unknown	GTR	Unknown	Unknown	NA	Death
17	50	M	HPC	Lt. parietal	NA	Unknown	GTR	Unknown	Unknown	NA	Death
18	53	F	SFT	Rt. parietal	NA	Visual disturbance	GTR	None	No	NA	Alive
19	35	F	HPC	Falx	NA	Headache	GTR	None	Unknown	NA	Death

SFT, solitary fibrous tumor; HPC, hemangiopericytoma; Tx, therapy; F, female; HPC, hemangiopericytoma; GTR, gross total resection; RT, radiotherapy; DBD, death by disease; Rt., right; L/E, lower extremity; CT, chemotherapy; VIP, VP-16, ifosfamide, cisplatin; Lt., left; GKS, gamma knife surgery; M, male; STR, subtotal resection; EAC, external auditory canal; CPA, cerebellopontine angle; T-P-O, temporoparietooccipital lobe; SFT, solitary fibrous tumor; F-T, frontotemporal; NA, not applicable.

Dako, Glostrup, Denmark), epithelial membrane antigen (EMA; Dako, 1:200), and MIB-1 (Ki-67) (Dako, 1:1,000) were used. A verified SFT or antibody-specific known positive control was used as a positive control. The primary antibodies were omitted in the negative control. For STAT6, robust nuclear positivity in >90% of the tumor cells was considered positive. For CD34, cytoplasmic staining in >10%, and for EMA, membranous staining in >10% of the tumor cells were considered positive. A nuclear algorithm of the Aperio ScanScope image analysis program (Aperio Technologies, Vista, CA, USA) was used to calculate the nuclear positivity in hot spots for the Ki-67 labeling index.

Statistical analyses were performed using Fisher exact tests. Kaplan-Meier survival analysis was performed to compare overall survival according to the patients' age, tumor grade, mitoses, necrosis, Ki-67 labeling index, CD34 expression, and the occurrence of systemic metastasis. All statistical analyses were carried out using SPSS ver. 22 (IBM Co., Armonk, NY, USA).

The mean patient ages in the metastatic and non-metastatic groups were 37.1 years (range, 26.1 to 55.9 years) and 52.5 years (range, 34 to 76.2 years), respectively (Table 2). The mean follow-up periods for the metastatic and non-metastatic groups were 215 months (range, 124 to 351 months) and 99 months (range, 33 to 174 months), respectively. This study was designed to clarify the clinicopathological characteristics of metastatic and non-metastatic meningeal SFTs. In order to identify prognostic factors, several parameters were compared between the two groups, including Ki-67 labeling indices, mitotic rates, initial meningeal tumor size, and the presence or absence of necrosis.

This study abides by the World Medical Association Declaration of Helsinki recommendations. It was approved by the Institutional Review Board of Seoul National University Hospital (IRB No. 1501-046-639).

RESULTS

Six of the ten patients in the metastatic group were women, and four were men. There was an average age of 37.1 years

(range, 24 to 56 years). The initial symptoms included headache (6 patients), lower extremity weakness (2), double vision (1), and dizziness (1). In one patient, the diagnosis was an incidental finding. The disease originated in the supratentorial region in eight patients, and in the posterior fossa in the other two. There was no intracranial predilection site. Nine patients underwent gross total resections (GTR) of their tumors, while one (case 4) had a partial resection.

Radiologically, the tumors were large, well-enhanced, solid, and cystic masses attached to the dura. Typically, they had intratumoral vessels, and exhibited a severe mass effect. One patient (case 10) underwent preoperative radiotherapy (RT; 54 Gy) due to the tumor's excessive size (6.5 × 5.8 × 5.5 cm) (Fig. 1A). The solid and cystic tumor decreased in size, as evidenced by a post-RT brain magnetic resonance imaging (Fig. 1B). Nine of the 10 patients in this group were treated with adjuvant therapies following GTR (Table 1). The types of adjuvant therapy included gamma knife surgery (GKS) in four patients, RT in three, Cyberknife RT in one, and chemotherapy in one.

In the non-metastatic group, all patients underwent GTR. During the follow-up period, one patient received RT and two received RT + GKS (Table 1).

In the metastatic group, seven patients (70%) had extracranial metastases after local recurrence was detected. In the remaining three, the tumors metastasized without local recurrence. Common extracranial metastatic sites included the lungs (6 patients), bone (4), and liver (3). Other less frequent metastatic sites included the breast (1 patient), orbit (1), and external auditory canal (1). When the disease was metastatic to the bone, common sites included the vertebrae, femur, and ischium. When the tumor invaded the lungs and bone, multiple metastases were observed. In contrast, metastatic foci in the liver and breast were usually single masses (Fig. 2). However, lymph node enlargement or lymph node metastases were not present. The average time from the initial diagnosis of a meningeal tumor to systemic metastasis was 14.2 years (range, 5.6 to 24.2 years). The findings of these 10 cases with systemic metastasis are summarized in Table 1.

Table 2. The differences between the meningeal SFTs according to the presence or absence of systemic metastases

Item	SFT with systemic metastases (metastatic group, n = 10)	SFT without systemic metastases (non-metastatic group, n = 9)
Age (yr)	37 (24.1–55.9)	51 (33.9–76.4)
Median mitotic rate	7/10 HPF (1–27)	7/10 HPF (1–26)
Median Ki-67 labeling index (%)	5.0	6.0
Median tumor size (cm)	3.5 (2.2–6.0)	5.0 (1.5–7.5)
Median survival	202 mo (16.8 yr)	56 mo (4.7 yr)

SFT, solitary fibrous tumor; HPF, high-power field.

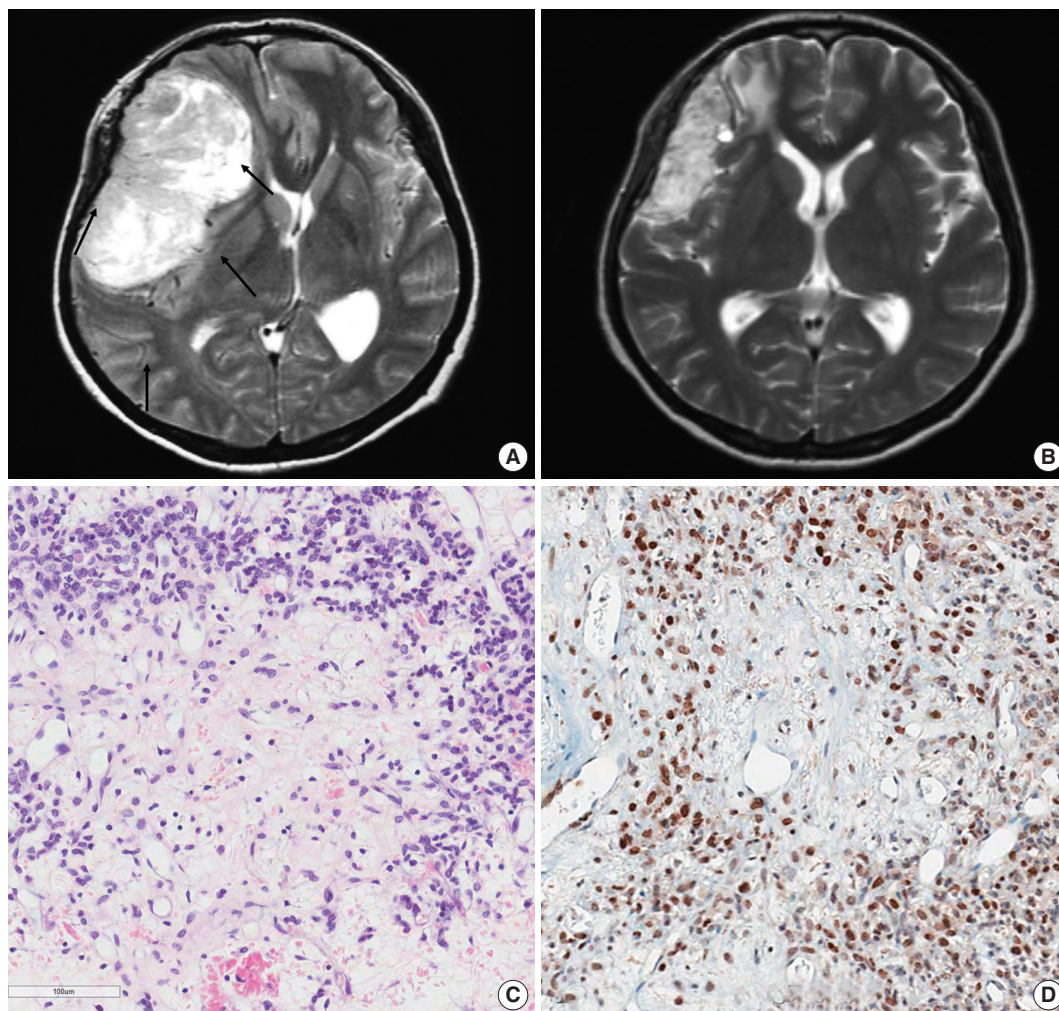


Fig. 1. Representative brain magnetic resonance images and histopathology of the primary brain tumor from case 10. (A) Prior to radiation therapy. A large, solid and cystic mass is observed in the right frontoparietal lobe with strong enhancement. There was severe mass effect. Intratumoral vessels were identified. (B) After preoperative radiation therapy. The tumor decreased in the size after radiation therapy. (C) The tumor demonstrates low cellular and edematous areas with staghorn-shaped vasculature. The tumor cells may have been ablated by radiotherapy. (D) Aberrant STAT6 nuclear positivity is observed in the primary brain tumor.

Histopathologically, the initial meningeal and metastatic tumors are identical to cellular SFTs (previously called intracranial HPC-like tumors of a cellular nature) (Figs. 1 and 2 are from the same patient, case 10). Interestingly, multinucleated osteoclast-type giant cells (OGCs) were widely present in one metastatic tumor to the liver (Fig. 2C). There was necrosis in 30% and 28% of tumors with and without systemic metastases, respectively. All of the tumors exhibited robust, but heterogeneous STAT6 immunopositivity. In most cases, the STAT6 immunostaining was stronger at the periphery of the tumor or in the perivascular areas (Figs. 1, 2). However, 40% of systemically metastatic tumors had positive CD34 immunostaining, while 85% of non-metastatic tumors showed at least focal CD34 positivity. EMA immunostaining was focally positive in two cases. The mean

Ki-67 indices were 8.7% and 8.8% (1.0% to 27.3%) in the tumors of metastatic and non-metastatic groups, respectively. There were no differences in the Ki-67 labeling indices, mitoses, necrosis, or tumor size based on the presence or absence of systemic metastasis (Table 2).

Ultrastructural studies were carried out in three patients from the metastatic group and seven from the non-metastatic group. There were no differences between the two groups. Ultrastructural examination revealed sheets of oval to elongated cells around the small capillaries. The tumor nuclei were oval or indented in appearance. The nuclear chromatin was fine and granular, with skein-like nucleoli. The individual tumor cells were surrounded by thick, electron-dense external laminar material (Fig. 2F).

Over the 10–29-year (average, 17.2 years) follow-up period,

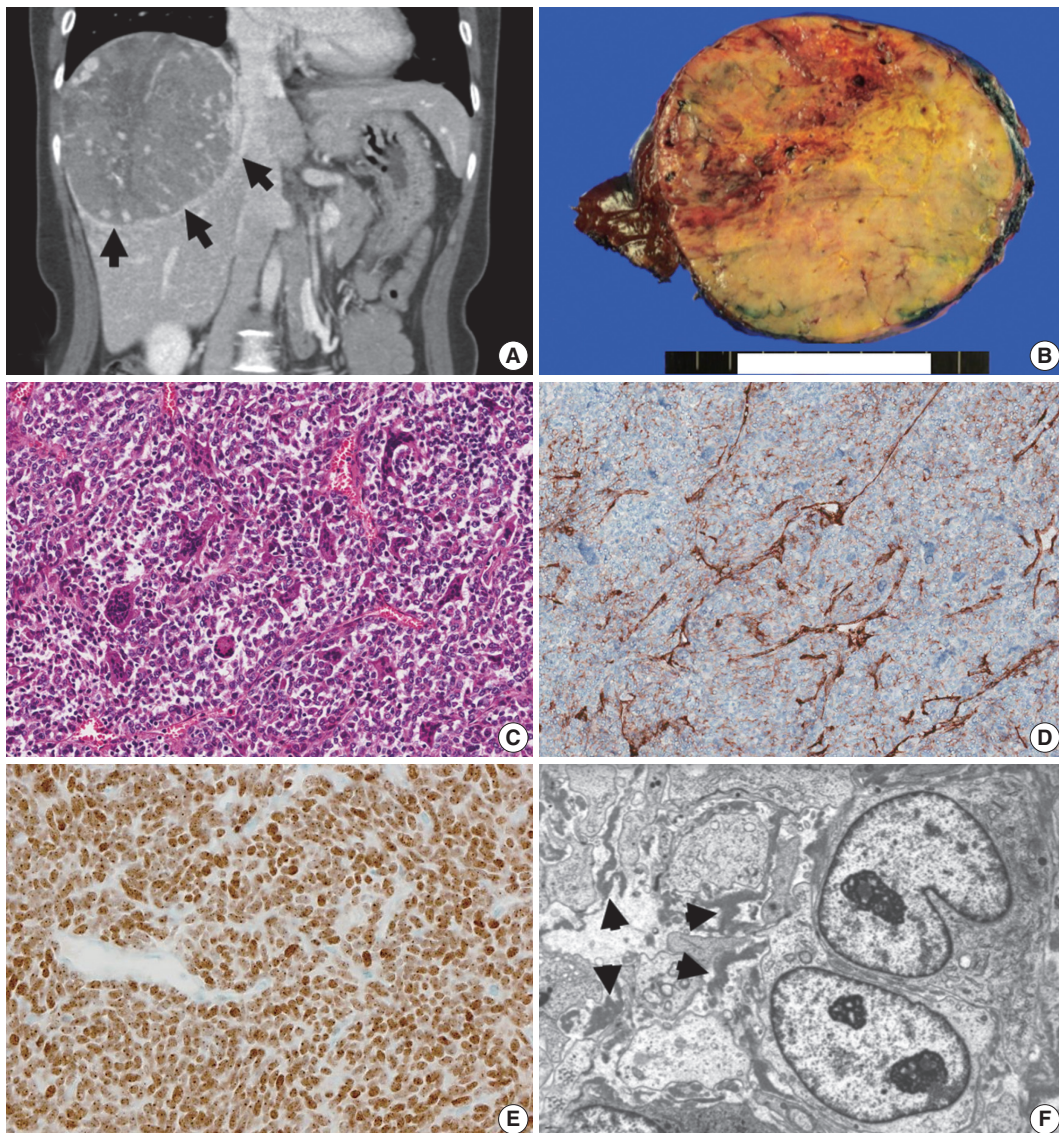


Fig. 2. Computed tomography (CT) and pathology of a metastatic solitary fibrous tumor from case 10. (A) Liver CT scan showing a large, 12-cm soft tissue mass in the right lobe with prominent feeding vessels. (B) The cut surface of a hepatic tumor specimen showing a well-circumscribed, yellowish-tan-colored, solid tumor with multifocal necrosis, and hemorrhage with dilated vessels. (C) Microscopic examination of the liver mass reveals small, discohesive tumor cells with oval nuclei and fine chromatin. Staghorn-shaped hyalinized vessels and osteoclast-like multinucleated giant cells are identified. (D) Tumor cells are focally positive for CD34 on immunohistochemical staining. (E) Aberrant STAT6 nuclear positivity is observed in the metastatic tumor cells in the liver. (F) Ultrastructurally, the tumor is composed of sheets of oval to elongate cells around small capillaries. The tumor cells have nuclei with an oval or indented appearance, and fine, granular chromatin. Skein-like nuclei are also present. The individual tumor cells are surrounded by a thick, electron-dense, amorphous, external lamina material (arrowheads; uranyl acetate and lead citrate, $\times 5,000$).

five patients (50%) in the metastatic group died of their disease. The 10-year survival rate was 100%, but by 15 years, this rate dropped to 60%. In the non-metastatic group, the 10-year survival rate was 33%. This rate was sustained for 14.5 years of follow-up.

Paradoxically, the Kaplan-Meier survival analysis revealed that patients with metastatic disease had significantly better over-

all survival times than did those without systemic metastases ($p = .04$) (Fig. 3). The mean survival of patients with systemic metastases was 215 ± 79 months, and that of patients without systemic metastases was 99 ± 47 months. The median survival time was 202 months and 99 months for patients with and without systemic metastases, respectively.

Both univariate and multivariate analyses revealed that an

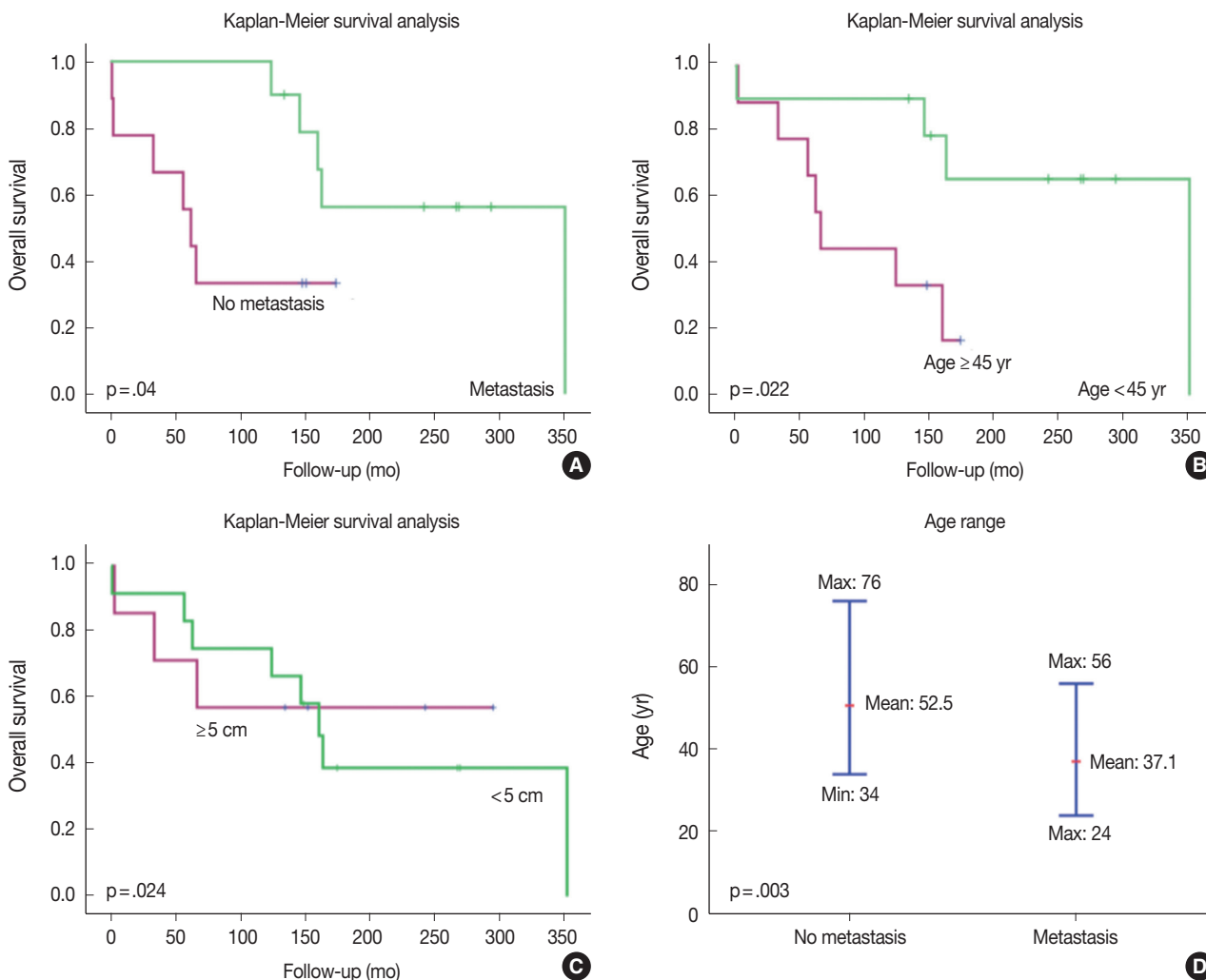


Fig. 3. Kaplan-Meier survival curves of patients with solitary fibrous tumors according to the presence or absence of systemic metastases. (A) Paradoxically, the patients with systemic metastases had better prognosis than did those without metastasis. Metastases usually arose approximately 10 years after the initial tumor development. Therefore, only longer survivors developed systemic metastases. (B) Younger patients lived longer and had better survival. The age cut-off to demonstrate a meaningful survival difference is 45 years. (C) Patients with an initial tumor size > 5 cm have poorer survival than did those with smaller tumors. (D) The age of tumor onset is significantly younger in patients with systemic metastases than it is in patients without metastases. The median ages of onset in patients with and without systemic metastases are 37.1 years and 52.5 years, respectively.

age of onset > 45 years and an initial tumor size > 5 cm were significant markers of poor prognosis. There was no prognostic significance of increased mitoses ($\geq 5/10$ high-power fields), high Ki-67 index ($\geq 5\%$), necrosis, high tumor grade, or the absence of CD34 expression on univariate and multivariate analyses. However, these factors did suggest a poor prognosis on multivariate analysis (Table 3).

DISCUSSION

A SFT is an uncommon type of spindle-cell mesenchymal tumor. It is most commonly found in the visceral pleura, but also

has been reported in virtually all extrapleural soft tissues.^{5,8} Recently, SFTs and HPCs in soft tissue have been reclassified as a single entity.³ Gengler and Guillou⁹ introduced the concept of an SFT spectrum. They recommend that a conventional SFT is designated as a fibrous variant of an SFT, while a conventional HPC is considered a cellular variant of an SFT.

Regardless of where they develop in the CNS, there is morphological, immunohistochemical, and genetic overlap between SFTs and HPCs.¹⁰ However, in the CNS, HPCs are still considered separate entities from SFTs.¹¹ The so-called meningeal SFTs have generally been regarded as indolent, non-aggressive tumors.^{3,12} Conversely, meningeal HPCs have a high tendency to

Table 3. The results of univariate and multivariate analysis

Variable	Univariate analysis p-value	Multivariate analysis		
		Hazard ratio	95% CI	p-value
Age (<45 yr vs ≥45 yr)	.022	0.172	0.009–3.277	.241
Systemic metastasis	.040	0.126	0.01–1.675	.117
Tumor size (<5 cm vs ≥5 cm)	.377	2.815	0.364–21.796	.322
Necrosis	.352	1.28	0.225–7.291	.781
Mitoses (<5/10HPF vs ≥5/10HPF) or grade	.603	6.602	0.12–362.385	.356
Ki-67 labeling index (<5/10HPF vs ≥5/10HPF)	.377	0.261	0.009–7.773	.438
CD34 (positive vs negative)	.983	0.246	0.26–2.319	.22

CI, confidence interval; HPF, high-power field.

Table 4. Summary of the patients with meningeal SFT/HPC with extracranial metastasis in the literature

Reference	Age (yr)/Sex	Diagnosis	Metastatic location	Time for metastasis (yr)
Ng <i>et al.</i> (2000) ¹⁴	55/F	SFT	Lung and neck	9
Someya <i>et al.</i> (2001) ¹⁵	42/F	HPC	Bone, lung, and liver	12
	37/F	HPC	Bone	7
Dufour <i>et al.</i> (2001) ¹⁶	23/M	HPC	Bone	12
	22/F	HPC	Extracranial site	13
	30/M	HPC	Extracranial site	14
Ogawa <i>et al.</i> (2004) ¹³	44/F	SFT	Lung	25
Pistolesi <i>et al.</i> (2004) ⁷	42/F	HPC	Bone, lung and adrenal gland	13
Chang <i>et al.</i> (2004) ¹⁷	43/F	HPC	C2–C3 vertebrates, lung, liver and kidney	5
Metellus <i>et al.</i> (2007) ¹⁰	34/M	SFT	Systemic metastasis	10.5
Hayashi <i>et al.</i> (2009) ¹⁸	45/M	HPC	Extracranial site	NM
	30/M	HPC	Extracranial site	NM
	47/F	HPC	Extracranial site	NM
	35/M	HPC	Extracranial site	NM
Ambrosini-Spaltro and Eusebi (2010) ¹¹	51/F	HPC	Hip	13
Robinson <i>et al.</i> (2013) ²⁰	40/M	Malignant SFT	Lung	NM
	33/F	Malignant SFT	Kidney	NM
	29/M	Malignant SFT	Pancreas	NM
	32/M	Malignant SFT	Small bowel	NM

SFT, solitary fibrous tumor; HPC, hemangiopericytoma; F, female; M, male; NM, not metastasized.

recur and to metastasize outside of the CNS; therefore, these are classified as World Health Organization grade II or III lesions.¹² Histopathologically, meningeal HPCs tend to have higher rates of mitosis and a higher Ki-67 index than do HPCs/SFTs in soft tissues. They also stain less intensely for CD34 and B-cell lymphoma 2 (BCL2) proteins.¹¹ However, two previous studies reported that several cases of SFTs progressed to HPCs at recurrence.^{3,10} There have also been reports of extracranial metastases of conventional SFTs.¹³

In the English-language literature, we identified 19 reports of meningeal SFTs/HPCs with extracranial metastasis (Table 4).^{14–18} The median age of tumor onset of these cases was 37 years, and there was no sex dominance (male:female = 9:10). The median time between the initial tumor development and extracranial metastasis was 14.2 years (range, 5.6 to 24.2 years).

In our series, patients with metastatic meningeal SFTs were a

mean of 15 years younger than were those in the non-metastatic group. There was a female sex predominance (male:female = 2:3). Similar to the prior report, the mean time between the initial tumor development and extracranial metastasis was 14.2 years in our study.¹⁹ Hoshi *et al.*¹⁹ reported that two cases had metastasized to the bone, 17 and 19 years after resection of primary leptomeningeal HPCs and introduced that median time from primary tumor to the occurrence of systemic metastases was 149 years from literature review. The most common metastatic sites were the lungs, bone, and liver, but rarely, the breast, orbit, and external auditory canal were the metastatic site. There were no lymph node metastases. Therefore, the meningeal SFTs studied here present with very similar clinical features to those previously reported.

Two recent studies found that the *NAB2-STAT6* gene fusion was a distinct molecular feature of SFTs and HPCs, in both men-

ingeal and extracranial tumors.^{4,20} Schweizer *et al.*²¹ also found that nuclei stained positive for anti-STAT6 in 35 of 37 meningeal HPCs and in all 25 meningeal SFTs, but not in 87 meningiomas. This provided additional evidence in support of unifying the terms SFT and HPC. Robinson *et al.*²⁰ noted that overexpression of the fusion protein NAB2-STAT6 induces the proliferation of cultured cells and activates early growth response genes. These findings suggest that the *NAB2-STAT6* fusion is a driver mutation of SFT.²⁰

In this study, strong aberrant nuclear expression of STAT6 was detected in all meningeal and extracranial metastatic SFTs (including the cases previously diagnosed as HPCs). This suggests that these tumors had the same pathogenesis. Verifying nuclear STAT6 immunoreexpression or *NAB2-STAT6* gene fusion may be useful to confirm the diagnosis, especially when only small biopsies are available for pathology, or in cases that are CD34-negative. Although CD34 is a good marker of SFTs/HPC, its sensitivity is < 100%. Overall, there is 95% CD34 positivity in SFTs.²² However, the CD34 positivity is lower in meningeal SFTs, as mentioned above.¹¹

To our knowledge, this is the first report of prominent OGCs described in an SFT/HPC (case 9). Previously, OGCs have been reported in various malignancies including breast, pancreatic, and gastric carcinomas,²³⁻²⁵ gastrointestinal stromal tumors,²⁶ clear cell sarcoma-like tumors,²⁷ squamous cell carcinoma of the skin,²⁸ and malignant melanoma.²⁹ It is thought that OGCs result from a host reaction to degeneration and necrosis of the tumor. However, it is not well understood why OGCs are so exaggerated in non-histiocytic tumors.

Kaplan-Meier survival analysis revealed that patients with metastatic disease had significantly better survival than did those without systemic metastasis ($p = .04$) (Fig. 3). The mean age of the metastatic group was younger than that of the non-metastatic group (37.1 years vs 52.5 years, respectively), suggesting that the age might be the most important prognostic factor (Fig. 3). Younger patients lived longer, but also had a higher risk of metastasis than did older patients. The Ki-67 labeling index ($\geq 5\%$), presence of necrosis, and absence of CD34 expression were not significant prognostic factors on univariate and multivariate analyses. The statistical insignificance of these latter factors may reflect the small number of cases involved.

In this study, two patients received adjuvant chemotherapy, one patient received a single cycle of VIP (VP-16, ifosfamide, cisplatin) chemotherapy and one received a single cycle of ifosfamide. There is no optimal chemotherapy regimen that has been established for SFTs/HPCs to date.³⁰ There are limited case

reports describing chemotherapy use. One case report described a patient with meningeal SFTs/HPCs who received two cycles of ICE (ifosfamide, carboplatin, and etoposide) chemotherapy and lived at least 151 months.⁶ Another study reported the relative success of various chemoregimens in 15 patients.³¹ In that study, only two patients were treated with adjuvant chemotherapy, but the treatment was stopped after one cycle in one patient due to a severe adverse effect.

In conclusion, we have reported 10 cases of meningeal SFTs with delayed extracranial metastasis. Systemic metastases developed after a long latent period, a mean of 14.2 years after the initial surgery. Metastases were associated with younger patient age and longer survival. Leptomeningeal SFTs can be divided into two groups by prognosis. The poor prognostic group is characterized by an initially locally aggressive tumor and early death. The better prognostic group is characterized by younger age of tumor onset, successful control of local recurrence, and a life expectancy > 10 years. However, despite intensive treatment, this group eventually developed delayed systemic metastases. The median survival rates of patients with and without systemic metastases were 202 months and 99 months, respectively. The age of onset was the most important prognostic factor. The best prognostic group was < 45 years old on Kaplan-Meier survival analysis. Therefore, meningeal SFTs arising in young patients (< 45 years) require careful surveillance for the early detection of systemic metastases, especially because extracranial metastases usually occur after a latency period of > 10 years.

Conflicts of Interest

No potential conflict of interest relevant to this article was reported.

Acknowledgments

This work was supported by the National Research Foundation of Korea (NRF) grant funded by the Korean government (MSIP) (No. 2010-0028631). The authors would like to thank U-ri Chae (Department of Industrial Engineering, Ajou University) for her precise statistical analysis of our data. In addition, the authors are very grateful to Professor Je G. Chi, who passed away last winter (November 26, 2014). He was a great mentor and friend to all of us. This work is dedicated to his memory.

REFERENCES

1. Klemperer P, Coleman BR. Primary neoplasms of the pleura: a re-

- port of five cases. *Am J Ind Med* 1992; 22: 1-31.
2. Fletcher CD, Bridge JA, Hogendoorn P, Mertens F. WHO classification of tumours of soft tissue and bone. Lyon: IARC Press, 2013.
 3. Tihan T, Viglione M, Rosenblum MK, Olivi A, Burger PC. Solitary fibrous tumors in the central nervous system: a clinicopathologic review of 18 cases and comparison to meningeal hemangiopericytomas. *Arch Pathol Lab Med* 2003; 127: 432-9.
 4. Chmielecki J, Crago AM, Rosenberg M, *et al.* Whole-exome sequencing identifies a recurrent *NAB2-STAT6* fusion in solitary fibrous tumors. *Nat Genet* 2013; 45: 131-2.
 5. Yu HC, Cho BH, Kim YK, Noh SJ, Moon WS. Solitary fibrous tumor of the liver: a case report. *Korean J Pathol* 2010; 44: 536-9.
 6. Park BJ, Kim YI, Hong YK, Jeun SS, Lee KS, Lee YS. Clinical analysis of intracranial hemangiopericytoma. *J Korean Neurosurg Soc* 2013; 54: 309-16.
 7. Pistolesi S, Fontanini G, Barellini L, *et al.* Meningeal hemangiopericytoma metastatic to the adrenal gland with multiple metastases to bones and lungs: a case report. *Tumori* 2004; 90: 147-50.
 8. Kim NR, Ro JY, Shin KH, Paik HJ, An JS, Ha SY. Solitary fibrous tumor of the conjunctiva with heretofore undescribed pathologic findings. *Korean J Pathol* 2011; 45: 315-8.
 9. Gengler C, Guillou L. Solitary fibrous tumour and haemangiopericytoma: evolution of a concept. *Histopathology* 2006; 48: 63-74.
 10. Metellus P, Bouvier C, Guyotat J, *et al.* Solitary fibrous tumors of the central nervous system: clinicopathological and therapeutic considerations of 18 cases. *Neurosurgery* 2007; 60: 715-22.
 11. Ambrosini-Spaltro A, Eusebi V. Meningeal hemangiopericytomas and hemangiopericytoma/solitary fibrous tumors of extracranial soft tissues: a comparison. *Virchows Arch* 2010; 456: 343-54.
 12. Fuller C. WHO classification of tumours of the central nervous system, fourth edition. *J Neuropathol Exp Neurol* 2008; 67: 260.
 13. Ogawa K, Tada T, Takahashi S, *et al.* Malignant solitary fibrous tumor of the meninges. *Virchows Arch* 2004; 444: 459-64.
 14. Ng HK, Choi PC, Wong CW, To KF, Poon WS. Metastatic solitary fibrous tumor of the meninges: case report. *J Neurosurg* 2000; 93: 490-3.
 15. Someya M, Sakata KI, Oouchi A, Nagakura H, Satoh M, Hareyama M. Four cases of meningeal hemangiopericytoma treated with surgery and radiotherapy. *Jpn J Clin Oncol* 2001; 31: 548-52.
 16. Dufour H, Métellus P, Fuentes S, *et al.* Meningeal hemangiopericytoma: a retrospective study of 21 patients with special review of postoperative external radiotherapy. *Neurosurgery* 2001; 48: 756-62.
 17. Chang CC, Chang YY, Lui CC, Huang CC, Liu JS. Meningeal hemangiopericytoma with delayed multiple distant metastases. *J Chin Med Assoc* 2004; 67: 527-32.
 18. Hayashi Y, Uchiyama N, Nakada M, *et al.* A reevaluation of the primary diagnosis of hemangiopericytoma and the clinical importance of differential diagnosis from solitary fibrous tumor of the central nervous system. *Clin Neurol Neurosurg* 2009; 111: 34-8.
 19. Hoshi M, Araki N, Naka N, *et al.* Bone metastasis of intracranial meningeal hemangiopericytoma. *Int J Clin Oncol* 2005; 10: 208-13.
 20. Robinson DR, Wu YM, Kalyana-Sundaram S, *et al.* Identification of recurrent *NAB2-STAT6* gene fusions in solitary fibrous tumor by integrative sequencing. *Nat Genet* 2013; 45: 180-5.
 21. Schweizer L, Koelsche C, Sahn F, *et al.* Meningeal hemangiopericytoma and solitary fibrous tumors carry the *NAB2-STAT6* fusion and can be diagnosed by nuclear expression of STAT6 protein. *Acta Neuropathol* 2013; 125: 651-8.
 22. Fisher C. Immunohistochemistry in diagnosis of soft tissue tumours. *Histopathology* 2011; 58: 1001-12.
 23. Tavassoéli FA, Devilee P. World Health Organization classification of tumours: pathology and genetics of tumours of the breast and female genital organs. Lyon: IARC Press, 2003.
 24. Sakai Y, Kupelioglu AA, Yanagisawa A, *et al.* Origin of giant cells in osteoclast-like giant cell tumors of the pancreas. *Hum Pathol* 2000; 31: 1223-9.
 25. Ushiku T, Shinozaki A, Uozaki H, *et al.* Gastric carcinoma with osteoclast-like giant cells: lymphoepithelioma-like carcinoma with Epstein-Barr virus infection is the predominant type. *Pathol Int* 2010; 60: 551-8.
 26. Insabato L, Di Vizio D, Ciancia G, Pettinato G, Tornillo L, Terracciano L. Malignant gastrointestinal leiomyosarcoma and gastrointestinal stromal tumor with prominent osteoclast-like giant cells. *Arch Pathol Lab Med* 2004; 128: 440-3.
 27. Friedrichs N, Testi MA, Moiraghi L, *et al.* Clear cell sarcoma-like tumor with osteoclast-like giant cells in the small bowel: further evidence for a new tumor entity. *Int J Surg Pathol* 2005; 13: 313-8.
 28. Wooff J, Werner D, Murphy J, Walsh N. Osteoclast-like giant cell reaction associated with cutaneous squamous cell carcinoma: a report of 2 cases and review of the literature. *Am J Dermatopathol* 2009; 31: 282-7.
 29. Al-Brahim N, Salama S. Malignant melanoma with osteoclast-like giant cells: an unusual host response: immunohistochemical and ultrastructural study of three cases and literature review. *Am J Dermatopathol* 2005; 27: 126-9.
 30. Park MS, Patel SR, Ludwig JA, *et al.* Activity of temozolomide and bevacizumab in the treatment of locally advanced, recurrent, and metastatic hemangiopericytoma and malignant solitary fibrous tumor. *Cancer* 2011; 117: 4939-47.
 31. Chamberlain MC, Glantz MJ. Sequential salvage chemotherapy for recurrent intracranial hemangiopericytoma. *Neurosurgery* 2008; 63: 720-6.

Prognostic Significance of Aquaporin 5 Expression in Non-small Cell Lung Cancer

Young Min Jo · Tae In Park
Hwa Young Lee¹ · Ji Yun Jeong
Won Kee Lee²

Department of Pathology, Kyungpook National University Hospital, Kyungpook National University School of Medicine, Daegu; ¹Department of Pathology, Kyungpook National University School of Medicine, Daegu; ²Biostatistics, Biomedical Research Institute, Kyungpook National University School of Medicine, Daegu, Korea

Received: August 31, 2015
Revised: October 30, 2015
Accepted: October 30, 2015

Corresponding Author

Tae In Park, MD, PhD
Department of Pathology, Kyungpook National University Hospital, Kyungpook National University School of Medicine, 680 Gukchaebosang-ro, Jung-gu, Daegu 41944, Korea
Tel: +82-53-200-4854
Fax: +82-53-426-1525
E-mail: tipark@knu.ac.kr

Background: Aquaporins are water channel proteins that play a major role in the movement of water in various human tissues. Recently, it has been found that aquaporins have influence in the carcinogenesis of human malignancies. We analyzed the prognostic impact of aquaporin 5 (AQP5) in non-small lung cancer (NSCLC). **Methods:** Seventy-six cases of NSCLC were studied, including 44 cases of adenocarcinoma (ADC) and 32 cases of squamous cell carcinoma (SQCC). Tissue microarray was constructed and immunohistochemical staining for AQP5 was performed. **Results:** AQP5 was positive in 59.2% of the total enrolled NSCLCs (63.7% in ADC and 53.1% in SQCC). The difference in expression of AQP5 according to the histologic grade of the tumor was significant ($p < .047$), but not in a serial order. When ADC and SQCC were separately evaluated, no significant difference was observed according to the histologic grade of the tumor ($p = .076$ in ADC and $p = .631$ in SQCC). No difference was observed between AQP5 expression and other demographic data and tumor characteristics. Disease-free survival (DFS) was higher in AQP5 negative cases than positive cases in ADC ($p = .047$), but no significance was found in SQCC ($p = .068$). We were unable to find a significance between AQP5 overexpression and overall survival in either ADC ($p = .210$) or SQCC ($p = .533$). **Conclusions:** AQP5 expression is associated with DFS in ADC of the lung and tumor grade of NSCLC. The present study suggests that AQP5 can be a prognostic factor of NSCLC.

Key Words: Aquaporin 5; Carcinoma, non-small cell lung; Adenocarcinoma; Carcinoma, squamous cell

Lung cancer is a leading cause of cancer-related morbidity and mortality worldwide, and non-small cell lung cancer (NSCLC), which includes adenocarcinoma (ADC) and squamous cell carcinoma (SQCC), is the most prevalent subtype.¹ Despite the discovery of molecular mutations and advances in diagnosis and treatment, the prognosis for patients with NSCLC remains poor, and a considerable number of patients experience recurrence of their disease. Therefore, there is a strong need for reliable biomarkers associated with various characteristics of patients with tumors that can predict the prognosis of NSCLCs.

In recent years, molecules expected to reflect the prognosis of patients with NSCLCs have been studied worldwide. Aquaporin (AQP) is one of such molecules. AQP is a water channel protein and plays a major role in transcellular water movement and homeostasis in various human tissues.^{2,3} It is a family of transmembrane proteins, and about 10 distinct subtypes of AQPs have been discovered.³ Recent studies have reported that certain

subtypes of AQPs play a role in carcinogenesis and tumor progression in many human malignancies including colon cancer, pancreatic cancer, brain tumors, and renal cell carcinoma.⁴⁻⁷ Although the role of AQPs in carcinogenesis has not been clearly defined, an ectopic overexpression of AQPs is known to promote the phosphorylation of a cAMP-protein kinase consensus site in the cytoplasmic area of AQP, which is the transcellular protein. This phosphorylation is also preferentially found in tumors.⁸ AQPs are also thought to be related to angiogenesis, an essential step in the growth, invasion, and metastasis of a tumor. Vacca *et al.*⁹ reported that AQPs are expressed in higher levels in the bone marrow tissues in active multiple myeloma than in non-active multiple myeloma tissues. In this study, immunohistochemical staining for AQP1 revealed significantly greater microvessel staining patterns in active multiple myeloma tissues compared to non-active multiple myeloma tissues. In view of the functional role of AQPs, AQP1 is one of the delayed response genes, and it

is thought to be involved in cell migration and angiogenesis.^{10,11} AQP3 and AQP5, other members of transmembrane channel proteins, are known to induce the process of lymphocyte activation.¹² Notably, a few studies have been conducted regarding AQPs in lung cancer. In one study, Chae *et al.*¹³ reported that the ectopic expression of AQP5 in the NIH3T3 cell, the murine fibroblast cell line, and BEAS-SB cell, the normal lung cell line, resulted in a phenotypic change both *in vivo* and *in vitro*. This change seemed to be caused by the signaling pathway activated by Ras. In another study, Guo and Jin¹⁴ reported that the nuclear factor of activated T-cells 5 (NFAT5), which is an osmoregulated transcription factor, and AQP5 are upregulated in ADC of the lung. In addition, knockdown of each *NFAT5* or *AQP5* gene inhibits proliferation and migration of ADC cells.

Laboratories worldwide are studying the molecules and pathways associated with the carcinogenesis of lung cancer, looking for a correlation with prognostic significance in these patients. In our study, we evaluated the expression of AQP5 in NSCLC and its relationship with various clinicopathologic features. We also examined the prognostic impact of AQP5 in NSCLC.

MATERIALS AND METHODS

Patients and tissue selection

All tissues used in this study were formalin-fixed and paraffin-embedded NSCLC tissues obtained from the Kyungpook National University Hospital between 1998 and 2008. Clinicopathologic information was obtained from electronic medical records. Two pathologists examined the slides of selected cases and reconfirmed the diagnoses of ADC and SQCC according to the World Health Organization classifications. The pathologic TNM stages were evaluated based on the seventh edition of the American Joint Committee on Cancer (AJCC) cancer staging system. A total of 385 cases of NSCLC were identified, of which 338 cases were ADC and SQCC. Other types of NSCLC such as large cell neuroendocrine carcinoma were excluded due to their rare incidence. However, only 76 cases were used in this study; cases with loss of tissue due to other experiments, cases lost to follow-up, and cases that lacked certain clinicopathologic data were all excluded. Consequently, 44 cases of ADC and 32 cases of SQCC were enrolled in the study. This study has been approved by the Institutional Review Board of Kyungpook National University.

Tissue microarray and immunohistochemical staining

Tissue microarrays were constructed from the representative

tumor areas, each core measuring 3 mm in diameter. Normal human lung tissues were used as controls. Immunohistochemical staining was performed using the BenchMark automated staining instrument (Ventana Medical System, Tucson, AZ, USA). The AQP5 antibody was an affinity-purified goat antibody, used at a dilution of 1:50. Tissue sections were cut in 4 μ m thickness and deparaffinized in xylene, rehydrated in three graded alcohol chambers, and treated with 3% hydrogen peroxide in methanol. The avidin-biotin-peroxidase technique was used for visualization (DAKO LSAB Kit, DAKO Cytomation, Carpinteria, CA, USA). All the stained slides were examined by two pathologists who were blinded from all clinicopathologic data.

Scoring of AQP5 immunohistochemistry

For semi-quantitative analysis of the AQP5 immunoreactivity, we used H-score method.¹⁵ All cells had cytoplasmic staining pattern. We counted 100 tumor cells in the hot spot, and the H-score was calculated by adding the percentages of strongly stained (3 \times), moderately stained (2 \times), and weakly stained (1 \times) nuclei, resulting in a possible range of 0–300. Two pathologists evaluated and obtained this score. We divided the H-score interval into 0–15 (less than 5% of the maximum score, AQP5 negative), 15–75 (5%–25%, AQP5 weak positivity, 1 +), 75–150 (25%–50%, AQP5 moderate positivity, 2 +), and over 151 (50%–100%, AQP5 strong positivity, 3 +). The median values of H-score for each interval were 4 for negative cases, 53 for weak, 108 for moderate, and 267 for strong staining. We considered over 1 + immunohistochemical staining as positive.

Statistical analysis

Statistical analysis was performed using SAS ver. 9.4 (SAS Institute Inc., Cary, NC, USA) and R ver. 3.2.1 (R Foundation for Statistical Computing, Vienna, Austria), and the t test and log-rank test were used. Patient's mean age, histologic grade, and tumor stage were evaluated by t test. Survival curves were produced by log-rank test to evaluate the disease-free survival (DFS) status and overall survival (OS) status. Age, sex, histological grade, and tumor stage were accounted. All p-values were two-sided, and differences at $p < .05$ were considered statistically significant.

RESULTS

Patient characteristics

Patient characteristics are shown in Table 1. Of the 76 cases, 52 were men and 24 were women. The mean age was 64 years (range, 41 to 82 years). All cases were diagnosed as either ADC

Table 1. Association between AQP5 expression, demographic data, and tumor characteristics

Clinical and tumor characteristic	AQP5 status in NSCLC		p-value
	AQP5 (-) (n=31, 40.8%)	AQP5 (+) (n=45, 59.2%)	
Age, mean ± SD (range, yr)	64 ± 8.3 (41–78)	64 ± 8.1 (49–82)	.985
Sex			
Male	22 (42.3)	30 (57.7)	.692
Female	9 (37.5)	15 (62.5)	
Histologic subtype			
Adenocarcinoma	16 (36.4)	28 (63.6)	.357
Squamous cell carcinoma	15 (47)	17 (53)	
Grade			
Well differentiated	7 (36.9)	12 (63.1)	.047
Moderately differentiated	22 (51.2)	21 (48.8)	
Poorly differentiated	2 (14.3)	12 (85.7)	
Grade among ADCs			
Well differentiated	5 (38.5)	8 (61.5)	.076
Moderately differentiated	10 (50)	10 (50)	
Poorly differentiated	1 (9.1)	10 (90.9)	
Grade among SQCCs			
Well differentiated	2 (33.3)	4 (66.7)	.631
Moderately differentiated	12 (52.2)	11 (47.8)	
Poorly differentiated	1 (33.3)	2 (66.7)	
T stage			
T1	7 (43.7)	9 (56.3)	.305
T2	16 (38.1)	26 (61.9)	
T3	4 (36.4)	7 (63.6)	
T4	4 (57.2)	3 (42.8)	
N stage			
N0	20 (40.8)	29 (59.2)	.479
N1	4 (30.8)	9 (69.2)	
N2	4 (40)	6 (60)	
N3	3 (75)	1 (25)	
TNM stage			
I	18 (50)	18 (50)	.094
II	7 (28)	18 (72)	
III	4 (30.8)	9 (69.2)	
IV	0	0	

Values are presented as number (%) unless otherwise indicated.

AQP5, aquaporin 5; NSCLC, non-small lung cancer; SD, standard deviation; ADC, adenocarcinoma; SQCC, squamous cell carcinoma.

(n = 44) or SQCC (n = 32). The most prevalent histologic grade was moderately differentiated, with 43 cases (56.6%). The pathologic stages were as follows: stage I (n = 36, 47.3%), stage II (25, 32.9%), stage III (15, 19.8%), and stage IV (0, 0%). AQP5 showed significantly different expressions depending on the histologic grade ($p < .047$), but not in a serial order. When ADC and SQCC were separately evaluated, there was no significance regarding the histologic grade (in ADC, $p = .076$ and in SQCC, $p = .631$). No difference was identified between AQP5 expression and other clinical and tumor characteristics. We included N3 patients who underwent surgery due to tumor burden. In all cases, complete resection was performed, and resection margins were free from tumor in all cases.

AQP5 immunoexpression

Following immunohistochemical staining, AQP5 expression was evaluated by H-score with staining intensity in the hot spot and categorized into the following: no staining (-), weak or mild staining (1+), moderate staining (2+), and strong staining (3+). The representative images of each score are shown in Fig. 1 and the results are shown in Table 2. The positive cases totaled 28 (57.9%) in ADC and 17 (42.1%) in SQCC. Specifically, 1+, 2+, and 3+ were scored in six ADC and three SQCC cases (total nine), seven ADC and six SQCC cases (total 13), and 15 ADC and eight SQCC cases (total 23), respectively.

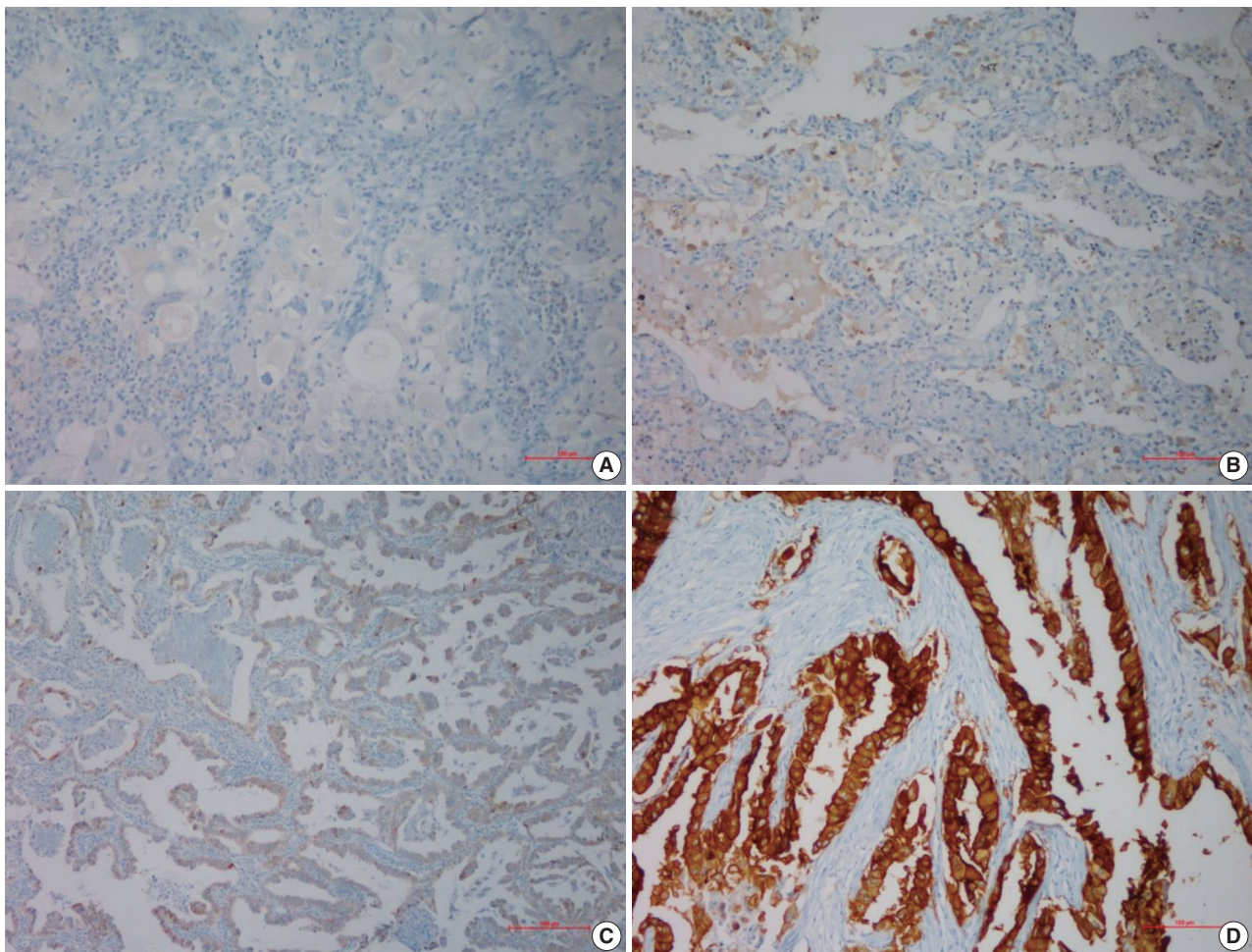


Fig. 1. Immunohistochemical staining with aquaporin 5. (A) No staining (0). (B) Weak, mild staining (1+). (C) Moderate staining (2+). (D) Strong staining (3+).

Table 2. Histologic subtype of non-small cell lung cancer and aquaporin 5 immunohistochemical staining status

Aquaporin 5 immunohistochemical staining status	0	1+	2+	3+	Total
Adenocarcinoma	16 (36.3)	6 (13.6)	7 (15.9)	15 (34.2)	44 (57.9)
Squamous cell carcinoma	15 (46.9)	3 (9.3)	6 (18.8)	8 (25)	32 (42.1)
Total	31 (40.8)	9 (11.8)	13 (17.1)	23 (30.3)	76 (100)

Values are presented as number (%).

Prognostic impact of AQP5 in NSCLC

We had long-term follow-up data for all patients included in this study, ranging from 1 year to 9 years. Within that period, 31 patients died of primary lung cancer or related complications. Eighteen of the 44 patients with ADC and 13 of the 32 patients with SQCC died. Seven cases of death in ADC were due to the primary disease and others deaths were due to complications including pneumonia, cachexia and treatment related death. In SQCC, five cases were died due to the primary disease and others were due to complications. The number of patients with re-

current lung cancer was 21 in ADC and 12 in SQCC. DFS and OS along with AQP5 positive and negative cases are shown in Fig. 2 for ADC and in Fig. 3 for SQCC. In the log-rank test graph, AQP5 positive cases are represented with a dotted line and AQP5 negative cases are represented with a solid line in both ADC and SQCC with 95% confidence interval.

In the DFS graph, the p-value of AQP5 positive patients is .047 in ADC, which shows the significance in terms of prognostic impact. However, the other parameters were not significant, as shown in Figs. 2 and 3. We did find more correlation with

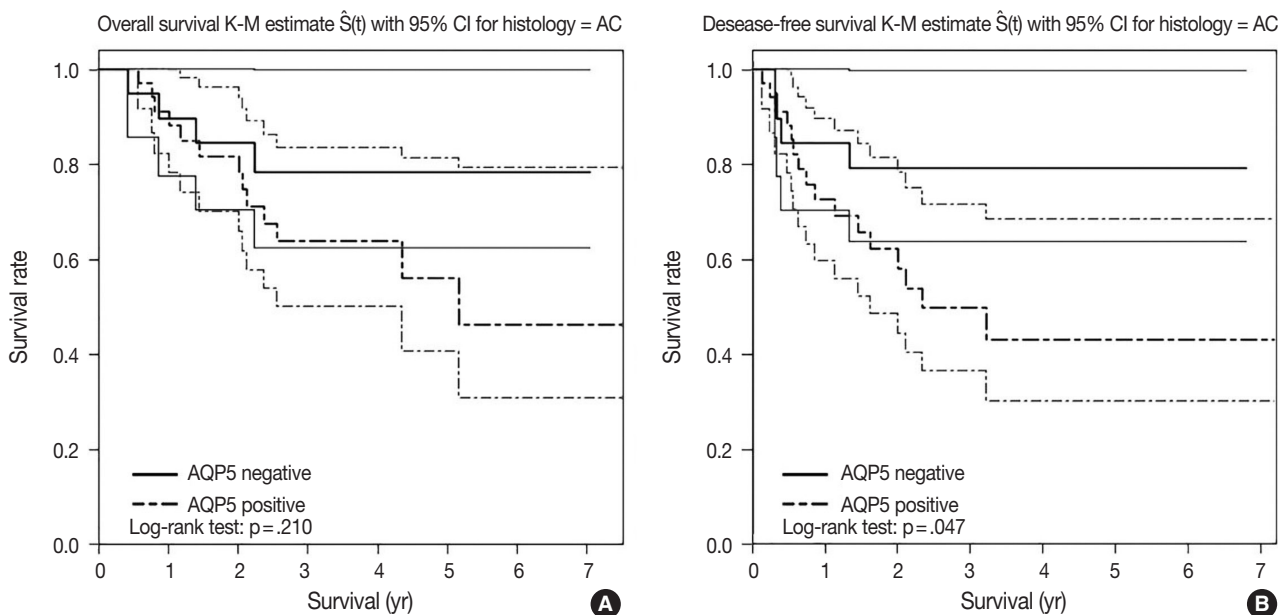


Fig. 2. Overall survival (A) and disease-free survival (B) graphs with log-rank test in adenocarcinoma. Aquaporin 5 (AQP5) positive and negative cases are illustrated with bold dotted and solid lines, respectively. A 95% confidence interval (CI) is included in this graph and illustrated with fine dotted and solid lines. KM, Kaplan-Meier; AC, adenocarcinoma.

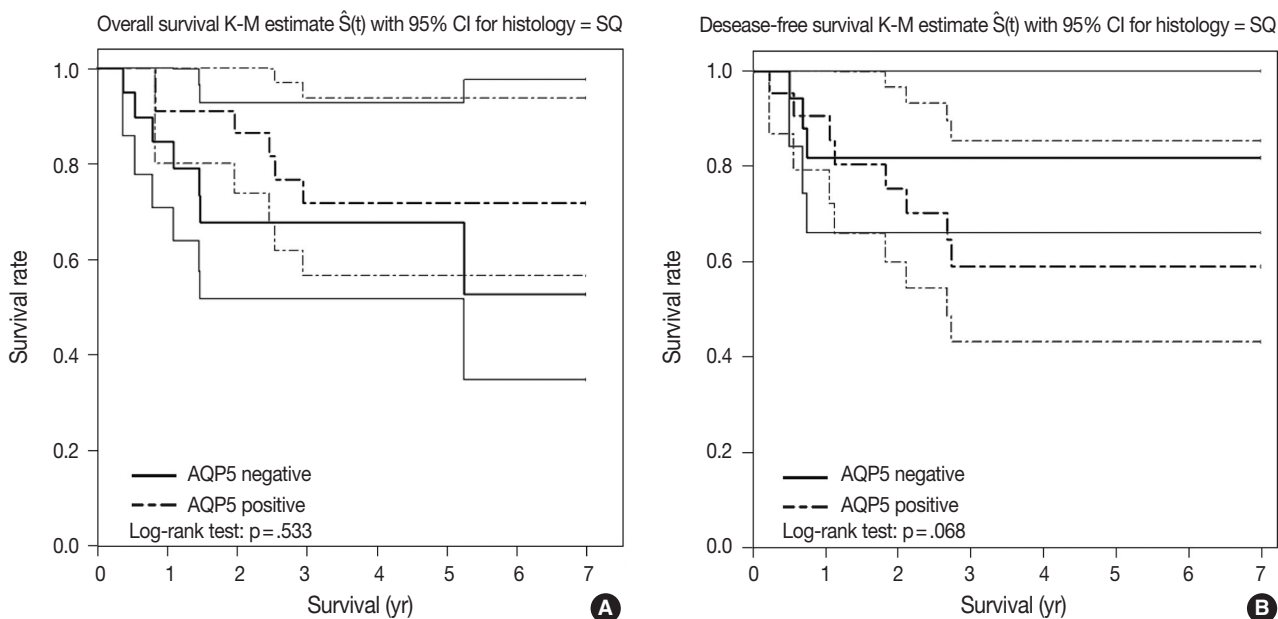


Fig. 3. Overall survival (A) and disease-free survival (B) graph with log-rank test in squamous cell carcinoma. Aquaporin 5 (AQP5) positive and negative cases are illustrated with bold dotted and solid lines, respectively. A 95% confidence interval (CI) is included in this graph and illustrated with fine dotted and solid lines. KM, Kaplan-Meier; SQ, squamous cell carcinoma.

AQP5 positive status in the earlier stage (stage I) than in the higher stages in the DFS, but statistical correlation was not significant ($p = .152$ vs. $p = .929$). Meanwhile, recurrence rate, stage at the time of diagnosis and the cause of patient death (primary disease vs. other complications) did not correlate with the AQP5 status.

DISCUSSION

Although the role of AQP5 in both normal control and tumor tissue has not been clarified, few studies have reported the effect of AQPs in carcinogenesis and tumor progression. Some studies reported that expression of AQP1 was frequently involved in the

development of colon cancer, pancreatic cancer, brain tumors, and renal cell carcinoma with paralleling angiogenesis.^{5,6} Additionally, AQP5 expression in various human cancers has been studied. Burghardt *et al.*⁷ reported the expression of AQP5 in pancreatic cancer and ovarian cancer. In another study conducted by Kang *et al.*,¹⁶ AQP5 showed a good correlation with lymph node metastasis in patients with colon cancer, but the OS or DFS was not found to be significant. Lee *et al.*¹⁷ showed that the AQP5 upregulation led to unfavorable prognoses in patients with estrogen receptor positive breast cancer, and it led to significantly worse prognosis especially in the case of early breast cancer. In lung cancer, Guo and Jin¹⁴ showed that NFAT5 promotes proliferation and migration of ADC partly via regulation of AQP5 expression. However, very few studies have been conducted in this field until recently. Based on these observations, we hypothesized that the NSCLCs with AQP5 positive staining would have more frequent tumor recurrence, shorter DFS, and poorer OS.

In our study, AQP5 was expressed in the portion of the lung cancer patients in both ADC and SQCC. Among various clinicopathologic features, tumor grade was significantly correlated with p-value of .047. This is suggestive of a prognostic implication of AQP5 in NSCLCs. Although the percentage of AQP5 positive cases is not serially ordered as the degree of differentiation in our results, more extensive study should be conducted to verify the exact significance. In addition, when we separately evaluated the tumor grade with AQP5 in both ADC and SQCC, no significant correlation was identified. For the other variables, we could not find any significant correlation with AQP5 expression.

AQP5 positive cases showed a poorer DFS rate than the negative ones ($p = .047$) in ADC. However, the AQP5 positive status was not significantly correlated with OS in ADC cases ($p = .210$). The crude hazard ratio (HR) and 95% confidence interval of ADC in DFS were 2.291 (0.97–8.75) and the HR and 95% confidence interval after adjustment for smoking status, age, tumor stage, etc. were 2.95 (0.98–8.92). Median survival rate in AQP5 positive cases was 1.94 year. While median survival rate in AQP5 negative cases was not evaluated. Its level was not fall below the 0.75. In the DFS graph for SQCC, the p-value of AQP5 positive patients is .068, and the prognostic impact was not significant for OS between AQP5 positive and negative cases ($p = .533$). Additionally, neither recurrence rate nor tumor stage correlated with the AQP5 status. That is, no parameter correlated with AQP5 positivity in SQCC cases. This may be explained by the small number of cases involved in the study, and perhaps a study with a large number of cases can demonstrate its significance as a prognostic marker.

In addition to the relatively small sample size, our study had several limitations. We originally sought to determine the clinical usefulness of immunohistochemical staining for AQP5 protein for determining prognosis in NSCLC. We examined earlier studies for the significance of AQP5 in detecting and predicting prognosis in patients with ADC or SQCC. In addition, we focused on correlating DFS rate, OS rate, recurrence rate, and histological stage with AQP5. However, the correlation of immunoeexpression of AQP5 in malignant tissue with poor prognosis has already been reported. However, to date, only a few studies on this topic have been published, and our study will provide an additional evidence to support the correlation of AQP5 with survival rates in ADC.

We examined the usefulness of immunohistochemical staining of AQP5 for clinical significance. However, we did not evaluate the molecular pathogenesis, molecular pathway, or carcinogenetic mechanisms. Many such pathways and molecules were unknown until recently. More molecules and carcinogenetic processes related to invasion, adhesion, migration, and motility should be identified and studied.

Lung cancer subtypes may have distinct carcinogenetic pathways. Although ADC and SQCC are the predominant subtypes, others such as large cell neuroendocrine carcinoma and small cell carcinoma do exist. Even though they are rare, they should be included when studying carcinogenetic molecules and pathways in NSCLC. Lastly, many studies referenced in our study had been performed using a single cell line. More studies using other cell lines and subtypes of NSCLC can be the basis for future research.

In conclusion, the results of the current study show a correlation between AQP5 expression and poorer DFS in the ADC subtype of NSCLC. We believe that AQP5 can be a potential novel prognostic biomarker in ADC. Further research is needed to determine its utility in other subtypes of lung cancer.

Conflicts of Interest

No potential conflict of interest relevant to this article was reported.

Acknowledgments

This research was supported by Kyungpook National University Research Fund, 2012.

REFERENCES

1. Travis WD, Brambilla E, Burke AP, Marx A, Nicholson AG. WHO

- classification of tumours of the lung, pleura, thymus and heart. 4th ed. Lyon: IARC Press, 2015; 26-52.
2. King LS, Agre P. Pathophysiology of the aquaporin water channels. *Annu Rev Physiol* 1996; 58: 619-48.
 3. Verkman AS, van Hoek AN, Ma T, *et al.* Water transport across mammalian cell membranes. *Am J Physiol* 1996; 270(1 Pt 1): C12-30.
 4. Vogelstein B, Kinzler KW. Cancer genes and the pathways they control. *Nat Med* 2004; 10: 789-99.
 5. Saadoun S, Papadopoulos MC, Davies DC, Bell BA, Krishna S. Increased aquaporin 1 water channel expression in human brain tumours. *Br J Cancer* 2002; 87: 621-3.
 6. Moon C, Soria JC, Jang SJ, *et al.* Involvement of aquaporins in colorectal carcinogenesis. *Oncogene* 2003; 22: 6699-703.
 7. Burghardt B, Elkaer ML, Kwon TH, *et al.* Distribution of aquaporin water channels AQP1 and AQP5 in the ductal system of the human pancreas. *Gut* 2003; 52: 1008-16.
 8. Woo J, Lee J, Chae YK, *et al.* Overexpression of AQP5, a putative oncogene, promotes cell growth and transformation. *Cancer Lett* 2008; 264: 54-62.
 9. Vacca A, Frigeri A, Ribatti D, *et al.* Microvessel overexpression of aquaporin 1 parallels bone marrow angiogenesis in patients with active multiple myeloma. *Br J Haematol* 2001; 113: 415-21.
 10. Moon C, Williams JB, Preston GM, *et al.* The mouse aquaporin-1 gene. *Genomics* 1995; 30: 354-7.
 11. Saadoun S, Papadopoulos MC, Hara-Chikuma M, Verkman AS. Impairment of angiogenesis and cell migration by targeted aquaporin-1 gene disruption. *Nature* 2005; 434: 786-92.
 12. Moon C, Rousseau R, Soria JC, *et al.* Aquaporin expression in human lymphocytes and dendritic cells. *Am J Hematol* 2004; 75: 128-33.
 13. Chae YK, Woo J, Kim MJ, *et al.* Expression of aquaporin 5 (AQP5) promotes tumor invasion in human non small cell lung cancer. *PLoS One* 2008; 3: e2162.
 14. Guo K, Jin F. NFAT5 promotes proliferation and migration of lung adenocarcinoma cells in part through regulating AQP5 expression. *Biochem Biophys Res Commun* 2015; 465: 644-9.
 15. Ishibashi H, Suzuki T, Suzuki S, *et al.* Sex steroid hormone receptors in human thymoma. *J Clin Endocrinol Metab* 2003; 88: 2309-17.
 16. Kang BW, Kim JG, Lee SJ, *et al.* Expression of aquaporin-1, aquaporin-3, and aquaporin-5 correlates with nodal metastasis in colon cancer. *Oncology* 2015; 88: 369-76.
 17. Lee SJ, Chae YS, Kim JG, *et al.* AQP5 expression predicts survival in patients with early breast cancer. *Ann Surg Oncol* 2014; 21: 375-83.

Interobserver Variability of Ki-67 Measurement in Breast Cancer

Yul Ri Chung¹ · Min Hye Jang²
So Yeon Park^{1,2} · Gyungyub Gong³
Woo-Hee Jung⁴
The Korean Breast Pathology Ki-67
Study Group*

¹Department of Pathology, Seoul National University College of Medicine, Seoul;

²Department of Pathology, Seoul National University Bundang Hospital, Seongnam;

³Department of Pathology, Asan Medical Center, University of Ulsan College of Medicine, Seoul;

⁴Department of Pathology, Gangnam Severance Hospital, Yonsei University College of Medicine, Seoul, Korea

Received: November 26, 2015

Revised: December 21, 2015

Accepted: December 24, 2015

Corresponding Author

So Yeon Park, MD, PhD

Department of Pathology, Seoul National University Bundang Hospital, 82 Gumi-ro 173beon-gil, Bundang-gu, Seongnam 13620, Korea

Tel: +82-31-787-7712

Fax: +82-31-787-4012

E-mail: syumd@snu.ac.kr

*Lists of participants and their affiliations appear at the end of the paper.

Background: As measurement of Ki-67 proliferation index is an important part of breast cancer diagnostics, we conducted a multicenter study to examine the degree of concordance in Ki-67 counting and to find factors that lead to its variability. **Methods:** Thirty observers from thirty different institutions reviewed Ki-67–stained slides of 20 different breast cancers on whole sections and tissue microarray (TMA) by online system. Ten of the 20 breast cancers had hot spots of Ki-67 expression. Each observer scored Ki-67 in two different ways: direct counting (average vs. hot spot method) and categorical estimation. Intraclass correlation coefficient (ICC) of Ki-67 index was calculated for comparative analysis. **Results:** For direct counting, ICC of TMA was slightly higher than that of whole sections using average method (0.895 vs 0.858). The ICC of tumors with hot spots was lower than that of tumors without (0.736 vs 0.874). In tumors with hot spots, observers took an additional counting from the hot spot; the ICC of whole sections using hot spot method was still lower than that of TMA (0.737 vs 0.895). In categorical estimation, Ki-67 index showed a wide distribution in some cases. Nevertheless, in tumors with hot spots, the range of distribution in Ki-67 categories was decreased with hot spot method and in TMA platform. **Conclusions:** Interobserver variability of Ki-67 index for direct counting and categorical estimation was relatively high. Tumors with hot spots showed greater interobserver variability as opposed to those without, and restricting the measurement area yielded lower interobserver variability.

Key Words: Ki-67; Observer variation; Multicenter; Breast neoplasms

Breast cancer is a heterogeneous group of diseases with different molecular bases, histologies, and prognoses.¹ Current classification is based on molecular subtyping with cDNA microarrays into five categories: luminal A, luminal B, human epidermal growth factor receptor 2 (HER2)–positive, basal-like, and normal breast-like.^{2,3} In daily practice, however, immunohistochemistry is a simple and economic method that provides as much valuable information as gene expression profiling. Thus, breast cancer subtyping using immunohistochemical surrogates has been proposed.^{4,6} Cheang *et al.*⁶ classified breast cancers into luminal A, luminal B, HER2-positive, and triple negative using estrogen receptor, progesterone receptor, HER2, and Ki-67. They used a 14% cutoff value for Ki-67 with hormone receptor–positive breast cancer having Ki-67 < 14% as luminal A and those with ≥ 14% as luminal B.⁶ The St. Gallen Consensus for treat-

ment of early breast cancer adopted the surrogate definitions of breast cancer subtypes proposed by Cheang *et al.*⁶ and established guidelines according to each subtype, which are now held standard of treatment in breast cancer.^{7,8} Because classification of luminal A and luminal B subtypes depends on Ki-67 index, its accurate measurement is a critical factor in deciding therapeutic modalities.

Ki-67 is a protein expressed in all phases of the cell cycle (except for resting Go) used as a tumor proliferation marker.⁹ Ki-67 index is defined by the percentage of tumor cells with positive nuclear staining out of all tumor cells within a given histological field. Several studies have shown the prognostic and predictive value of Ki-67 with a high Ki-67 index having higher risks of recurrence and treatment response in breast cancer.¹⁰⁻¹³ Furthermore, a more recent study has shown that for neoadjuvant

endocrine therapy, Ki-67 indices before treatment and 2 weeks after treatment are strongly associated with time to relapse as well as response to endocrine treatment.¹⁴ Despite such critical role of Ki-67 index in breast cancer treatment, there exist dilemma in using it as a standard prognostic or predictive marker owing to the lack of standard methodologies in its measurement.

There are some methodological issues concerning Ki-67 index interpretation, which can cause variabilities in its measurement. First, the number of tumor cells counted and the areas selected for counting may be different for each observer. Second, as with other tumors, breast cancers may exhibit intratumoral heterogeneity in cell proliferation with areas of higher proliferation indicated by more intense staining of Ki-67 known as “hot spots.” In tumors with such hot spots, an observer may decide to measure Ki-67 index from the hot spot or take the average of a few different fields in the same section. Third, some may proceed with manual counting while others may utilize digital image analysis (DIA). Fourth, some may record Ki-67 index in continuous numbers while others may record it in categorical values. Together, these various factors inevitably lead to interobserver variability in Ki-67 measurement, the degree of which is unknown. Thus, suggestions have been put forth by the International Ki-67 in Breast Cancer Working Group in an attempt to standardize Ki-67 measurement.¹⁵ The need for standard criteria regarding the number of tumor cells and the area of the field to be counted, as well as the method of counting is becoming all the more urgent.

In this study, we chose 20 samples of invasive breast cancer, of which 10 had hot spots and performed a multicenter study with participation from 30 institutions to assess the degree of

interobserver variability in Ki-67 index measurement and clarify the factors affecting its measurement by comparing whole sections versus tissue microarray (TMA) platforms, average counting versus hot spot counting, and continuous versus categorical counting.

MATERIALS AND METHODS

Case selection and TMA construction

Twenty cases (T1–T20) of invasive ductal carcinoma (IDC) were selected from the pathologic archives of Seoul National University Bundang Hospital after reviewing the Ki-67 immunostained slides upon diagnosis. All cases were surgically resected tissue specimens fixed in 10% formalin and paraffin-embedded in 2012. To analyze the effect of the presence of hot spots in Ki-67 measurement, we purposely chose 10 IDCs (T11–T20) which had localized high Ki-67 staining areas (Fig. 1). The remaining (T1–T10) showed a relatively even distribution of positive tumor cells. All twenty cases were arranged into a 2 mm, single-core TMA to set limits for the area of analysis, as opposed to whole section slides. TMA was constructed using a trephine apparatus (Superbiochips Laboratories, Seoul, Korea). Hot spot areas were selected to be incorporated into the TMA in 10 IDCs (T11–T20) while areas most representative of the tumor were selected for the remaining 10 cases (T1–T10) for TMA construction. This study was exempt from Institutional Review Board (IRB) deliberation (IRB No. X-1508/312-901).

Immunohistochemical staining and measurement of Ki-67

Immunohistochemical staining of Ki-67 was re-performed

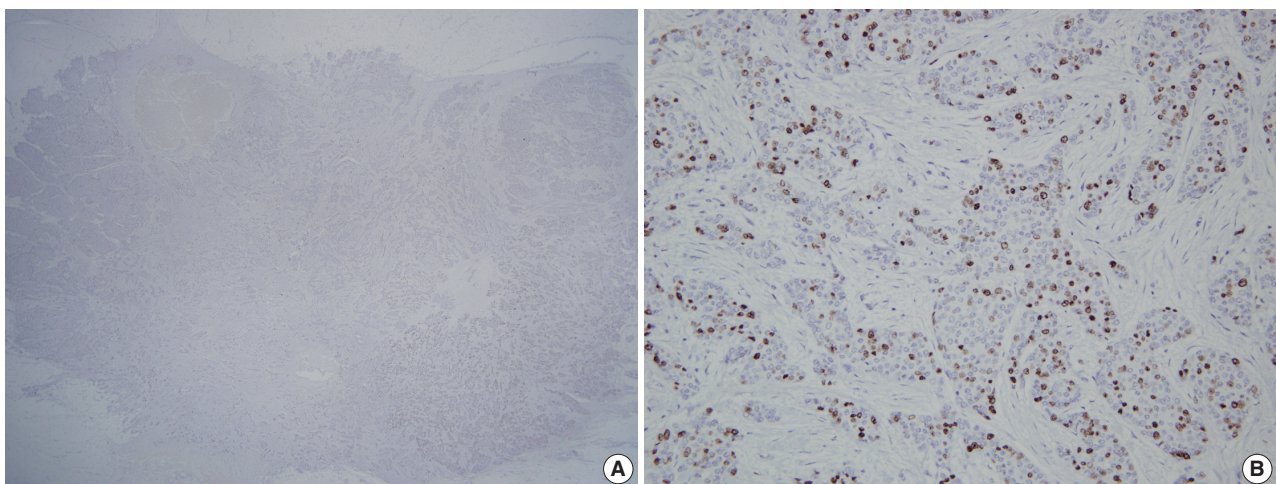


Fig. 1. A representative case with hot spots in Ki-67 immunohistochemistry. (A) Scan power view of Ki-67 immunostained slides with a hot spot in right lower corner. (B) High power view of the hot spot.

using MIB-1 clone (1:500; DAKO, Carpinteria, CA, USA) in whole sections and a TMA section. Four-micrometer-thick tissue sections were cut, dried, deparaffinized, and rehydrated following standard procedures. All sections were subjected to heat-induced antigen retrieval. Immunohistochemical staining was carried out in a BenchMark XT autostainer (Ventana Medical Systems, Tucson, AZ, USA) using an UltraView detection kit. All immunostained slides were scanned using ScanScope CS system (Aperio, Vista, CA, USA) and the files of such scanned slides were uploaded to an online system. Thirty different pathologists (O1–O30) from thirty different institutions (25 of which are academic teaching hospitals including all of the major hospitals in the country) participated in this study and examined the scanned slides using ImageScope viewing software with specific guidelines for Ki-67 measurement.

All observers measured Ki-67 index in two different ways for both whole section slides and a TMA slide. First, direct counting method consisted of counting at least 500 tumor cells in each of three representative areas in whole sections and counting of at least 500 tumor cells or all of the tumor cells (if the number of tumor cells were less than 500) in a TMA, either manually or digitally using an image analyzer, and the positive percentage was calculated; two out of 30 participants utilized DIA for direct counting. Second, rough estimation method consisted of visual estimation of Ki-67 index into five categories: 0 (<5%), 1 (5% to <10%), 2 (10% to <20%), 3 (20% to <50%), and 4

(≥50%). In tumors with hot spot areas (T11–T20), direct counting on whole section slides consisted of two different methods. The first was to count the number of positive tumor cells in one representative hot spot area which we designated as the “hot spot method.” The other method was counting in three representative areas including the hot spot and then calculating its average, which we named as the “average method.” For rough estimation, the observers made separate categorical estimations of Ki-67 from the hot spot and the entire field in whole section slides in tumors with hot spot areas (T11–T20). The schematic representation of study design and counting methods is provided in Fig. 2.

Statistical analyses

To assess interobserver variability in the 20 cases, we calculated intraclass correlation coefficient (ICC) with a 95% confidence interval (CI). Since there is no consensus on standard criteria for ICC, we used this value only for comparison of interobserver variabilities of different Ki-67 measurement methods. The ICC has a range of 0 to 1, with 1 defining perfect agreement. To evaluate the distribution of Ki-67 proliferation indices measured by different observers for each case, we calculated the mean, median, standard error of mean, and standard deviation of each case, for every method. We drew a side by side box plot for Ki-67 indices. All data analyses were performed using IBM SPSS ver. 21.0.0 (IBM Co., Armonk, NY, USA).

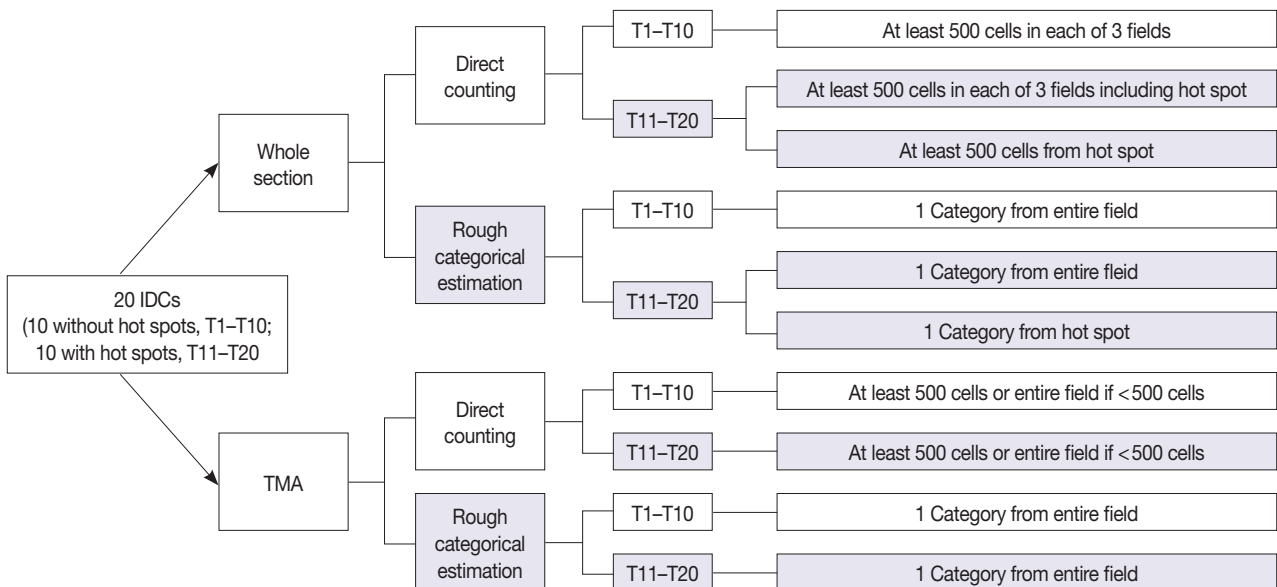


Fig. 2. A schematic diagram of study design and counting methods. Twenty cases of invasive ductal carcinoma (IDC) were prepared in two platforms-whole sections and a tissue microarray (TMA), and then digitally scanned for analysis in online system. Each observer was instructed to measure Ki-67 index in two platforms in two different ways (direct counting or rough categorical estimation) employing the average method and hot spot method.

RESULTS

Direct counting

The Ki-67 indices in each tumor calculated by direct counting in whole sections and a TMA are presented in Fig. 3. The mean and median values of Ki-67 indices were relatively lower

in T1–T10 than in T11–T20 for both whole sections and TMA. To evaluate the effect of restricting area of measurement on Ki-67 counting, we compared the ICCs of Ki-67 indices in whole sections and TMA. The ICC of 20 cases among 30 observers was 0.802 (95% CI, 0.696 to 0.897) for whole sections by the average method. The ICC of Ki-67 indices measured in TMA was

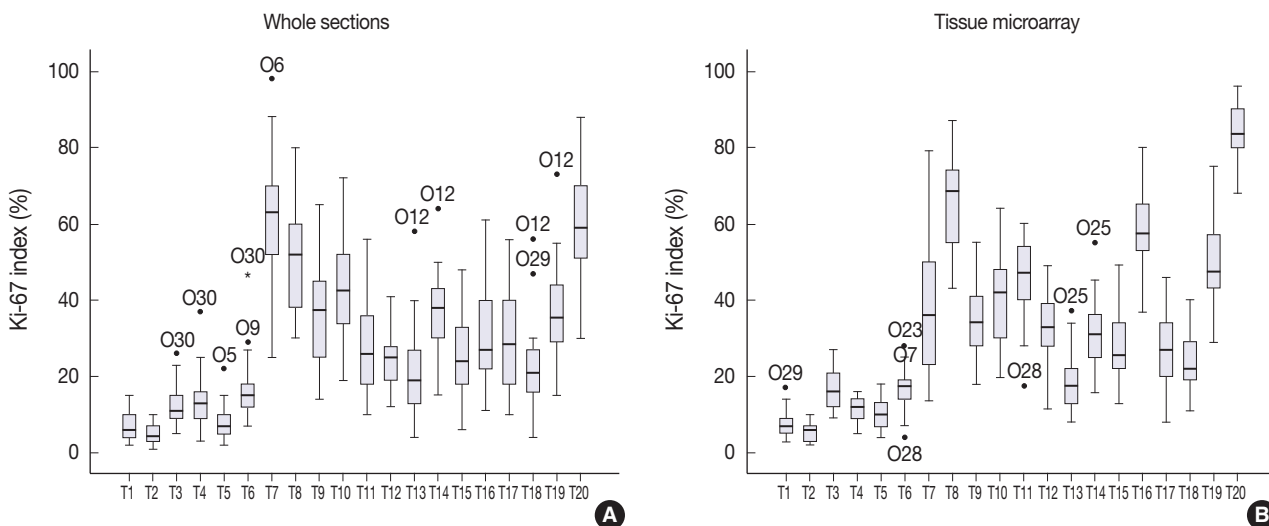


Fig. 3. Side-by-side box plots of Ki-67 distribution using whole sections (A) and tissue microarray slides (B) in direct counting method. The box shows the first to third quartiles, the horizontal line inside the box represents the median, the whiskers extend to minimum and maximum values within 1.5 times the interquartile range (IQR) from the first and third quartiles. Outliers are represented by small circles and extreme values (more than 3 times IQR) by asterisks. The Ki-67 indices measured in whole section show wider distribution than those in tissue microarray.

Table 1. Comparison of Ki-67 assessment in whole sections and tissue microarray in T11–T20

	T11	T12	T13	T14	T15	T16	T17	T18	T19	T20
Whole section, average method										
Minimum	10.00	12.00	4.00	15.00	6.00	11.00	10.00	4.00	15.00	30.00
Maximum	56.00	41.00	58.00	64.00	48.00	61.00	56.00	56.00	73.00	88.00
Mean	28.20	24.43	20.50	37.20	24.97	31.30	29.27	21.93	37.13	59.90
Median	26.00	25.00	19.00	38.00	24.00	27.00	28.50	21.00	35.50	59.00
SD	12.50	7.12	11.77	10.09	10.24	13.08	12.76	10.58	12.74	14.68
SE	2.28	1.30	2.15	1.84	1.87	2.39	2.33	1.93	2.33	2.68
Whole section, hot spot method										
Minimum	24.80	23.50	13.50	20.60	17.50	27.00	15.80	16.50	33.30	62.50
Maximum	62.20	56.00	36.50	59.50	61.00	79.30	54.50	49.00	72.50	94.00
Mean	44.59	35.74	26.73	41.71	34.40	56.43	37.03	29.38	51.58	82.50
Median	46.00	34.00	26.85	41.75	35.80	55.85	39.00	28.45	49.75	83.35
SD	9.65	8.71	6.14	8.42	9.26	11.46	9.60	7.81	9.35	7.86
SE	1.76	1.59	1.12	1.54	1.69	2.09	1.75	1.43	1.71	1.44
Tissue microarray										
Minimum	17.50	11.60	8.00	15.80	13.00	37.00	8.00	11.00	29.00	68.00
Maximum	60.00	49.00	37.00	55.00	49.00	80.00	46.00	40.00	75.00	96.00
Mean	45.62	32.99	18.19	31.46	28.42	59.07	26.83	24.09	50.33	83.97
Median	47.00	33.00	17.50	31.00	25.50	57.50	27.00	22.00	47.50	83.50
SD	10.78	9.11	6.98	8.38	8.97	10.11	9.61	7.14	10.72	7.40
SE	1.97	1.66	1.27	1.53	1.64	1.85	1.76	1.30	1.96	1.35

Values are presented as percentage.
SD, standard deviation; SE, standard error of mean.

0.895 (95% CI, 0.829 to 0.948). Because the TMA was constructed from the hot spot areas in T11–T20, we also compared the Ki-67 indices acquired by hot spot method in whole sections with those in TMA (Table 1). In T11–T20, the ICC of TMA was higher than that of whole sections using hot spot method (TMA: ICC, 0.895 [95% CI, 0.798 to 0.966]; whole section: ICC, 0.737 [95% CI, 0.561 to 0.905]).

To assess the effect of the presence of hot spots on direct counting, we compared the ICC of tumors without hot spots (T1–T10) with that of tumors with hot spots (T11–T20). Ki-67 indices using the average method were used for analysis in both T1–T10 and T11–T20. The ICC of T1–T10 was 0.874 with a 95% CI of 0.761–0.959, and the ICC of T11–T20 was 0.736 with a 95% CI of 0.559–0.904 in whole sections. The ICC of tumors with hot spots was significantly lower than that of tumors without hot spots using the same method of counting.

We also compared the ICC of two different counting methods applied in T11–T20: hot spot method versus average method (Table 1). In general, the mean Ki-67 indices resulting from the hot spot method was higher than those yielded using the average method. However, there was no difference between the ICC value of the former (ICC, 0.737 [95% CI, 0.561 to 0.905]) and latter ICC, 0.736 [95% CI, 0.559 to 0.904].

Categorical estimation

The Ki-67 indices in each tumor calculated by rough estimation for whole sections and TMAs are presented in Fig. 4. In whole sections, Ki-67 indices belonged to two categories in six

cases, three categories in six cases, four categories in seven cases, and five categories in the remaining one case. In TMAs, they were assigned to one category in one case, two in six, three in eight, and four in the remaining five cases. Ki-67 for T15 in particular, showed a poor concordance between observers in the whole section. One observer assessed Ki-67 index as less than 5% while another assessed it as more than 50%. Rough estimation in TMA resulted in a narrower distribution of Ki-67 categories in six cases (T11 and T15 through 20) and a wider distribution of Ki-67 in three cases (T7, T10, and T14) compared with that in whole sections. Based on the distribution of Ki-67 indices, the rough estimation method was not better than the direct counting method.

Additionally, we compared the Ki-67 indices acquired by rough estimation in whole section using hot spot method with those in TMA for T11–T20 (Table 2). The distribution of Ki-67 categories was mainly restricted to two continuous categories in both platforms. In T11–T20, we also compared the Ki-67 indices acquired by categorical estimation in two different ways: hot spot method versus average method (Table 2). We observed that tumors tended to be categorized into higher categories and the range of distribution was decreased using the hot spot method compared with the average method.

DISCUSSION

Although Ki-67 index in breast cancer has predictive and prognostic values, it has not been accepted as a standard predic-

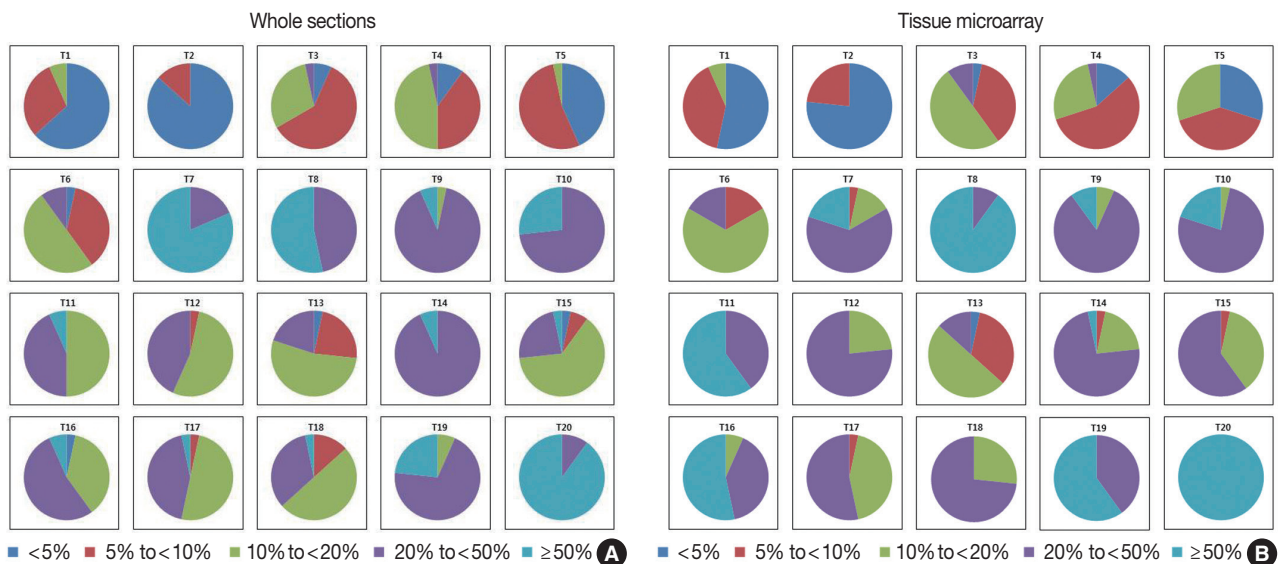


Fig. 4. Distribution of Ki-67 indices in whole sections (A) and tissue microarray slides (B) in categorical estimation. The Ki-67 indices measured by categorical estimation in whole sections and TMAs show a wide distribution in some cases.

Table 2. Ki-67 index assessment by rough estimation method in whole sections and tissue microarray in T11–T20

	T11	T12	T13	T14	T15	T16	T17	T18	T19	T20
Whole section, average method										
<5%	0	0	1	0	1	1	0	0	0	0
5 to <10%	0	1	7	0	2	0	1	4	0	0
10 to <20%	15	16	16	0	19	11	15	15	2	0
20 to <50%	13	13	6	28	7	16	13	10	21	3
≥50%	2	0	0	2	1	2	1	1	7	27
Whole section, hot spot method										
<5%	0	0	0	0	0	0	0	0	0	0
5 to <10%	0	0	1	0	0	0	0	0	0	0
10 to <20%	0	4	8	0	6	1	0	6	0	0
20 to <50%	22	24	20	15	22	8	20	22	8	0
≥50%	8	2	1	15	2	21	10	2	22	30
Tissue microarray										
<5%	0	0	1	0	0	0	0	0	0	0
5 to <10%	0	0	10	1	1	0	1	0	0	0
10 to <20%	0	7	15	6	11	2	13	8	0	0
20 to <50%	12	23	4	22	18	12	16	22	12	0
≥50%	18	0	0	1	0	16	0	0	18	30

The numbers presented indicate the number of cases that belong to each category.

tive or prognostic biomarker due to variability in its measurement. Thus, in this study, we performed a multicenter study to assess the degree of interobserver variability in Ki-67 index measurement and to find factors that contribute to its variability.

As there is no statistical criterion defining “high” concordance, one study assumed it to be having an ICC of approximately 0.9.¹⁶ The ICCs for various measurements taken in our study were in the range of 0.7–0.8. Thus, interobserver concordance in Ki-67 measurement was moderately good at best for all settings. We were, however, able to deduce some important conclusions from our study. With the participation of thirty different institutions, we evaluated interobserver variability in Ki-67 index measurement specifically depending on the area of selection, intratumoral heterogeneity, and counting method, which we held especially important among several factors that are known to influence Ki-67 measurement variability.

Previous studies evaluating interobserver variability of Ki-67 measurement have used either core biopsy samples or TMAs. However, this study is the first one, to our best knowledge, to have made direct comparisons between the whole section and TMA preparations from the same tumor sample. While restricting the area of counting increased concordance between the observers by a small amount (TMA: ICC, 0.895 [95% CI, 0.829 to 0.948]; whole section: ICC, 0.858 [95% CI, 0.774 to 0.929]), the difference was not significantly large. However, in tumors with hot spots (T11–T20), the ICC of TMA was much higher than that of whole sections using either average method or hot

spot method (TMA: ICC, 0.895 [95% CI, 0.798 to 0.966]; whole section, average method: ICC, 0.736 [95% CI, 0.559 to 0.904]; whole section, hot spot method: ICC, 0.737 [95% CI, 0.561 to 0.905]). Similarly, in categorical estimation, the range of distribution in Ki-67 categories was decreased when counting in TMA in the cases with hot spots. Thus, restricting the area of counting seems to be a critical factor affecting concordance in Ki-67 measurement.

Because some breast cancers possess intratumoral heterogeneity in tumor cell proliferation, a manifestation of which is the presence of hot spots in Ki-67 expression, we attempted to analyze the degree of difference in Ki-67 measurement between observers in two ways. Dividing those cancers with and without hot spots and measuring ICCs of the two groups for the average counting method yielded an ICC of 0.874 for T1–T10 (95% CI, 0.761 to 0.959) and 0.736 (95% CI, 0.559 to 0.904) for T11–T20 in whole sections. Thus, the ICC of tumors with hot spots was much lower than that of tumors without hot spots; such finding that tumors with hot spots exhibit greater interobserver variability is not counterintuitive. A more interesting finding is that within this subset of tumors with hotspots, when we measured the degree of difference in Ki-67 measurement with regards to counting an average of the entire field or taking a single count from the hot spot only, there was no difference between the ICC value of the former (ICC, 0.736 [95% CI, 0.559 to 0.904]) and latter (ICC, 0.737 [95% CI, 0.561 to 0.905]). We expected that the ICC for whole section using hot spot

method would be higher than that for whole section using average method. However, even within the hot spots, it was likely that observers chose different areas for counting, and the distribution of Ki-67–stained tumor nuclei was variable.

Interpretation of the weakly stained nuclei as either positive or negative staining may be an important factor contributing to variability in Ki-67 measurement. However, we did not investigate this interpretative issue in the current study. We used a mouse monoclonal antibody MIB-1 for Ki-67 immunostaining. It yielded similar yet less intense staining results compared with rabbit monoclonal antibody SP6 using the central laboratory equipment (data not shown). SP6 was employed in many previous pivotal studies^{6,17–20} and showed increased sensitivity compared to mouse monoclonal antibodies.^{17,18,20} However, the current recommendations from the International Ki-67 in Breast Cancer Working Group states only MIB-1 as the antibody endorsed in Ki-67 measurement.^{15,21} Further comparative studies using different clones for Ki-67 and interpretation of weakly stained nuclei will be needed.

In order to assess interobserver variability depending on the counting method (in categories or direct numbers), each observer was instructed to take these two counting methods for each sample: for direct counting, more than five hundred cells were counted from at least three representative areas. For categorical counting, the observers made an estimate of the percentage of positive tumor cells into five categories (category 0, < 5%; category 1, 5%–10%; category 2, 10%–20%; category 3, 20%–50%; and category 4, ≥ 50%). Although Ki-67 indices belonged to two categories in six cases on whole section and TMA (one case on TMA belonged to only one category), they had a wide distribution belonging to more than three categories in the remaining cases. Moreover, the cases with Ki-67 index within 10%–20%, which includes the cutoff value of 14% used for distinction of luminal A and luminal B subtypes in breast cancer, showed wide distribution in rough estimation from category 0 to 4. Therefore, rough estimation methods may be worse than direct counting method in terms of interobserver concordance.

A limitation of our study includes a small number of tumor samples. Although each tumor sample was presented in two platforms of whole section and TMA, and each observer made at least a few countings for each sample for various settings, the absolute sample number was only twenty, which is the major reason we restricted our statistical analysis to evaluating ICCs.

Finally, all of the observers were given the liberty of using either manual or digital counting, and two observers made direct counting via DIA. However, we were not able to make direct

comparisons between the two methods due to the small sample size. DIA enables a much quicker measurement, and its clinical utility seems promising. One group has reported that automated Ki-67 measurement was almost as comparable as visual estimation in precision and prognostic ability,²² and Laurinavicius *et al.*²³ have suggested specific methodologies in using DIA for Ki-67 measurement. Standardization of DIA techniques may offer more consistent results between observers in the future, and its application using standard protocols should be studied in further studies.

In conclusion, our nationwide thirty-center study of Ki-67 interobserver variability showed that interobserver variability in measuring this critical biomarker is high. Although direct comparison between direct counting and rough estimation into categories was impossible due to statistical issues, direct counting seems to result in less interobserver variability. Thus, we recommend that Ki-67 measurement be performed by direct counting rather than by rough categorical estimation. Tumors with hot spots generally showed greater interobserver variability than those without hot spots. However, restricting the area of measurement to TMA platform resulted in decreased interobserver variability, even in tumors with hot spots. At this point, we cannot put down a specific number for the area of selection, and further studies are needed; however, we can propose that the area of selection should be confined to a specific area, such as the periphery of the tumor or hot spots (in cases with hot spots). Lastly, we urge future analyses comparing manual counting versus DIA in Ki-67 measurement since DIA seems to reduce not only intraobserver variability but also interobserver variability so that this critical biomarker can be used with a greater confidence in clinical practice.

*The Korean Breast Pathology Ki-67 Study Group

Sun Young Kwon; Department of Pathology, Keimyung University School of Medicine, Daegu, Korea

Youngmee Kwon; Department of Pathology, National Cancer Center, Goyang, Korea

Dae Cheol Kim; Department of Pathology, College of Medicine, Dong-A University, Busan, Korea

Dong Sug Kim; Dr. Kim's Pathology Clinic, Daegu, Korea

Eun Kyung Kim; Department of Pathology, Eulji University College of Medicine, Seoul, Korea

Wan Seop Kim; Department of Pathology, Konkuk University School of Medicine, Seoul, Korea

Yee Jeong Kim; Department of Pathology, National Health Insurance Service Ilsan Hospital, Goyang, Korea

Chungyeul Kim; Department of Pathology, College of Medicine, Korea University, Seoul, Korea

Ji-Young Kim; Department of Pathology, CHA Gangnam Medical Center, CHA University School of Medicine, Seoul, Korea

Hee Jung Kim; Department of Pathology, MizMedi Hospital, Seoul, Korea

Sung-Im Do; Department of Pathology, Kangbuk Samsung Hospital, Sungkyunkwan University School of Medicine Seoul, Korea

Young Hee Maeng; Department of Pathology, Jeju National University School of Medicine, Jeju, Korea

Kyeongmee Park; Department of Pathology, Inje University Sanggye Paik Hospital, Seoul, Korea

So Young Park; Department of Pathology, MizMedi Hospital, Seoul, Korea

Young Kyung Bae; Department of Pathology, Yeungnam University College of Medicine, Daegu, Korea.

Kwang-Sun Suh; Department of Pathology, Chungnam National University School of Medicine, Daejeon, Korea

Jeong Yun Shim; Department of Pathology, CHA Gangnam Medical Center, CHA University School of Medicine, Seoul, Korea

Hoon Kyu Oh; Department of Pathology, Catholic University of Daegu College of Medicine, Daegu, Korea

Jin Ye Yoo; Department of Pathology, Saegyaero Hospital, Busan, Korea

Hye Kyoung Yoon; Department of Pathology, Inje University Busan Paik Hospital, Busan, Korea

Ah Won Lee; Department of Hospital Pathology, Seoul St. Mary's Hospital, The Catholic University of Korea College of Medicine, Seoul, Korea

Ji Shin Lee; Department of Pathology, Chonnam National University Medical School, Gwangju, Korea

Hyun Ju Lee; Department of Pathology, Soonchunhyang University Cheonan Hospital, Soonchunhyang University College of Medicine, Cheonan, Korea

Hee Jin Lee; Department of Pathology, Asan Medical Center, Seoul, Korea

Hyunee Yim; Department of Pathology, Ajou University Hospital, Suwon, Korea

Yi Kyeong Chun; Department of Pathology, Cheil General Hospital and Women's Healthcare Center, Dankook University College of Medicine, Seoul, Korea

Min Jung Jung; Department of Pathology, Kosin University Gospel Hospital, Busan, Korea

Eun Yoon Cho; Department of Pathology, Samsung Medical Center, Sungkyunkwan University School of Medicine, Seoul, Korea

Yoon-Mi Jeon; Department of Pathology, Soonchunhyang University Hospital, Seoul, Korea

Hyun Joo Choi; Department of Hospital Pathology, St. Vincent's Hospital, The Catholic University of Korea College of Medicine, Suwon, Korea

Conflicts of Interest

No potential conflict of interest relevant to this article was reported.

Acknowledgments

This study was supported by Korean Society of Pathologists Grant 2013, and by a grant from the Basic Science Research Program through the National Research Foundation of Korea (NRF) funded by the Ministry of Science, ICT and Future Planning (Grant No. NRF-2015R1A2A2A01007907) to Park SY.

REFERENCES

1. Polyak K. Breast cancer: origins and evolution. *J Clin Invest* 2007; 117: 3155-63.
2. Sørlie T, Perou CM, Tibshirani R, *et al.* Gene expression patterns of breast carcinomas distinguish tumor subclasses with clinical implications. *Proc Natl Acad Sci U S A* 2001; 98: 10869-74.
3. Perou CM, Sørlie T, Eisen MB, *et al.* Molecular portraits of human breast tumours. *Nature* 2000; 406: 747-52.
4. Nielsen TO, Hsu FD, Jensen K, *et al.* Immunohistochemical and clinical characterization of the basal-like subtype of invasive breast carcinoma. *Clin Cancer Res* 2004; 10: 5367-74.
5. Carey LA, Perou CM, Livasy CA, *et al.* Race, breast cancer subtypes, and survival in the Carolina Breast Cancer Study. *JAMA* 2006; 295: 2492-502.
6. Cheang MC, Chia SK, Voduc D, *et al.* Ki67 index, HER2 status, and prognosis of patients with luminal B breast cancer. *J Natl Cancer Inst* 2009; 101: 736-50.
7. Goldhirsch A, Winer EP, Coates AS, *et al.* Personalizing the treatment of women with early breast cancer: highlights of the St Gallen International Expert Consensus on the Primary Therapy of Early Breast Cancer 2013. *Ann Oncol* 2013; 24: 2206-23.
8. Goldhirsch A, Wood WC, Coates AS, Gelber RD, Thurlimann B, Senn HJ. Strategies for subtypes: dealing with the diversity of breast cancer: highlights of the St. Gallen International Expert Consensus on the Primary Therapy of Early Breast Cancer 2011. *Ann*

- Oncol 2011; 22: 1736-47.
9. Bruno S, Darzynkiewicz Z. Cell cycle dependent expression and stability of the nuclear protein detected by Ki-67 antibody in HL-60 cells. *Cell Prolif* 1992; 25: 31-40.
 10. Luporsi E, André F, Spyrtos F, *et al.* Ki-67: level of evidence and methodological considerations for its role in the clinical management of breast cancer: analytical and critical review. *Breast Cancer Res Treat* 2012; 132: 895-915.
 11. Yerushalmi R, Woods R, Ravdin PM, Hayes MM, Gelmon KA. Ki67 in breast cancer: prognostic and predictive potential. *Lancet Oncol* 2010; 11: 174-83.
 12. Viale G, Giobbie-Hurder A, Regan MM, *et al.* Prognostic and predictive value of centrally reviewed Ki-67 labeling index in postmenopausal women with endocrine-responsive breast cancer: results from Breast International Group Trial 1-98 comparing adjuvant tamoxifen with letrozole. *J Clin Oncol* 2008; 26: 5569-75.
 13. Penault-Llorca F, André F, Sagan C, *et al.* Ki67 expression and docetaxel efficacy in patients with estrogen receptor-positive breast cancer. *J Clin Oncol* 2009; 27: 2809-15.
 14. Dowsett M, Smith IE, Ebbs SR, *et al.* Prognostic value of Ki67 expression after short-term presurgical endocrine therapy for primary breast cancer. *J Natl Cancer Inst* 2007; 99: 167-70.
 15. Dowsett M, Nielsen TO, A'Hern R, *et al.* Assessment of Ki67 in breast cancer: recommendations from the International Ki67 in Breast Cancer working group. *J Natl Cancer Inst* 2011; 103: 1656-64.
 16. Polley MY, Leung SC, McShane LM, *et al.* An international Ki67 reproducibility study. *J Natl Cancer Inst* 2013; 105: 1897-906.
 17. Wong SC, Chan JK, Lo ES, *et al.* The contribution of bifunctional SkipDewax pretreatment solution, rabbit monoclonal antibodies, and polymer detection systems in immunohistochemistry. *Arch Pathol Lab Med* 2007; 131: 1047-55.
 18. Zabaglo L, Salter J, Anderson H, *et al.* Comparative validation of the SP6 antibody to Ki67 in breast cancer. *J Clin Pathol* 2010; 63: 800-4.
 19. Ekholm M, Beglerbegovic S, Grabau D, *et al.* Immunohistochemical assessment of Ki67 with antibodies SP6 and MIB1 in primary breast cancer: a comparison of prognostic value and reproducibility. *Histopathology* 2014; 65: 252-60.
 20. Fasanella S, Leonardi E, Cantaloni C, *et al.* Proliferative activity in human breast cancer: Ki-67 automated evaluation and the influence of different Ki-67 equivalent antibodies. *Diagn Pathol* 2011; 6 Suppl 1: S7.
 21. Colozza M, Azambuja E, Cardoso F, Sotiriou C, Larsimont D, Piccart MJ. Proliferative markers as prognostic and predictive tools in early breast cancer: where are we now? *Ann Oncol* 2005; 16: 1723-39.
 22. Mohammed ZM, McMillan DC, Elsberger B, *et al.* Comparison of visual and automated assessment of Ki-67 proliferative activity and their impact on outcome in primary operable invasive ductal breast cancer. *Br J Cancer* 2012; 106: 383-8.
 23. Laurinavicius A, Plancoulaine B, Laurinaviciene A, *et al.* A methodology to ensure and improve accuracy of Ki67 labelling index estimation by automated digital image analysis in breast cancer tissue. *Breast Cancer Res* 2014; 16: R35.

Comparison of Analytical and Clinical Performance of HPV 9G DNA Chip, PANArray HPV Genotyping Chip, and Hybrid-Capture II Assay in Cervicovaginal Swabs

Ho Young Jung · Hye Seung Han
Hyo Bin Kim¹ · Seo Young Oh¹
Sun-Joo Lee² · Wook Youn Kim

Department of Pathology, Konkuk University School of Medicine, Seoul; ¹Department of Pathology, Konkuk University Medical Center, Seoul; ²Department of Obstetrics and Gynecology, Konkuk University School of Medicine, Seoul, Korea

Received: September 30, 2015

Revised: October 16, 2015

Accepted: October 21, 2015

Corresponding Author

Wook Youn Kim, MD, PhD
Department of Pathology, Konkuk University School of Medicine, 120-1 Neungdong-ro, Gwangjin-gu, Seoul 05030, Korea
Tel: +82-2-2030-5646
Fax: +82-2-2030-5629
E-mail: 20100182@kuh.ac.kr

Background: Human papillomavirus (HPV) infection can be detected by using several molecular methods, including Hybrid-Capture II (HC2) assay and variable HPV DNA chip tests, although each method has different sensitivities and specificities. **Methods:** We performed HPV 9G DNA Chip (9G) and PANArray HPV Genotyping Chip (PANArray) tests on 118 cervicovaginal swabs and compared the results with HC2, cytology, histology, and direct sequencing results. **Results:** The overall and high-risk HPV (HR-HPV) positivity rates were 62.7% and 44.9% using 9G, and 61.0% and 30.5% using PANArray, respectively. The positivity rates for HR-HPV with these two chips were significantly lower than 55.1% when HC2 was used. The sensitivity of overall HPV positivity in detecting histologically confirmed low-grade cervical squamous intraepithelial lesions or higher was 88.7% for all three tests. The specificity was 58.5% for 9G and 61.5% for PANArray, which was significantly lower than the 72.3% for HC2. With the HR-HPV⁺ genotype threshold, the sensitivity decreased to 75.5% for 9G and 52.8% for PANArray, which was significantly lower than the 88.7% for HC2. Comparison of the two chips showed concordant results in 55.1% of the samples, compatible results in 16.9%, and discordant results in 28.0%, exhibiting poor agreement in detecting certain HPV genotypes. Compared with direct sequencing, 9G yielded no discordant results, whereas PANArray yielded 31 discordant results (26.7%). **Conclusions:** Compared with HC2, the HPV genotyping tests showed lower sensitivity in histologic correlation. When the two chips were compared, the 9G was more sensitive and accurate for detecting HR-HPV than the PANArray.

Key Words: Human papillomavirus; Hybrid-Capture II assay; Oligonucleotide array sequence analysis; Cervix uteri

The causal role of human papillomavirus (HPV) infection has been well established in the pathogenesis of cervical cancer and precancerous lesions.¹ Among the large number of HPV genotypes identified to date, about 40 genotypes infect the mucosal lining of the human body, including the anogenital tract. Based on their epidemiological association with cervical lesions, the mucosal HPV strains are classified into high-risk (HR) and low-risk (LR) genotypes.^{2,3} The HR-HPV genotypes are detected more frequently in precancerous or cancerous cervical lesions, whereas the LR-HPV genotypes cause genital warts and are rarely associated with premalignant or malignant cervical lesions.^{3,4} Although most LR- or HR-HPV infections are transient and successfully controlled by the host immune system, persistent infection with HR-HPV was highly associated with the development of high-grade dysplasia or invasive cervical cancers.^{5,6} Overall, 14 HR-HPV genotypes (HPV 16, 18, 31, 33, 35, 39,

45, 51, 52, 56, 58, 59, 66, and 68) have been identified in almost all cervical cancers worldwide.⁴ Among these types, HPV 16 is the most important genotype that causes more than 50% of cervical carcinomas, followed by HPV 18 that causes 10%–15% and HPV 45 that causes approximately 7%.⁷ HPV 18 is also identified in more than 35% of cervical adenocarcinomas.⁸ Therefore, detecting HR-HPV in cervical samples is an important ancillary test for screening cervical lesions.⁹ Furthermore, HPV testing has been shown to have a high negative predictive value (NPV) close to 100% for high-grade squamous intraepithelial lesions (HSILs) and invasive cancers, thereby emphasizing the usefulness of HPV tests in the triage of equivocal or low-grade cytological smears.^{10,11}

HPV infection can be detected by many molecular methods, including Hybrid-Capture II assay (HC2; Qiagen, Gaithersburg, MD, USA) and variable HPV genotyping tests, although these

methods have different sensitivities and specificities. HC2 detects 13 types of HR-HPV by means of an RNA cocktail probe and provides pooled data about HR-HPV infection, but does not indicate individual HPV types; further, it is the most widely used screening test with proven clinical performance.¹²⁻¹⁴ However, because a few HPV types, including HPV 16 and 18 among the many types of HPV, are responsible for most HPV-related cancers, a clinical necessity for HPV genotyping that can distinguish individual types has arisen. Genotyping for specific oncogenic HPV types has also been shown to improve the positive predictive value (PPV) and specificity in predicting HSIL and carcinoma in women with atypical squamous cells of undetermined significance (ASCUS) and low-grade cervical squamous intraepithelial lesions (LSIL).¹⁵ In addition, in vaccinated women, type-specific HPV testing can be useful to assess the prevalence of specific HPV types, including HPV types that do not have vaccines available.¹⁵ Reflecting this trend, the recently introduced Cobas HPV test (Roche Molecular Systems Inc., Branchburg, NJ, USA) provides specific genotyping data about HPV 16 and 18 in conjunction with pooled HR-HPV results.¹⁶

In Korea, several HPV genotyping tests that use polymerase chain reaction (PCR)-based microarray methods are commercially available, but they lack standardization compared to HC2 and show variable clinical efficacy. We therefore selected two widely used DNA chips, the HPV 9G DNA Chip (9G; Diatech Korea Co. Ltd., Seoul, Korea) and PANArray HPV Genotyping Chip (PANArray; Panagene, Daejeon, Korea), and compared their results with the results from HC2, cytological diagnoses, and histological diagnoses in terms of clinical efficacy. Additionally, genotyping results of these two chips were further validated by direct sequencing.

MATERIALS AND METHODS

Selection of study samples

A total of 118 histologically confirmed cervicovaginal swab specimens in which HPV infection status was examined by HC2, between January 2015 and March 2015 at Konkuk University Medical Center, were collected. Cytological diagnosis was obtained in 109 patients using liquid-based cervical cytology (Sure-

Path, TriPath Imaging Inc., Burlington, NC, USA) according to the Bethesda System for reporting cervical cytology.¹⁷ Histological confirmation was available in all 118 cases using cervical biopsy, loop electrosurgical excision procedure, and hysterectomy within one month from HC2. In total, nine cases have not been sent for cytological examination, but were submitted for histological examination. The cytological and histological diagnoses were reviewed and confirmed by two pathologists (H.S.H. and W.Y.K.). This study was approved by the Institutional Review Board (KUH 1210039).

HC2

Cervical specimens were collected using brush samplers and placed in a collection tube containing a preservative solution (Qiagen). A 200- μ L aliquot of each sample was removed and stored for DNA extraction and subsequent testing for HPV genotyping assays. The HC2 assay method was performed using residual sample materials with the automated HC2 assay system, according to the manufacturer's protocol (Qiagen). The samples were analyzed for the presence of 13 HR-HPV types (16, 18, 31, 33, 35, 39, 45, 51, 52, 56, 58, 59, and 68). Positive and negative controls (provided by the manufacturer) were included in each run. The relative light unit for all the samples was set to the degree of relative brightness compared to the positive control group. This ratio was considered positive when it was ≥ 1.0 and negative when it was < 1.0 .

DNA extraction

DNA was extracted from the above-mentioned 200- μ L aliquots of samples, as previously described.¹⁸

HPV genotype assay using the 9G

The 9G test detected 14 HR- and 5 LR-HPV types (Table 1). Analyses were performed according to the manufacturer's instructions.¹⁹ Briefly, the PCR mixture consisted of 10 μ L of the extracted target DNA, 10 μ L of the primer set (provided by the manufacturer), and PCR premix (provided by the manufacturer) that contained deoxyribonucleotide triphosphate and Taq DNA polymerase in an amplification buffer. Amplification was performed using the following steps: predenaturation for 5 minutes

Table 1. HPV genotypes identified by the 9G and PANArray

Risk level	Detection by both 9G and PANArray	Detection by PANArray only
High	16, 18, 31, 33, 35, 39, 45, 51, 52, 56, 58, 59, 66, 68	26, 69, 70, 73
Low	6, 11, 34, 40, 42	32, 43, 44, 54, 55, 62, 81, 83

HPV types in bold corresponds to the 13 high-risk genotypes detected by Hybrid-Capture II assay. HPV, human papillomavirus; 9G, HPV 9G DNA Chip; PANArray, PANArray HPV Genotyping Chip.

at 94°C, 40 cycles of 30 seconds each for denaturation at 94°C, 40 cycles of 30 seconds each for annealing at 45°C, 40 cycles of 30 seconds each for elongation at 72°C, and a final elongation step of 5 minutes at 72°C. The PCR products were electrophoresed in a 2% agarose gel to confirm successful amplification of the PCR product. Each hybridization chamber of the 9G was covered with a mixture of 35 µL of the hybridization reaction mixture and 15 µL of the PCR product and incubated at 25°C for 30 minutes. After washing, array images were scanned and taken using a fluorescent scanner (EasyScan-100, Xillux Co. Ltd., Seoul, Korea).

HPV genotype assay using the PANArray

The PANArray test detected 19 HR- and 13 LR-HPV types (Table 1). Analyses were performed according to the manufacturer's instructions.²⁰ Briefly, one PCR mix contained 5 µL of target DNA, 3 µL of PCR primer No. 1, and 17 µL of reaction mixture No. 1 supplied by the manufacturer (containing Taq DNA polymerase, PCR buffer, and deoxynucleoside triphosphate mixture) for a total volume of 25 µL. Another PCR mix contained 5 µL of the same target DNA, 3 µL of PCR primer No. 2, and 17 µL of reaction mixture No. 2. All tubes were incubated for 2 minutes at 50°C before PCR was started. Ten cycles of 30 seconds at 94°C, 30 seconds at 60°C, and 30 seconds at 72°C were performed, including pre-denaturation for 15 minutes at 94°C at the first step, followed by 40 cycles of 30 seconds at 94°C, 1 minute at 47°C, and 30 seconds at 72°C. The PCR products were electrophoresed in a 2% agarose gel to confirm successful amplification of the PCR product. A mixture of hybridization buffer No. 1 and No. 2 (70 µL) was mixed with 5 µL of PCR product No. 1 and 5 µL of PCR product No. 2 and then applied to the PANArray chip and incubated for 1 hour at 50°C. After washing, array images were scanned and taken using a fluorescent scanner (EasyScan-100, Xillux Co. Ltd.).

Direct sequencing

Genotyping results were confirmed by direct sequencing, as previously described.¹⁹ Direct sequencing was performed by an outside laboratory (Fammed Co. Ltd., Seongnam, Korea) using a universal HPV primer set (MY 09/11) that detects a wide range of HPV types. The primer sequences were as follows: MY 09 (reverse) 5'-CGTCCMARRGGAWACTGATC-3'; MY 11 (forward) 5'-GCMCAGGGWCATAAYAATGG-3'. In samples with multiple infections that were identified by the two HPV genotyping assays, type-specific primers were used to obtain specific PCR products, which were analyzed again by direct sequencing.

Gene accession numbers of type-specific primers for each HPV genotype were as follows: HPV 6 (HG793922), 16 (KP874716), 18 (KT070102), 31 (KF700156), 33 (KF700164), 34 (X74476), 35 (JX129488), 39 (KC470245), 40 (HE793074), 42 (GQ472847), 45 (KC470255), 51 (M62877), 52 (KF700237), 53 (JN393901), 56 (JX912947), 58 (AB819279), 59 (KC470266), 66 (JN122292), 68 (KC70283), and 70 (KC470291). Sequences of type-specific primers are shown in Table 2. A total of 116 cases were available by direct sequencing, with the exception of two cases.

Statistical analysis

We defined true-positive, true-negative, false-positive, and

Table 2. Type-specific primer sets used in direct sequencing

HPV type	Primer sequence
6	F: 5'-CAC CTA AAG GTC CTG TTT CGA GGC GGC TAT-3' R: 5'-CTG AAT CGT CCG CCA TCG TTG TTA GGT CTT-3'
16	F: 5'-TTT ATA CAT TAA AGG CTC TGG GTC TAC TGC-3', R: 5'-TAA GGT TTA TTG AAT ATT TGG GCA TCA GAG-3'
18	F: 5'-CAG TCT CCT GTA CCT GGG CAA TAT GAT GCT-3' R: 5'-CTA TGG TGG GCT TGC GAC GCA ATC CAG CCT-3'
31	F: 5'-TGC AAA GGT CAG TTA ACA GAA ACA GAG GTA-3' R: 5'-ACA GCT CTT GCA ATA TGC GAAA TAT CTA CTT-3'
33	F: 5'-AAC TAT ACA CAA CAT TGA ACT ACA GTG CGT-3' R: 5'-ATC TAA AAC ATA TTC CTT TAA CGT TGG CTT-3'
34	F: 5'-GGG TAT GTC AAC CGT GTT TAC TGT TTT ACT-3' R: 5'-ATT ATC AAT AAA ATC CCC CAT TTC AGA ATC-3'
35	F: 5'-AGA AGT GGA CAG ACA TTG TAA GGT GCG GTA T-3' R: 5'-GTC ATC TTC ATT TTC GTC CTC TAC ACT GGA-3'
39	F: 5'-AAG TAT GTA TGA CAG TTT CAT GTG TGA TTG-3' R: 5'-ACA AAA TGG CGA AGT ATA AAA TGT AGA AAC-3'
40	F: 5'-TTT AAT AAA GCT ATA TGT GTG GTG TGG TGT-3' R: 5'-TGC CAA AAC TGC TAT TAG CTA ACT TTT TAT-3'
42	F: 5'-CAG CTA AAC GTA AGA AAA CAC ACA AAT AGA-3' R: 5'-CTT ATT TTT CAA AGC CAG GAT TGT AGT TTA-3'
45	F: 5'-ATT GTA TAA TTG GCG TGT AGA ACC ACT TTC-3' R: 5'-TTT GCA ATA TAC ACA GGC AAT AGA TAC GTC-3'
51	F: 5'-TTC GGT TCG TGT ACT TTT AGT ATA TTT GCC-3' R: 5'-TTA AAT TAT TAT AGG GCG GAA AAC AGT GTG-3'
52	F: 5'-ATA CAG TTG CTC CTA ATC TAT TGC ATC TCC-3' R: 5'-GCA GGA CCT GTG AGT CAG CAA GAA GTC AGT-3'
53	F: 5'-GGA GTG TGC AAA TTC TGT TTG CTA TTT TAT-3' R: 5'-ATA AGC ATT TGT TGT AAA ATA CGC AGC TCT-3'
56	F: 5'-AGA AGC ACA GCT ATA ACA TGT CAA CGG GAA C-3' R: 5'-CTT ACA AAA CAA AAG CCA CAA TAA TGA CAC-3'
58	F: 5'-CAG ACT AAA ACG TTC GGC CCC TAC TAC CCG-3' R: 5'-GGA GGT AAA GTA AAA TGG AGGG CAG TAC TGT-3'
59	F: 5'-AAA CTA CTG TGC AAT CCA AGA ATG TGT CTA-3' R: 5'-ATA TCA TGC AGA GGA ATA TTC AAT GTT GTG-3'
66	F: 5'-TTG ATT GTA AAC AAA CCC AGT TAT GTA TTG-3' R: 5'-GGG CAT CAT ATT TAG TTA ATG TGC TTT TAG-3'
68	F: 5'-TTG TAT ATT AAG GGC ACT GAC ATA CGT GAC-3' R: 5'-TAC AAC CAC ACA TAC AAC CAA CAT ACA AAA-3'
70	F: 5'-AAG TAT GGA GGG AGC AAT CTA AAT AAA AGT-3' R: 5'-CTG TAA TAC TGT TTT TAG CTG TGC AGT AGG-3'

HPV, human papillomavirus.

false-negative results of each detection method to compare with the histological diagnosis as the gold standard. Sensitivity, specificity, PPV, and NPV were calculated according to the definitions. The McNemar test was used to compare the diagnostic sensitivity and specificity between HPV DNA tests, and to test the difference between paired proportions. Agreement between tests was assessed using Cohen's kappa statistic, where values in the range of 0.00–0.20 indicated poor agreement, 0.21–0.40 indicated fair agreement, 0.41–0.60 indicated moderate agreement, 0.61–0.80 indicated good agreement, and 0.81–1.00 indicated very good agreement. Two-sided $p < .05$ were considered statistically significant. The SPSS ver. 17.0 statistical software (SPSS Inc., Chicago, IL, USA) was used for the statistical evaluation.

RESULTS

Cytological and histological diagnoses

Of the 109 cases with cytological diagnoses, 47 cases were diagnosed as negative for intraepithelial lesion, 24 cases were diagnosed as ASCUS, 24 cases were diagnosed as LSIL, 10 cases were diagnosed as HSIL, two cases were diagnosed as atypical squamous cells—cannot exclude HSIL, and two cases were diagnosed as invasive squamous cell carcinomas (Table 3). Histological diagnosis was obtained in 118 cases, which included 65 cases of cervicitis, 24 cases of LSIL, 25 cases of HSIL, and four cases of cancers, including three cases of invasive squamous cell carcinomas, and one case of adenocarcinoma. The cytology was normal, but the histological findings indicated LSIL in four patients and cancer (adenocarcinoma) in one patient. Among the 24 patients with ASCUS, 15 patients had LSIL or HSIL. Although cytology indicated LSIL, the histological findings indicated HSIL in seven patients.

HPV positivity by HC2 and two genotyping assays

The overall HPV positivity rate was 62.7% for 9G and 61.0% for PANArray. The HR-HPV positivity rate was 44.9% using

the 9G and 30.5% with the PANArray, which was significantly lower than the HR-HPV positivity rate of 55.1% by HC2 ($p = .002$ and $p = .000$, respectively) (Table 4).

The rates of HPV positivity using the HC2 and two DNA chips according to the histological diagnosis are summarized in Table 4. LSIL or higher lesions ($n = 53$) showed significantly higher rates of HPV positivity compared to cervicitis by HC2 and two chips. The positivity rates for HR-HPV by PANArray in LSIL (41.7%) and HSIL (72.0%) were significantly lower than those by HC2: 79.2% and 100%, respectively ($p = .004$ and $p = .016$, respectively), but the positivity rates for HR-HPV using 9G in LSIL (58.3%) and HSIL (96.0%) did not show any statistically significant differences from those by HC2 ($p = .063$ and $p = 1.000$, respectively).

In comparison according to the cytological diagnoses, the prevalence of HR-HPV detected by PANArray in cases of ASCUS (50.0%) was significantly lower than that of HR-HPV detected by HC2 (83.3%) and that of HR-HPV detected by 9G (79.2%) ($p = .008$ and $p = .016$, respectively) (Table 4). The PANArray also showed lower positivity rates for HR-HPV in cases of LSIL (54.2%) or HSIL (30.0%) compared to HC2, which were 91.7% and 100%, respectively ($p = .004$ and $p = .016$, respectively).

Comparative evaluation of 9G and PANArray

All HPV genotypes detected by two chips were genotypes detectable by both 9G and PANArray, with the exception of one case. This case showed HPV type 70 (detectable by PANArray only) using PANArray and other type HPV by 9G.

Among the HPV⁺ cases detected using two chips, the frequency of multiple infections detected by 9G (23/74, 31.1%) was significantly higher compared to that detected by PANArray (5/72, 6.9%) ($p = .000$) (Table 4). This difference occurred because the majority of multiple infections detected by 9G (16/23, 69.5%) were identified as a single infection by PANArray. The pattern of mixed infection was mostly the combination

Table 3. Diagnostic comparison between histology and cytology

Histology	Cytology							Total
	Negative	ASCUS	ASC-H	LSIL	HSIL	Cancer	Not done	
Cervicitis	42	9	0	7	0	0	7	65
LSIL	4	8	0	10	1	0	1	24
HSIL	0	7	1	7	9	0	1	25
Cancer	1	0	1	0	0	2	0	4
Total	47	24	2	24	10	2	9	118

ASCUS, atypical squamous cells of undetermined significance; ASC-H, atypical squamous cells—cannot exclude HSIL; LSIL, low-grade squamous intraepithelial lesion; HSIL, high-grade squamous intraepithelial lesion.

Table 4. Prevalence of HPV and its distribution according to histological and cytological diagnosis

	Total	HC2	9G				PANArray			
			Overall	HR	LR	Other	Overall	HR	LR	Other
Total	118	65 (55.1)	74 (62.7)	53 (44.9)	6 (5.1)	15 (12.7)	72 (61.0)	36 (30.5)	8 (6.8)	28 (23.7)
Single	-	-	36	30	6	-	39	31	8	-
Multiple	-	-	23	23 ^a	0	-	5	5 ^a	0	-
Histology										
Cervicitis	65	18 (27.7)	27 (41.5)	13 (20)	3 (4.6)	11 (16.9)	25 (38.5)	8 (12.3)	4 (6.2)	13 (20)
LSIL	24	19 (79.2)	20 (83.3)	14 (58.3)	3 (12.5)	3 (12.5)	21 (87.5)	10 (41.7)	4 (16.7)	7 (29.2)
HSIL	25	25 (100.0)	24 (96.0)	24 (96.0)	0	0	24 (96.0)	18 (72.0)	0	6 (24.0)
Cancer	4	3 (75.0)	3 (75.0)	2 (50.0)	0	1 (25.0)	2 (50.0)	0	0	2 (50.0)
Cytology										
Negative	47	6 (12.8)	12 (25.5)	6 (12.8)	2 (4.3)	4 (8.5)	12 (25.5)	5 (10.6)	2 (4.3)	5 (10.6)
ASCUS	24	20 (83.3)	21 (87.5)	19 (79.2)	0	2 (8.3)	20 (83.3)	12 (50.0)	1 (4.2)	7 (29.2)
ASC-H	2	1 (50.0)	2 (100.0)	1 (50.0)	0	1 (50.0)	1 (50.0)	1 (50.0)	0	0
LSIL	24	22 (91.7)	23 (95.8)	16 (66.7)	3 (12.5)	4 (16.7)	24 (100.0)	13 (54.2)	4 (16.7)	7 (29.2)
HSIL	10	10 (100.0)	9 (90.0)	8 (80.0)	1 (10.0)	0	9 (90.0)	3 (30.0)	1 (10.0)	5 (50.0)
Cancer	2	2 (100.0)	1 (50.0)	1 (50.0)	0	0	1 (50.0)	0	0	1 (50.0)
Total	109	61 (56.0)	68 (62.4)	51 (46.8)	6 (5.5)	11 (10.1)	67 (61.5)	34 (31.2)	8 (7.3)	25 (22.9)

Values are presented as number (%).

HPV, human papillomavirus; HC2, Hybrid-Capture II assay; 9G, HPV 9G DNA Chip; PANArray, PANArray HPV Genotyping Chip; HR, high-risk HPV; LR, low-risk HPV; Other, other-type HPV; LSIL, low-grade squamous intraepithelial lesion; HSIL, high-grade squamous intraepithelial lesion; ASCUS, atypical squamous cells of undetermined significance; ASC-H, atypical squamous cells-cannot exclude HSIL.

^aThe combination of HR and LR HPV types was interpreted as HR HPV infection in the classification of multiple infection.

of HR- and LR-HPV types, followed by co-infection with two or more HR-HPV types, but rarely presented as co-infection with LR types.

When the two chips were compared, the detection rate of HR-HPV by 9G (44.9%) was significantly higher than that of PANArray (30.5%) ($p = .000$), whereas the positivity rate for the other type HPV with 9G (12.7%) was lower than that with PANArray (23.7%) (Table 4). When the genotyping results were classified as negative, LR-, HR-, or other type HPV, the two chip comparison showed that a substantial proportion of HR-HPV⁺ cases detected by 9G were detected as other type (18/53, 34.0%) by PANArray, which caused lower detection rates of HR-HPV by PANArray (Table 5). As a result, the overall strength of agreement between the two assays was considered to be moderate in risk-stratified comparison ($k = 0.579$).

Overall frequency of detection of each HPV genotype was compared in assay-common genotypes using both chip tests, and the results are shown in Table 6. The highest kappa values were observed for HPV 6, 45, 51, and 58 (very good agreement), followed by HPV 16, 34, 39, and 40 (good agreement), HPV 18 and 42 (moderate agreement), and HPV 33 and 56 (fair agreement). The lowest kappa values were observed for HPV types 11, 31, 35, 52, 66, and 68, which showed no agreement between the two chips.

Table 5. Comparison of two HPV genotyping assays according to risk-stratified results

PANArray	9G			
	Negative	LR	HR	Other
Negative	39 (88.6)	0	1 (1.9)	6 (40.0)
LR	1 (2.3)	5 (83.3)	1 (1.9)	1 (6.7)
HR	1 (2.3)	1 (16.7)	33 (62.3)	1 (6.7)
Other	3 (6.8)	0	18 (34.0)	7 (46.7)

Values are presented as number (%).

HPV, human papillomavirus; PANArray, PANArray HPV Genotyping Chip; 9G, HPV 9G DNA Chip; LR, low-risk HPV; HR, high-risk HPV; Other, other-type HPV.

Comparative evaluation of 9G and PANArray by direct sequencing

When genotyping results were classified as concordant (complete agreement in genotypes detected by two assays), compatible (partial agreement), or discordant (no same genotype result), the two chips showed concordant results in 55.1% of the samples, compatible results in 16.9%, and discordant results in 28.0% (Table 7).

Comparisons of two genotyping assays and direct sequencing were also classified as concordant, compatible, or discordant (Table 7). The 9G yielded no discordant results, whereas PANArray yielded 31 discordant results (26.7%). Twenty-three cases with multiple HPV infection by 9G were identified as a concordant multiple infection in 15 cases, a compatible multiple infec-

Table 6. Type-specific agreement for each HPV type, detected by both the 9G and the PANArray in 118 samples

HPV genotype	9G	PANArray	No. of cases positive by either test	Kappa value (95% CI)	Strength of agreement
LR 6	3	3	3	1.000	Very good
LR 11	1	0	0	0.000	Poor
HR 16	13	9	9	0.800 (0.612 to 0.989)	Good
HR 18	8	8	5	0.598 (0.305 to 0.891)	Moderate
HR 31	4	0	0	0.000	Poor
HR 33	5	1	1	0.324 (-0.156 to 0.804)	Fair
LR 34	3	2	2	0.796 (0.406 to 1.000)	Good
HR 35	5	0	0	0.000	Poor
HR 39	1	2	1	0.663 (0.043 to 1.000)	Good
LR 40	3	3	2	0.658 (0.214 to 1.000)	Good
LR 42	3	1	1	0.494 (-0.107 to 1.000)	Moderate
HR 45	2	2	2	1.000	Very good
HR 51	8	6	6	0.848 (0.642 to 1.000)	Very good
HR 52	5	0	0	0.000	Poor
HR 56	5	1	1	0.324 (-0.156 to 0.804)	Fair
HR 58	8	8	7	0.866 (0.683 to 1.000)	Very good
HR 59	0	0	0	-	-
HR 66	2	0	0	0.000	Poor
HR 68	9	0	0	0.000	Poor

HPV, human papillomavirus; 9G, HPV 9G DNA Chip; PANArray, PANArray HPV Genotyping Chip; CI, confidence interval; LR, low-risk HPV; HR, high-risk HPV.

Table 7. Agreement for HPV genotype, detected by the 9G, PANArray, and direct sequencing in 118 samples

Variable	9G vs PANArray	9G vs Sequencing	PANArray vs Sequencing
Concordant	65/118 (55.1)	88/116 (75.9)	59/116 (50.9)
Compatible	20/118 (16.9)	28/116 (24.1)	26/116 (22.4)
Discordant	33/118 (28.0)	0	31/116 (26.7)

Values are presented as number (%).

HPV, human papillomavirus; 9G, HPV 9G DNA Chip; PANArray, PANArray HPV Genotyping Chip.

tion in six cases, and a compatible single infection in two cases by direct sequencing. Five cases with multiple HPV infection by PANArray were identified as a compatible multiple infection in three cases and a compatible single infection in one case by direct sequencing, with the exception of one case, which was not available by direct sequencing.

Clinical performance of 9G, PANArray, and HC2

To evaluate the diagnostic value of each method for HPV detection, we compared the results of each method with the histological diagnosis as the gold standard (Table 8). The sensitivity of overall HPV positivity in detecting LSIL or higher was 88.7% for all three tests. The specificity was 58.5% for 9G and 61.5% for PANArray, which was significantly lower than the specificity of 72.3% for HC2 ($p = .002$ and $p = .03$, respectively). The PPV of HC2 (72.3%) was higher than that of the two genotyping assays (63.5% and 65.2%).

Table 8. Diagnostic accuracies of HPV DNA tests

Variable	HC2	Overall HPV positivity		High-risk HPV positivity	
		9G	PANArray	9G	PANArray
Sensitivity	88.7	88.7	88.7	75.5	52.8
Specificity	72.3	58.5	61.5	80.0	87.7
PPV	72.3	63.5	65.2	75.5	77.8
NPV	88.7	86.4	87.0	80.0	69.5

Values are presented as percentage.

HPV, human papillomavirus; HC2, Hybrid-Capture II assay; 9G, HPV 9G DNA Chip; PANArray, PANArray HPV Genotyping Chip; PPV, positive predictive value; NPV, negative predictive value.

With the HR-HPV⁺ genotype threshold, the sensitivity decreased to 75.5% for 9G and 52.8% for PANArray, which was significantly lower than the sensitivity of 88.7% for HC2 ($p = .008$ and $p = .000$, respectively). The PANArray also had lower sensitivity than 9G ($p = .0005$). The NPV of PANArray (69.5%) was lower than both the HC2 (88.7%) and 9G (80.0%). In contrast, the specificity of PANArray (87.7%) was significantly higher than that of HC2 (72.3%) ($p = .003$).

DISCUSSION

In this study, we performed 9G and PANArray tests on 118 cervicovaginal swabs and compared their clinical performance with HC2 through histological correlation. Genotyping results of the two DNA chips were further validated by direct sequencing. The detection rates of HR-HPV by the two genotyping as-

says were significantly lower than HC2 detection rates. The lower HR-HPV positivity rates also caused lower sensitivity of the two DNA chips in detecting LSIL or higher lesions in histologic correlation compared to that of HC2, which could limit their clinical applicability, considering the importance of HR-HPV detection in screening cervical lesions.

The PANArray, in particular, showed lowest positivity rates for HR-HPV among the three tests and it did not detect a substantial portion of HR-HPV⁺ cases identified by HC2. The PANArray also showed a distinctly lower prevalence of HR-HPV than HC2 in each group, according to the histological or cytological diagnosis. In contrast, this assay had higher detection rates of other-type HPV infection compared to 9G, because a substantial proportion of HR-HPV⁺ cases identified by the two other tests were detected as other-type or negative by PANArray. Due to the false negative results on PANArray, its sensitivity for HR-HPV detection showed a much lower value compared to that of HC2 and 9G, although the sensitivity for overall HPV detection, including LR- and other-type HPV, was identical to that of HC2 and 9G. Similarly, the NPV of this assay was inferior to that of the two tests with HR-HPV⁺ genotype threshold, whereas it showed a similar NPV for overall HPV detection. The lower sensitivity and NPV of PANArray indicate that it is not optimal to use as a screening tool for cervicovaginal samples.

There have been conflicting results about the PCR-based DNA chip method in previous studies in Korea. The majority of these studies reported that the HPV DNA chip method had higher or similar sensitivity or detection rates, compared to HC2 or other DNA tests,²¹⁻²⁴ whereas some reports showed that commercial DNA chips had lower sensitivity or detection rates for HR-HPV.^{25,26} Specifically, there were contradictory reports about comparative results of the PANArray method in the respective studies.^{24,26} These differences may be due to insufficient standardization of the DNA chip method.

Insufficient standardization was also observed in the differences in the frequency of multiple infections between the two chips. The proportion of cases with multiple infections using the 9G chip was approximately four times higher than when PANArray was used. These differences between DNA chips were consistently found in previous studies, showing a variable percentage of multiple infections that ranged from about 6%–30% in HPV⁺ cases.^{21,23-25} The high frequency of multiple infections may be associated with cross-reactivity due to the similarities in the DNA sequence between type-specific DNA probes attached within DNA chips, thereby yielding false-positive results that affect the sensitivity or specificity of DNA chips. Therefore, well-

balanced standardization is required during DNA chip manufacturing to achieve the desired level of HPV detection.

In this study, the HR-HPV positivity rate in normal cytology was 10.6%–12.8%, which was similar to those reported in previous studies, which ranged from 8.3% to 14.5%.^{13,27-29} The HR-HPV positivity rate in ASCUS was 83.3% based on HC2, which was higher than those described in previous studies, with ranges from 33.3% to 55.9%.^{13,27,29} This difference might occur because the majority of cases diagnosed with ASCUS, due to insufficient sampling or poor quality in cytology, were determined to be LSIL or HSIL in histology. In addition, our study population, which consisted only of histologically-confirmed cases, might have an enhanced HPV positivity in ASCUS cases because histological samples were more frequently taken from patients with HPV⁺ ASCUS lesions than those that were not related to HPV.

In this study, HPV 16 was the most frequently identified HR genotype, followed by HPV 68, 58, 51, 18, 52, 56, 33, and 35 by 9G. In PANArray, HPV 16, 58, 18, and 51 were frequently detected. The prevalence of HR-HPV genotypes is known to differ according to geographic distribution.²⁵ HPV 16, 18, 31, and 45 are frequently detected in Western countries, whereas HPV 16, 58, 52, and 56 are predominant in Korea.^{24,25} Considering the number of cases that were HPV 52 and 56 positive in two tests, 9G showed relatively similar patterns in the distribution of HPV genotypes compared to the PANArray method.

Comparison of the two chips indicated that the HPV genotypes showed variable differences in positivity for individual HPV types. Among the frequently detected genotypes, HPV 68, 35, and 52 were markedly different between the two chips with no agreement, as the PANArray showed negative results in HPV 68⁺ (n = 9), 35⁺ (n = 5), or 52⁺ (n = 5) cases detected by 9G. These differences need to be corrected, especially because these types are relatively common in Korean women.^{24,25} In contrast, the most important HR-HPV types that caused cervical cancer, HPV 16 and 18, showed relatively better agreement between the two genotyping assays.

When the results of the two chips were confirmed by direct sequencing, 9G yielded concordant or compatible results in all cases. In contrast, the PANArray yielded discordant results in approximately one fourth of the cases. Most of these discrepancies were attributable to the erroneous results of PANArray, discussed above, which detected HR-HPV as other-type. Given that the frequency of multiple infections was much higher with the 9G than by PANArray, these results suggest that the threshold value for detecting each HPV type may vary between chips

and 9G may have a more sensitive threshold for detection compared to PANArray.

In this study, HC2 was more sensitive with a high NPV, thereby increasing the possibility of avoiding unnecessary surgical procedures. However, the HC2 assay has some disadvantages compared to other HPV genotyping tests. This assay does not provide specific information about individual HPV genotypes, and it does not distinguish between persistent infection with the same genotype and infection with a new HPV genotype.²⁵ In addition, multiple infections also cannot be detected. However, the two HPV genotyping assays tested in the present study did not have diagnostic accuracies that were comparable to HC2. Therefore, it is necessary to improve the quality of HPV DNA chips, considering the importance of HPV genotyping, especially for detecting HPV 16 and 18, in clinical practice.

There were some limitations to this study. The present data included a small number of cases collected over a short time period. Furthermore, the number of HSIL or higher lesions in histology (n = 29) was too small to generalize the results. A larger study series conducted over a longer period of time is needed to confirm the clinical and analytical performance of the DNA chip method.

In conclusion, the HPV genotyping tests using the PCR-based DNA chip method showed lower sensitivity in histologic correlation compared with HC2, limiting their clinical applicability as an HPV screening test. When comparing the two chips, the 9G was more sensitive and accurate for detecting HR-HPV than the PANArray. The two DNA chips showed poor agreement in detecting certain HPV genotypes. These results indicate the necessity for standardization and validation of the HPV genotyping assays.

Conflicts of Interest

This study was supported by Diatech Korea Co., Ltd. The sponsor had no involvement in the study design, data interpretation, or writing of the manuscript.

REFERENCES

1. Kurman RJ, Carcangiu ML, Herrington CS, Young RH. WHO classification of tumours of female reproductive organs. 4th ed. Lyon: IARC Press, 2014.
2. Bzhalava D, Guan P, Franceschi S, Dillner J, Clifford G. A systematic review of the prevalence of mucosal and cutaneous human papillomavirus types. *Virology* 2013; 445: 224-31.
3. Muñoz N, Bosch FX, de Sanjosé S, *et al.* Epidemiologic classification of human papillomavirus types associated with cervical cancer. *N Engl J Med* 2003; 348: 518-27.
4. Walboomers JM, Jacobs MV, Manos MM, *et al.* Human papillomavirus is a necessary cause of invasive cervical cancer worldwide. *J Pathol* 1999; 189: 12-9.
5. Kjaer SK, van den Brule AJ, Paull G, *et al.* Type specific persistence of high risk human papillomavirus (HPV) as indicator of high grade cervical squamous intraepithelial lesions in young women: population based prospective follow up study. *BMJ* 2002; 325: 572.
6. Elfgren K, Jacobs M, Walboomers JM, Meijer CJ, Dillner J. Rate of human papillomavirus clearance after treatment of cervical intraepithelial neoplasia. *Obstet Gynecol* 2002; 100(5 Pt 1): 965-71.
7. Khan MJ, Castle PE, Lorincz AT, *et al.* The elevated 10-year risk of cervical precancer and cancer in women with human papillomavirus (HPV) type 16 or 18 and the possible utility of type-specific HPV testing in clinical practice. *J Natl Cancer Inst* 2005; 97: 1072-9.
8. Bosch FX, de Sanjosé S. Chapter 1: Human papillomavirus and cervical cancer: burden and assessment of causality. *J Natl Cancer Inst Monogr* 2003; (31): 3-13.
9. Cuschieri KS, Cubie HA. The role of human papillomavirus testing in cervical screening. *J Clin Virol* 2005; 32 Suppl 1: S34-42.
10. Rozendaal L, Westerga J, van der Linden JC, *et al.* PCR based high risk HPV testing is superior to neural network based screening for predicting incident CIN III in women with normal cytology and borderline changes. *J Clin Pathol* 2000; 53: 606-11.
11. Denise Zielinski G, Snijders PJ, Rozendaal L, *et al.* High-risk HPV testing in women with borderline and mild dyskaryosis: long-term follow-up data and clinical relevance. *J Pathol* 2001; 195: 300-6.
12. Poljak M, Brencic A, Seme K, Vince A, Marin IJ. Comparative evaluation of first- and second-generation digene hybrid capture assays for detection of human papillomaviruses associated with high or intermediate risk for cervical cancer. *J Clin Microbiol* 1999; 37: 796-7.
13. Sandri MT, Lentati P, Benini E, *et al.* Comparison of the Digene HC2 assay and the Roche AMPLICOR human papillomavirus (HPV) test for detection of high-risk HPV genotypes in cervical samples. *J Clin Microbiol* 2006; 44: 2141-6.
14. Castle PE, Wheeler CM, Solomon D, Schiffman M, Peyton CL; ALTS Group. Interlaboratory reliability of Hybrid Capture 2. *Am J Clin Pathol* 2004; 122: 238-45.
15. Huh W, Einstein MH, Herzog TJ, Franco EL. What is the role of HPV typing in the United States now and in the next five years in a vaccinated population? *Gynecol Oncol* 2010; 117: 481-5.
16. Lindemann ML, Dominguez MJ, de Antonio JC, *et al.* Analytical comparison of the cobas HPV Test with Hybrid Capture 2 for the detection of high-risk HPV genotypes. *J Mol Diagn* 2012; 14: 65-70.

17. Solomon D, Davey D, Kurman R, *et al.* The 2001 Bethesda System: terminology for reporting results of cervical cytology. *JAMA* 2002; 287: 2114-9.
18. Oh SY, Kim WY, Hwang TS, Han HS, Lim SD, Kim WS. Development of an ammonium sulfate DNA extraction method for obtaining amplifiable DNA in a small number of cells and its application to clinical specimens. *Biomed Res Int* 2013; 2013: 546727.
19. An H, Song KS, Nimse SB, *et al.* HPV 9G DNA chip: 100% clinical sensitivity and specificity. *J Clin Microbiol* 2012; 50: 562-8.
20. Choi JJ, Kim C, Park H. Peptide nucleic acid-based array for detecting and genotyping human papillomaviruses. *J Clin Microbiol* 2009; 47: 1785-90.
21. An HJ, Cho NH, Lee SY, *et al.* Correlation of cervical carcinoma and precancerous lesions with human papillomavirus (HPV) genotypes detected with the HPV DNA chip microarray method. *Cancer* 2003; 97: 1672-80.
22. Lee GY, Kim SM, Rim SY, Choi HS, Park CS, Nam JH. Human papillomavirus (HPV) genotyping by HPV DNA chip in cervical cancer and precancerous lesions. *Int J Gynecol Cancer* 2005; 15: 81-7.
23. Kim TJ, Jung CK, Lee A, *et al.* Comparison of clinical efficacy between an HPV DNA chip and a Hybrid-Capture II assay in a patient with abnormal colposcopic findings. *Korean J Cytopathol* 2008; 19: 119-25.
24. Song HJ, Lee JW, Kim BG, Song SY, Bae DS, Kim DS. Comparison of the performance of the PANArray™ HPV test and DNA chip test for genotyping of human papillomavirus in cervical swabs. *BioChip J* 2010; 4: 167-72.
25. Um TH, Lee EH, Chi HS, Kim JW, Hong YJ, Cha YJ. Comparison of HPV genotyping assays and Hybrid Capture 2 for detection of high-risk HPV in cervical specimens. *Ann Clin Lab Sci* 2011; 41: 48-55.
26. Park KS, Kim JY, Ki CS, Lee NY. Comparison of the digene HPV genotyping LQ test and the PANArray HPV genotyping chip for detection of high-risk or probable high-risk human papillomavirus genotypes. *Ann Lab Med* 2014; 34: 279-85.
27. de Cremoux P, Coste J, Sastre-Garau X, *et al.* Efficiency of the hybrid capture 2 HPV DNA test in cervical cancer screening. A study by the French Society of Clinical Cytology. *Am J Clin Pathol* 2003; 120: 492-9.
28. Trope A, Sjoborg K, Eskild A, *et al.* Performance of human papillomavirus DNA and mRNA testing strategies for women with and without cervical neoplasia. *J Clin Microbiol* 2009; 47: 2458-64.
29. Clavel C, Masure M, Bory JP, *et al.* Human papillomavirus testing in primary screening for the detection of high-grade cervical lesions: a study of 7932 women. *Br J Cancer* 2001; 84: 1616-23.

Morphologic Analysis of Cytomegalovirus Infected Cells in Bronchial Washing Cytology: Comparison of Liquid-Based Preparation and Conventional Smear

Jae Yeon Seok* · Jungsuk An*
Seung Yeon Ha · Dong Hae Chung
Sangho Lee · Hyunchul Kim

Department of Pathology, Gachon University Gil Medical Center, Incheon, Korea

Received: November 3, 2015
Revised: December 15, 2015
Accepted: December 24, 2015

Corresponding Author

Seung Yeon Ha, MD, PhD
Department of Pathology, Gachon University Gil Medical Center, 21 Namdong-daero 774beon-gil, Namdong-gu, Incheon 21565, Korea
Tel: +82-32-460-3073
Fax: +82-32-460-2394
E-mail: syha@gilhospital.com

*Jae Yeon Seok and Jungsuk An contributed equally to this work.

Background: The cytopathic effects of cytomegalovirus (CMV) infection have been well described since the virus was first reported; however, the morphology of CMV infection has not been clearly studied. We examined the difference in detailed cytologic findings in bronchial washing cytology between liquid-based and conventionally prepared smears. **Methods:** Bronchial washing cytology was processed using either the conventional preparation (CP) or liquid-based preparation (LBP). Sixty-nine cells with typical cytopathic effects of CMV infection were detected on CP slides and 18 cells on LBP slides. Using the image analyzer, area, circumference, major axis, and minor axis of the cytoplasm, nucleus, and intranuclear inclusion were measured in singly scattered CMV-infected cells, and histiocytes were used as a control. **Results:** The mean cytoplasmic area of CMV-infected cells was 1.47 times larger than that of histiocytes in CP and 2.92 times larger in LBP ($p < .05$). The mean nuclear area of CMV-infected cells was 2.61 times larger than that of histiocytes in CP and 4.25 times larger in LBP ($p < .05$). The nucleus to cytoplasm ratio and intranuclear inclusion to cytoplasm ratio of the mean area, circumference, major axis, and minor axis in CP were larger than those in LBP ($p < .05$). **Conclusions:** The sizes of cytoplasm, nucleus, and intranuclear inclusion were larger in LBP than in CP, indicating that CMV-infected cells are easily detectable in LBP. However, the nucleus-to-cytoplasm ratio was larger in CP, suggesting that differentiation from malignancy or regenerative atypia requires caution in CP.

Key Words: Cytomegalovirus; Bronchial washing; Cytology; Lung

The morphologic alteration of cytomegalovirus (CMV) infected cells is well described in that they have enlarged cytoplasm and nuclei, sharply demarcated nuclear membranes, and chromatin condensation with a surrounding halo. A distinguishing feature of CMV-infected cells was first described by Ribbert¹ in kidney and parotid glands of a syphilitic stillborn in 1904.² Jesonek and Kiolemenoglou³ reported similar unusually large cells as protozoan-like cells and clearly described the cellular morphology: the cells were 20–30 μm in diameter, with large eccentrically placed nuclei. Each contained a ‘central nuclear body’ surrounded by two zones, a darker inner zone and a clear outer zone.³ In 1921, Goodpasture and Talbot⁴ suggested that these cells were similar to Varicella-infected cells of the skin and that they were products of viral infection, and thus they were named cytomegalia infantum. Cole and Kuttner⁵ demonstrated inclusion body formation by viral injection into guinea pig cells. Various terminologies have been used for CMV, including “salivary gland virus disease,” “inclusion body disease,” “generalized sali-

vary gland virus infection,” “inclusion disease,” and “cytomegalic inclusion disease.” In 1957, Weller isolated viral particles from cells of cytomegalic inclusion disease and suggested CMV as the etiologic virus.⁶ However, the exact size of enlarged CMV-infected cells has not been studied in detail.

CMV is a common infectious agent in immunocompromised hosts, and early detection is clinically important. The characteristic features have been used for pathognomonic diagnostic findings of CMV infections in various cytology specimens, including urine, sputum, bronchial brushing, and bronchoalveolar lavage.⁷⁻¹¹ In practice, the first diagnosis that used cytologic preparation was made by Fetterman in 1952.⁷ Urine was obtained from a 2-day-old premature infant; after alcohol fixation and hematoxylin and eosin staining, several inclusion containing cells with enormous cellular hypertrophy and large intranuclear inclusions were observed in urine exfoliative cytology. The infant died of generalized inclusion disease, and typical inclusions were found in tissue sections of the brain, pituitary gland, thyroid

gland, lungs, liver, pancreas, and kidneys. In 1964, Warner *et al.*⁸ described the cellular morphology of CMV-infected cells in sputum cytology. CMV-infected cells in sputum contained a spherical nucleus, sharply demarcated nuclear membrane, centrally located chromatin mass surrounded by halo, and an occasional binucleated form that resembled a syncytium. In a tissue section of lung in this patient, typical cytomegaly with nuclear inclusion was observed throughout the alveolar spaces and septa, measuring 15–25 µm in cell size. Round or oval nuclear inclusion with halo, sharply delineated nuclear membrane, parasol bodies, and occasional clusters of cytoplasmic inclusions were noted. Although detection of CMV-infected cells in cytology specimens is a less sensitive method than virus isolation, it is quite time saving in terms of effectiveness. Culture for viral isolation requires several weeks, and CMV titer in serology also requires weeks before diagnosis. Detection of CMV-infected cells using a cytologic specimen is an easy and widely used approach in immunocompromised patients and in those with conditions suspicious for congenital infection.

The application of cytologic specimens associated with respiratory tract infection including sputum, bronchial brushing, bronchoalveolar lavage, bronchial washing, and fine-needle aspiration was well-defined in a clinical setting of acquired immunodeficiency syndrome, idiopathic pulmonary fibrosis, lung transplantation, and kidney transplantation.⁸⁻¹⁵ Cytology specimens of other organs described as diagnostic tools for CMV infection including uterine cervical Pap smear,¹⁶⁻²¹ salivary gland aspiration,^{22,23} pleural fluid,²⁴⁻²⁶ cerebrospinal fluid,²⁷ esophagus,²⁸ and thyroid aspiration²⁹ have been reported. In cytologic specimens, the individual cellular morphology is well-preserved, and the diagnostic usability is particularly useful for CMV infection in which cellular alteration is pathognomonic.

In liquid-based preparation (LBP), the cytologic detail of CMV

infection has not been described except in two gynecologic samples, which highlighted the difference between CMV and human papillomavirus infection.^{19,30} Several studies that compared the difference between LBP and conventional preparation (CP) in cytologic specimens focused mainly on neoplastic diseases.³¹⁻⁴⁰ We studied the difference in detailed cytologic findings between bronchial washing in LBP and CP for cellular morphologic parameters.

MATERIALS AND METHODS

Patient selection

Five cases diagnosed with CMV infection based on bronchial washing cytology specimens at Gachon University Gil Medical Center between 2003 and 2014 were selected and reviewed. This study was approved by the Institutional Review Board (IRB) of Gachon University Gill Medical Center (IRB No. GBIRB 2015-284). Clinical information on the five patients is summarized in Table 1. Each bronchial washing cytology specimen was treated in CP and LBP.

Cytologic preparations

The obtained samples were treated with both CP and LBP, simultaneously. The bronchus was washed with normal saline, and the washing samples were centrifuged for five minutes. The cytopsin technique was used as in the CP method. The sample was centrifuged (2,000 rpm, 5 minutes), and two cytopsin (1,500 rpm, 4 minutes) were prepared for each bronchial washing sample. Slides were fixed in 95% alcohol for 60 minutes and stained with a Papanicolaou stain. For LBP, mucolysis was performed using dithiothreitol. After rinsing with Cytolyt (Cytoc Co., Boxborough, MA, USA), the sample was centrifuged for five minutes at 1,500 rpm. The supernatant was discarded,

Table 1. Clinical history of patients with cytomegaloviral infection detected in bronchial washing cytology and the number of cytomegalovirus infected cells and histiocytes by the cytologic preparation method

No.	Sex	Age (yr)	History	Other finding	CMVinf-CP	CMVinf-LBP	Histiocyte-CP	Histiocyte-LBP
1	F	39	Renal transplantation ^a	Serum cytomegalovirus > 1,000	9	0	7	0
2	M	45	Renal transplantation ^a	Acute rejection	1	0	1	0
3	M	18	Bone marrow transplantation ^b	Cytomegaloviral retinitis, influenza A virus +	15	5	11	1
4	F	66	Myasthenia gravis	Aspergillus antigen +, gram-positive bacteremia	27	12	55	21
5	M	71	Acquired immunodeficiency syndrome	Cytomegalovirus PCR +, tuberculosis	17	1	36	0

CMVinf-CP, cytomegalovirus infected-cells in smear processed by conventional preparation; CMVinf-LBP, cytomegalovirus infected-cells in cytology processed by liquid-based preparation; Histiocyte-CP, histiocytes in smear processed by conventional preparation; Histiocyte-LBP, histiocytes in cytology processed by liquid-based preparation; PCR, polymerase chain reaction.

^aChronic renal failure; ^bAplastic anemia.

and the sample was transferred to a vial containing cytopreservative solution (PreservCyt, Cytyc Co.). PreservCyt solution mildly fixed the cells for 15 minutes. The sample was run on a ThinPrep Processor (Cytyc Co.) using sequence 3 (for mucoid specimen). A single slide was prepared for each sample and was stained using the Papanicolaou method.

Imaging and analysis

Using a DP70 digital camera (Olympus, Tokyo, Japan) and BX51 microscope (Olympus), pictures were taken at high power magnification ($\times 1,000$) for each singly scattered CMV-infected cell and histiocyte. Cells with artifacts such as drying, squeezing, and overlapping were excluded. Sixty-nine cells with typical cytopathic effects of CMV infection on CP slides and 18

cells on LBP slides were selected (patient 1, 9 cells on CP; patient 2, 1 cell on CP; patient 3, 15 cells on CP and 5 cells on LBP; patient 4, 27 cells on CP and 12 cells on LBP; patient 5, 17 cells on CP and 1 cell on LBP) (Table 1). The area, circumference, major axis, and minor axis of cytoplasm, nucleus, and intranuclear inclusion were measured using the image analyzer software package i-Solution ver. 10.1 (IMT i-Solution, Vancouver, BC, Canada). The major axis was the longest diameter, and the minor axis was the dimension perpendicular to the major axis (Fig. 1A, B).

Statistical analysis

SPSS ver. 18.0 (SPSS Inc., Chicago, IL, USA) was used for statistical analysis. Student's t test was used to compare the area,

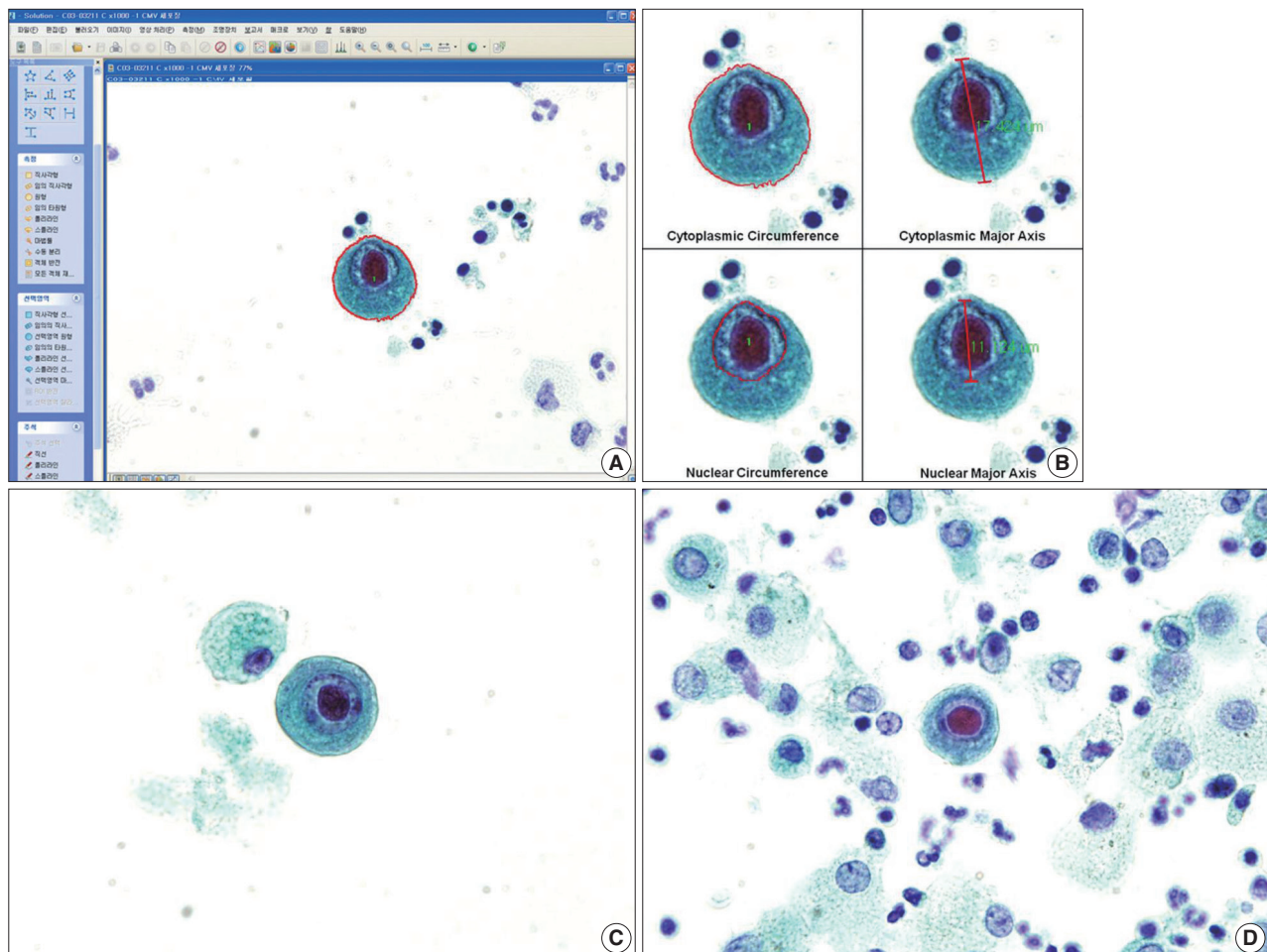


Fig. 1. (A, B) Well-prepared microscopic photographs from the image analyzer program. Specific shape and color are detected by the program. The researcher selects an area of interest, and the area, circumference, major axis, and minor axis are automatically calculated by the image analyzer. The major axis is the longest diameter, and the minor axis is the dimension perpendicular to the major axis. (C) A singly scattered cytomegalovirus infected cell and a histiocyte in a cytology specimen processed by liquid-based preparation are noted with a clean background. The cytoplasm and nucleus are enlarged and show dense cytoplasm with a well-demarcated cytoplasmic border. (D) In a conventionally-prepared cytology smear, a cytomegalovirus infected cell shows a prominent intranuclear inclusion.

circumference, major axis, and minor axis results to assess the differences in CMV-infected cells and histiocytes in each preparation method and the differences in CMV-infected cell morphology in different preparations. A p-value less than .05 was considered statistically significant.

RESULTS

CMV-infected cell morphology in bronchial washing cytology

Sixty-nine cells with typical cytopathic effects of CMV infection were detected on CP slides, and 18 cells were noted on LBP slides (Fig. 1C, D). Each CMV-infected cell was singly scattered with an enlarged cytoplasm and nucleus, compared to histiocytes around the cell. The nuclear membrane was distinct, and a well-demarcated large intranuclear inclusion was observed

with a peri-inclusion halo. Cytoplasmic inclusion was variably noted.

CMV-infected cells and histiocytes in CP

Details on the morphologic parameter measurements are shown in Tables 2 and 3. The mean cytoplasmic area of CMV-infected cells was $189.94 \pm 49.27 \mu\text{m}^2$ ($t = 8.136$, $p < .001$), and the mean nuclear area of CMV-infected cells was $73.87 \pm 19.54 \mu\text{m}^2$ ($t = 18.021$, $p < .001$). The nucleus to cytoplasm ratio of the mean area in CMV-infected cells was 0.40 ± 0.09 ($t = 13.817$, $p < .001$).

CMV-infected cells and histiocytes in LBP

The mean cytoplasmic area of CMV-infected cells was $299.74 \pm 94.90 \mu\text{m}^2$ ($t = 8.414$, $p < .001$), and the mean nuclear area of

Table 2. Comparison of cellular morphology

Parameter	CMVinf-CP (A) (n=69)	CMVinf-LBP (B) (n=18)	Histiocyte-CP (C) (n=110)	Histiocyte-LBP (D) (n=22)	p-value			
					A vs B	A vs C	B vs D	C vs D
Cytoplasm								
Area (μm^2)	189.94 ± 49.27	299.74 ± 94.90	129.48 ± 47.82	102.64 ± 50.39	.000*	.000*	.000*	.019*
Circumference (μm)	59.26 ± 10.81	74.59 ± 17.56	56.76 ± 15.76	50.55 ± 24.03	.000*	.209	.001*	.128
Major axis (μm)	15.89 ± 2.26	19.87 ± 2.92	13.29 ± 2.62	11.74 ± 2.93	.000*	.000*	.000*	.014*
Minor axis (μm)	15.71 ± 2.27	19.60 ± 3.29	13.35 ± 2.72	11.50 ± 2.70	.000*	.000*	.000*	.004*
Nucleus								
Area (μm^2)	73.87 ± 19.54	100.89 ± 47.87	28.35 ± 9.64	23.76 ± 8.43	.030*	.000*	.000*	.039*
Circumference (μm)	34.92 ± 5.50	40.00 ± 7.99	21.43 ± 3.82	20.15 ± 4.48	.002*	.000*	.000*	.164
Major axis (μm)	9.94 ± 1.53	11.72 ± 2.88	6.18 ± 1.21	5.81 ± 1.44	.020*	.000*	.000*	.201
Minor axis (μm)	9.91 ± 1.42	11.58 ± 2.08	6.06 ± 1.15	5.50 ± 1.10	.000*	.000*	.000*	.038*
N/C ratio								
Area (μm^2)	0.40 ± 0.09	0.33 ± 0.07	0.23 ± 0.07	0.26 ± 0.09	.005*	.000*	.008*	.174
Circumference (μm)	0.60 ± 0.09	0.54 ± 0.07	0.40 ± 0.10	0.44 ± 0.13	.021*	.000*	.002*	.092
Major axis (μm)	0.63 ± 0.08	0.59 ± 0.07	0.48 ± 0.10	0.51 ± 0.13	.049*	.000*	.020*	.187
Minor axis (μm)	0.64 ± 0.08	0.59 ± 0.07	0.46 ± 0.09	0.49 ± 0.10	.053	.000*	.001*	.217
INI								
Area (μm^2)	29.48 ± 8.46	36.94 ± 14.23	-	-	.006*			
Circumference (μm)	22.51 ± 3.23	26.20 ± 4.81	-	-	.006*			
Major axis (μm)	6.27 ± 1.17	7.05 ± 1.41	-	-	.017*			
Minor axis (μm)	6.50 ± 1.06	7.28 ± 1.48	-	-	.013*			
INI/N ratio								
Area (μm^2)	0.41 ± 0.09	0.38 ± 0.09	-	-	.282			
Circumference (μm)	0.65 ± 0.08	0.66 ± 0.10	-	-	.597			
Major axis (μm)	0.63 ± 0.09	0.61 ± 0.09	-	-	.345			
Minor axis (μm)	0.66 ± 0.09	0.63 ± 0.08	-	-	.199			
INI/C ratio								
Area (μm^2)	0.16 ± 0.04	0.12 ± 0.02	-	-	.000*			
Circumference (μm)	0.39 ± 0.07	0.36 ± 0.05	-	-	.075			
Major axis (μm)	0.40 ± 0.06	0.35 ± 0.04	-	-	.002*			
Minor axis (μm)	0.42 ± 0.07	0.37 ± 0.05	-	-	.010*			

CMVinf-CP, cytomegalovirus infected cells in smear processed by conventional preparation; CMVinf-LBP, cytomegalovirus infected cells in cytology processed by liquid-based preparation; Histiocyte-CP, histiocytes in smear processed by conventional preparation; Histiocyte-LBP, histiocytes in cytology processed by liquid-based preparation; N, nucleus; C, cytoplasm; INI, intranuclear inclusion.

* $p < .05$.

Table 3. Comparison of cytomegalovirus infected cells and histiocytes

Parameter	CMVinf-CP (n=69)	CMVinf-LBP (n=18)	CMVinf-CP/Histiocyte-CP	CMVinf-LBP/Histiocyte-LBP
Cytoplasm				
Area (μm^2)	189.94 \pm 49.27	299.74 \pm 94.90	1.47*	2.92*
Circumference (μm)	59.26 \pm 10.81	74.59 \pm 17.56	1.04	1.48*
Major axis (μm)	15.89 \pm 2.26	19.87 \pm 2.92	1.20*	1.69*
Minor axis (μm)	15.71 \pm 2.27	19.60 \pm 3.29	1.18*	1.70*
Nucleus				
Area (μm^2)	73.87 \pm 19.54	100.89 \pm 47.87	2.61*	4.25*
Circumference (μm)	34.92 \pm 5.50	40.00 \pm 7.99	1.63*	1.99*
Major axis (μm)	9.94 \pm 1.53	11.72 \pm 2.88	1.61*	2.02*
Minor axis (μm)	9.91 \pm 1.42	11.58 \pm 2.08	1.64*	2.11*
N/C ratio				
Area (μm^2)	0.40 \pm 0.09	0.33 \pm 0.07	1.74*	1.27*
Circumference (μm)	0.60 \pm 0.09	0.54 \pm 0.07	1.50*	1.23*
Major axis (μm)	0.63 \pm 0.08	0.59 \pm 0.07	1.31*	1.16*
Minor axis (μm)	0.64 \pm 0.08	0.59 \pm 0.07	1.39*	1.20*

CMVinf-CP, cytomegalovirus infected cells in smear processed by conventional preparation; CMVinf-LBP, cytomegalovirus infected cells in cytology processed by liquid-based preparation; Histiocyte-CP, histiocytes in smear processed by conventional preparation; Histiocyte-LBP, histiocytes in cytology processed by liquid-based preparation; N, nucleus; C, cytoplasm.

* $p < .05$.

CMV-infected cells was $100.89 \pm 47.87 \mu\text{m}^2$ ($t = 6.751$, $p < .001$). The nucleus to cytoplasm ratio of the mean area in CMV-infected cells was 0.33 ± 0.07 ($t = 2.781$, $p = .008$) (Tables 2, 3).

CMV-infected cell morphology in CP and LBP

The mean area, circumference, major axis, and minor axis of the cytoplasm, nucleus, and intranuclear inclusion of CMV-infected cells in LBP were larger than those in CP ($p < .05$) (Table 4). However, the mean area, circumference, and major axis of the nucleus to cytoplasm ratio in CP were larger than those in LBP ($p < .05$) (Table 4).

Histiocytes in CP and LBP

The mean cytoplasmic area of histiocytes in CP was $129.48 \pm 47.82 \mu\text{m}^2$, which was 1.26 times larger than that in LBP ($t = 2.382$, $p = .019$). The mean nuclear area of histiocytes in CP was $28.35 \pm 9.64 \mu\text{m}^2$ ($t = 2.081$, $p = .039$). The nucleus to cytoplasm ratio of the mean area, circumference, major axis, and minor axis of histiocytes in CP was not significantly different from that in LBP.

DISCUSSION

CMV-infected cells are distinguishable by an enlarged morphology compared to normal counterpart cells. However, the exact numerical measurements of the cytoplasm or nucleus have not been described. In this study, we clarify the sizes of the cytoplasm, nucleus, and intranuclear inclusion in terms of area,

circumference, major axis, and minor axis. In CP, the mean cytoplasmic area of CMV-infected cells was 1.47 times larger than that of histiocytes, and the mean nuclear area was 2.61 times larger. In LBP, the mean cytoplasmic area of CMV-infected cells was 2.92 times larger than that of histiocytes, and the mean nuclear area was 4.25 times larger. We measured the size of histiocytes near CMV-infected cells and of those that were singly scattered and well-preserved. Histiocytes were selected as a control for the following reasons: (1) the selected CMV-infected cells were singly scattered with a round cytoplasmic contour, which mainly appeared to be CMV-infected histiocytes, (2) histiocytes are the most frequently encountered cells in bronchial washing cytology specimens, and (3) the exact difference between CMV-infected cells and histiocytes can be easily determined in daily practice.

The mean nuclear cytoplasmic area ratio of the CMV-infected cells was 1.74 times larger than that of histiocytes in CP and 1.27 times in LBP. The nuclear cytoplasmic area ratio was 0.83 times smaller in LBP (0.33 ± 0.07) than in CP (0.40 ± 0.09). Attention should be paid to the relatively high nuclear cytoplasmic ratio in CP for a practical differential diagnosis of other pathologic cellular alterations, such as neoplastic conditions and reparative changes.

The results of specimen collections from five patients were analyzed as CMV-infected cells in CP, CMV-infected cells in LBP, histiocytes in CP, and histiocytes in LBP. When the four grouped cells were analyzed separately in each patient, the result was the same as shown above. Several reports on compari-

Table 4. Comparison of cytomegalovirus infected cells on cellular morphology in conventional preparation and liquid-based preparation

Parameter	CMVinf-LBP (n=18)	CMVinf-CP (n=69)	CMVinf-LBP/CMVinf-CP	p-value
Cytoplasm				
Area (μm^2)	299.74 \pm 94.90	189.94 \pm 49.27	1.58*	.000*
Circumference (μm)	74.59 \pm 17.56	59.26 \pm 10.81	1.26*	.000*
Major axis (μm)	19.87 \pm 2.92	15.89 \pm 2.26	1.25*	.000*
Minor axis (μm)	19.60 \pm 3.29	15.71 \pm 2.27	1.25*	.000*
Nucleus				
Area (μm^2)	100.89 \pm 47.87	73.87 \pm 19.54	1.37*	.030*
Circumference (μm)	40.00 \pm 7.99	34.92 \pm 5.50	1.15*	.002*
Major axis (μm)	11.72 \pm 2.88	9.94 \pm 1.53	1.18*	.020*
Minor axis (μm)	11.58 \pm 2.08	9.91 \pm 1.42	1.17*	.000*
N/C ratio				
Area (μm^2)	0.33 \pm 0.07	0.40 \pm 0.09	0.83*	.005*
Circumference (μm)	0.54 \pm 0.07	0.60 \pm 0.09	0.90*	.021*
Major axis (μm)	0.59 \pm 0.07	0.63 \pm 0.08	0.94*	.049*
Minor axis (μm)	0.59 \pm 0.07	0.64 \pm 0.08	0.92	.053
INI				
Area (μm^2)	36.94 \pm 14.23	29.48 \pm 8.46	1.25*	.006*
Circumference (μm)	26.20 \pm 4.81	22.51 \pm 3.23	1.16*	.006*
Major axis (μm)	7.05 \pm 1.41	6.27 \pm 1.17	1.12*	.017*
Minor axis (μm)	7.28 \pm 1.48	6.50 \pm 1.06	1.12*	.013*
INI/N ratio				
Area (μm^2)	0.38 \pm 0.09	0.41 \pm 0.09	0.93	.282
Circumference (μm)	0.66 \pm 0.10	0.65 \pm 0.08	1.02	.597
Major axis (μm)	0.61 \pm 0.09	0.63 \pm 0.09	0.97	.345
Minor axis (μm)	0.63 \pm 0.08	0.66 \pm 0.09	0.95	.199
INI/C ratio				
Area (μm^2)	0.12 \pm 0.02	0.16 \pm 0.04	0.75*	.000*
Circumference (μm)	0.36 \pm 0.05	0.39 \pm 0.07	0.92	.075
Major axis (μm)	0.35 \pm 0.04	0.40 \pm 0.06	0.88*	.002*
Minor axis (μm)	0.37 \pm 0.05	0.42 \pm 0.07	0.88*	.010*

CMVinf-LBP, cytomegalovirus infected cells in cytology processed by liquid-based preparation; CMVinf-CP, cytomegalovirus infected cells in smear processed by conventional preparation; N, nucleus; C, cytoplasm; INI, intranuclear inclusion.

* $p < .05$.

son of CP with LBP have highlighted the smaller sizes of the nucleus and cytoplasm in LBP,³⁷⁻⁴⁰ clear morphologic detail in LBP,³⁶ higher diagnostic accuracy,³³⁻³⁵ and superior quantity of diagnostic cells³⁴ or infectious organisms.³² Son *et al.*³¹ reported that, in urine, the cell and nuclear sizes in LBP are larger than in CP. In this study, CMV-infected cells of LBP were significantly larger in the nucleus (1.58 times), cytoplasm (1.37 times), and intranuclear inclusion (1.25 times) areas compared with CP. Enlargement of cells in CMV infection is characteristic and is more easily detectable in LBP than in CP, which may help to increase the diagnostic accuracy. It is unclear why the LBP specimen showed larger CMV-infected cells. It is possible that several factors influenced this result, such as delayed time for the fixative from the moment the specimen was obtained, CMV-infected cellular characteristics, and degeneration. Additional studies with a larger number of cases are needed to determine causative

factors for the larger size of histiocytes in CP.

The LBP method has an advantage in detecting CMV-infected cells in daily practice because of the large cytoplasm and nucleus, which are enhanced by a clean background and a small field, which emphasize the enlarged cells and cellular details. However, in this study, the number of CMV-infected cells in LBP tended to be lower than in CP. The CP slides contained more CMV-infected cells. However, the CMV-infected cells were scattered throughout the entire smear slide. In addition, CMV-infected cells in CP showed a higher nuclear cytoplasmic ratio than those in LBP, which requires a clearer differentiation from other conditions that result in a high nuclear cytoplasmic ratio.

To the best of our knowledge, this is the first analysis of the cytoplasm, nucleus, and intranuclear inclusion of CMV-infected cells that includes numerical measurements of area, circumference, and major and minor axes. The exact extent of CMV-in-

ected cell enlargement compared to histiocytes was calibrated, and it might be helpful in diagnosing CMV infection in bronchial washing cytology specimens. The preparation method affects the extent of cellular alteration, specifically the cell size, and further study is needed to elucidate the mechanism. In addition, CMV-infected cells in LBP were significantly larger than those in CP.

Conflicts of Interest

No potential conflict of interest relevant to this article was reported.

Acknowledgments

This work was supported by the Gachon University Gil Medical Center (Grant number: 2011-01).

REFERENCES

- Ribbert H. Über protozoenartige Zellen in der Niere eines syphilitischen Neugeborenen und in der Parotis von Kindern. *Zentralbl Allg Pathol* 1904; 15: 945-8.
- Halwachs-Baumann G. Congenital cytomegalovirus infection: epidemiology, diagnosis, therapy. Wien: Springer Vienna, 2011.
- Jesionek A, Kiolemenoglou B. Ueber einen Befund von protozoenartigen Gebilden in den Organen eines hereditär-luetischen Foetus. *Munch Med Wochenschr* 1904; 51: 1905-7.
- Goodpasture EW, Talbot FB. Concerning the nature of "protozoan-like" cells in certain lesions of infancy. *Am J Dis Child* 1921; 21: 415-25.
- Cole R, Kuttner AG. A filterable virus present in the submaxillary glands of guinea pigs. *J Exp Med* 1926; 44: 855-73.
- Craig JM, Macauley JC, Weller TH, Wirth P. Isolation of intranuclear inclusion producing agents from infants with illnesses resembling cytomegalic inclusion disease. *Proc Soc Exp Biol Med* 1957; 94: 4-12.
- Fetterman GH. A new laboratory aid in the clinical diagnosis of inclusion disease of infancy. *Am J Clin Pathol* 1952; 22: 424-5.
- Warner NE, McGrew EA, Nanos S. Cytologic study of the sputum in cytomegalic inclusion disease. *Acta Cytol* 1964; 8: 311-5.
- An-Foraker SH, Haesaert S. Cytomegalic virus inclusion body in bronchial brushing material. *Acta Cytol* 1977; 21: 181-2.
- Frale WJ, Frable MA, Seney FD Jr. Virus infections of the respiratory tract cytopathologic and clinical analysis. *Acta Cytol* 1977; 21: 32-6.
- Martin WJ 2nd, McDougall JC. Cytomegalovirus infection with idiopathic pulmonary fibrosis: diagnosis suggested by bronchoalveolar lavage. *Chest* 1983; 84: 500-2.
- Duggan MA, Pomponi C, Robboy SJ. Pulmonary cytology of the acquired immune deficiency syndrome: an analysis of 36 cases. *Diagn Cytopathol* 1986; 2: 181-6.
- Buchanan AJ, Gupta RK. Cytomegalovirus infection of the lung: cytomorphologic diagnosis by fine-needle aspiration cytology. *Diagn Cytopathol* 1986; 2: 341-2.
- Selvaggi SM, Gerber M. Pulmonary cytology in patients with the acquired immunodeficiency syndrome (AIDS). *Diagn Cytopathol* 1986; 2: 187-93.
- Solans EP, Yong S, Husain AN, Eichorst M, Gattuso P. Bronchioalveolar lavage in the diagnosis of CMV pneumonitis in lung transplant recipients: an immunocytochemical study. *Diagn Cytopathol* 1997; 16: 350-2.
- Gideon K, Zaharopoulos P. Cytomegalovirus endocervicitis diagnosed by cervical smear. *Diagn Cytopathol* 1991; 7: 625-7.
- Hunt JL, Baloch Z, Judkins A, LiVolsi VA, Montone KT, Gupta PK. Unique cytomegalovirus intracytoplasmic inclusions in ectocervical cells on a cervical/endocervical smear. *Diagn Cytopathol* 1998; 18: 110-2.
- Henry-Stanley MJ, Stanley MW, Burton LG, Samuelson J. Cytologic diagnosis of cytomegalovirus in cervical smears. *Diagn Cytopathol* 1993; 9: 364-5.
- Sekhon HS, Press RD, Schmidt WA, Hawley M, Rader A. Identification of cytomegalovirus in a liquid-based gynecologic sample using morphology, immunohistochemistry, and DNA real-time PCR detection. *Diagn Cytopathol* 2004; 30: 411-7.
- Oei AL, Salet-van de Pol MR, Borst SM, van den Berg AP, Grefte JM. "Owl's eye" cells in a cervical smear of a transplant recipient: don't forget to inform the referring physician. *Diagn Cytopathol* 2007; 35: 227-9.
- Venkataraman G, Kouria G, Mehrotra S, Hammadeh R, Wojcik EM, Booth CN. Cytomegalovirus inclusions on a cervical pap test: report of a well-known organism at an uncommon site. *Diagn Cytopathol* 2007; 35: 618-20.
- Wax TD, Layfield LJ, Zaleski S, *et al.* Cytomegalovirus sialadenitis in patients with the acquired immunodeficiency syndrome: a potential diagnostic pitfall with fine-needle aspiration cytology. *Diagn Cytopathol* 1994; 10: 169-72.
- Santiago K, Rivera A, Cabaniss D, Dhurhar N, Moroz K. Fine-needle aspiration of cytomegalovirus sialadenitis in a patient with acquired immunodeficiency syndrome: pitfalls of diff-quick staining. *Diagn Cytopathol* 2000; 22: 101-3.
- Goodman ZD, Gupta PK, Frost JK, Erozan YS. Cytodiagnosis of viral infections in body cavity fluids. *Acta Cytol* 1979; 23: 204-8.
- Delfs-Jegge S, Dalquen P, Hurwitz N. Cytomegalovirus-infected cells in a pleural effusion from an acquired immunodeficiency syn-

- drome patient: a case report. *Acta Cytol* 1994; 38: 70-2.
26. Armbruster C, Schalleschak J, Vetter N, Pokieser L. Pleural effusions in human immunodeficiency virus-infected patients: correlation with concomitant pulmonary diseases. *Acta Cytol* 1995; 39: 698-700.
 27. Katz RL, Alappattu C, Glass JP, Bruner JM. Cerebrospinal fluid manifestations of the neurologic complications of human immunodeficiency virus infection. *Acta Cytol* 1989; 33: 233-44.
 28. Teot LA, Ducatman BS, Geisinger KR. Cytologic diagnosis of cytomegaloviral esophagitis: a report of three acquired immunodeficiency syndrome-related cases. *Acta Cytol* 1993; 37: 93-6.
 29. Zhang X, el-Sahrigy D, Elhosseiny A, Melamed MR. Simultaneous cytomegalovirus infection and Kaposi's sarcoma of the thyroid diagnosed by fine needle aspiration in an AIDS patient: a case report and first cytologic description of the two entities occurring together. *Acta Cytol* 2003; 47: 645-8.
 30. Shi Q, Nilson E, Singh M, David O, Cabay RJ. Uncommon cervical viral cytopathic changes in a liquid-based cytology preparation. *Diagn Cytopathol* 2012; 40: 1088-9.
 31. Son SM, Koo JH, Choi SY, *et al.* Evaluation of urine cytology in urothelial carcinoma patients: a comparison of CellprepPlus(R) liquid-based cytology and conventional smear. *Korean J Pathol* 2012; 46: 68-74.
 32. Takei H, Ruiz B, Hicks J. Cervicovaginal flora: comparison of conventional pap smears and a liquid-based thin-layer preparation. *Am J Clin Pathol* 2006; 125: 855-9.
 33. Konofaos P, Tomos P, Malagari K, *et al.* The role of ThinPrep cytology in the investigation of lung tumors. *Surg Oncol* 2006; 15: 173-8.
 34. Lee KR, Papillo JL, St John T, Eyerer GJ. Evaluation of the ThinPrep processor for fine needle aspiration specimens. *Acta Cytol* 1996; 40: 895-9.
 35. Astall E, Atkinson C, Morton N, Goddard MJ. The evaluation of liquid-based 'Cyto-SED' cytology of bronchioalveolar lavage specimens in the diagnosis of pulmonary neoplasia against conventional direct smears. *Cytopathology* 2003; 14: 143-9.
 36. Hayama FH, Motta AC, Silva Ade P, Migliari DA. Liquid-based preparations versus conventional cytology: specimen adequacy and diagnostic agreement in oral lesions. *Med Oral Patol Oral Cir Bucal* 2005; 10: 115-22.
 37. Kobayashi Y, Uehara T, Ota H. Liquid-based thin-layer cytology can be routinely used in samples obtained via fiberoptic bronchoscope. *Acta Cytol* 2011; 55: 69-78.
 38. Kim S, Owens CL. Analysis of ThinPrep cytology in establishing the diagnosis of small cell carcinoma of lung. *Cancer* 2009; 117: 51-6.
 39. Lee JD, Oh YH, Lee SO, Kim JY. Comparison of diagnostic cytomorphology of atypical squamous cells in liquid-based preparations and conventional smears. *Korean J Pathol* 2012; 46: 365-9.
 40. Norimatsu Y, Shigematsu Y, Sakamoto S, *et al.* Nuclear characteristics of the endometrial cytology: liquid-based versus conventional preparation. *Diagn Cytopathol* 2013; 41: 120-5.

Clear Cell Adenocarcinoma Arising from Adenofibroma in a Patient with Endometriosis of the Ovary

Inju Cho · Sung-Chul Lim

Department of Pathology, Chosun University
School of Medicine, Gwangju, Korea

Received: April 9, 2015
Revised: July 23, 2015
Accepted: August 7, 2015

Corresponding Author

Sung-Chul Lim, MD, PhD
Department of Pathology, Chosun University
Hospital, 365 Pilmun-daero, Dong-gu, Gwangju
61453, Korea
Tel: +82-62-230-6343
Fax: +82-62-226-5860
E-mail: sclim@chosun.ac.kr

Ovarian clear cell adenocarcinomas (CCACs) are frequently associated with endometriosis and, less often with clear cell adenofibromas (CCAFs). We encountered a case of ovarian CCAC arising from benign and borderline adenofibromas of the clear cell and endometrioid types with endometriosis in a 53-year-old woman. Regions of the adenofibromas showed transformation to CCAC and regions of the endometriosis showed atypical endometriotic cysts. This case demonstrates that CCAC can arise from CCAF or endometriosis.

Key Words: Adenocarcinoma, clear cell; Adenofibroma; Endometriosis; Ovary

Histological and epidemiological analyses have demonstrated a close relationship between endometriosis and ovarian clear cell adenocarcinoma (CCAC).¹⁻³ Clear cell adenofibroma (CCAF) is a major benign or borderline type of ovarian clear cell tumor.⁴ However, benign CCAF is extremely rare.^{5,6} One study demonstrated the coexistence of CCAF components (14 cases) in 21% of surgically resected ovarian CCACs. Of these 14 CCAF (+) cases, CCAF with atypia were found adjacent to CCAF without atypia in 10, and adjacent to obvious CCACs in 13 cases.⁷ Therefore, we can speculate that both CCAF and endometriosis may be precursors of CCAC. Several studies have demonstrated that there is a genetic linkage between CCAF and CCAC,⁸ as well as between endometriosis and CCAC.⁹⁻¹¹

Here, we report a case of CCAC in a 53-year-old woman with both benign and borderline ovarian adenofibromas of the clear cell and endometrioid types, in addition to endometriosis.

CASE REPORT

A 53-year-old woman visited a local obstetrics and gynecology clinic for a routine examination. Ultrasonography demonstrated a right ovarian cystic mass. The patient was referred to the Department of Obstetrics and Gynecology at Chosun Uni-

versity Hospital for further evaluation and treatment. The patient had a history of laparoscopic left salpingo-oophorectomy and adhesiolysis due to left ovarian teratoma and intestinal adhesion seven years earlier. She had also experienced an intracranial hemorrhage 3 years earlier, and had suffered from medication-controlled hypothyroidism for 5 years.

Abdominal computed tomography revealed a 5.5-cm cystic mass in her right ovary (Fig. 1A). The cyst was unilocular with fluid attenuation, and there was no contrast-enhancing solid mass. Laparoscopy findings revealed a fluid-containing cystic mass that had a smooth surface with focal hemorrhage (Fig. 1B). Laparoscopic right salpingo-oophorectomy and adhesiolysis was undertaken under the clinical impression of benign cystadenoma.

Gross findings revealed a previously collapsed cystic mass measuring 5 cm × 4.5 cm × 2.5 cm. The mass showed a 2.3 cm × 1.2 cm solid part on one side. Histologic examination revealed benign and borderline CCAFs, endometriosis, atypical endometriotic cysts, and CCAC. The solid portion consisted of benign and borderline CCAF, CCAC, and endometriosis in descending order of prevalence. The cystic portion was merged into the solid portion of CCAF and CCAC, and consisted of benign and atypical endometriotic cysts.

The benign CCAF constituted a major portion of the tumor

and demonstrated a compact arrangement of variably sized tubulocystic structures in the cellular stroma with no nuclear atypia. Flattened indiscernible, flat cuboidal, and polygonal cells with relatively abundant cytoplasm and no nuclear atypia lined the mass (Fig. 2). The glands in the borderline CCAF showed a greater degree of crowding and variation in size and shape compared with the benign CCAF. Focal nuclear atypia was observed in the glandular linings. The glands were delineated with one to three layers of cells with abundant cytoplasm and mildly pleomorphic, hyperchromatic nuclei. In some areas, stratified epithelium showed tiny buds with atypical nuclei. However, the glands in many areas were lined with non-atypical flat to cuboidal epithelium (Fig. 2).

The CCAC had a tubulocystic pattern with hobnail, cuboidal or flat atypical cell lining, characterized by nuclear enlargement and hyperchromasia. The glands were separated by fibrous stro-

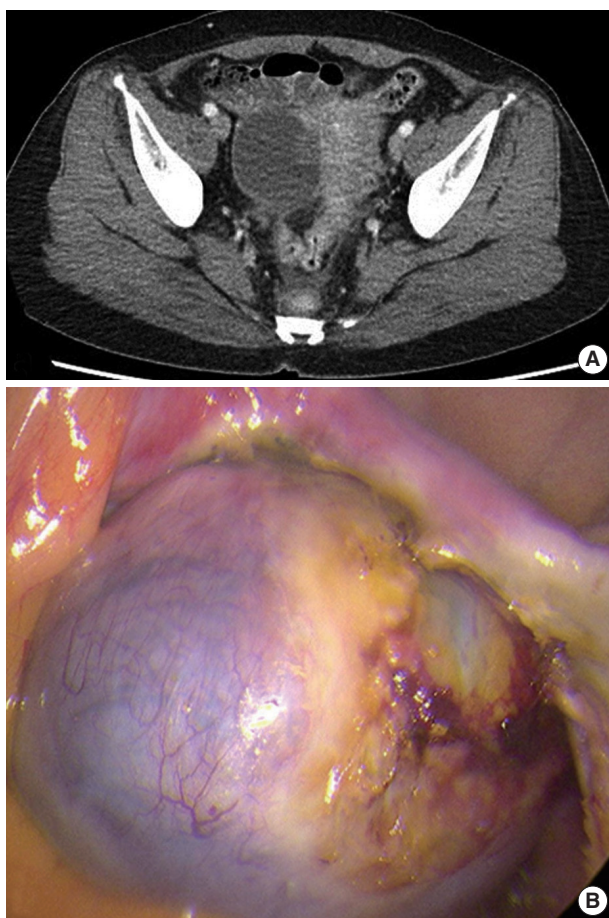


Fig. 1. Abdominal computed tomography (CT) and laparoscopic findings. (A) Abdominal computed tomography showing a 5.5-cm cystic mass in the right ovary. (B) Laparoscopy findings reveal a fluid containing cystic mass with a smooth surface and focal hemorrhage.

ma, and foci of altered stromal responses were noted. There was crowding of tubules with a slightly haphazard arrangement in some areas. The borderline CCAF had microinvasion characterized by a few cells scattered haphazardly in the surrounding stroma. The borderline CCAF and CCAC were scattered, and a histologic continuum between borderline CCAF and CCAC was found within the same tumor (Fig. 2).

The benign endometriotic cysts had a predominantly cystic gross appearance. Typical endometriotic cysts showed minimally stratified tubal-type epithelium overlying the scant endometrial-type stroma. This endometriotic epithelium gradually showed greater nuclear atypia, demonstrating a multilayered epithelium with hyperchromatic, enlarged and irregular nuclei with prominent nucleoli as it merged with possible intraepithelial carcinomatous areas (Fig. 3).

The presence of benign and borderline CCAFs, borderline CCAF with microinvasion, CCAC, endometriosis, and benign and atypical endometriotic cysts within this single ovarian mass suggests a histologic continuum among endometriosis, CCAF and CCAC.

DISCUSSION

Sampson¹² was the first to report malignant transformation of ovarian endometriosis. Endometrioid adenocarcinoma and CCAC are the most common types of malignancy arising from ovarian endometriosis.¹³ Ovarian endometriosis is therefore considered a precursor lesion to endometrioid adenocarcinoma and CCAC of the ovary. Sampson¹² and Scott¹⁴ suggested the following criteria for determining whether a tumor has arisen from endometriosis: the presence of both malignant and benign endometrial tissue in the same ovary; cancer arising from ovarian endometriosis without other invasion; tissue resembling endometrial stroma surrounding characteristic epithelial glands; and a transition between benign endometriosis and malignant epithelium. In the present case, we found typical endometriosis, benign and atypical endometriotic cysts, and possible intraepithelial carcinomatous areas in the same ovary. CCAC arising in ovarian endometriosis or CCAF without other invasion was also found.

Malignant transformation of ovarian endometriosis occurs in more than 1% of the cases.¹² CCAC is the most common type of malignant transformation of ovarian endometriosis, and endometrioid adenocarcinoma is the second most common.¹³

Adenofibromas are also usually associated with ovarian endometriosis.^{5,15} In the present case, we identified benign and bor-

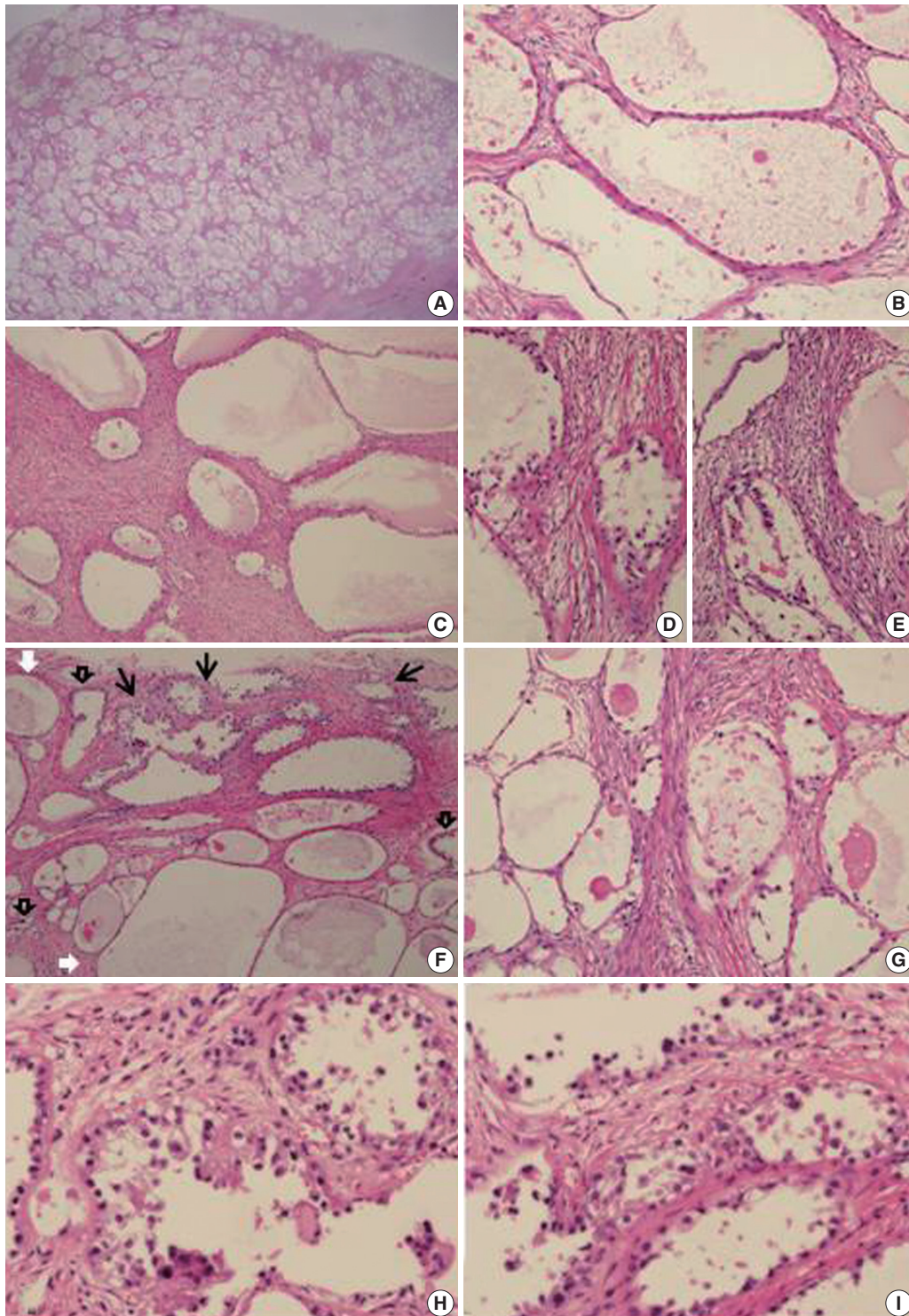


Fig. 2. Histopathologic findings of the solid part of the mass. (A) The compact arrangement of variably-sized tubulocystic structures in the stroma is consistent with adenofibroma. The cell lining consisted of flattened indiscernible cells or flat cuboidal cells (B) and polygonal cells with abundant clear cytoplasm (C). (D, E) In some areas, stratified epithelium shows tiny buds with atypical nuclei. (F) The transitional zone from benign (white arrows) to borderline (black open arrows) clear cell adenofibromas to clear cell adenocarcinoma (black arrows). (G) Higher magnification shows benign (left) and atypical (right) adenofibromas. (H, I) Area of clear cell adenocarcinoma shows a tubulocystic pattern with hobnail, cuboidal, or flat atypical lining cells characterized by nuclear enlargement and hyperchromasia, and foci of altered stromal responses.

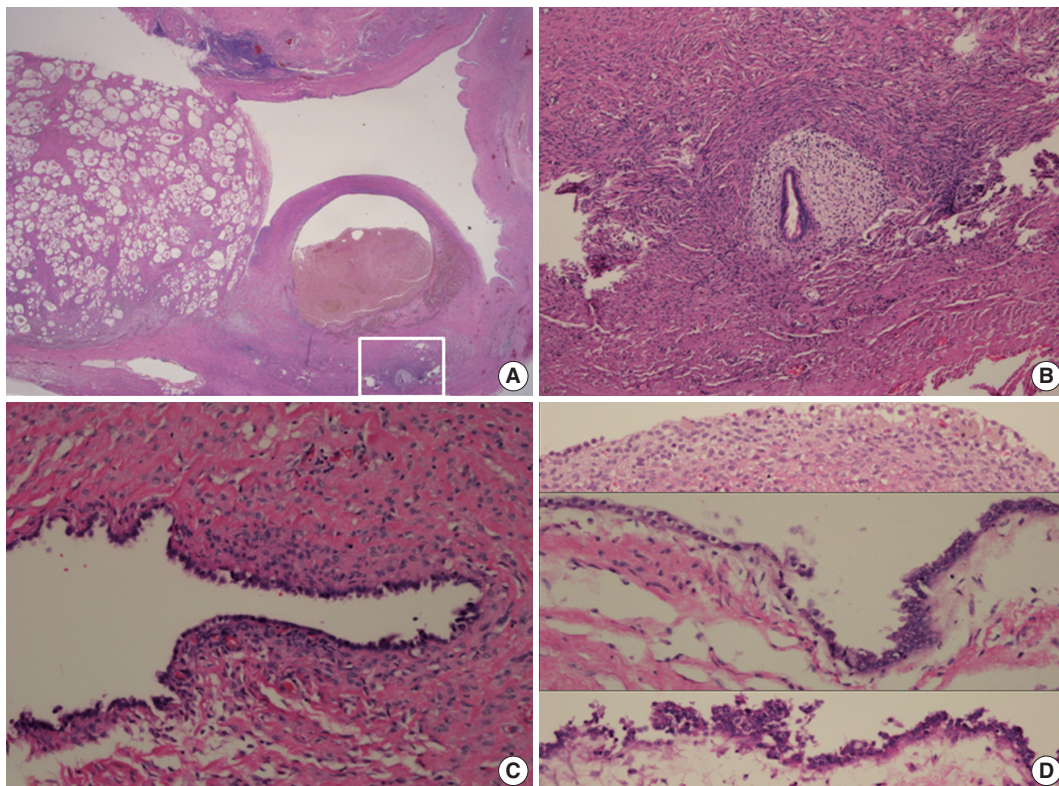


Fig. 3. Histopathologic findings of adenofibroma, endometriotic cyst, and endometriosis (A). Higher magnification of the inset shows endometriosis (B). (C) Endometriotic cyst with tubal-type epithelium overlying scant endometrial-type stroma. (D) Endometriotic cyst with simple cuboidal epithelium overlying endometrial stroma with hemosiderin pigmentation (upper) and gradual transition to nuclear atypia demonstrating stratification with hyperchromatic, enlarged, and irregular nuclei with prominent nucleoli (middle and lower).

derline adenofibromas, and the borderline adenofibromas demonstrated a transition to CCAC. Slow and progressive transformation of CCAC from benign to borderline to a microinvasive pattern has been suggested.³ In addition, patients with ovarian CCAF are younger than those with CCAC.^{5,6} This supports the suggestion of transformation of CCAC from benign to malignant tumors.

CCAC containing CCAFs are occasionally found.^{6,16,17} According to the classification of CCAC into groups with and without CCAF components, the CCAF (+) group showed a higher frequency of histologically low-grade tumors, a lower Ki-67 labeling index, less frequent endometriosis, and better patient prognosis than the CCAF (-) group.⁷

There are two types of ovarian carcinogenesis, type I and type II. Type I tumors are usually low grade and in low stage, behave in an indolent fashion, and develop slowly from precursor lesions. However, type II tumors are highly aggressive high grade tumors characterized by frequent *TP53* mutations. They are not associated with the usual precursor lesions. CCAC is associated with precursor lesions such as endometriosis, adenofibromas, bor-

derline/atypical adenofibromas and endometriotic cysts. It is also found in a low stage, showing a low frequency of *TP53* mutations. However, CCAC is high grade and associated with poor prognosis when it is found in high stage.¹⁸ Zhao *et al.*¹⁸ speculated that ovarian CCAC have two pathways. In one, epithelial atypia arises in an endometriotic cyst and then evolves into CCAC, and in the other, non-cystic endometriosis induces a fibromatous reaction resulting in the formation of an adenofibroma, which then develops into borderline adenofibroma and subsequently CCAC. Therefore, CCACs with or without adenofibromas are more closely related to type I tumors. Adenofibromatous and cystic types of CCAC appear to be derived from endometriosis. Adenofibromatous CCAC develops from non-cystic endometriosis and is associated with an adenofibromatous background, while the cystic type of CCAC develops from an endometriotic cyst and is not associated with an adenofibromatous background.¹⁸ The two pathways may overlap in some cases. The present case showed benign and borderline CCAFs, borderline CCAF with microinvasion, CCAC, endometriosis, and benign and atypical endometriotic cysts. Thus, the two pathways

overlapped in the present case. *ARID1A* mutation and loss of the corresponding protein, BAF250a, are common in CCAC. However, loss of BAF250a expression is significantly more common in CCAC with endometriosis than in cases with adenofibroma.¹⁹

There is a common genetic linkage between endometriosis and ovarian cancers such as CCAC, including losses of heterozygosity (LOHs) and alleles at the *PTEN* locus.⁹⁻¹¹ Moreover, there is also a common genetic linkage between CCAF and ovarian CCAC, such as LOHs on 5q, 10q, and 22q.⁷ Therefore, possible alternative ovarian clear cell carcinogenic pathways are endometriosis to CCAC, CCAF to CCAC, or endometriosis to CCAF/adenofibroma to CCAC.

The present case demonstrates that both CCAF and endometriosis should be regarded as precursors to CCAC.

Conflicts of Interest

No potential conflict of interest relevant to this article was reported.

Acknowledgments

This study was supported by research fund from Chosun University, 2014.

REFERENCES

- Seidman JD, Russell P, Kurman RJ. Surface epithelial tumors of the ovary. In: Kurman RJ, editor. Blaustein's pathology of the female genital tract. 5th ed. New York: Springer-Verlag, 2001; 791-904.
- Vercellini P, Parazzini F, Bolis G, *et al.* Endometriosis and ovarian cancer. *Am J Obstet Gynecol* 1993; 169: 181-2.
- Fukunaga M, Nomura K, Ishikawa E, Ushigome S. Ovarian atypical endometriosis: its close association with malignant epithelial tumours. *Histopathology* 1997; 30: 249-55.
- Tavassoli FA, Devilee P. World Health Organization classification of tumours of pathology and genetics of tumours of the breast and female genital organs. Lyon: IARC Press, 2003; 218-28.
- Bell DA, Scully RE. Benign and borderline clear cell adenofibromas of the ovary. *Cancer* 1985; 56: 2922-31.
- Roth LM, Langley FA, Fox H, Wheeler JE, Czernobilsky B. Ovarian clear cell adenofibromatous tumors: benign, of low malignant potential, and associated with invasive clear cell carcinoma. *Cancer* 1984; 53: 1156-63.
- Yamamoto S, Tsuda H, Yoshikawa T, *et al.* Clear cell adenocarcinoma associated with clear cell adenofibromatous components: a subgroup of ovarian clear cell adenocarcinoma with distinct clinicopathologic characteristics. *Am J Surg Pathol* 2007; 31: 999-1006.
- Yamamoto S, Tsuda H, Takano M, Hase K, Tamai S, Matsubara O. Clear-cell adenofibroma can be a clonal precursor for clear-cell adenocarcinoma of the ovary: a possible alternative ovarian clear-cell carcinogenic pathway. *J Pathol* 2008; 216: 103-10.
- Jiang X, Morland SJ, Hitchcock A, Thomas EJ, Campbell IG. Allelotyping of endometriosis with adjacent ovarian carcinoma reveals evidence of a common lineage. *Cancer Res* 1998; 58: 1707-12.
- Obata K, Hoshiai H. Common genetic changes between endometriosis and ovarian cancer. *Gynecol Obstet Invest* 2000; 50 Suppl 1: 39-43.
- Sato N, Tsunoda H, Nishida M, *et al.* Loss of heterozygosity on 10q23.3 and mutation of the tumor suppressor gene *PTEN* in benign endometrial cyst of the ovary: possible sequence progression from benign endometrial cyst to endometrioid carcinoma and clear cell carcinoma of the ovary. *Cancer Res* 2000; 60: 7052-6.
- Sampson JA. Endometrioid carcinoma of the ovary, arising in endometrial tissue in that organ. *Arch Surg* 1925; 10: 1-72.
- Russell P. The pathological assessment of ovarian neoplasms. I: Introduction to the common 'epithelial' tumours and analysis of benign 'epithelial' tumours. *Pathology* 1979; 11: 5-26.
- Scott RB. Malignant changes in endometriosis. *Obstet Gynecol* 1953; 2: 283-9.
- Kao GF, Norris HJ. Unusual cystadenofibromas: endometrioid, mucinous, and clear cell types. *Obstet Gynecol* 1979; 54: 729-36.
- Russell P, Merkur H. Proliferating ovarian "epithelial" tumours: a clinico-pathological analysis of 144 cases. *Aust N Z J Obstet Gynaecol* 1979; 19: 45-51.
- Bell DA. Ovarian surface epithelial-stromal tumors. *Hum Pathol* 1991; 22: 750-62.
- Zhao C, Wu LS, Barner R. Pathogenesis of ovarian clear cell adenofibroma, atypical proliferative (borderline) tumor, and carcinoma: clinicopathologic features of tumors with endometriosis or adenofibromatous components support two related pathways of tumor development. *J Cancer* 2011; 2: 94-106.
- Nishikimi K, Kiyokawa T, Tate S, Iwamoto M, Shozu M. *ARID1A* expression in ovarian clear cell carcinoma with an adenofibromatous component. *Histopathology* 2015 Apr 23 [Epub]. <http://dx.doi.org/10.1111/his.12721>.

An Adult Case of Bartter Syndrome Type III Presenting with Proteinuria

Eun Jung Cha · Won Min Hwang¹
Sung-Ro Yun¹ · Moon Hyang Park

Department of Pathology, ¹Division of Nephrology, Department of Internal Medicine, Konyang University Hospital, Konyang University College of Medicine, Daejeon, Korea

Received: June 12, 2015
Revised: August 4, 2015
Accepted: August 31, 2015

Corresponding Author

Moon Hyang Park, MD
Department of Pathology, Konyang University Hospital, Konyang University College of Medicine, 158 Gwanjeodong-ro, Seo-gu, Daejeon 35365, Korea
Tel: +82-42-600-9280
Fax: +82-42-600-9280
E-mail: parkmh@hanyang.ac.kr

Bartter syndrome (BS) I-IV is a rare autosomal recessive disorder affecting salt reabsorption in the thick ascending limb of the loop of Henle. This report highlights clinicopathological findings and genetic studies of classic BS in a 22-year-old female patient who presented with persistent mild proteinuria for 2 years. A renal biopsy demonstrated a mild to moderate increase in the mesangial cells and matrix of most glomeruli, along with marked juxtaglomerular cell hyperplasia. These findings suggested BS associated with mild IgA nephropathy. Focal tubular atrophy, interstitial fibrosis, and lymphocytic infiltration were also observed. A genetic study of the patient and her parents revealed a mutation of the *CLCNKB* genes. The patient was diagnosed with BS, type III. This case represents an atypical presentation of classic BS in an adult patient. Pathologic findings of renal biopsy combined with genetic analysis and clinicolaboratory findings are important in making an accurate diagnosis.

Key Words: Bartter syndrome; Hypokalemia; Juxtaglomerular cell hyperplasia

Bartter syndrome (BS) is a rare renal tubulopathy that was first described by Bartter in 1962.¹ The condition is characterized by polyuria, hypokalemia, metabolic alkalosis, and hyperreninemic-hyperaldosteronism with normal or slightly low blood pressure due to renal loss of sodium and hyperplasia of the juxtaglomerular apparatus (JGA). The condition is also referred to as salt-wasting nephropathy.¹ The prevalence of BS is 1 in 1,000,000, compared with 1 in 40,000 for Gitelman syndrome (GS).² The classification depends on the severity of the symptoms and type of genetic mutation. Clinically, BS can be classified into two variants, antenatal/neonatal BS and classic BS, according to the onset of age. Genetically, BS can be classified into five variants according to type of gene mutation.³ Type III BS presents as classic BS, which is characterized by polyuria, polydipsia, and a tendency for dehydration, but with normal or slightly increased urinary calcium excretion and no tendency to develop kidney stones. Patients with classic BS might have symptoms in the first two years of life, but most cases are usually diagnosed at school age or in adolescence.⁴ However, age of onset and clinical severity are highly variable.⁵⁻⁷

Here, we present a case of late onset BS, with typical hyperplasia of juxtaglomerular cells on renal biopsy and molecular di-

agnostic confirmation of a familial chloride channel K_b (*CLCNKB*) gene mutation.

CASE REPORT

Mild proteinuria had been incidentally detected in a 22-year-old woman during a regular health check-up 2 years prior to presentation. She visited a local clinic for a follow-up check. She took medication to treat hyperlipidemia for 1 year and did not take any other drugs including diuretics or laxatives. She was admitted to our hospital for evaluation of persistent mild proteinuria.

The prenatal course was unremarkable. On physical examination, her height was 153 cm, her body weight was 49 kg and her blood pressure was 100/60 mm Hg. No edema was found, and normal muscle strength and reflexes were noted. The rest of the physical examination was unremarkable. The laboratory examination revealed blood urea nitrogen of 10.9 mg/dL, creatinine of 0.68 mg/dL, sodium of 137 mmol/L, potassium of 2.59 mmol/L, chloride of 94.7 mmol/L, magnesium of 2.05 mEq/L, and bicarbonate of 31.2 mEq/L. Serum levels of IgG, IgA, IgM, C3, and C4 were normal. Anti-nuclear antibody was negative. Urinalysis showed a specific gravity of 1.007, trace protein, pH

8.0, and no red blood cells. The spot urine protein/creatinine ratio was 0.95 g/g creatinine. Abdominal sonography revealed normal-sized kidneys, without nephrocalcinosis or stones. Plasma renin activity was elevated at 27.98 ng/mL/hr (normal range, 0.50 to 1.90 ng/mL/hr in a supine position), but serum aldosterone was 13.2 pg/mL within normal limits (normal range, 1 to 16 pg/mL in a supine position). The urine prostaglandin E2 level was elevated at 2,815 ng/day (normal range, 400 to 620 ng/day). These findings suggested BS or pseudo-BS/GS caused by vomiting or diuretics.

Light microscopy of renal biopsy demonstrated 14 glomeruli, two of which were globally sclerotic. Most glomeruli appeared moderately increased in size and cellularity due to prominence of the mesangium and JGA. Five glomeruli showed marked enlargement with hyperplasia (Fig. 1A) and hypergranulosis of the JGA (Fig. 1B). The mesangium was diffusely expanded due

to mild to moderate increase in cells and matrix (Fig. 1A). There was moderate tubular atrophy and interstitial fibrosis with infiltration of lymphocytes. The interlobular arteries and arterioles displayed mild to moderate intimal fibrous thickening and medial sclerosis. Immunofluorescence revealed weak positive (1+) staining for IgG, IgA, and fibrinogen and trace (+/-) of staining for C3 and lambda in the mesangium (Fig. 1C). Electron microscopy revealed mild increase in the mesangial cells and matrix with rare small mesangial electron-dense deposits and hyperplastic juxtaglomerular cells with increased electron dense renin and progranules (Fig. 1D).

Genetic analysis revealed a homozygous deletion of exon 1–14 and heterozygous deletion of exon 15–19 in the *CLCNKB* gene (Fig. 2A). Her father had heterozygous deletion of exon 1–14 (Fig. 2B), and her mother had heterozygous deletion of all examined exons of the *CLCNKB* gene (Fig. 2C). However, her

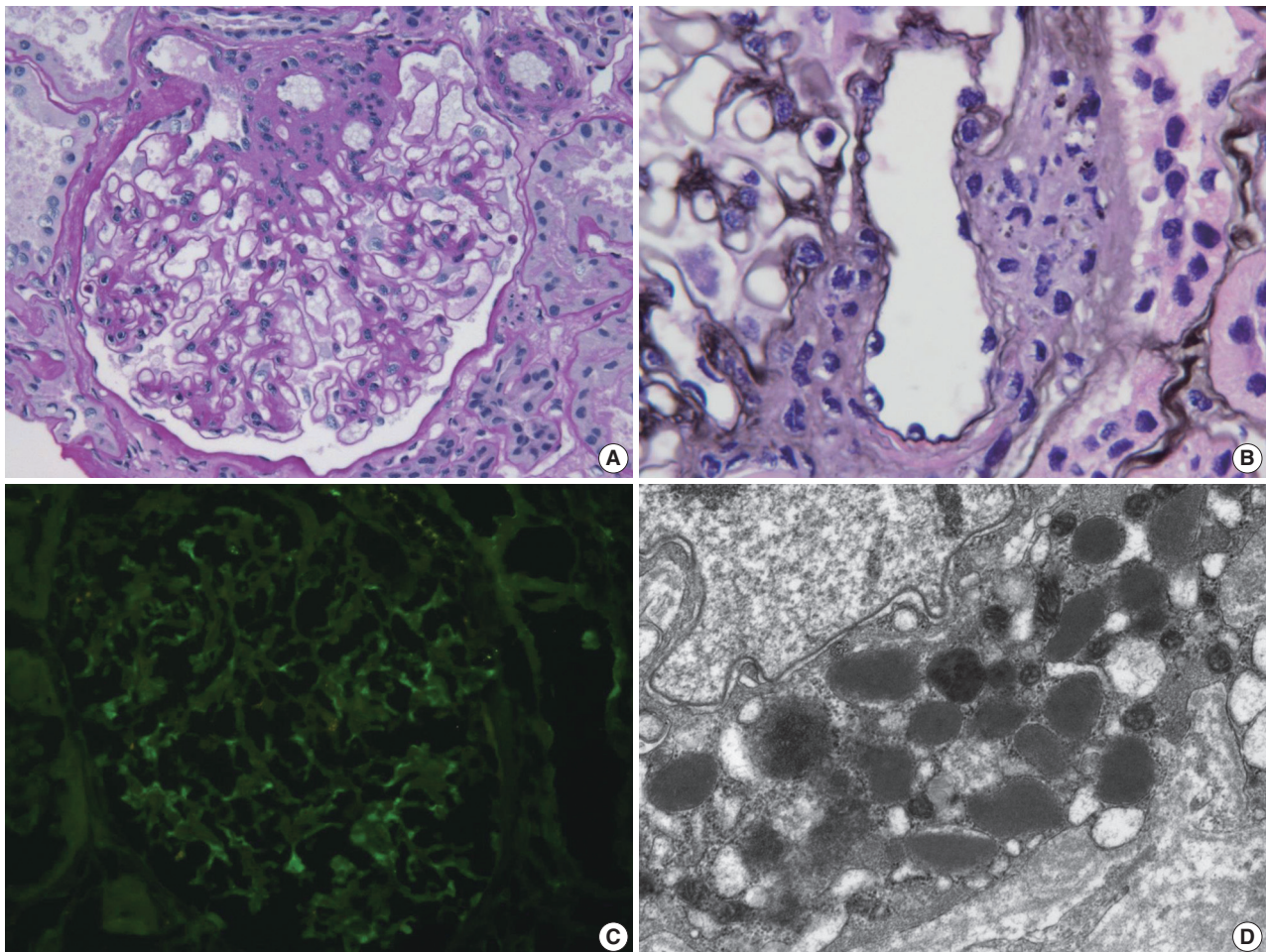


Fig. 1. Renal biopsy in a patient with Bartter syndrome with IgA nephropathy. (A) Glomerulus shows hyperplasia of juxtaglomerular cells with increased mesangial cells and matrix (periodic acid-Schiff). (B) Glomerulus shows hyperplasia and hypergranulosis of juxtaglomerular cells (Jones' methenamine silver, $\times 1,000$). (C) Immunofluorescence reveals weak (1+) staining for IgA in the mesangium. (D) Electron micrograph of the juxtaglomerular apparatus shows abundant progranules and mature renin granules (Hitach HT7700 EM, $\times 6,000$).

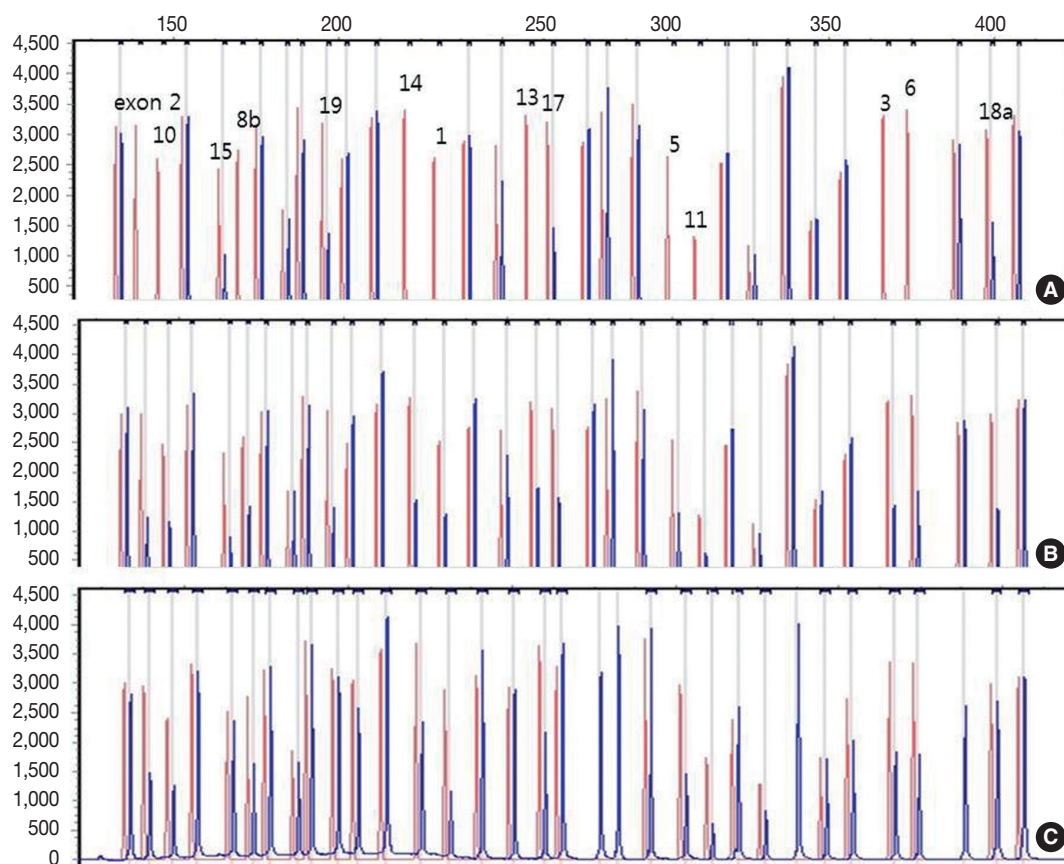


Fig. 2. Capillary electrophoretic pattern of the multiplex ligation-dependent probe amplification products of the patient's family. (A) The patient has a large homozygous deletion and a large heterozygous deletion. (B) Her father has a heterozygous deletion of exon 1–14. (C) Her mother has a heterozygous deletion of all examined exons of the *CLCNKB* gene.

parents displayed no renal symptoms or abnormal renal function.

DISCUSSION

BS is an autosomal recessive genetic disorder whose primary pathogenic mechanism is defective transepithelial chloride reabsorption in the thick ascending limb of the loop of Henle. The disorder is the result of defective function of proteins responsible for transporting ions to renal cells. Five types of genetic mutations are associated with the five different forms of the disease. Type I is due to an *SLC12A1* mutation encoding the bumetanide-sensitive $\text{Na}^+ - \text{K}^+ - 2\text{Cl}^-$ cotransporter (NKCC2), and type II is the result of *KCNJ1* encoding the inward rectifying K^+ channel (ROMK). Type III or classic BS results from a mutation of *CLCNKB*, encodes for the kidney-specific basolateral chloride channel (ClC-Kb). The ClC-Kb protein is required to ensure the exit of chloride (Cl^-) on the basolateral side. Impaired ClC-Kb function reduces Cl^- efflux and decreases Na-K-Cl reabsorption through NKCC2 by modifying the transepithelial voltage

gradient and causing salt loss in urine.⁴ Type IV is due to mutations of *BSND* encoding barttin (the β -subunit of the basolateral chloride channel). Finally, type V, with the features of autosomal dominant hypocalcemia, is caused by gain-of-function mutations of the calcium-sensing receptor.^{3,5,8,9} Types I, II, and IV are classified as antenatal BS.

Renal calcium handling can be used to differentiate between classic BS and GS. Hypomagnesemia is considered a well-defined characteristic of GS but it also affects a considerable number of patients with BS. The most definitive diagnostic method of BS is molecular analysis.^{10,11} The patient in the current case had no symptoms in the neonatal period or in childhood. This patient had no symptoms of polyuria, dehydration, or polydipsia except for nocturia and presented with mild proteinuria and mild hypokalemic metabolic alkalosis at 22 years of age. Clinically, this patient's diagnosis raised a suspicion of GS rather than BS, but deletion of the *CLCNKB* gene in the genetic analysis confirmed type III BS.

Although proteinuria is not a classic symptom in BS, it has

been a presenting symptom in cases associated with other glomerular diseases, such as focal segmental glomerulosclerosis, C1q nephropathy or immune complex glomerulopathy.¹²⁻¹⁵ Our patient had mild proteinuria for 2 years. The presence of mild to moderate mesangial proliferation in the renal biopsy, in addition to the weak positive immunofluorescence staining for IgA in the mesangium pointed to the possibility of mild IgA nephropathy coexistent with BS. Electron microscopy revealed rare small paramesangial electron dense deposits.

Renal changes in BS are probably caused by stimulation of the renin-angiotensin axis and activation of transforming growth factor β (TGF- β).¹⁶ Laboratory studies have suggested that exposure of mesangial cells to angiotensin II results in proliferation, hypertrophy, and TGF- β production.¹³ Although patients with BS have high angiotensin II level and activation of the renin-angiotensin axis, they also demonstrate normo/hypotension, reduced peripheral resistance, and hyporesponsiveness to vasopressor agents. Patients with BS and GS, as well as heterozygous carriers of both disorders, have lower blood pressure than the general population.² In addition to volume depletion, another possible contributor to the lower blood pressure in BS is increased renal release of vasodilator prostaglandins E2 (PGE2). The increased renal production of PGE2 results from impaired entry of sodium chloride into the macula densa cells at the end of the thick ascending limb of the loop of Henle, which increases the expression of cyclooxygenase 2.¹⁷ Therefore, these patients do not develop hypertension or associated complications such as cardiovascular remodeling and atherogenesis.¹⁸ The cause of renal dysfunction in patients with BS is unclear.

The histologic and molecular features of BS have been well described in the literature,^{3,5,6} and histologic findings of BS consistently show juxtaglomerular hyperplasia, interstitial fibrosis and nephrocalcinosis. Juxtaglomerular hyperplasia is a characteristic finding but is not a necessary finding for diagnosis. Juxtaglomerular hyperplasia can be associated with a variety of causes, such as chronic hypovolemic states with hypokalemia due to chronic vomiting or laxative abuse, familial chloride diarrhea, or cystinosis.⁴ The ingestion of diuretics is perhaps the most common cause of chronic hypokalemic alkalosis. For an accurate diagnosis, other causes must be ruled out through careful history taking, plasma and urine electrolyte measurement, or various diuretic screening methods.¹⁹

Accounting for the patient's clinical, laboratory, and pathological findings of BS, in conjunction with the results of genetic analysis of both the patient and her parents, the patient was diagnosed with type III BS. This case shows the importance of renal

biopsy and molecular analysis in delineating the cause of an atypical presentation of classic BS in an adult patient.

Conflicts of Interest

No potential conflict of interest relevant to this article was reported.

Acknowledgments

We thank Prof. HaeIl Cheong for performing the genetic study.

REFERENCES

1. Bartter FC, Pronove P, Gill JR Jr, Maccardle RC. Hyperplasia of the juxtaglomerular complex with hyperaldosteronism and hypokalemic alkalosis: a new syndrome. *Am J Med* 1962; 33: 811-28.
2. Ji W, Foo JN, O'Roak BJ, *et al*. Rare independent mutations in renal salt handling genes contribute to blood pressure variation. *Nat Genet* 2008; 40: 592-9.
3. Lee BH, Cho HY, Lee H, *et al*. Genetic basis of Bartter syndrome in Korea. *Nephrol Dial Transplant* 2012; 27: 1516-21.
4. Naesens M, Steels P, Verberckmoes R, Vanreterghem Y, Kuypers D. Bartter's and Gitelman's syndromes: from gene to clinic. *Nephron Physiol* 2004; 96: p65-78.
5. Xiumin W, Zheng S, Meichun X, Junfen F, Li L. A Chinese girl with Bartter syndrome type III due to a novel mutation and/or single nucleotide polymorphisms (SNPs) in *CLCNKB* gene. *Iran J Pediatr* 2013; 23: 89-94.
6. García Castaño A, Pérez de Nanclares G, Madariaga L, *et al*. Genetics of type III Bartter syndrome in Spain, proposed diagnostic algorithm. *PLoS One* 2013; 8: e74673.
7. Simon DB, Bindra RS, Mansfield TA, *et al*. Mutations in the chloride channel gene, *CLCNKB*, cause Bartter's syndrome type III. *Nat Genet* 1997; 17: 171-8.
8. Bhat YR, Vinayaka G, Sreelakshmi K. Antenatal Bartter syndrome: a review. *Int J Pediatr* 2012; 2012: 857136.
9. Krämer BK, Bergler T, Stoelcker B, Waldegger S. Mechanisms of disease: the kidney-specific chloride channels *CICKA* and *CICKB*, the Barttin subunit, and their clinical relevance. *Nat Clin Pract Nephrol* 2008; 4: 38-46.
10. Knoers NV, Levchenko EN. Gitelman syndrome. *Orphanet J Rare Dis* 2008; 3: 22.
11. Nakhoul F, Nakhoul N, Dorman E, Berger L, Skorecki K, Magen D. Gitelman's syndrome: a pathophysiological and clinical update. *Endocrine* 2012; 41: 53-7.
12. Su IH, Frank R, Gauthier BG, *et al*. Bartter syndrome and focal seg-

- mental glomerulosclerosis: a possible link between two diseases. *Pediatr Nephrol* 2000; 14: 970-2.
13. Sardani Y, Qin K, Haas M, Aronson AJ, Rosenfield RL. Bartter syndrome complicated by immune complex nephropathy: case report and literature review. *Pediatr Nephrol* 2003; 18: 913-8.
 14. Hanevold C, Mian A, Dalton R. C1q nephropathy in association with Gitelman syndrome: a case report. *Pediatr Nephrol* 2006; 21: 1904-8.
 15. Lee SE, Han KH, Jung YH, *et al.* Renal transplantation in a patient with Bartter syndrome and glomerulosclerosis. *Korean J Pediatr* 2011; 54: 36-9.
 16. Yamamoto T, Noble NA, Cohen AH, *et al.* Expression of transforming growth factor-beta isoforms in human glomerular diseases. *Kidney Int* 1996; 49: 461-9.
 17. Kömhoff M, Reinalter SC, Gröne HJ, Seyberth HW. Induction of microsomal prostaglandin E2 synthase in the macula densa in children with hypokalemic salt-losing tubulopathies. *Pediatr Res* 2004; 55: 261-6.
 18. Pagnin E, Davis PA, Semplicini A, Calò LA. The search for a link between inflammation and hypertension: contribution from Bartter's/Gitelman's syndromes. *Nephrol Dial Transplant* 2006; 21: 2340-2.
 19. Colussi G, Rombolà G, Airaghi C, De Ferrari ME, Minetti L. Pseudo-Bartter's syndrome from surreptitious diuretic intake: differential diagnosis with true Bartter's syndrome. *Nephrol Dial Transplant* 1992; 7: 896-901.

A Rare Case of Thymic Gangliocytic Paraganglioma

Jung Wook Yang · Joung-ho Han · Hyun Woo Lee · Soo Youn Cho · Hong Kwan Kim¹

Departments of Pathology and ¹Thoracic Surgery, Samsung Medical Center, Sungkyunkwan University School of Medicine, Seoul, Korea

Gangliocytic paraganglioma (GP) is a rare neuroendocrine tumor characterized by epithelioid endocrine cells, spindled schwann-like cells, and ganglion cell-like elements.¹ These tumors almost always arise in the duodenum, particularly in the periampullary region. Extra-duodenal GPs are extremely unusual,² and we could not find any case of thymic GP in the English literature. Here, we report a case of thymic GP and describe its histological and immunohistochemical characteristics.

CASE REPORT

A 1.6-cm-sized anterior mediastinal mass was incidentally found in a 55-year-old female on computed tomography (CT) during work-up for thyroid carcinoma (Fig. 1A). During 12 months of follow-up, CT images showed no interval change. Partial thymectomy was performed, and the cut surface showed an ovoid, well-circumscribed, gray-tan mass measuring 2 × 1.3 cm. Microscopically, the mass had an expanding border surrounded by normal thymic tissue (Fig. 1B). It was composed of spindle cells, ganglion-like cells, epithelioid cells, and fibrillary cells (Fig. 1C), which were haphazardly intermixed in most areas. The spindle cells were arranged in an intersecting fascicular pattern. The scattered ganglion-like cells showed large round nuclei with prominent nucleoli and a large amount of eosinophilic cytoplasm. The epithelioid cells had medium-sized round nuclei with indistinct nucleoli and a small or moderate amount of eosinophilic cytoplasm; they formed vague nests in some areas (Fig. 1D). The fibrillary cells also formed a vague or confluent

nesting pattern in some areas. These cells had small round to ovoid dark nuclei with a fine chromatin pattern and fibrillary cytoplasm. Benign epithelial cells were also observed in approximately half of the cut surface area (Fig. 1F). These cells were intermixed with other components and showed a branching pattern (Fig. 1E). In some areas, they were located between nests of the fibrillary cells. There were several compressed cords and ducts formed by the epithelial cells. No cellular components showed atypia, and no mitosis was seen. On immunohistochemical stains (IHC) (Fig. 1G–K), spindle cells were positive for CD56 (1:200, Leica, Newcastle upon Tyne, UK), synaptophysin (1:50, Thermo Scientific, Rockford, IL, USA), and S-100 (1:5,000, Dako, Glostrup, Denmark). S-100 staining showed that some spindle cells were located adjacent to and in the nests of fibrillary cells. Ganglion-like cells were positive for CD56 and synaptophysin but negative for S-100 and AE1/AE3 (1:500, Dako). The epithelioid and fibrillary cells had the same results on IHC for CD56, synaptophysin, S-100, and AE1/AE3 as did the ganglion-like cells. However, the epithelial cells were only positive for AE1/AE3 with a reticular or race-like cytoplasmic staining pattern (Fig. 1J). Some of the fibrillary and epithelioid cells were positive (Fig. 1K) for progesterone receptor (PR; 1:800, Leica), but most of them were negative (Fig. 1L).

DISCUSSION

The duodenum is the most common site of GP.² Only one case of GP in the posterior mediastinum has been reported,³ and we could not find any English literature cases of GP involving the thymus. We hypothesize that the rarity of thymic GP is due to minimal ganglioneuronal component in the thymus, as GP seems to be related to the amount of ganglioneuronal content in the involved organ. According to the World Health Organization classification, GP is a distinctive triphasic tumor

Corresponding Author

Joung-ho Han, MD
Department of Pathology, Samsung Medical Center, Sungkyunkwan University School of Medicine, 81 Irwon-ro, Gangnam-gu, Seoul 06351, Korea
Tel: +82-2-3410-2800, Fax: +82-2-3410-0025, E-mail: hanjho@skku.edu

Received: June 18, 2015 Revised: July 14, 2015

Accepted: July 14, 2015

consisting of haphazardly distributed epithelioid endocrine cells, spindled schwann-like cells, and ganglion cell-like elements.¹ Composite paragangliomas with a ganglioneuromatous compo-

nent also show the above three elements;⁴ however, the paraganglioma and ganglioneuroma components of the tumor are usually minimally admixed with an abrupt transition. The present

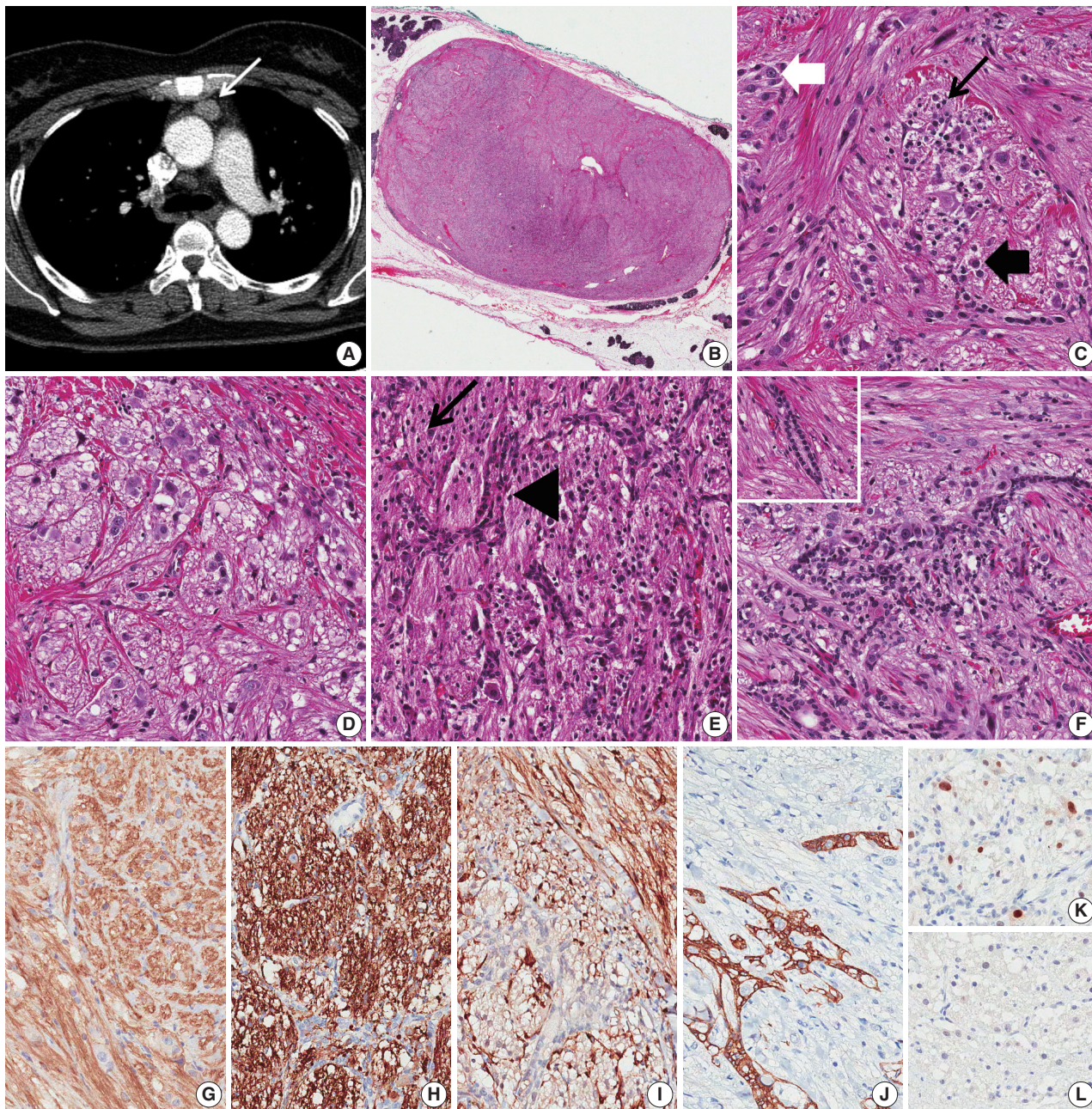


Fig. 1. Thymic gangliocytic paraganglioma. (A) Chest computed tomography reveals a well-circumscribed ovoid mass (white arrow) in the anterior mediastinum. (B) On low-power view, the mass shows an expanding border surrounded by normal thymic tissue. (C) Spindle cells show an intersecting fascicular pattern, and fibrillary cells show a vague or confluent nesting pattern (black arrow). Scattered ganglion-like cells (white thick arrow) and epithelioid cells (black thick arrow) are also noted. (D) Epithelioid cells form a vague nesting pattern. (E) Epithelial cells show a branching pattern (arrowhead) between the nests of fibrillary cells (black arrow). (F) In focal areas, the epithelial cells form compressed cords and ducts (left upper corner). (G, H) Staining with CD56 (G) and synaptophysin (H) is positive for spindle cells, ganglion-like cells, epithelioid cells, and fibrillary cells. (I) Only spindle cells are positive for S-100. Spindle cells are located adjacent to and within the nests of fibrillary cells. (J) On staining for AE1/AE3, the epithelial cells show a reticular or race-like cytoplasmic pattern. (K, L) Some of the fibrillary cells and epithelioid cells are positive (K) for progesterone receptor, but most of them are negative (L).

case is consistent with GP, but there are two unusual components: fibrillary cells and epithelial cells. The fibrillary cells appeared similar to neuronal cells at first glance. Though the fibrillary cells showed a vague nesting pattern similar to carcinoids in some areas, the cells did not express AE1/AE3. Weissferdt *et al.*⁵ reported that all of the studied thymic carcinoid tumors were positive for pancytokeratin. Based on these results, the tumors seem to be composed of neuronal-like cells rather than carcinoid-like cells. Okubo *et al.*⁶ reported that epithelioid cells in almost all cases of duodenal GP were positive for PR. In the present case, some fibrillary and epithelioid cells expressed PR. The fibrillary cells were most likely derived from the same progenitor cell as the epithelioid cells.

The epithelial cells might be entrapped thymic epithelial cells. The staining pattern for AE1/AE3 resembles that of thymic epithelial cells; however, the tumor had an expanding border, and the epithelial component was too extensive to be composed of entrapped thymic cells. Furthermore, the cells formed ducts in focal areas. Thus, the epithelial cells were probably one of the tumor components. Ogata *et al.*⁷ reported a case of duodenal GP with regional lymph node metastasis and a glandular component. The duodenal GP had small amounts of distinct glandular component with mucin. The metastatic tumor deposit in the dissected lymph nodes more prevalently exhibited glandular components with mucus compared to the primary site.

In conclusion, this rare case of thymic GP with neuronal-like and epithelial components shows an extremely unusual site of involvement and unusual tumor components.

Conflicts of Interest

No potential conflict of interest relevant to this article was reported.

REFERENCES

1. DeLellis RA, Lloyd RV, Heitz PU, Eng C. World Health Organization classification of tumors of pathology and genetics of tumors of endocrine organs. Lyon: IARC Press, 2004; 162-3.
2. Okubo Y, Wakayama M, Nemoto T, *et al.* Literature survey on epidemiology and pathology of gangliocytic paraganglioma. *BMC Cancer* 2011; 11: 187.
3. Weinrach DM, Wang KL, Blum MG, Yeldandi AV, Laskin WB. Multifocal presentation of gangliocytic paraganglioma in the mediastinum and esophagus. *Hum Pathol* 2004; 35: 1288-91.
4. de Montpréville VT, Mussot S, Gharbi N, Darteville P, Dulmet E. Paraganglioma with ganglioneuromatous component located in the posterior mediastinum. *Ann Diagn Pathol* 2005; 9: 110-4.
5. Weissferdt A, Kalhor N, Liu H, *et al.* Thymic neuroendocrine tumors (paraganglioma and carcinoid tumors): a comparative immunohistochemical study of 46 cases. *Hum Pathol* 2014; 45: 2463-70.
6. Okubo Y, Nemoto T, Wakayama M, *et al.* Gangliocytic paraganglioma: a multi-institutional retrospective study in Japan. *BMC Cancer* 2015; 15: 269.
7. Ogata S, Horio T, Sugiura Y, Aiko S, Aida S. Duodenal gangliocytic paraganglioma with regional lymph node metastasis and a glandular component. *Pathol Int* 2011; 61: 104-7.

Primary Neurilemmoma of the Thyroid Gland Clinically Mimicking Malignant Thyroid Nodule

Young Sub Lee · Jee Soon Kim · Arthur Minwoo Chung · Woo Chan Park¹ · Tae-Jung Kim

Departments of Hospital Pathology and ¹Surgery, College of Medicine, The Catholic University of Korea, Seoul, Korea

Neurilemmomas, also known as schwannomas, are benign, slow-growing tumors that arise from Schwann cells of nerve roots. They can occur anywhere in the body, but those arising in the head and neck account for 25% to 45% of the cases.¹ Primary neurilemmomas of the thyroid gland are very rare. Only 20 cases of primary thyroid neurilemmoma have been documented in the English literature.² They were usually asymptomatic, and only two cases were found in children.^{3,4} Here we report this rare tumor in a 14-year-old girl, which was clinically mistaken for a malignant thyroid nodule.

CASE REPORT

A 14-year-old girl visited our hospital with a neck mass that had been present for 3 weeks without any symptoms. Ultrasonographic examination showed a lobulated, heterogeneous and hypoechoic nodule in the right thyroid lobe (Fig. 1A). Computed tomography with contrast showed a large hypodense mass in the right thyroid lobe with exophytic extension into the right strap muscle. The tumor was closely abutting and compressing the right tracheal wall (Fig. 1B). Fine needle aspiration cytology (FNAC) of the tumor showed a paucicellular smear composed of bland spindle-shaped cells in loosely cohesive aggregates (Fig. 1C). The patient underwent surgical resection. Intraoperative histological examination of a frozen section favored a benign mesenchymal tumor. Total thyroidectomy was performed; however,

because the lesion was severely adhered to the right tracheal wall, and the surgeon interpreted it as an invasion.

The entire thyroid gland was submitted for pathologic evaluation. On section, a well-demarcated, gray, firm mass was noted in the right thyroid lobe, measuring 3.0 × 2.5 × 2.0 cm (Fig. 1D). The tumor was completely surrounded by the capsule of the thyroid gland. Microscopic examination revealed a proliferation of uniformly spindled cells with a thick fibrous capsule (Fig. 2A). The tumor showed cellular areas with nuclear palisading (Antoni A) and pauci-cellular areas with myxoid change (Antoni B), a characteristic histologic feature of a neurilemmoma (Fig. 2B). There was extensive fibrosis around the tumor, but no perithyroidal tumor extension was found. Immunohistochemically, the tumor cells were positive for S-100 (Fig. 2C), Bcl-2, and fibroblast growth factor receptor 1 (FGFR1) (Fig. 2D), but negative for CD34 and platelet-derived growth factor receptor. Electron microscopy revealed complex intertwinings of slender cell processes outlined by a continuous basal lamina (Fig. 3). Publication of the case information and materials was approved by the Institutional Review Board of Yeouido St. Mary's Catholic Medical Center (SCMC IRB, Project Number SC12ZISE0225).

DISCUSSION

Non-epithelial thyroid tumors, including neurilemmomas, are very rare, accounting for less than 1% of all thyroid tumors.² Delaney and Fry in 1964⁵ first reported a neurilemmoma arising in the thyroid gland. Only 20 cases of a primary thyroid neurilemmoma have been reported.² All but two cases occurred in adults, ranging in age from 20 to 57 years. Baglaj *et al.* in 2004³ first described a primary neurilemmoma of the thyroid gland in a child. A 12-year-old girl underwent left thyroid lobectomy due

Corresponding Author

Tae-Jung Kim, MD, PhD
Department of Pathology, Yeouido St. Mary's Hospital, 10 Yaksam-ro, Yeongdeungpo-gu, Seoul 07345, Korea
Tel: +82-2-3779-2157, Fax: +82-2-783-6648, E-mail: kimecho@catholic.ac.kr

Received: July 19, 2015 Revised: August 11, 2015

Accepted: August 26, 2015

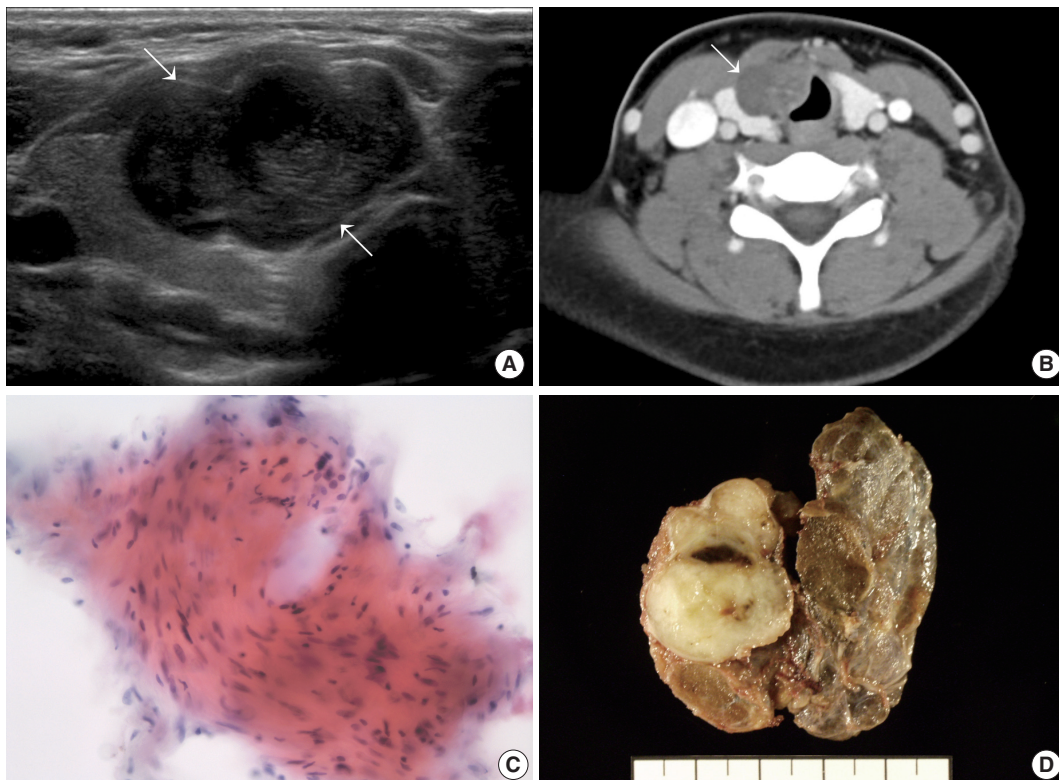


Fig. 1. Imaging, cytologic analysis, and gross examination of thyroidal mass. (A) Ultrasonography showing a lobulated, hypoechoic mass (arrow) in the subcapsular region of the right thyroid lobe. (B) Postcontrast computed tomography imaging revealing a hypodense right thyroidal mass (arrow) compressing the right tracheal wall. (C) Fine needle aspiration cytology with a loose cluster of bland-looking spindle cells. (D) The complete thyroidectomy specimen showing an encapsulated, gray, firm mass replacing the right upper lobe.

to an asymptomatic left lower neck swelling that had been present for 9 months. Ultrasonography showed a predominantly hypoechoic solid lesion measuring $1.7 \times 1.2 \times 2.6$ cm within the left lobe. The second case of a primary thyroid neurilemmoma in a child was reported by An *et al.* in 2010.⁴ A 14-year-old male presented with an asymptomatic left intrathyroidal mass. Radiologic studies showed a hypoechoic left thyroid mass measuring $6.0 \times 4.5 \times 3.0$ cm with cystic portions that was pushing the trachea toward the right. Both cases were diagnosed via postoperative pathological diagnosis as a neurilemmoma. The present case is the third occurrence of a primary thyroid neurilemmoma in a child.

Primary thyroid neurilemmomas should be differentiated from other benign spindle cell neoplasms of the thyroid glands, including vascular, smooth muscle, and fibroblastic tumors.⁶ The diagnosis can be made easily by identifying characteristic histologic features of neurilemmomas: alternating Antoni A and B areas with Verocay bodies (nuclear palisading around cell processes).⁶ Immunohistochemically, diffuse nuclear and cytoplasmic staining of S-100 protein can be helpful. Neurilemmomas arise

from the soft tissues of the neck and secondarily involving the thyroid gland should also be differentiated.⁷ Features suggesting the possibility of a primary thyroid origin may include a rim of thyroid tissue around the capsule and the tumor replacing a major portion of the thyroid gland.

The fibroblast growth factors and their receptors (FGFRs) are known to have a mitogenic effect on Schwann cells.⁸ In vestibular neurilemmomas, overexpression of FGFR1 is positively correlated with the incidence and growth rate of the tumor.⁹ Moreover, activation of FGFR1 may promote invasive behavior in vestibular neurilemmomas through ERK and Akt signaling pathways.¹⁰ In the present case, FGFR1 expression in tumor cells was identified by immunohistochemistry. Although there have been no studies of FGFR1 expression in primary thyroid neurilemmomas, it is suspected that increased expression of FGFR1 in tumor cells might play a role in the rapid growth of the tumor and its aggressive clinical behavior such as extensive tracheal adhesion.

In conclusion, it should be noted that primary neurilemmomas of the thyroid gland with marked adhesion can be clinical-

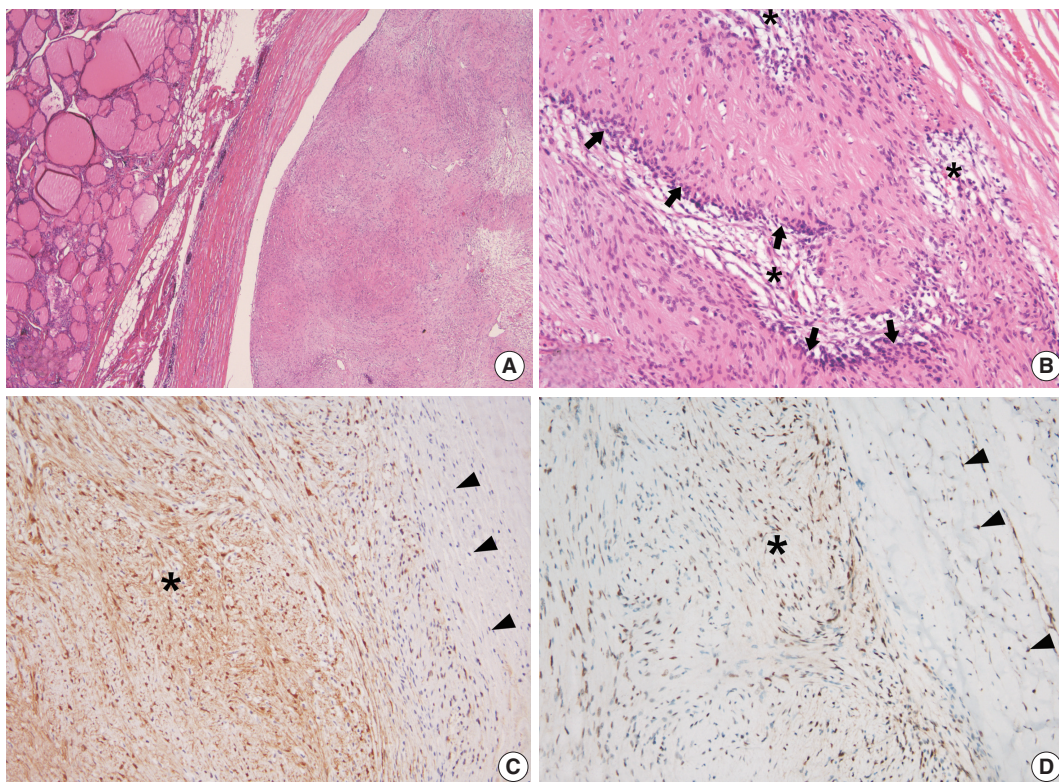


Fig. 2. Histologic and immunohistochemical analysis of the mass. (A) Low magnification view showing a spindle cell lesion (right) sharply demarcated from the adjacent normal thyroid tissue (left) by a thick fibrous capsule. (B) High magnification view revealing both cellular Antoni A areas (arrows) and loose paucicellular Antoni B areas (asterisks). (C) Tumor cells (asterisk) are positive and fibroblasts (arrowheads) are negative for S-100 protein on immunohistochemical staining. (D) Both tumor cells (asterisk) and fibroblasts (arrowheads) are positive for fibroblast growth factor receptor 1 on immunohistochemical staining.

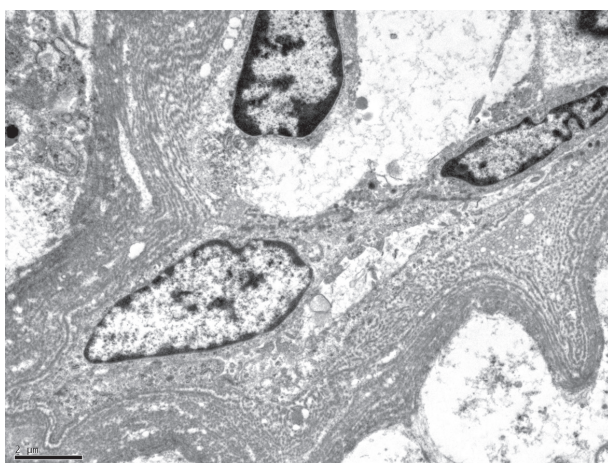


Fig. 3. Electron microscopy displaying long, enveloping cytoplasmic processes outlined by layers of discrete basal lamina.

ly misinterpreted as malignant thyroid nodules. Preoperative FNAC and intraoperative frozen section may help clinicians in making a proper decision on the surgical management of thyroid masses in children.

Conflicts of Interest

No potential conflict of interest relevant to this article was reported.

REFERENCES

1. Uri O, Baron E, Lefel O, Bitterman A. Primary schwannoma of the thyroid gland presenting as an asymptomatic cold nodule. *Am J Otolaryngol* 2009; 30: 427-9.
2. Graceffa G, Cipolla C, Florena AM, Gentile I, Pompei G, Latteri MA. Primary schwannoma of the thyroid gland involving the isthmus: report of a case. *Surg Today* 2013; 43: 106-9.
3. Bağlaj M, Markowska-Woyciechowska A, Sawicz-Birkowska K, Dorobisz U. Primary neurilemmoma of the thyroid gland in a 12-year-old girl. *J Pediatr Surg* 2004; 39: 1418-20.
4. An J, Oh YL, Shin JH, Jeong HS. Primary schwannoma of the thyroid gland: a case report. *Acta Cytol* 2010; 54: 857-62.
5. Delaney WE, Fry KE. Neurilemmoma of the thyroid gland. *Ann Surg* 1964; 160: 1014-7.

6. Kandil E, Abdel Khalek M, Abdullah O, *et al.* Primary peripheral nerve sheath tumors of the thyroid gland. *Thyroid* 2010; 20: 583-6.
7. Badawi RA, Scott-Coombes D. Ancient schwannoma masquerading as a thyroid mass. *Eur J Surg Oncol* 2002; 28: 88-90.
8. Tzeng SF, Deibler GE, DeVries GH. Myelin basic protein and myelin basic protein peptides induce the proliferation of Schwann cells via ganglioside GM1 and the FGF receptor. *Neurochem Res* 1999; 24: 255-60.
9. O'Reilly BF, Kishore A, Crowther JA, Smith C. Correlation of growth factor receptor expression with clinical growth in vestibular schwannomas. *Otol Neurotol* 2004; 25: 791-6.
10. Blair KJ, Kiang A, Wang-Rodriguez J, Yu MA, Doherty JK, Ongkeko WM. EGF and bFGF promote invasion that is modulated by PI3/Akt kinase and Erk in vestibular schwannoma. *Otol Neurotol* 2011; 32: 308-14.